UNIVERSITY OF CAPE TOWN

Faculty of Engineering and the Built Environment

Department of Civil Engineering

MSc. Dissertation

Philbert HABIMANA

Behaviour of FRP Strengthened RC Beams with Concrete Patch Repairs Subjected to Impact Loading

Supervisor: Professor Pilate MOYO

Co-Supervisor: Mr Kabani MATONGO

March, 2017

Behaviour of FRP Strengthened RC Beams with Concrete Patch Repairs Subjected to Impact Loading

Philbert HABIMANA

Thesis submitted to the faculty of Engineering and the Built Environment, University of Cape Town, South Africa, in partial fulfilment of the requirements for the degree of Masters of Science in Engineering.

Cape Town, 2017

TABLE OF CONTENT

DECLARATION

I know the meaning of plagiarism and declare that all the work in the document, save for that which is properly acknowledged, is my own. This thesis/dissertation has been submitted to the Turnitin module (or equivalent similarity and originality checking software) and I confirm that my supervisor has seen my report and any concerns revealed by such have been resolved with my supervisor. It is being submitted for the degree of Master of Science in Civil Engineering at the University of Cape Town, Republic of South Africa. I also confirm that no part of this work has been submitted previously to any university, college or other institution for the award of any degree.

…Signed by candidate… …Signed by candidate……..

Philbert HABIMANA

Date: …*06th March 2017*……

Supervisor: Professor Pilate MOYO

Date: ……6/3/2017

ABSTRACT

The acceptable performance levels and serviceability of reinforced concrete (RC) structures are always the priorities of asset managers, engineers and researchers in any country. RC structures in service may fail to adequately perform due to changes in functionality, corrosion attack on the reinforcing bars, lack of proper and timely maintenance, and loading and standards updating, among other reasons. Impact loading is an extreme form of loading that can damage RC structures such as bridges, interchanges and flyovers during their life span. The repair and strengthening of deteriorating RC structures in service, by using concrete patch repairs and fibre reinforced polymers (FRP) respectively, has attracted a lot of attention from researchers and engineers. Nevertheless, these rehabilitated RC structures in service are susceptible to future deterioration with adverse effects. Inspection and periodic maintenance of strategic RC structures in use are essential for their safe serviceability and to avoid or mitigate economic loss.

This experimental study was conducted on fifteen RC beams with the size of 155 x 254 x 2000 mm, in order to study their behaviour under impact loading testing. Twelve out of these fifteen RC beams were intentionally damaged by uniformly reducing 14 % of the cross-section of their main reinforcing bars, as this simulated the effects of corrosion on RC structures. The drop test, with the impactor applied from varying drop heights, was selected from the different types of impact loading testing methods and used in this research. Each tested RC beam was subjected to eight consecutive drop tests. During this experimental study 120 tests were performed and, from these tests, dynamic responses were recorded for analysis. Two transducers, a load cell and high-speed camera (HSC), were used to record data. In general the captured and stored dynamic responses led to the extraction of contact forces and deflections results. In addition, the HSC recorded video footage of the impact scenarios of the RC beams. The combined use of software such as Photron FASTCAM Analysis (PFA) and Matlab R2014a enables the acquisition of deflection results and, on the basis of these results, residual deflection and maximum deflection have been extracted for further analysis. The computation of bending and inertial forces was also performed on the basis of deflection results. The recorded video footage allowed analysis of the propagation of damage including the cracking patterns and mode(s) of failure of tested RC beams.

The maximum deflection results showed that patch-repaired and FRP-strengthened RC beams generally had a higher flexural rigidity than the control beams. The brittle behaviour of FRP-

strengthened RC beams has also been noted in the maximum deflection findings. Except for the residual deflection results of SB2 group, the results of the remaining tests indicate that at least 60 % of the total bending stiffness ability was lost after the seventh drop test. Regardless of the type of the RC beam tested, deflection half cycle duration increased as drop height increased; however an exception has been made with the first drop tests.

In this study the propagation of damage, including cracking patterns and mode(s) of failure, was assessed and evaluated. All tested RC beams exhibited mainly flexural cracks, some flexure-shear cracks and a few shear cracks. Tested RC beams failed locally in concrete crushing and spalling, followed by the formation of shear plug that started from the point of impact. They also failed globally in permanent bending with the production of important residual deflections. In addition, the FRP-strengthened RC beams failed in the debonding of strengthening material i.e. FRP strip delamination. More than half of the patch-repaired and FRP-strengthened RC beams (that is, 58.3%) exhibited their total FRP debonding after the sixth drop test. Hence, the bond formed between the FRP strengthening materials and concrete soffit of all tested RC beams withstood the impact loading perfectly up to the third drop test, while the fastest total FRP debonding was observed after the fifth drop test.

Furthermore, it was noticed that the longer the patch-repair length, the more the stiffness of the FRP-strengthened RC beams increased, with a corresponding increase in brittle behaviour. The FRP-strengthened RC beams experienced relatively less cracking density compared to the control beams. These FRP strengthening methods may improve the ability of RC beams to withstand the easy propagation of cracks and, consequently, reduce the associated cracking density. The combined application of the concrete patch repairs and the FRP strengthening provides an acceptable approach for the repair and rehabilitation of any deteriorating RC beams that have been subjected to consecutive impact loading.

DEDICATION

To the Almighty God

To my loving mother, my sister and my beloved son Giuseppe Henry M H

To whoever contributed in one way or another to the successful completion of this work

ACKNOWLEDGEMENTS

My appreciation is extended to the following people and organisations:

My supervisor, Professor Pilate MOYO, for all the time he dedicated towards my study, his positive criticisms and kind guidance throughout this research work.

My co-supervisor, Mr Kabani MATONGO a PhD researcher at the University of Cape Town (UCT), for helping me during the experimental testing, reviewing my work and providing me with a stimulating and enjoyable research environment.

Dr Steeve CHUNG KIM YUEN from Blast, Impact and Survivability Research Unit (BISRU), for supervising and ensuring my experimental programme was successfully completed. Special thanks to all other members of BISRU for their kindness.

The following organisations for the financial supports during this studying period at UCT: the government of Rwanda through Rwanda Education Board (REB) and the Concrete Materials and Structural Integrity Research Unit (CoMSIRU).

The management of the former Kigali Institute of Science and Technology (KIST) currently College of Science and Technology (CST) under the University of Rwanda (UR), for allowing me to pursue these postgraduate studies.

Mr Steve CROSSWELL and Pretoria Portland Cement (PPC) De Hoek, for kindly providing the cement used in this study. Mr Kevin KIMBREY and SIKA South Africa, for gently and timely providing all patch repair and FRP strengthening materials used in this research work.

All the members of CoMSIRU, for their kindness, discussion and encouragement during my studies, particularly the late night group; the following PhD researchers: Mr Philemon ARITO, Mr Patrick BUKENYA and Mr Rakesh GOPINATH; Mr Feroz A. MULLAJEE and Mr Thabiso DLADLA, for their assistance, particularly by sharing useful information and experience; Mr Cedric Adam, for his assistance in laboratory works; Dr Björn HÖHLIG a former post-doctoral research fellow, for his advice.

All Civil Engineering laboratory staff, particularly Mr N. HASSEN and Mr H. MAFUNGWA.

All my housemates for their kindness, patience and advice during my studies. Special thanks to Mr Didace HABUMUGISHA and Mr Asaph Mercy KABAASHA.

My landlord Dr Moira E. Niehaus, for accommodating me through my study period.

LIST OF TABLES

LIST OF FIGURES

LIST OF ABBREVIATIONS AND ACRONYMS

ACI: American Concrete Institute

AFRP: Aramid Fibre Reinforced Polymers/ Plastics

AR-glass: Alkali resistant glass

BISRU: Blast Impact & Survivability Research Unit

CAE: Complete Abaqus Environment

CEM I: Cement type I

CEM II/A-L: Cement type II

C-glass: Chemical glass

CFRP: Carbon Fibre Reinforced Polymers/ Plastics

CoMSIRU: Concrete Materials & Structural Integrity Research Unit

DIF: Dynamic Increase Factor

EB: Externally bonded

EBR: Externally bonded reinforcement

ECR: Electrochemical corrosion resistant

E-glass: Electrical glass

EMPA: Swiss Federal Laboratories for Materials Testing and Research

ETS: Embedded through-section

FIB: Fédération internationale du béton (International Federation for Structural Concrete)

fps: frames per second

FRP: Fibre Reinforced Polymers / Plastics

GFRP: Glass Fibre Reinforced Polymers/ Plastics

HSC: High-Speed Camera

HSFC: High Strength Fibre Composite

i.e.: id est

ISIS: Intelligent Sensing for Innovative Structures organization

LVDT: Linear Variable Displacement Transducer/ Linear Variable Differential Transformer

Matlab: Matrix laboratory

NDRC: National Defence Research Committee

NI: National Instruments Corporation

N^{o}: Number

NSM: Near-surface mounted

NSMR: Near Surface Mounted Reinforcement

PFA: Photron FASTCAM Analysis

PFV: Photron FASTCAM Viewer

PPC: Pretoria Portland Cement

RC: Reinforced Concrete

SB1: 450 mm patch-repaired and FRP-strengthened beam group

SB2: 800 mm patch-repaired and FRP-strengthened beam group

SB3: 1300 mm patch-repaired and FRP-strengthened beam group

SB4: 1800 mm patch-repaired and FRP-strengthened beam group

SHPBs: Split Hopkinson Pressure Bars

S-glass: Structural glass

SVM: Super High modulus Fibre

Tg: glass transition temperature

UCT: University of Cape Town

LIST OF SYMBOLS

$\ddot{u}$ (x, t) : acceleration of the specimen

δ_{max} : Maximum deflection

%: Percentage

δ_{u0} (t) : a virtual displacement at the centre of the beam compatible with boundary conditions

D_{max} : Total deflection

A_s : Area of rebar

$\sum \delta_{rs}$: Cumulative residual deflection

ϕ: Diameter of steel bars

A_{lt} : Lost area of steel bar due to grinding

$\overline{m}$: Mass per unit length

δ_{rs} : Residual deflection

c_1: damping coefficient for overall response

c_2: damping coefficient for local response

GPa: gigapascal

h: drop height

I (t): Impact force

k_1: load-mid span deflection of RC beam

k_2: load-displacement relationship of contact spring

kg: kilogram

kN: kilonewton

L: FRP strip length / FRP sheet length

m/s: meter per second

m: meter

m_1: equivalent mass of RC beam

m_2: mass of drop hammer

m^3: cubic meter

μs: microseconds

ms: milliseconds

mm: millimeter

MPa: megapascal

N/mm^2: Newton per square millimeter

N: Newton

^oC: Degree Celcius

P_b (t): actual bending load

P_b: Bending force

P_i (t): Generalised inertia load

P_i: Inertial force

P_t (t): Generalised total load

R_N: Support reaction at the north support

R_S: Support reaction at the south support

s: Second

t: FRP strip thickness / FRP sheet thickness

t_d: duration of the first pulse formation

t_r: rebound time

u_0 (t): displacement at the centre of the beam

u_1: mid-span deflection of RC beam

u_2: displacement of drop hammer

vs: versus

w: FRP strip width / FRP sheet width

CHAPTER 1: INTRODUCTION

1.1. Background

There is a growing need to repair, strengthen and rehabilitate reinforced concrete (RC) structures in service as they are deteriorating due to ageing, revision of loading standards, changes in functionality, corrosion of reinforcing steel bars, and a lack of adequate and timely maintenance, among other reasons (Jumaat & Alam, 2006; Täljsten, 2006; Jumaat & Alam, 2007). The economic loss from damage caused by the corrosion of steel in concrete is arguably the largest single infrastructure problem facing industrialized countries (Broomfield, 2007). Corrosion of reinforcement steel bars is one of the main causes of deterioration of RC structures such as bridges, parking garages and coastal structures, and this results in many defects, including concrete cracking which leads to concrete spalling and the consequent reduction of the load-carrying capacity of the structure. The quality of concrete cover, its depth and design (taking into consideration durability issues, together with the good supervision of all construction work) may constitute an effective approach to mitigate or relatively avoid the deterioration of RC structures due to corrosion attacks. However despite the protection provided to embedded steel by concrete, RC structures are not immune to the ravages of corrosion (Mackechnie & Alexander, 2001).

The patch repair is an effective strategy for maintaining and restoring the serviceability of RC structures. This successful method is used throughout the world provided that the effective treatment of localised zones of corroded reinforcement steel has already been done. Nevertheless concrete repair is a complex process and it presents unique challenges to those associated with new concrete construction (Vaysburd, 2006).

Deteriorating RC structures in service require appropriate remedial measures to restore their load-carrying capacity up to an acceptable performance level (Täljsten, 2006). Patch repair and strengthening methods are currently adapted to achieve this. Strengthening methods include steel plate bonding, external post-tensioning, near surface mounted reinforcement (NSMR) and fibre reinforced polymers (FRP) laminate bonding. However some shortcomings have been observed from conventional strengthening techniques: steel plates are prone to corrosion and fatigue failure, and they are difficult to install on existing RC members owing to their weight (Tavakkolizadeh & Saadatmanesh, 2003). FRP composites, on the other hand, present the following advantages when compared to the other conventional strengthening methods: high

strength-to-weight ratios, flexibility, ease of handling during construction, immunity to corrosion and excellent resistance to environmental degradation (Zhao & Zhang, 2007). While FRP strengthening of existing RC members offers a better solution, debonding failure of such systems is still an issue. It is worth noting that debonding is the separation of the FRP plate from the parent concrete.

Studies conducted under different loading conditions, and in combination with various loading rates, have highlighted various modes of failure of FRP-strengthened RC structures and members. On the one hand, the following modes of failure occurred under static loading: the rupture of FRP strips, compression failure before yielding of steel, compression failure after yielding of steel, delamination of FRP strips, and concrete cover separation (Gao, et al., 2007). The same modes of failure were observed under similar loading conditions were observed during a study conducted by Büyüköztürk & Hearing (1998). On the other hand, when Erki & Meier (1999) conducted a study on FRP laminates subjected to impact loading, the following was noticed: failure of bonded carbon fibre reinforced polymers (CFRP) laminates, yielding of steel and concrete crushing followed by the rupture of the whole beam into two pieces. Furthermore, Tang & Saadatmanesh (2003), in their study of FRP laminates under impact loading, noticed general shear accompanied by the local crushing of concrete in the compression zone of the beam, and delamination of FRP composites from the concrete substrate.

FRP composites for both new and old structures were introduced in the construction industry following their successful use in the aerospace and mechanical engineering fields. However numerical, analytical and experimental studies are necessary in order to gain a full understanding of the behaviour of such FRP-strengthened RC structures and make possible the investigation of all mechanisms involved in the different layers of the system, under various loading conditions. Although FRP laminates are increasingly used to strengthen structural elements, little is known about the effects of impact loads on RC structures strengthened with FRP laminates (Erki & Meier, 1999). Most of the previous studies done on FRP strengthening and repair of RC structures focused on structures subjected to static loading; however in the engineering field, RC structures serve not only under static loads but also under dynamic loadings including impact loading (Tang & Saadatmanesh, 2003). Characterisation of the behaviour of concrete material under impulsive or impact loading is a precondition for the analysis and design of concrete and concrete-like structures (Grote, et al., 2001). The focus of

this study is to experimentally investigate the FRP-strengthened RC beams which have been patch-repaired under impact loading. The results of this study might serve as a basis for: (i) the elaboration of the code of practice and design specifications and (ii) the validation of the analytical and numerical models for FRP-strengthened RC structures when subjected to high loading rates including impact loading.

1.2. Problem statement

RC is a versatile material in construction technology and most RC structures are designed to serve for 50 years and more. These structures are exposed to different loading regimes under various environment conditions. As they are prone to deterioration they therefore need adequate maintenance and rehabilitation to ensure an acceptable level of performance throughout their lifespan. The FRP strengthening method is widely accepted as a viable and durable solution for deteriorating RC structures.

Most studies and researches have been carried out on the FRP-strengthened RC structures under static loading, but few of them are done under impact loading (Tang & Saadatmanesh, 2003). In addition, most of the available literature on RC structures subjected to impact loading has focused on developing the empirical formulae for predicting and assessing the effects of impact loads on concrete structures (Sangi, 2011). Furthermore, these empirical formulae have limitations which exclude them from being generally applied to any concrete structure as they have little theoretical basis and the emphasis is mostly on localised effects.

Practically, for the external application of FRP strengthening RC structures, the sequence of activities is as follows: the removal of all loose concrete material; the proper cleaning and treatment of damaged steel bars; the application the concrete patch repair to the rehabilitated zone; the cleaning of the concrete substrate surface; and the application of the adhesive (usually an epoxy) followed by the FRP strengthening composites. According to the literature that I have been able to access, no research has been published on the FRP strengthening of RC structures that are patch-repaired with concrete under high loading rates such as impact loading.

It is essential to conduct various studies and researches on the general/structural behaviour of FRP-strengthened RC beams - not only under normal loading conditions but also under extreme loading conditions such as impact loads, natural hazards, man-made disasters, and etc. RC structures in service, including the rehabilitated ones, must be able to safely withstand various

impact loads resulting from: (i) falling loads in factories; (ii) rock falls in hilly areas on protective structures; (iii) the dynamic interaction between vehicles' tyres and underlying RC structures and (iv) car accidents on RC flyovers and bridges.

From the foregoing discussions, the present experimental research is conducted to investigate the behaviour of FRP-strengthened RC beams with patch repairs under impact loading. This research will help to bridge the gap in understanding of how FRP composites perform in the civil engineering field.

1.3. Key questions

i. How do FRP strengthening material and patch-repaired RC beams behave compositely under impact loading?
ii. What are the mechanisms involved in the cracking pattern and mode(s) of failure of FRP-strengthened RC beams under impact loading?

1.4. Research objectives

The main aim of this research is to experimentally investigate the behaviour of RC beams patch-repaired with concrete and strengthened with FRP composites under impact loading. To achieve this, the following assessments should be done:

i. Investigate the flexural rigidity and bending stiffness of tested RC beams, and the associated deflection responses.
ii. Assess the effects of varying patch-repair lengths on the stiffness, the resulting deflection and cracking patterns of patch-repaired and FRP-strengthened RC beams.
iii. Investigate the propagation of damage, including the cracking patterns and the mode(s) of failure of patch-repaired and FRP-strengthened RC beams.
iv. Assess the composite action between various layers of materials of patch-repaired and FRP-strengthened RC beams under impact loading.

1.5. Scope of the research

The present research was limited to the behaviour of FRP-strengthened beams with patch repairs as shown in Figure 1.1. Four different groups of FRP-strengthened beams with three specimens for each group were experimentally studied, together with a control group of three unrepaired and unstrengthened RC beams. A total number of fifteen RC beams with the following dimensions 155 x 254 x 2000 mm were studied in this research. The FRP strengthening materials were CFRP strips, with the same size for all strengthened RC beams. The patch-repaired length varied within the FRP-strengthened RC beams groups, although each of these groups had the same patch-repaired length.

Corrosion attack on RC structures usually lead to adverse effects such as cover cracking, spalling, and degradation of structural performance. These adverse effects are caused by: (i) the loss of steel bar cross section; (ii) the volumetric expansion of corroded steel bars and (iii) the weak interfacial layer between concrete and steel bars. However the present research placed emphasis only on the adverse effects of corrosion related to the loss of steel bar cross section (Figure 2.1). The grinding technique was used to reduce the diameter of the steel bars. Nevertheless, the dynamic properties of the materials used to produce all tested RC beams were not explicitly assessed.

This research only took into consideration simply supported rectangular beams cast in-situ, damaged by simulated corrosion, patch-repaired with concrete-based repair material and strengthened with FRP composites. The various unstrengthened and FRP-strengthened RC beams were tested up to the point of failure. The drop hammer method with the hard striking body (impactor) was selected for this research from the various methods of testing RC beams under impact loading.

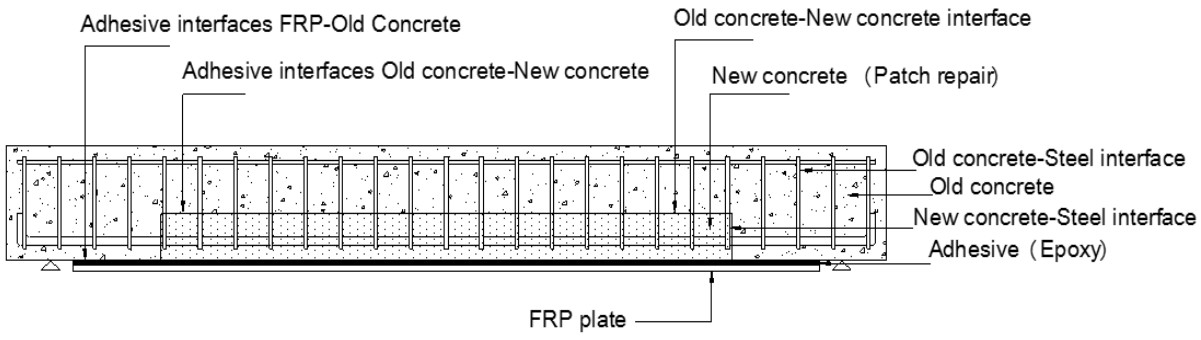

Figure 1.1. Typical labelled FRP-strengthened RC beam with concrete patch repair.

1.6. Layout of the thesis

This thesis is presented in five chapters as follows:

i. The first chapter is an introduction to the study. It provides the background to the research problem and specifies the key questions of the research as well as the research objectives. The scope of the research is also presented.

ii. The second chapter provides a review of published works, journal papers and theses. A detailed background to the RC structures subjected to impact loading system, deterioration of RC structures due to corrosion attacks, patch repairs technique of corroded RC structures, and conventional/traditional and FRP strengthening of RC structures.

iii. The third chapter contains the experimental methodology. All the parameters investigated in this research, the materials and equipment used, as well as different groups of beams tested, are presented here.

iv. The fourth chapter contains the results that were gathered during this research study. The analysis of experimental data is presented in this chapter. The discussions and interpretation of the results obtained are also presented here.

v. The fifth chapter contains the conclusions that have been extracted, based on all collected and analysed data. The recommendations also are provided in this chapter.

CHAPTER 2: LITERATURE REVIEW

2.1. Introduction

Under certain circumstances, strategic infrastructures such as bridges, high-rise buildings and historic monuments deteriorate and need rehabilitation to provide continuously good service. However, rehabilitated structures, particularly RC beams, also deteriorate in time due to various reasons including impact loads. The deterioration of RC structures and corroded RC beam repair are reviewed here, along with the strengthening techniques for RC structures. Impact loading and other high-rate loadings on RC structures, as well as modes of failure of non-FRP-strengthened and FRP-strengthened RC beams under those loading systems are also reviewed to a considerable extent.

2.2. Deterioration of RC structures

Deterioration of RC structures refers to the degradation of the structure from its original condition. A number of internal and external factors are involved in the deterioration of reinforced concrete structures such as the aging of the structure, environmentally induced degradation, poor initial design and lack of maintenance (Täljsten, 2006). Corrosion of reinforcement steel is one of the main causes of deterioration of RC structures (Zhang, et al., 2009; Zhang, et al., 2010). However as corrosion occurs over a relatively long period, it should be assessed carefully and handled accordingly. Moreover, the corrosion process leads to several coupled effects: longitudinal cracking of concrete cover due to expansive corrosion products, steel cross section reduction, and the degradation of the steel-concrete bond (Vidal, et al., 2007). Since corrosion damage happens slowly, it is essential to timely detect, monitor and rehabilitate corrosion defects on RC beams through patch repair and FRP strengthening.

2.2.1. Corrosion damage of RC structures

Concrete is a durable material and, if designed and properly placed, will give long service under normal conditions (Beushausen & Alexander, 2009). The durability of concrete structures depends on the resistance of concrete against chemical and physical factors and its ability to protect the embedded reinforcement steel bars against corrosion (Kapasny & Zembo, 1993; Capozucca, 1995). However, when RC structures in service are exposed to aggressive

environmental conditions in combination with the presence of other unfavourable conditions such as moisture, penetrable concrete cover and insufficient cover depth, they are prone to corrosion. The main causes of corrosion in RC structures are carbonation and chloride penetration. Reinforcement steel bars within the RC structures are depassivated when the pH of the concrete cover drops below critical levels due to carbonation or when the chloride concentration reaches the threshold levels on the rebar surface (Mackechnie & Alexander, 2001; Badawi & Soudki, 2005).

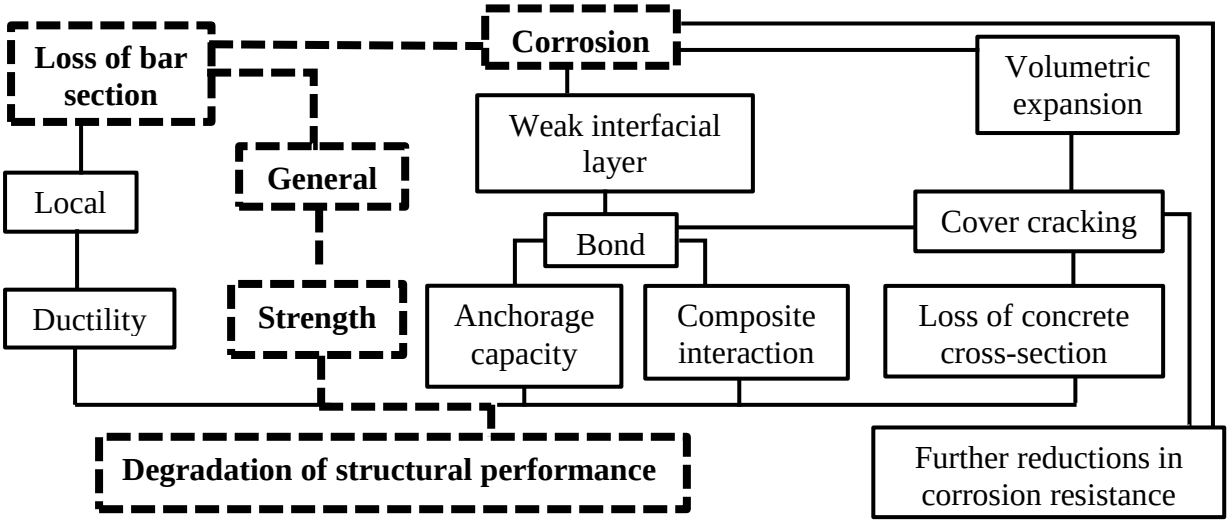

Figure 2.1. Effects of reinforcement steel corrosion on the residual structural capacity (Crains, et al., 2008).

The products of steel corrosion create volumetric expansion in the steel bars and damage the concrete (Capozucca, 1995). Longitudinal corrosion cracks form along the corroding reinforcing steel bars when the tensile stress of the concrete surrounding the rebar exceeds the tensile strength of the concrete (Bentur, et al., 1997). Damage to concrete appears as cracks due to rust pressure and causes a reduction of bar confinement with a weakening of the bond between the concrete and reinforcement steel (Capozucca, 1995). Corroded reinforcement steel bars lead to the reduction of its cross-sectional area and cracking of concrete matrix, followed by spalling and delamination of concrete cover. In addition, the following adverse effects in RC structures are observed: the bond strength between reinforcement steel and the concrete matrix is reduced and consequently, the load-carrying capacity is decreased and deflection of the member increased (Soudki, 2011). Also, the flexural strength of corroded member is reduced. Therefore, following an adequate and timely conditions assessment and the

application of appropriate measures before the failure stage is reached, the service life of corroded RC structures should be extended. The adverse effects of corrosion attacks on RC structures are summarised and presented in Figure 2.1 above. On the same Figure 2.1, the studied case of corroded RC structures is highlighted in dashed line and bold text.

2.3. Repair of corroded RC beams

Modification of a structure to partially or fully restore its serviceability characteristics and to improve its durability is known as repair. A good repair process must take into account a deep and well-detailed conditions assessment of the concrete structure in association with reasonable costs for the desired service life extension. All causes of deterioration of RC structures under study must be accurately investigated, clearly established and addressed based on an effective conditions assessment. Durable solutions and remedial measures to the damaged RC structures, including the repair and rehabilitation of those structures, must be done in good time. Repair of RC structure involves the replacement of corrosion contaminated concrete and all loose materials with new materials, by providing adequate cover to the reinforcement steel and thereby improving the durability of the concrete structures. The repair process must successfully integrate new materials and old materials, forming a composite system capable of enduring exposure to service loads, environment and time (Vaysburd, 2006).

2.3.1. Repair strategies

Concrete repair is not a “band-aid” to a structure in trouble; it is a complex engineering task (Vaysburd, 2006). There is no single solution for repairing deteriorating RC structures. However, an approximated solution to an exact problem is more meaningful than the exact solution to an approximate problem (Vaysburd, et al., 2009). In addition, the suitability and the cost-effectiveness of repairs depend on the level of deterioration and specific conditions of the structure (Mackechnie & Alexander, 2001). Therefore, depending on the circumstances, different repairs strategies can be applied to deteriorating RC structures. When RC structures are damaged by corrosion attacks, the following repair strategies may be adopted: patch repairs, coating systems, migrating corrosion inhibitors, electromechanical techniques, cathodic protection systems, and demolition/reconstruction (Mackechnie & Alexander, 2001). In this present research, patch repair is adopted as a solution to deteriorating RC structures.

2.3.2. Patch repair

Minor, major and localised defects can be addressed using patch repair. The purpose of the patch repair is to restore the damaged structure to its original surface profile (that is, geometry) and to provide adequate protection against further accelerated deterioration, thus ensuring the durability at the location of damage of the structure. Patch repairs consist of the following activities: (i) removal of cracked and delaminated concrete to fully expose the corroded reinforcement, (ii) cleaning of corroded reinforcement and the application of a protective coating to steel reinforcement surface, (iii) application of repair mortar or micro-concrete to replace the damaged concrete, and (iv) application of possible coating or sealant applied to the entire concrete surface to reduce moisture levels in the concrete (Mackechnie & Alexander, 2001; Sika, 2013). Patch repairs are generally successful, provide that all of the corroded reinforcement are well treated (Mackechnie & Alexander, 2001; Beushausen & Alexander, 2009).

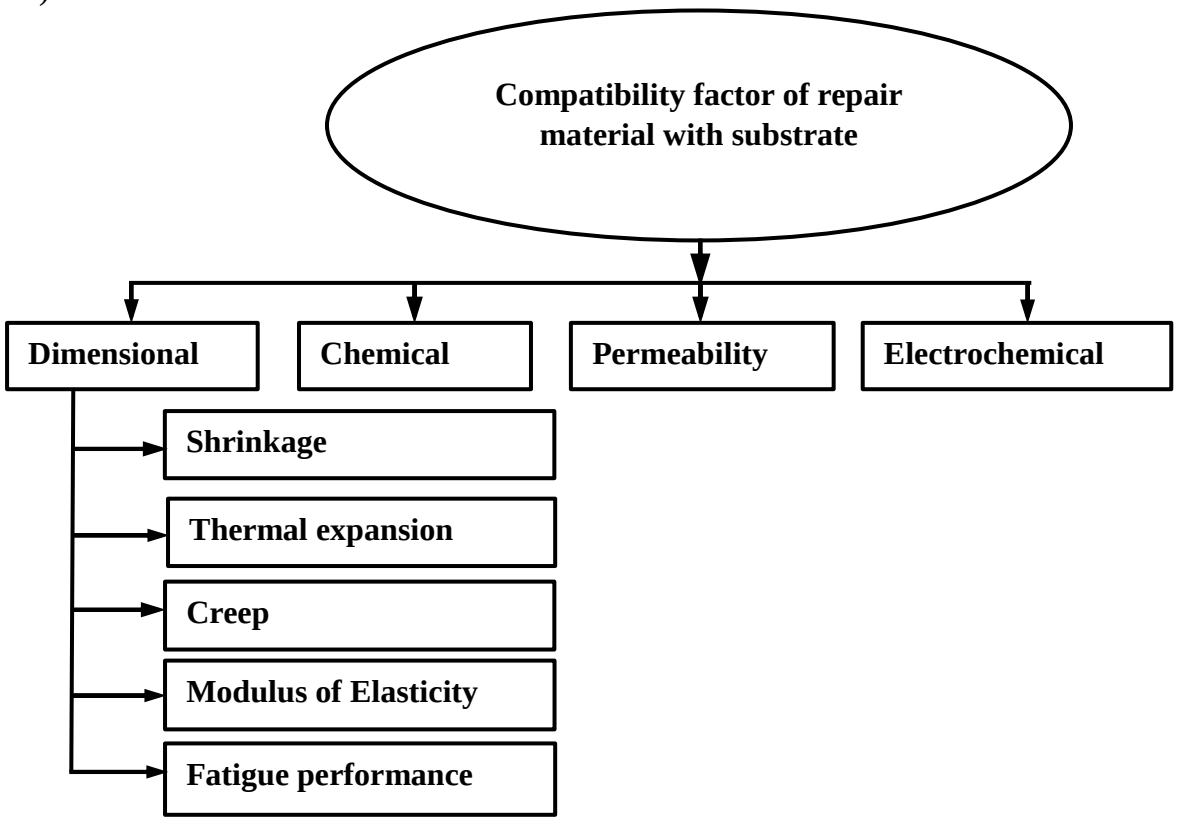

Figure 2.2. Compatibility factors in a concrete repair system adapted from Vaysburd, (2006).

One of the main causes of failure of patch repair is the lack of compatibility between the patch repair and the substrate. Compatibility of a repair system refers to the balance of dimensional

(geometrical), chemical, permeability and electrochemical properties of the substrate and the repair mortar, in order to ensure that the repair system is able to withstand stresses induced due to volumetric changes, chemical and electrochemical effects, without premature failure over designed period of time (Vaysburd, 2006). Therefore, successful repair methods must have good compatibility behaviour between the substrate and the repair material. Further maintenance should be also minimized for a good patch repair. The compatibility factors involved between the substrate and patch repair are summarized in Figure 2.2 above.

2.4. FRP composite materials

An advanced composite material is a term generally used to describe the material formed by mechanically bonding together two or more different materials to produce a new material with optimal desired properties (Mazumdar, 2002). Those individual materials are commonly known as constituents. Typically, an advanced composite material is formed by reinforcing fibres embedded in a matrix resin as shown in Figure 2.3. On the one hand, the matrix binds together the reinforcing fibres, to protect the fibres from both mechanical damages and environmental attacks such as corrosion and chemical attacks, and transfers and evenly distributes the load to the reinforcing fibres. On the other hand, the reinforcing fibres constitute the backbone of the composite material, and are therefore the main load-carrying constituents that provide other structural properties of the entire composite material.

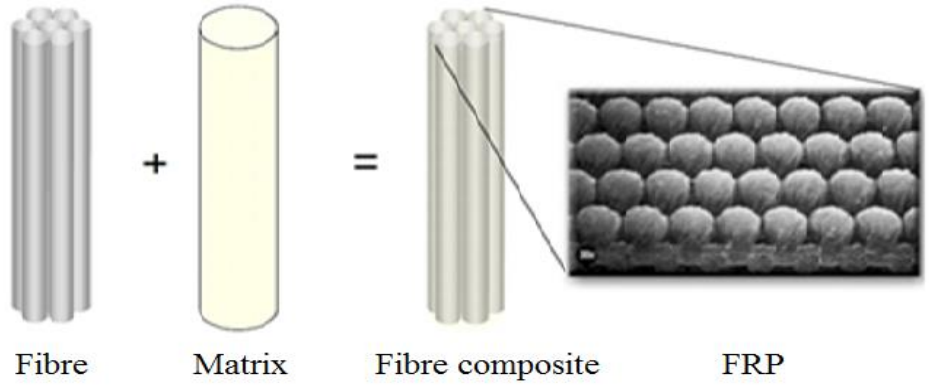

Figure 2.3. Typical advanced composite material i.e. FRP (Täljsten, 2006).

An increase in the amount of the reinforcing fibres leads to a proportional increase in both strength and stiffness of the composite material. The typical volume of fibres in FRP composites equals about 50-70% for laminates/strips and 25-35% for sheets (fib, 2001;

Täljsten, 2006). The strongest properties of fibres are oriented in parallel with the direction of fibres. Hence, in flexural strengthening the unidirectional composites are commonly used, thus the fibres are oriented in the longitudinal direction of the composite materials. Furthermore, depending on the nature and direction of the load to compensate, bidirectional and multidirectional composites can be used.

Despite their recent introduction as building materials for both new and old structures, the FRP composite materials are popular with the civil engineering community. Thus, FRP composites material as structural reinforcement and rehabilitation of RC members are commercially available in various sizes and forms including bars, tendons, ropes, grids, strips (laminates), sheets or fabrics (Matthys, 2000). Figure 2.4 illustrates different forms and sizes of FRP composites.

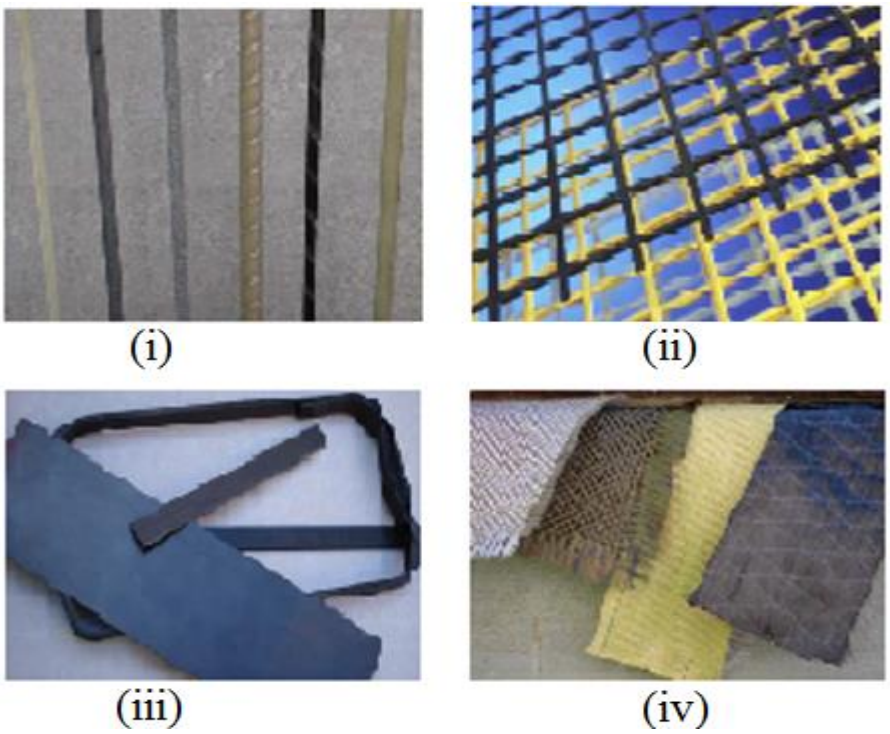

Figure 2.4. Various sizes and forms of FRP composites; (i) FRP rebar, (ii) FRP grids, (iii) FRP plates and strips, (iv) FRP sheets or fabrics (FIB, 2007).

The FRP composites materials are most suitable for rehabilitating RC structures due to their mechanical properties and behaviour, especially in aggressive environmental conditions. Also, the FRP composites materials have more advantages than conventional strengthening systems, including steel plates. In line with this research, the FRP constituents, the FRP applications, and the FRP strengthening systems are presented with more details.

2.4.1. Constituents of FRP composites materials

Matrix

In a composite material (that is, reinforced polymers or plastics) the matrix material can be regarded as both a structural and a protection component. Matrix material is a polymer made of molecules formed with much simpler and smaller units; these are commonly called monomers (Tuakta, 2005). A polymer is generally known as a resin system during the processing stage and becomes a matrix once the polymer has fully cured (FIB, 2007). Some of the important functions played by the matrix in the composite material system have been already mentioned above. Moreover, the matrix fulfils the other functions: (i) it isolates the reinforcing fibres so that the fibres can act separately as individual; hence this ability slows or stops the propagation of the crack; (ii) the performance characteristics such as impact strength, ductility, and etc. are influenced depending on the selected matrix material; (iii) the type of the matrix material may also strongly affect the mode of failure and the fracture toughness of the resulting composite and (iv) it controls the overall stress-strain behaviour of the composite.

There are two main groups of matrix material types: thermoplastics and thermosetting matrices. In the civil engineering field, thermosetting matrices are most commonly used together with high performance reinforcing fibres (Täljsten, 2006). The thermosetting matrices have strong intramolecular and intermolecular bonds than the thermoplastics matrices. Polyester, epoxy and vinyl ester are all thermosetting matrices. On the following Table 2.1, the thermosetting matrices are presented together with their various engineering properties. Most of these matrices were tests at room temperature. Among the thermosetting matrices, epoxies are more expensive; however, they generally possess better mechanical properties and high durability.

Table 2.1. Typical properties of thermosetting matrices (FIB, 2007).

Property	Matrix		
	Polyester	**Epoxy**	**Vinyl ester**
Density (kg/m^3)	1200-1400	1200-1400	1150-1350
Tensile strength (MPa)	34.5-104	55-130	73-81
Longitudinal modulus (GPa)	2.1-3.45	2.75-4.10	3.0-3.5
Poisson's coefficient	0.35-0.39	0.38-0.40	0.36-0.39
Thermal expansion coefficient (10^{-6}/ºC)	55-100	45-65	50-75
Moisture content (%)	0.15-0.60	0.08-0.15	0.14-0.30

Fibres

A fibre is a constituent material formed with a long filament having a 5-20μm diameter (fib, 2001; Tuakta, 2005). Reinforcing fibres can be manufactured in chopped (discontinuous) or continuous form. In this review, the emphasis was made on continuous fibres. The main functions of reinforcing fibres in a composite material are: (i) to carry the load (they carry 70 to 90 % of the overall applied load in a structural composite); (ii) to provide strength, thermal stability, stiffness, and other structural properties; and (iii) to provide insulation or electrical conductivity, depending on the type of fibre used. In addition, the desirable functional and structural requirements of the fibres in composite are: high elastic modulus for effective use of reinforcement; low deviation of strength between single/individual fibres; stability of properties during fabrication and handling; uniformity in diameter and surface of the fibre; high toughness; acceptable durability; availability in appropriate forms; and acceptable cost (FIB, 2007).

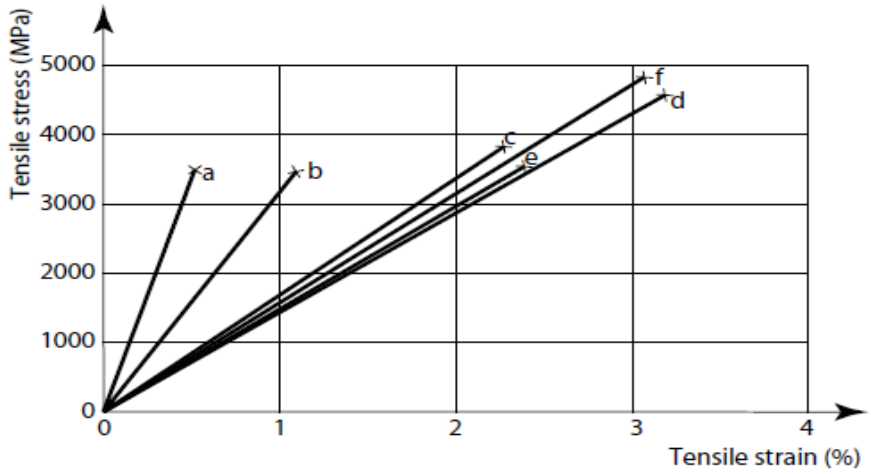

Figure 2.5. Stress-strain curves of typical reinforcing fibres: a) Carbon (high modulus); b) Carbon (high strength); c) Kevlar 49; d) S-glass; e) E-glass; f) Basalt (Hollaway, 1993; fib, 2007).

AFRP (Aramid Fibre Reinforced Polymers), CFRP and GFRP (Glass Fibre Reinforced Plastics) are the most common fibres used to produce FRP composite materials applied in civil engineering works. Also, basalt fibre type has recently been made commercially available. According to Hollaway (1993), all the fibres subjected to tensile loading show a linear elastic behaviour up to their failure point without displaying any yield. Figure 2.5 above illustrates the stress-strain curves of the most used reinforcing fibres in civil engineering. The properties of commercially available reinforcing fibres are presented in Table 2.2.

Table 2.2. Typical properties of reinforcing fibres for FRP composite materials (FIB, 2007).

Fibre type \ Property		Density	Tensile strength	Young modulus	Ultimate tensile strain	Thermal expansion coefficient	Poisson's coefficient
		(kg/m^3)	(MPa)	(GPa)	(%)	($10^{-6}/^oC$)	
Glass	E-glass	2500	3450	72.4	2.4	5	0.22
	S-glass	2500	4580	85.5	3.3	2.9	0.22
	AR-glass	2270	1800-3500	70-76	2.0-3.0	-	-
	ECR	2620	3500	80.5	4.6	6	0.22
Carbon	High modulus	1950	2500-4000	350-650	0.5	-1.2…-0.1	0.20
	High strength	1750	3500	240	1.1	-0.6…-0.2	0.20
Aramid	Kevlar 29	1440	2760	62	4.4	-2.0 longitudinal 59 radial	0.35
	Kevlar 49	1440	3620	124	2.2	-2.0 longitudinal 59 radial	0.35
	Kevlar 149	1440	3450	175	1.4	-2.0 longitudinal 59 radial	0.35
	Technora H	1390	3000	70	4.4	-2.0 longitudinal 59 radial	0.35
	SVM	1430	3800-4200	130	3.5	-	-
Basalt	Albarie	2800	4840	89	3.1	8	-

In Table 2.2 the temperature from which various FRP fibres were tested is not indicated in reference used. However, the FRP composite materials should not be used at temperatures above their glass transition temperature (Tg) (FIB, 2007). The value of Tg depends upon to the type of resin (polyester, epoxy, vinyl ester, etc.) and it is normally in the range of 70 ^{o}C to 175 ^{o}C. According to FIB, (2007) considerable reductions in bond strength were observed from the FRP materials tested at temperatures above Tg. Moreover, negative temperatures acting on FRP composite materials can lead to adverse effects such as matrix hardening, matrix micro-cracking and fibre-matrix bond degradation (FIB, 2007).

2.4.2. The applications of FRP composite materials

The FRP composites materials have been successfully used in aerospace and mechanical engineering fields for many years. However, the use of FRP materials did not experienced a rapid evolution in civil engineering community till the 1980s. The initial development of the FRP strengthening technique took place in Switzerland by Meier of the Swiss Federal Laboratories for Materials Testing and Research (EMPA) in 1987 (Täljsten, 2006). Due to their many advantages and good mechanical properties for fewer reported disadvantages and drawbacks, the FRP materials are now popular in civil engineering works. High strength, light weight, easy installation and easy transportation, high resistance to corrosion and chemical attacks are some of many others characteristics that make the FRP composites reliable and attractive construction materials. In addition, the emerging field of renewal engineering may best describe the use of FRP in civil engineering (Seible, 2001; Einde, et al., 2003). They are nowadays successfully applied in rehabilitation (that is, repair, strengthening and retrofitting of concrete structures) and the new structures such as bridge decks, building roofs, and etc. Figure 2.6 illustrates the use of FRP composites in civil engineering.

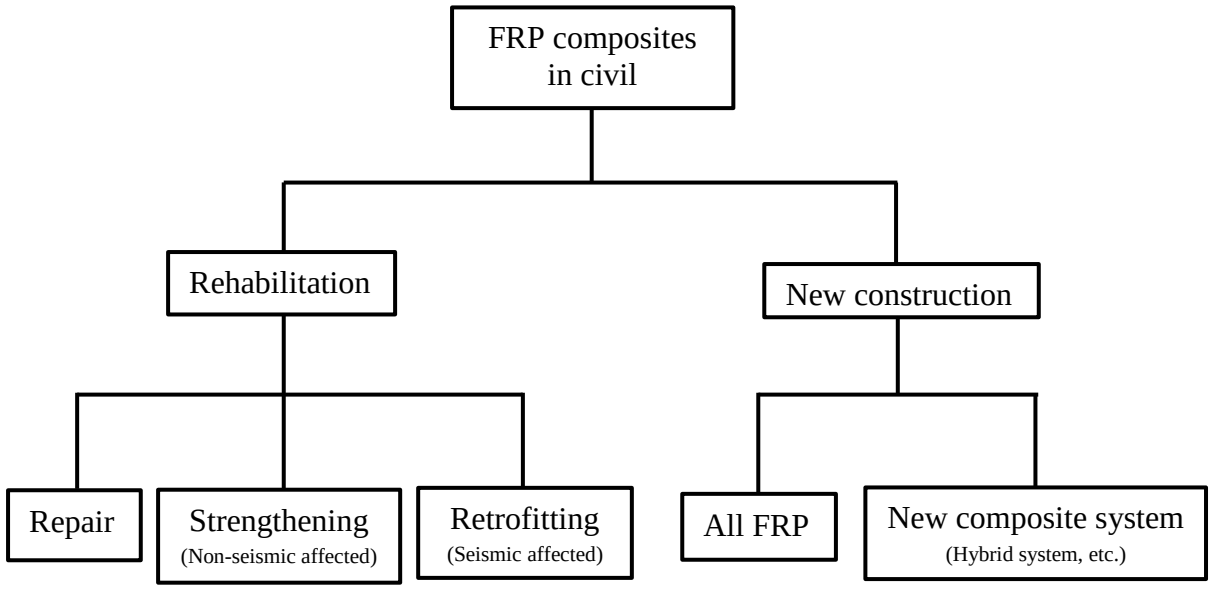

Figure 2.6. The use of FRP composite in civil engineering adopted from Seible, (2001); Einde, et al., (2003).

2.5. Strengthening of RC structures

Reinforced concrete is a versatile material and its ability to form complex shapes have led to its popular and successful use in the civil engineering community. Nevertheless, the durability of concrete and concrete-like structures depends on their capacity to protect the embedded steel reinforcement against corrosion and their resistance against chemical and physical factors (Kapasny & Zembo, 1993). There are several reasons and situations in which the structural capacity of existing RC structures needs to be upgraded to a certain performance level; that is, they require to be rehabilitated and/or strengthened. The structural capacity deficiencies may consist of one or more of the following factors: lack of strength (flexure and shear), stiffness, ductility and durability. Structural capacity deficiencies of the RC structures are usually due to corrosion attacks that then lead to the deterioration of the material, change in use, new loading criteria, aging, poor design and construction errors among other reasons (Nezamian & Setunge, 2004). It follows that a large number of RC structures worldwide are in urgent need of repair and strengthening to safely serve and fulfil their intended uses. It is becoming both economically and environmentally preferable and advisable to upgrade structures rather than to reconstruct them, particularly if efficient, rapid and strengthening methods are available (Garden & Hollaway, 1998). Furthermore, strengthening of RC beams is a common task of concrete structures maintenance nowadays (Jumaat & Alam, 2006).

The strengthening of RC structures in need can be classified when based on: (i) the direction of created stresses by the applied loads within the structure in the study; (ii) the location of the structural strengthening material and (iii) the type of the material used to strengthen those RC structures. The flexural strengthening, shear strengthening and confinement reinforcement are classes of strengthening that are based on the direction of stresses induced into the structure in the study. However if the classification of strengthened RC structures is based on the location of the strengthening materials, they are commonly called external and internal strengthening methods. Lastly, when the classification of strengthened RC structures is based on the type of materials, these methods are known as steel plate strengthening, concrete strengthening, prestressed concrete, FRP strengthening, among others.

The rehabilitation and/or the strengthening of existing structures to correct deterioration-related damage, increase structural load-carrying capacity or ductility has traditionally been accomplished through the utilisation of conventional materials and techniques (Setunge, et al., 2002). Some of many traditional strengthening techniques include steel plate bonding, concrete

or steel column jacketing, and external post-tensioning, and all these have been successfully used. However, some drawbacks and shortcomings have been experienced on RC structures strengthened using traditional/conventional techniques and advanced strengthening materials such as FRP composites have been introduced to overcome these challenges. FRP composites generally offer many excellent properties in comparison to conventional materials such as steel and aluminium (Täljsten, 2006). Corrosion resistance, high strength-to-weight ratio, general versatility and relatively low maintenance cost and of FRP materials make them more attractive and suitable for plate bonding applications (Quantrill & Hollaway, 1998). In the present research work, the emphasis is on the flexural strengthening of RC beams with FRP sheet anchorage applied at both ends of the FRP plate. Both traditional/conventional and FRP composites strengthening techniques are reviewed, presented and discussed in detail.

2.5.1. Externally bonded steel plating system

Steel plate is one of the most commonly used materials for strengthening RC structures (Jumaat & Alam, 2006). During the upgrading of reinforced concrete structures using steel material, a steel plate is bonded to the concrete surface by an epoxy adhesive. The bonding of a steel plate to the soffit of a RC member leads to the creation of three-phase concrete-adhesive-steel composite system. Hence, the most common form of plating is to stick steel plates to the faces of beams in the tension region, as the plate is at its furthest extremity from the compression region and, as a result, the composite flexural action will be at its maximum (Oehlers & Ali, 1998). Figure 2.7 illustrates most commonly used types of steel plating, and takes debonding issues into account.

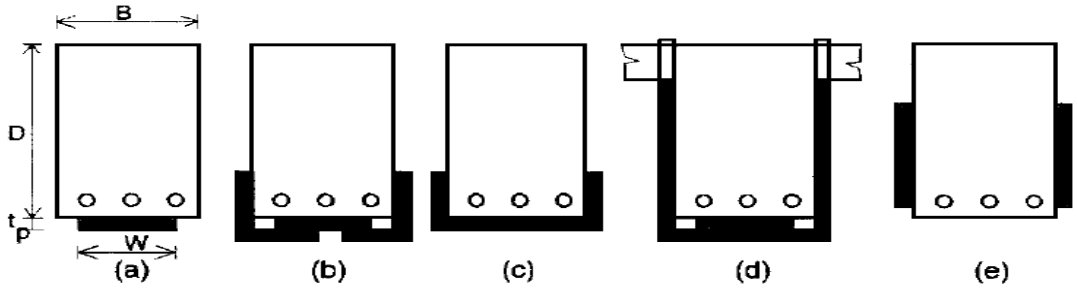

Figure 2.7. Types of steel plating (Oehlers & Ali, 1998).

2.7 (a) Steel plate at the tension face of the beam; 2.7 (b) steel plate at the tension faces of the beam plus steel angles to overcome premature debonding of the strengthening material; 2.7 (c)

steel channel is used instead of steel plate as this is relatively less prone to debonding ; 2.7 (d) tension face plates and external stirrups are combined together; thus, the external stirrups increase the shear ability and prevent debonding of the tension face plate and 2.7 (e) straps are applied on RC beam to enhance the shear performance.

It has been reported by a considerable number of researchers that the steel bonding to the RC beams can substantially contribute to the flexural stiffness, reduce cracking density and structural deformations at all load levels, as well as contribute positively to the ultimate flexural capacity (Jumaat & Alam, 2006; Arslan, et al., 2008). The ultimate and cracking loads of the strengthened RC beams glued steel plate depend mainly on the following parameters: (i) the compressive strength of concrete; (ii) nominal strength of the web reinforcement ratio; (iii) the yield strength of longitudinal reinforcing bars; (iv) the tensile reinforcement ratio; (v) the shear span-to-depth ratio; (vi) the strength of steel plates; (vii) mechanical properties of epoxy adhesive and (viii) friction coefficient between concrete and steel plate (Arslan, et al., 2008). The effectiveness of the steel plate bonding as a strengthening method of RC beams depends on the surface preparation, bonding materials and methods used between steel plates and the existing beam (Jumaat & Alam, 2006). Figure 2.8 shows steel plate material bonding for the flexural strengthening of a RC bridge.

Figure 2.8. Typical steel plate bonding for flexural strengthening RC beams of a RC bridge (Alkhrdaji, 2013).

Strengthening of RC structures generally requires the performance assessment of the structure before and after it is upgraded to acceptable serviceability level. Most of the time, the desired performance level is generally reached when certain requirements are met, and this includes

revising and upgrading the design of the structure. Various standards and codes of practice are used to better achieve the intended targets in the repair and strengthening of RC structures.

According to Hussain, et al., (1995), the repaired beams exhibited higher strength than the original beams, providing that the plates did not exceed a certain restricted thickness. Increasing the plate thickness led to the shift of the mode of failure of the repaired beams from flexural to premature failure. This resulted from the shear and/or tearing of the plate, and caused a reduction in ductility (Hussain, et al., 1995). Bonding steel plates on the tension faces of the beams led to an increase of their shear capacity from 9% up to 15%. This may have happened due to dowelling action from those plates which had the largest contact area with concrete, rather than a counterpart amount of internal steel reinforcing bars (Charif, 1983). Also, the glued plates can increase the ultimate flexural strength of structures by about 15% (Swamy, et al., 1987).

Steel plates have successfully been used as an externally bonded strengthening method to upgrade the structural capacity of RC structures for many years. RC structures are strengthened by using steel plates to effectively increase both shear and flexural capacity. Furthermore, with steel plate strengthening, the following advantages have also been reported: uniform material properties (isotropic), cheapness, availability, high fatigue strength and high ductility (Jumaat & Alam, 2006). However, the heavy weight of steel material, corrosion of steel material, the awkwardness of forming joints, and the intensive work required for surface preparation are among the major drawbacks of using steel plate as a strengthening material (Nurbaiah, et al., 2010).

2.5.2. Jacketing system

Jacketing is one of the most favoured and widely known strengthening methods of poor detailed or deficient RC members and structures (Chalioris, et al., 2013). Jacketing of reinforced concrete structures is based on improving the structural characteristics of structures in need of strengthening by adding a sleeve around the member/structure perimeter. Jackets may be built using different materials: these include concrete, steel and FRP composites. For example, the self-compacting concrete jacketing seems to be an effective rehabilitation technique to shear-damaged reinforced concrete beams. Figure 2.9 shows a RC rectangular beam strengthened with RC jacketing.

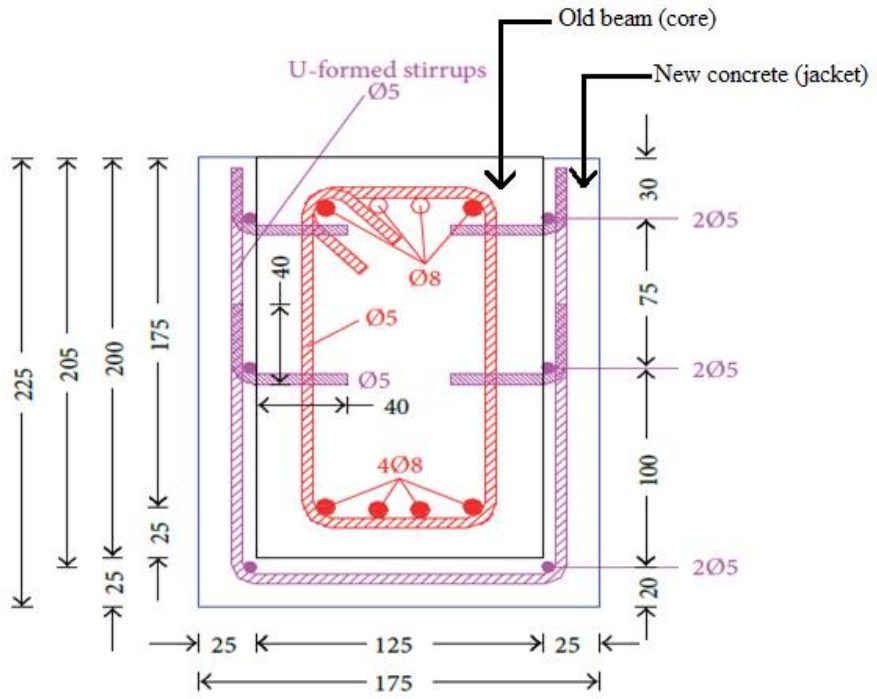

Figure 2.9. Cross-sectional dimensions and steel reinforcement of the jacketed beams (Chalioris, et al., 2013).

Compared to the initially tested specimens, the load bearing capacity and the overall structural performance of the jacketed beams were enhanced (Chalioris & Pourzitidis, 2012). A variety of techniques in placing concrete jackets have been used to rehabilitate columns, beams and joints (Vandoros & Dritsos, 2008). Jacketing can be partially or fully applied to a RC structure in need. Jacketing is partially applied once it covers a part of the member and it is fully applied once it covers the entire member.

The principal purposes of jacketing are: (i) to upgrade concrete confinement by transverse fibre reinforcement, particularly for circular cross-sectional columns; (ii) to enhance shear strength by transverse fibre reinforcement and (iii) to upgrade flexural strength by longitudinal fibre reinforcement (Waghmare, 2011).

The jacketing system enlarges the cross-sectional area of the column and decreases the slenderness ratio of the column (Klaiber & Wipf, 2000). Jacketing of structural elements, such as columns, consists of carefully adding concrete as longitudinal and transverse reinforcement around the existing columns. Jacketing of beams is highly recommended as it gives continuity to the neighbouring columns and stiffness of the structure. While jacketing a beam, its flexural resistance must be carefully computed to avoid the creation of a strong-weak column system

(Waghmare, 2011). It has long been recognized worldwide that RC jackets do provide enhanced strength, stiffness, and overall improvement of the structural performance (Thermou, et al., 2007).

Nevertheless, the difficulty most experienced with this strengthening technique is establishing continuity between the old and new material. This is very critical if the load is to be transmitted to the new material (Klaiber & Wipf, 2000). Therefore, the effectiveness of this strengthening method depends on the degree of bonding between the existing and the new concrete, which can range between 30% and 80% of the total in-situ concrete (Klaiber & Wipf, 2000). Hence there is a direct correlation between the amount of care taken in preparing the surface of the existing structure with appropriate tools, and the ultimate bond strength.

The effectiveness of adequately constructing concrete jackets was proved when it was realised that, under special circumstances and conditions, an almost monolithic behaviour could be reached. Even when the jacket was built with no treatment at the interface, a significant increase in both strength and stiffness was observed (Vandoros & Dritsos, 2008). Figure 2.10 illustrates practical examples of reinforced concrete structures that have been strengthened with jacketing systems.

(a). Enlargement of a RC beam. (b). Enlargement of a RC column.

Figure 2.10. Jacketing of RC members for higher loads (Alkhrdaji, 2013).

In the case of steel jackets, the following methods are used to bind together the new jacketing material and the existing member: (i) welding through bend-down bars or intermediate bars; (ii) heat tensioning of tie plates or full thin steel plates; (iii) bonding of thin steel sheets on damaged members by spreading epoxy adhesive gently onto the steel sheets and concrete surfaces; (iv) tie the damaged parts of the column with steel ties in the form of collars; (v) mild steel is attached around the damaged element, then heated and hammered to form a spiral and (vi) enfold a column with a high strength fibre composite (HSFC) jacket as a possible

replacement method to steel jackets (Frangou, et al., 1995). Figure 2.11 illustrates different techniques used to install a steel jacket on strengthened structures.

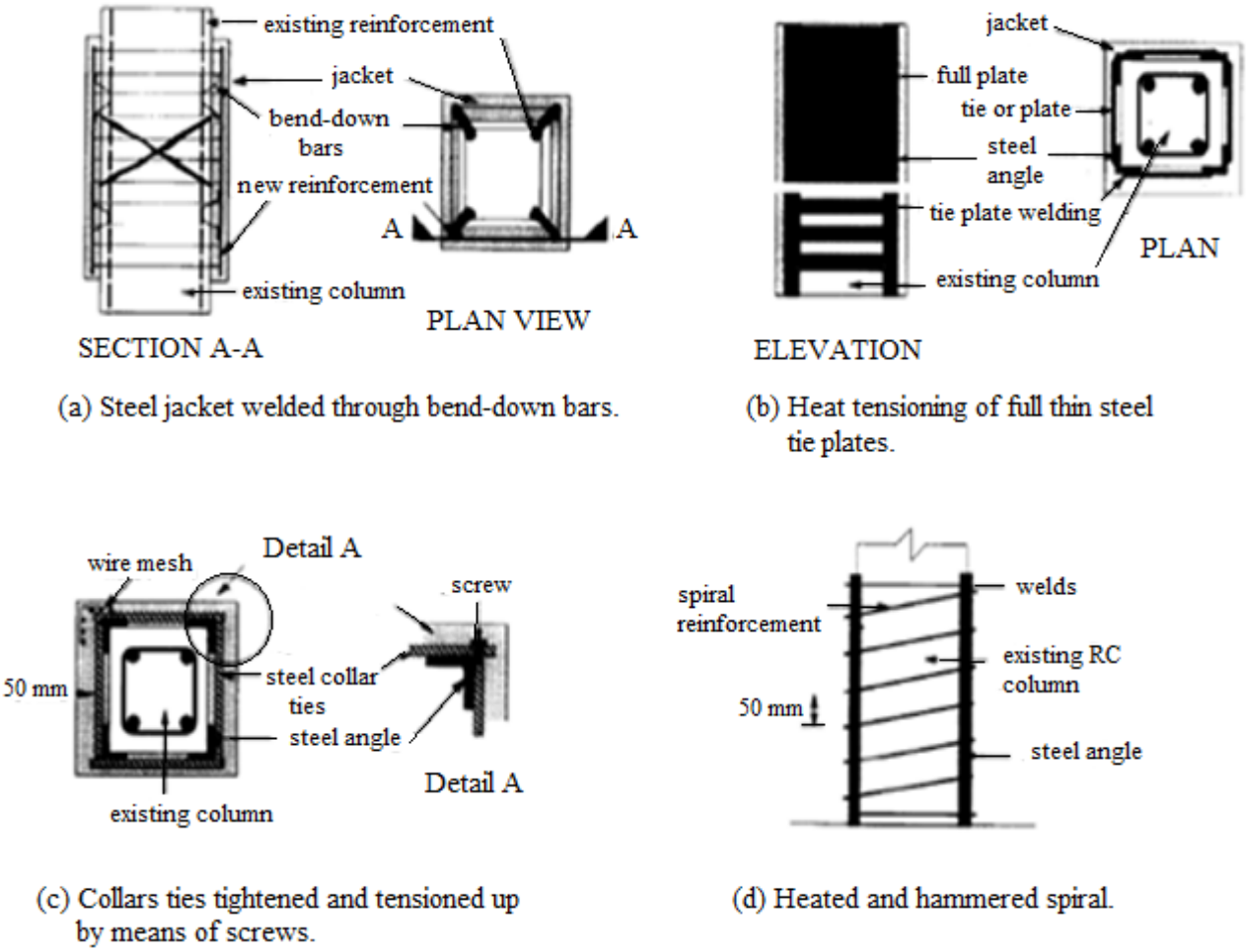

Figure 2.11. Various techniques used to install steel jackets on RC members (Frangou, et al., 1995).

Jacketing, although a conventional strengthening technique, has some disadvantages and this has led researchers to look for better methods. Jacketing is sometimes very costly and time-consuming, and it requires that the utilisation of the structure is interrupted while work is executed (Frangou, et al., 1995). Furthermore, when the important dead load is added to the strengthened structures, significant dimensions change and bulk formwork is needed. In addition, when steel jackets are installed and bonded with welding, the following drawbacks are experienced: (i) the lack of a globally-accepted analytical tool for determining the efficiency of the welding is a drawback, as the operator on site has sole responsibility for the standard of the work; (ii) time-consuming process; (iii) high cost; (iv) sophisticated/specialized

equipment and electrical power supply are required on site; (v) properly skilled staff are needed (Frangou, et al., 1995). Besides the challenges related to welding, steel jackets are also prone to corrosion attacks. The associated effects of corrosion may lead to the failure of the jacketing system. Thus as most of the time the initial cost of repair and strengthening measures is considerable, researchers need to find solutions that are more economical as well as durable.

2.5.3. External post-tensioning system

The aim of prestressing concrete beams may be either to enhance the serviceability of the structural system to which the beams belong, or to expand its limit state (Garden & Mays, 1999). In addition, the general aim of providing an external post-tensioning system to an existing bridge is to reinstate its serviceability by considerably reducing the dead load bending effects, thus leading to decreased deflections and/or elimination of cracking. The additional post-tensioning material will also upgrade the ultimate limit capacity in shear and bending (Ryall, 2001). Moreover, post-tensioning technique can be used for repair, rehabilitation, modification, and strengthening of both RC and post-tensioned structures (Krauser, 2006). Figure 2.12 shows a RC beam strengthened with the use of external tendons.

Figure 2.12. Deviated RC Beam strengthened with external tendons (Krauser, 2006).

The external prestressing system can be used on existing and new structures (Garden & Hollaway, 1998). This strengthening method can be effectively applied by the use of unbonded tendons or bonded composite plates (Garden & Mays, 1999). Unbonded tendons can take one of two forms: they can be internally embedded into the concrete material, as in unbonded post-tensioned slabs, or they can be externally applied to it, as in externally post-tensioned box girder bridges. The utilisation of unbonded tendons in general, and external prestressing, in particular, is currently gaining popularity because of cost-effectiveness and simplicity of construction (Alkhairi & Naaman, 1993). Also, the fatigue behaviour of concrete members is enhanced by this method because prestressing the tension flange of a beam decreases the tensile

component of the stress cycle. External prestressing can delay or prevent fatigue crack initiation and growth in reinforcement steel bars embedded in concrete or steel girders (Garden & Hollaway, 1998). Figure 2.13 shows a typical external prestressing arrangement.

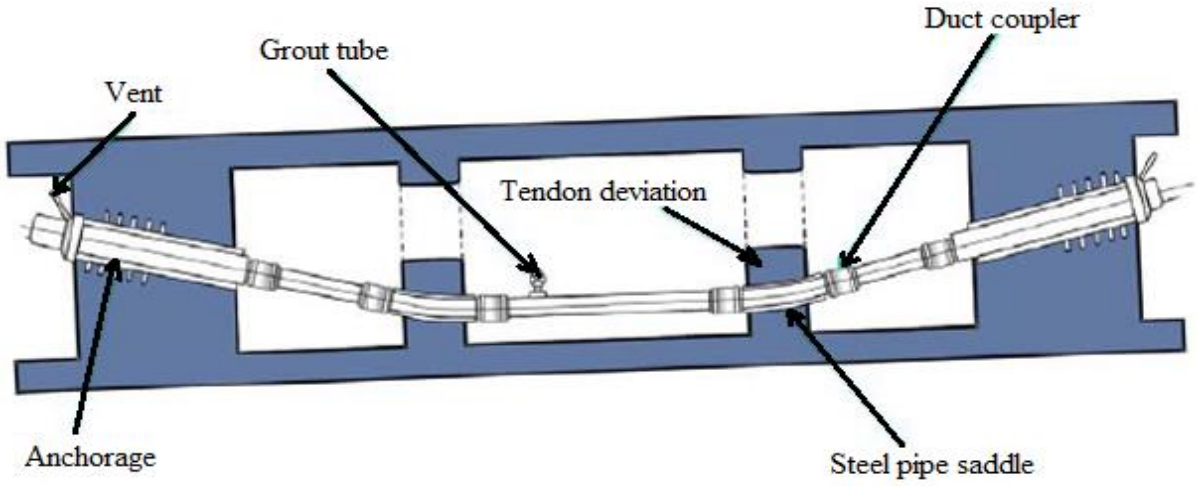

Figure 2.13. Typical post-tensioning strengthening method (Azizinamini & Gull, 2012).

Nevertheless, care must be taken with any prestressing system to ensure that the deviators and anchorage points are sound and that the additional prestressing forces can be adequately and safely transferred to the existing structure. Also, the deviators should be well shaped to host the curvature of the tendon sheathing. The entire prestressing system should be designed in such a way that once the deviators and anchorages are in position, it is relatively easy to install the tendons (Ryall, 2001). Post-tensioned-structures involve a timely and detailed monitoring of post-tensioning systems since damage to these systems is not obvious and can result in loss of integrity, expensive repairs/replacements and decrease in bridge safety (Azizinamini & Gull, 2012).

Post-tensioning system as a strengthening technique has many advantages including (i) easier and simpler inspections of external tendons profiles during and after installation; (ii) grouting is enhanced because of a better visual inspection of the operation and, consequently, a better protection of prestressing steel is achieved; (iii) it is also possible to monitor the tendons more easily during the lifespan of the structure; (iv) external tendons can be taken off and changed if the corrosion protection of the external tendons permits the release of the prestressing force and (v) friction losses are remarkably reduced because external tendons are tied to the structure solely at the deviation and anchorage zones (Picard, et al., 1995). Some disadvantages of this technique are listed: (i) external tendons are more easily reached than internal tendons and,

consequently, are more exposed to sabotage and fire damage; (ii) external tendons are prone to vibrations and, consequently, their free length should be restricted; (iii) anchorage zones and deviation are important and are challenging additions to the cross section; thus, these elements should be well designed and carefully detailed and adequately reinforced (Picard, et al., 1995). Figure 2.14 illustrates the post-tensioning strengthening technique placement.

Figure 2.14. Post-tensioning strengthening system placement (Alkhrdaji & Thomas, 2009).

In spite of all the advantages associated with new and old post-tensioned structures, there have been various concerns about the utilisation of external and internal post-tensioning tendons due to corrosion related issues (Azizinamini & Gull, 2012). Furthermore, there have been reports of corrosion issues in post-tensioned structures such as bridges after only five years of service life. Many of the problems related to post-tensioned systems can be assigned to grouting which is used for the corrosion protection of steel strands inside the duct (Azizinamini & Gull, 2012). Therefore, there is a need to use FRP tendons and do as many researches as possible for fully understand their behaviour as strengthening materials.

2.5.4. FRP strengthening systems

The FRP composites are now accepted by the construction industry all over the world as an application for rehabilitation and strengthening activities. They are generally reported as providing high performance, durable and reliable materials for strengthening of different structures including RC structures (Setunge, et al., 2002; Tang & Saadatmanesh, 2003; Esfahani, et al., 2007). FRP composites have been used as construction materials to strengthen various horizontally and vertically orientated structural RC members. Therefore, FRP composites is a cost-effective way of rehabilitating and upgrading existing RC structures such as columns, beams, slabs, and domes. Table 2.3 illustrates different FRP strengthening applications with an emphasis on externally bonded FRP methods.

Table 2.3. Applications of FRP strengthening of RC structures adopted from Setunge, et al., (2002).

Type	Applica-tion	Fibre direction	Schematic
Flexural	Tension and / or side face of beam	Along longitudinal axis of beam	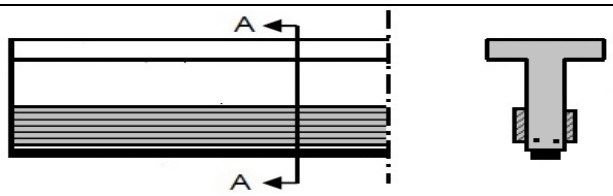
Shear	Side face of beam (U-Wrap or L-shape)	Perpendicular to longitudinal axis of beam	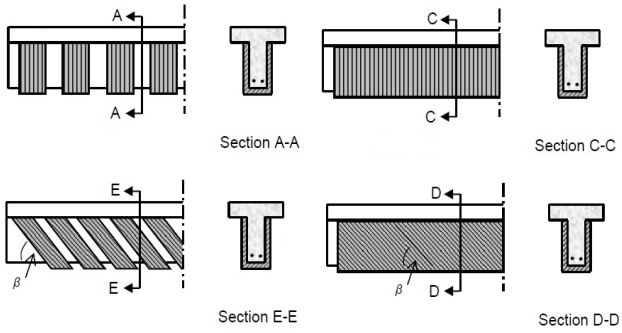
Confine-ment	Around column	Circumferential	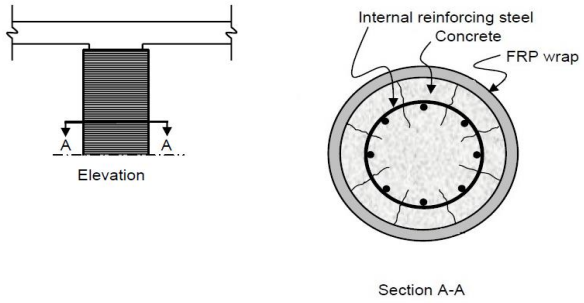

There are three main applications of FRP composites in strengthening of RC structures with deficiencies in structural capacity: flexural strengthening, shear strengthening and confining reinforcement. The FRP strengthening materials for RC structures can also be applied by internally and/or externally bonding them to the affected RC structure. An appropriate adhesive such as epoxy is used to effectively bond the FRP composites to concrete substrate. The used adhesive also serves as a shear load path between the concrete substrate layer and the FRP reinforcement material (Setunge, et al., 2002). Therefore, the bonding strength between FRP composite materials and concrete substrate plays an important role in the general performance of strengthened RC structures.

Shear and flexural strengthening of RC structures utilising FRP composites are two popular strengthening groups. External and internal application of FRP composites are two major methods among the popular groups of FRP strengthening of RC beams. Externally bonded (EB) FRP technique can be applied for both flexural and shear strengthening of RC beams. In addition, two emerging techniques namely embedded through-section (ETS) and NSMR are internally applied for shear strengthening of RC beams. Furthermore, NSMR technique can also be applied for flexural strengthening of RC structures. Various methods, externally and internally applied in FRP strengthening of RC beams for both flexural and shear strengthening are reviewed and presented. However, the emphasis is on flexural strengthening methods.

Externally bonded FRP systems

FRP composites materials may be glued to the tension side of RC beams, slabs and girders to supply additional flexural strength, and/or on the side faces of beams and girders to supply additional shear strength. FRP composites may also be used to envelop columns to improve the ductility due to confinement of the concrete (Rizkalla, et al., 2003). According to Rahimi & Hutchinson, (2001), the plate bonding technique is established as a simple and suitable repair/rehabilitation method for improving the flexural performance of concrete structures in general and, in particular, bridge decks including both beams and slabs. The advantages of this repair/rehabilitation technique are that the work can be executed while the structure is still in use (without interruption) and it is relatively low-cost in comparison to other methods (Rahimi & Hutchinson, 2001). The most important characteristic of EB FRP systems in strengthening/repair uses is the quick and easy installation (Rizkalla, et al., 2003).

According to ISIS, (2004), although various techniques can be utilised to apply external FRP reinforcement to RC structures, two similar installation techniques are most extensively used. The first technique is commonly termed as wet lay-up. In the wet lay-up technique, the fabrics of raw or pre-impregnated fibres or flexible sheets are saturated with epoxy adhesive resin before they are applied to the surface of the concrete member. As a result, the adhesive resin acts both as the FRP matrix and as the bonding material. The second installation technique consists of bonding of pre-cured rigid FRP strips/laminates or plates to the surface of the concrete member using an epoxy adhesive resin. While this last technique is closer to conventional rehabilitation/strengthening techniques which utilise steel plates material, it does not provide the flexibility gained from the wet lay-up method (Rizkalla, et al., 2003; ISIS,

2004). Despite all the advantages associated with externally bonded FRP reinforcements, the followings problems may be encountered which will adversely affect the mechanical properties of FRP: exposure to fire and a rise in temperature; sensitivity to damage from impact collision and moisture absorption; and susceptibility to damage from ultraviolet rays (ACI Committee, 1996). In some of the cases, poor protection may lead to a reduction in the lifespan of the FRP-strengthened structures (El-Hacha & Rizkalla, 2004). Some externally bonded FRP systems including special FRP strengthening systems are presented in the following section.

External bonded FRP strengthening systems based on FRP composites forms and sizes

FRP composites which will be used as strengthening materials are available in different forms and sizes (Figure 2.4). Sheet/fabrics system, laminate/strip system, bar system are among the FRP strengthening systems commonly used. Various FRP composite materials are externally bonded to RC structures in an urgent need to address deficiencies in flexural, shear or confinement capacity. Laminate system and sheet systems are the most popular externally bonded FRP strengthening systems, and are named after their forms. However, some other strengthening systems such as bar systems, are fully or partial applied internally. These bar systems are named after the FRP bars.

CFRP laminate systems were first used as strengthening materials on a concrete bridge in in Switzerland. This bridge required strengthening after an accident damaged the prestressing cables (Meier, 1995; Täljsten, 2006). Laminates and/or strips are most suitable for strengthening an application for flat surfaces such as slabs, beams and walls (Täljsten, 2006). The build-up of a laminate strengthening system is made by gluing of the FRP laminates/strips: the adhesive resin is applied as a relatively thin layer on the concrete and as a roof-shaped layer on the FRP (Matthys, 2000). The laminate strengthening process takes less time than the sheet strengthening process (Täljsten, 2006).

Sheet systems are more sensitive to the irregularities in the concrete surface and often require more pre-treatment (Täljsten, 2006). The application of sheets and fabrics onto the prepared concrete is performed by means of hand lay-up (Matthys, 2000). Sheet systems are more flexible and can be easily adapted to most surfaces, including the strengthening of curved surfaces and surfaces with openings. These types of strengthening systems have also found their application in seismic retrofitting (Täljsten, 2006). Some protective measures are often added to the sheet system such as post-treatment by painting, plaster or a thin layer of polymer

concrete (Täljsten, 2006). Figure 2.15 shows examples of the sheet and laminate strengthening systems.

Figure 2.15. (a) Hand lay-up of CFRP sheets or fabrics, (b) Application of prefabricated FRP strips (FIB, 2001).

Special strengthening systems

Automated wrapping and curing

Wrapping of structural elements such as columns (or other upright elements including chimneys) with flexible FRP fabrics or sheets is made possible nowadays by using automated machinery. The machine can also pertain heat and vacuum to facilitate the curing process (Bakis, et al., 2002). With this kind of system, a tow or tape is automatically wrapped around columns (Täljsten, 2006). There are two methods of automated wrapping, wet wrapping or dry wrapping. In the case of wet wrapping, the tow is drawn trough a resin bath and automatically wound around the column. The ambient temperature is enough to harden the wet wrapping (Täljsten, 2006). In the case of dry wrapping, pre-impregnated tow is wound around the column or structure to be strengthened. The finishing work on the wrap is performed by using heat. In some of the cases, the used heat is applied from the external source of heat, and in other cases infrared heaters are used (Täljsten, 2006). Figure 2.16 shows a typical automated wrapping system.

Figure 2.16. Automated wrapping strengthening system (FIB, 2001).

The automated wrapping system is most suitable when the strengthening works are performed on many columns of approximately the same size. Otherwise, when only a few columns have to be strengthened, traditional hand lay-up systems are more economical (Täljsten, 2006).

Prestressed FRP strengthening systems

Various researches and studies on prestressing systems for external reinforcement in form of FRP laminates and FRP rods are very appealing. The pressing need to optimise the efficient use of FRP materials has led to the development of these prestressing systems. According to El-Hacha, et al., (2001), when non-prestressed FRP laminates are adequately glued to the tensile face of a flexural element, they simultaneously lead to an increase of the ultimate loads and a decrease of the deflections. In addition, these FRP laminates can only sustain additional live loads that are exerted on a structure, and they are not able to bear a dead load. However prestressed FRP laminates can support both the additional live load and a portion of the dead load that is borne by the structure to be rehabilitated/strengthened. The use of prestressed FRP laminates enhances the serviceability and load-carrying capacity of concrete beams and slabs. Also the flexural members, such as beams strengthened with non-prestressed FRP laminates, are weak and the yielding load is remarkable, compared to members strengthened with prestressed FRP laminates (Figure 2.17). In many cases, the prestressing leads to a shift of the mode of failure of the structures under consideration, from a peeling failure of the concrete cover to a tensile rupture of FRP strip/laminate (El-Hacha, et al., 2001).

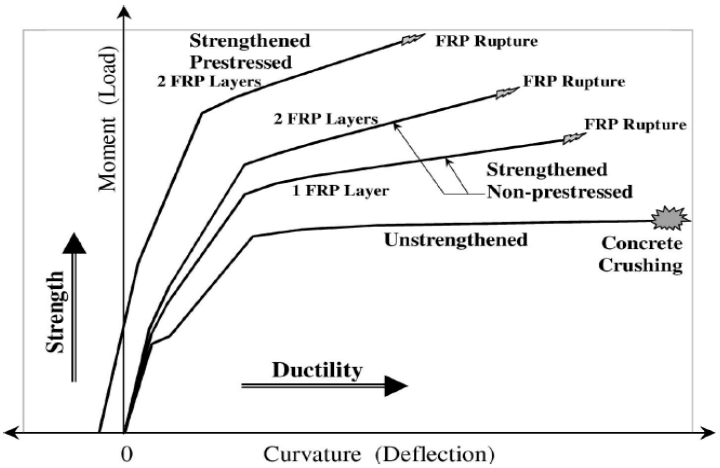

Figure 2.17. Typical load-deflection curves for beam strengthened with non-prestressed and prestressed FRP laminates (El-Hacha, et al., 2001).

According to fib, (2001); Täljsten, (2006), the use of prestressed laminates as strengthening materials exhibit the following advantages and disadvantages:

(1). The same strengthening results are obtained from small areas of stressed laminates/strips in comparison to non-stressed laminates/strips;

(2). Prestressed laminates provide stiffer characteristics. At early stages of this strengthening process, most of the concrete is in compression and, consequently, contribute to the moment of resistance;

(3). The use of prestressed FRP laminates is more costly than non-prestressed FRP laminates due to a large number of operations required and additional equipment needed;

(4). The operation takes a lot of time. The equipment used to push the laminate/strip up to the soffit of the concrete beam must remain in position until the adhesive has hardened sufficiently.

Internally applications of FRP systems

The FRP composites may be used to strengthen RC beams that are exposed to possible impact; thus they should be carefully protected to prevent impact damaged (Täljsten, 2006). Also, in some cases, the concrete surface of the RC beams to be strengthened is very uneven. FRP strengthening materials may also be exposed to vandalism. For these reasons, it is necessary to rehabilitate and strengthen those RC beams by the internal application of FRP composites. Slots are introduced into the RC beams to be strengthened, and FRP rods with circular or square shapes are being bonded into those slots with appropriate adhesives such as epoxies. As previously mentioned, the internal application of FRP strengthening of RC beams can be applied to both shear and flexural strengthening systems.

Near Surface Mounted Reinforcement methods

The NSMR technique consists of correctly placing the FRP reinforcing bars, strips or rods into well prepared grooves that are pre-cut into the concrete cover, with sufficient depth in the negative moment regions of decks and slabs or in the tension region of a beam (Rizkalla, et al., 2003; El-Hacha & Rizkalla, 2004). In these strengthening systems the FRP reinforcing bars, rods or strips are glued to the three sides of the readied groove using a cementitious grout material or high-strength epoxy adhesive. Also, the same adhesive has to cover the open side

of the groove. Some stresses including tensile stresses will develop around a NSM FRP bar; however increasing the epoxy cover leads to a significant reduction of such stress (Rizkalla, et al., 2003). Figures 2.18 (a) and 2.18 (b) show the typical strengthening application procedures with NSM FRP bars and tensile stress distribution around a given NSM FRP bar respectively.

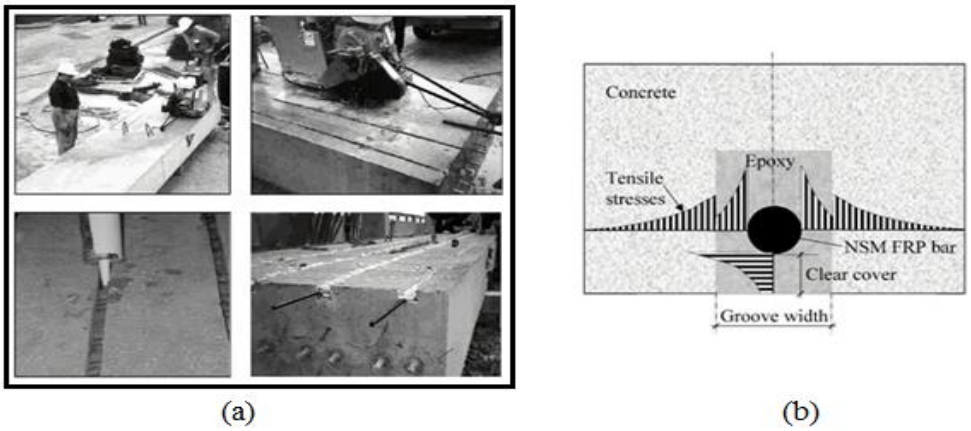

Figure 2.18. Strengthening application procedures with NSM FRP bars and tensile stress distribution around a given NSM FRP bar (Rizkalla, et al., 2003).

However, it is very important to carefully assess the concrete cover before deciding on this strengthening method. A concrete cover depth of at least 25 mm is needed (Täljsten, 2006). In addition, an acceptable distance between the existing reinforcement steel bars and the NSM FRP bars should be available to facilitate the pre-treatment process. The pre-treatment process includes preparation of grooves and placement of high-strength adhesives such as epoxies. The use of rectangular NSM CFRP rods with epoxy adhesive and cement grout as bonding agent increases the ultimate load-carrying capacity of strengthened beams by 77% and 58% respectively (Täljsten & Anders, 2001; El-Hacha, et al., 2001).

In comparison to EBR systems, NSMR technique has the following advantages (Szabó & Balázs, 2007, De Lorenzis & Teng, 2007):

(i). The required installation time is significantly reduced, as no surface preparation other than the prescribed grooving is needed;

(ii). The huge bonding surface induces better anchorage ability and prevents debonding failures;

(iii). Installed into grooves, NSM bars are well protected and so less exposed to fire, wear, vandalism, impact and mechanical damage.

Embedded Through-Section methods

FRP composite materials are commonly used to increase the structural performance shear resistance of RC beams. EBR FRP with FRP sheets/fabrics is the most popular method of significantly enhancing the shear capacity of RC beams when so required. The NSM FRP method is also applied to strengthen RC beams with a deficiency in shear capacity but, despite their successful application in strengthening and rehabilitation of RC beams, considerable drawbacks have been experienced. These include the high possibility of debonding failure, the necessity of surface preparation, the uncertain FRP/concrete bond and interface characteristics, and the protection against sabotage/vandalism, fire and temperature rise (Chaallal, et al., 2011). All aforementioned and other shortcomings encountered during shear strengthening of RC structures have led to the proposal of other viable solutions. The embedded through-section (ETS) method is one of those techniques.

The ETS technique is a relatively new method which uses FRP rods to overcome the shear capacity deficiencies. Vertical and/or inclined holes are made across the depth of the beam's cross-section; here FRP bars or rods are introduced and adequately bonded to the concrete substrate with appropriate adhesive materials (Chaallal, et al., 2011; Barros & Dalfré, 2013). The FRP rods used in ETS method rely on the strength of the RC beam's concrete core; however in EBR and NMSR systems, the FRP materials rely on the concrete cover of the RC beam (Chaallal, et al., 2011). In the ETS techinique, the improvement of both load and deflection capacities experince a better performance when inclined ETS strengthening is used rather than vertical ETS strengthening bars. Therefore, the use of inclined ETS bars is more effective than the use of vertical ETS bars (Barros & Dalfré, 2013). Figure 2.19 shows a typical ETS method.

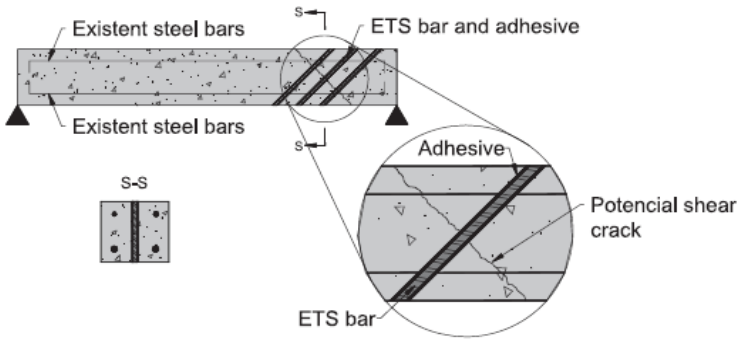

Figure 2.19. ETS strengthening technique concept for shear strengthening of RC beams (Barros & Dalfré, 2013).

According to Chaallal, et al., (2011), ETS strengthening methods can significantly improve the shear capacity of RC beams to be strengthened/rehabilitated, even in the presence of a restrained amount of transverse steel reinforcing material. An increase of shear capacity up to 60% for RC beams has been achieved using ETS FRP rods.

ETS vs other FRP strengthening techniques presented the following advantages (Chaallal, et al., 2011):

(1). The application of the ETS strengthening method requires less time;

(2). It requires less adhesive material, and needs neither surface preparation nor trained labourers for the installation;

(3). It is generally a cost-effective shear strengthening technique.

2.6. The effects of loading conditions on RC structures behaviour

RC structures and members are designed and built to serve safely during their predicted design life. Therefore, RC structures should be able to resist all types of design loading that they are likely encounter during their service life (Figure 2.20). In many previous research works and studies done, two popular categories of loading conditions applied on RC structures are quasi-static loading and dynamic loading (Wakabayashi, et al., 1980; Bischoff & Perry, 1991). On the one hand, the quasi-static loading is characterised by a relatively long duration of application on the structure under study in a progressive manner up to failure. On the other hand, the impact loading is an extremely severe loading condition, characterised by its application of a force of great intensity in a short duration (Tang & Saadatmanesh, 2003; Fujikake, et al., 2009).

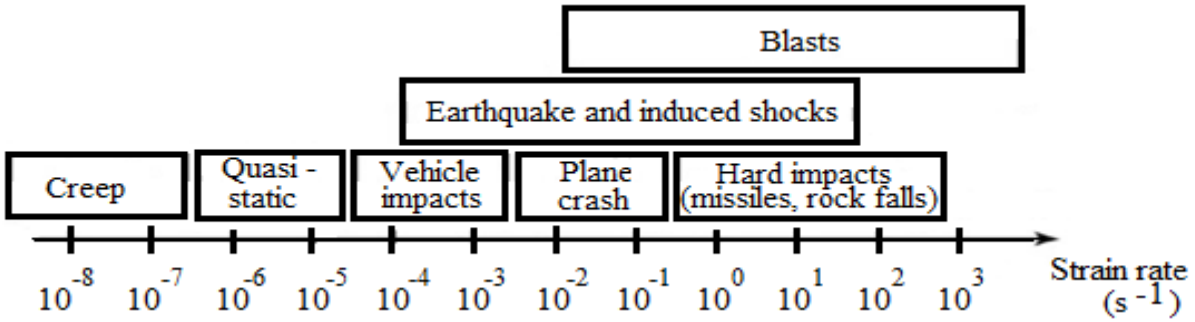

Figure 2.20. Various strain rate magnitude of different loading conditions associated with numerous loading events (Riisgaard, et al., 2007; Pająk, 2011).

RC structures under loading deform; and strain rate describes the rate of deformation of material subjected to dynamic loadings, including impact loading with respect to time. Strain rate is expressed in units of strain per second (s^{-1}). RC is a composite material in which reinforcing steel bars are embedded in a concrete matrix in such manner that the newly formed material acts to withstand the applied loads. The properties of the individual materials used in RC composite structures are practically all strain-rate dependent (Bischoff & Perry, 1991).

Different techniques are used to experimentally investigate the behaviour of RC structures subjected to different loading rates in combination with different loading conditions. Hence, the various strain regimes and the associated techniques developed to obtain them are shown in Figure 2.21. Among various experimental studies carried out under high loading rates including impact and dynamic loadings, this present research focuses on impact loading using a drop weight impact test apparatus.

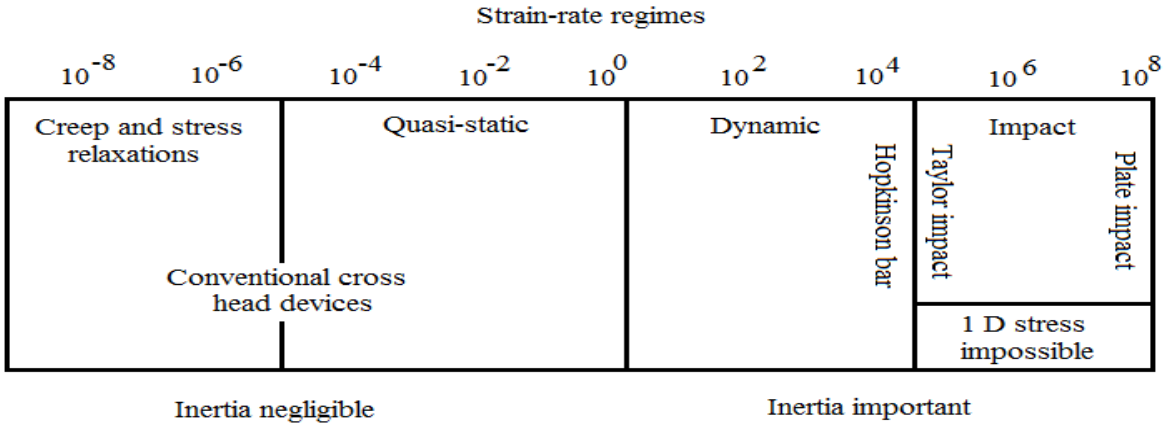

Figure 2.21. Schematic diagram of strain rate regimes (in reciprocal seconds) and the techniques that have been developed for obtaining them (Field, et al., 2004).

2.6.1. RC structures subjected to high loading rate

According to Chen & May (2009), for RC structures and members under high loading rates including dynamic and impact loadings, both steel and concrete are stress/strain rate sensitive. Therefore, an increase in the stress/strain rates can lead to an increase of both the compressive and tensile strengths and modulus of elasticity (Chen & May, 2009; Cusatis, 2011).

For many years, RC has been widely utilised by civil and military engineers in the design and construction of protective structures, in order to withstand severe extremely loading conditions such as explosive and impact loads (Li, et al., 2005). When RC structures are subjected to high

loading rates conditions such as impact loading, the impacted structure may respond in several ways, depending on the nature of the impact:

(1). It may experience local damage only, dissipating the majority of the impact energy at or around the impact zone;
(2). It may respond to the impact globally through the bending and deformation of the entire reinforced concrete member;
(3). It may respond in such way that it experiences a combination of both local and global damage (Saatci, 2007; Sangi, 2011).

The local responses produce local modes of failure which are directly observed in the vicinity of loading point after impact event, while global responses, including free vibration effect due to elastic-plastic deformation that occurs after impact event, produce global modes of failure which are experienced in the entire structural member over a long period (Fujikake, et al., 2009). Due to the complexity of impact phenomena, most of the researchers, scholars and engineers concentrated their efforts on developing empirical impact-resistant design methods and little effort was spent in understanding the shear and cracking mechanisms involved (Saatci & Vecchio, 2009).

Almost all the empirical formulae developed in this field of impact loading are based on experimental data and limited to those available data from which they were acquired; they are often elaborated by curve-fitting test data and are also unit-dependent; they are largely concerned with the effects of local modes of failure (Saatci & Vecchio, 2009; Sangi, 2011). The local and global modes of failure of RC structures subjected to impact loading are shown in Figure 2.22 (on the next page), according to Kennedy (1976) and later reviewed by Li et al., (2005). In the same Figure 2.22, local modes of failure are: penetration, cone cracking, spalling, scabbing and perforation; while global modes of failure are: cracking on (i) proximal and (ii) distal faces of the impactor, and overall target response.

The classification of impact phenomena may be based on (i) relative stiffness between the striking object (impactor) and the struck body, and (ii) velocity of the striking object. If the velocity of a striking body is less than or equal to $10m/s$, it is classified as low-velocity impact, otherwise, it is classified as high-velocity impact (Muda, et al., 2013). In addition, high-velocity impact response is normally dominated by stress wave propagation across the material, in which the structure under study does not have enough time to respond, leading to localised damage (Richardson & Wisheart, 1996). On the contrary, in low-velocity impact, the dynamic

structural response of the target (RC beam) is of paramount importance as the contact duration is long enough for the entire structure to respond to the exciting force due to the impact, and consequently more energy is absorbed elastically (Richardson & Wisheart, 1996). Therefore, RC structures generally experience: local modes of failure under high-velocity impact and global modes of failure under low-velocity impact. Figure 23 shows the modes of failure and dynamic response of a RC element (beam) subjected to impact loading. This present research, to investigate the behaviour of FRP strengthened RC beams with concrete patch repairs, will be done under relatively low-velocity impact loading with high loading rate.

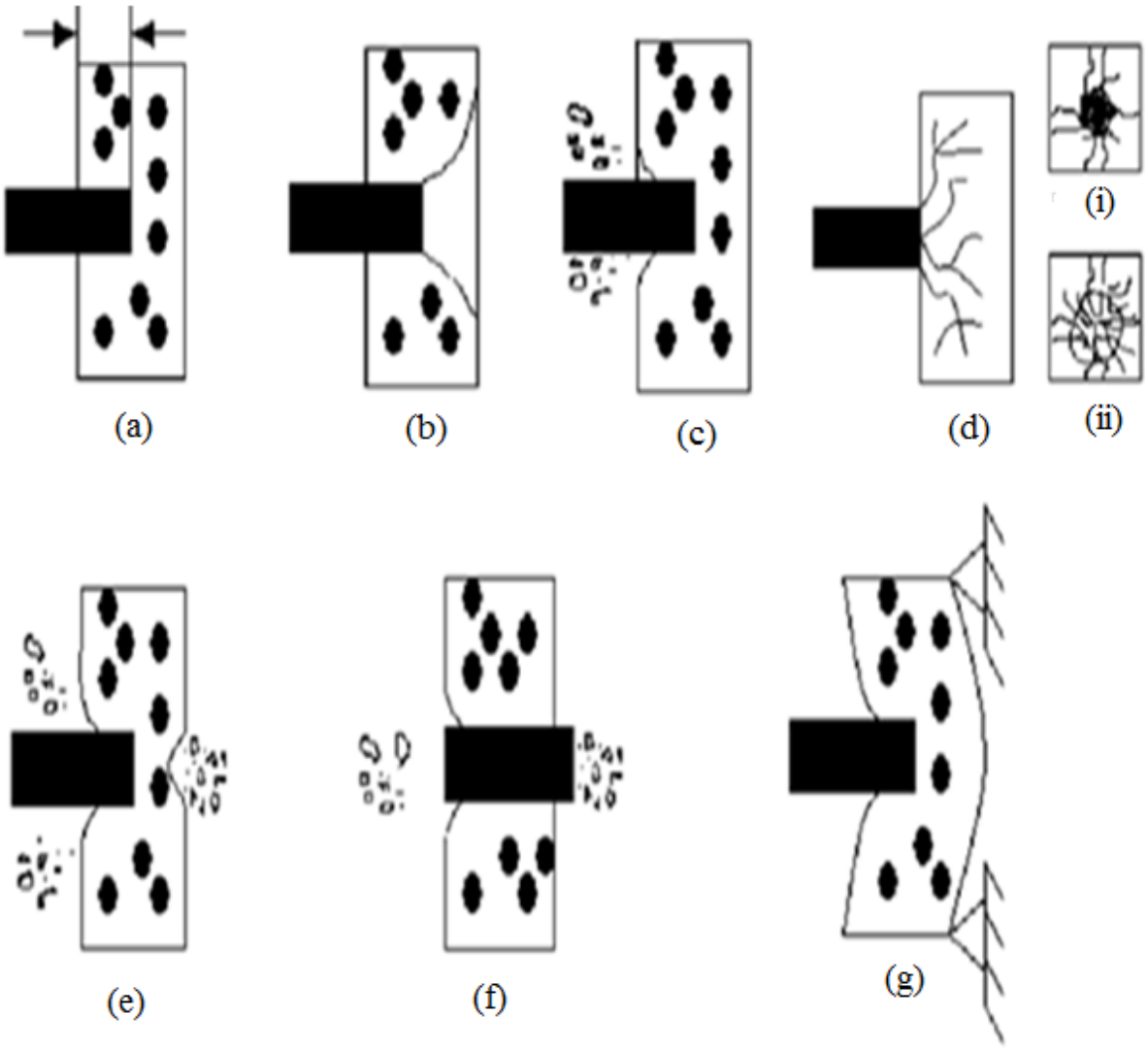

Figure 2.22. Missile impact effects on concrete target; (a) Penetration, (b) Cone Cracking, (c) Spalling, (d) Cracks on (i) Proximal face and (ii) Distal face, (e) Scabbing, (f) Perforation, and (g) Overall target response (Li, et al., 2005).

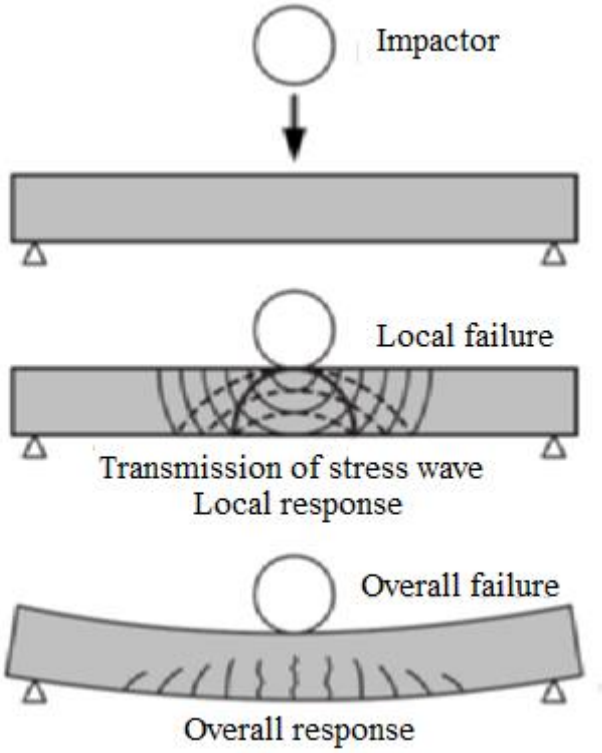

Figure 2.23. Modes of failure and dynamic response of a RC member (beam) subjected to impact loading (Fujikake, et al., 2009).

The term dynamic increase factor (DIF) is used to describe the relative strength enhancement (Riisgaard, et al., 2007). DIF is defined as the ratio of dynamic to static strength (Malvar & Crawford, 1998; Pająk, 2011). Increases in strength are observed to depend primarily on the loading rate, following either a log-log or linear-logarithmic relationship (Bischoff & Perry, 1991). In addition, the cracking stiffness, ultimate load resistance, and energy absorption of RC beams increases with increasing loading rates (Adhikary, et al., 2012). For concrete and concrete-like materials under dynamic loads such as impact loading, both strain rate and inertia forces effects should be carefully considered to have reasonable results (Cusatis, 2011). While under quasi-static loading, the aforementioned effects are negligible. Figure 2.24 shows the calculated DIF experimental results, with and without taking inertia effects into consideration (Cusatis, 2011). The comparison between those two entities is made both in tension and in compression on the basis of various experimental tests by researchers and engineers worldwide. The tensile DIF, computed without considering the inertia effect, experiences values comparable to the compressive (from 1 to 4). The DIF, calculated by taking into account the inertia effects and having an agreement with the experimental ones, vary from 1 to 1.6 for compression, and from 1 to 5 for tension, (Figure 2.24).

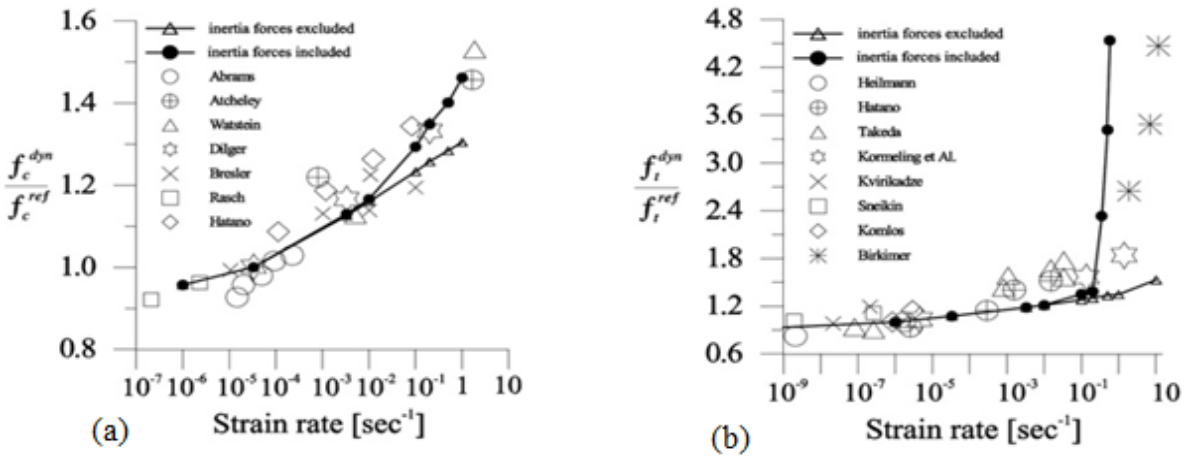

Figure 2.24. Comparison between the calculated DIF with and without inertia effects and experimental data gathered from literature: (a) compressive DIF; (b) tensile DIF (Cusatis, 2011).

According to Fu, et al., (1991), the maximum strains obtained in beams under dynamic loads are considerably higher than those obtained in beams under quasi-static loads of equal magnitude. They also added that the increase in strength of concrete subjected to dynamic conditions is less predictable than that for steel. Furthermore, Wakabayashi, et al., (1980), in their study noticed that the load-carrying capacity of the tested RC beam increased with increasing strain curve or curvature rate. The found increase was about 30% for a RC beam under the fastest rate of loading, in comparison to that under the slowest rate of loading. Thus, the effects of loading rates and associated DIF are also reviewed on individual materials that composed the R C composite material.

Behaviour of reinforcing steel under high loading rates

It has been reported by a many researchers and engineers that the overall behaviour (including the individual behaviour of constituent materials of RC beams) is affected by the loading rate associated with a particular loading type. The effect of strain rate on the concrete compressive and tensile strengths is normally reported as a DIF, that is, the ratio of the dynamic to static yield (or ultimate) stress (Malvar & Crawford, 1998). The yield strength of steel material increases with increasing strain rate, and that same approach of higher strength gain for lower strength materials under dynamic loading conditions seems to be applicable for both steel and concrete (Fu, et al., 1991). It should also be noted that most of the available data concerning the yield stress DIF refers to the upper yield stress (Malvar & Crawford, 1998).

Wakabayashi, et al., (1980), conducted an experimental study on rounded and deformed steel bars of 13 mm diameters. The following observations have been made; (1) evaluated stress-strain curves exhibit increases for both the lower and upper yield stresses with increasing strain rate, and (2) the average increase in lower yield strength was $7-8\%$ and $16-18\%$ respectively at a strain rate of $0.005s^{-1}$ and at $0.1s^{-1}$ for both types of steel reinforcing bars. Similar increases in upper yield strength evaluation were also found (Wakabayashi, et al., 1980). Under dynamic loading conditions, the mechanical properties of the steel reinforcing bars such as strength are known to increase by up to 60% resulting from strain rates of up to $10\ s^{-1}$ (Malvar, 1998). Besides this, beams under dynamic loading conditions had a 10% increase in stiffness before the first yield (Fu, et al., 1991). It was also found that for both yield and ultimate stress, the DIF is inversely in relation to the yield stress itself (Malvar, 1998).

The following DIF formulation was adopted for both yield and ultimate stress by (Malvar & Crawford, 1998):

$$DIF = \left(\frac{\dot{\varepsilon}}{10^{-4}}\right)^{\alpha} \qquad (2.1)$$

where for the yield stress, $\alpha = \alpha_{fy}$ was found to be:

$$\alpha_{fy} = 0.074 - 0.040\frac{fy}{60} \qquad (2.2)$$

and for the ultimate stress, $\alpha = \alpha_{fu}$ was found to be:

$$\alpha_{fy} = 0.019 - 0.009\frac{fy}{60} \qquad (2.3)$$

Where $\dot{\varepsilon}$ is the strain rate equation in s^{-1}; fy is the bar yield strength in ksi (if fy is in MPa, the $60\ ksi$ denominator should be replaced by $414 MPa$).

It should be also noted that in both cases α is a function of fy. In addition, the formulation above is valid for bars with yield stress between 42 and $103 ksi$ (290 and $710 MPa$) and for strain rates ranging between 10^{-4} and $10\ s^{-1}$ (Malvar, 1998).

Figure 2.25 was obtained from different experimental works by taking into consideration the DIF and its effects on the general behaviour of RC structures especially the steel bar reinforcement.

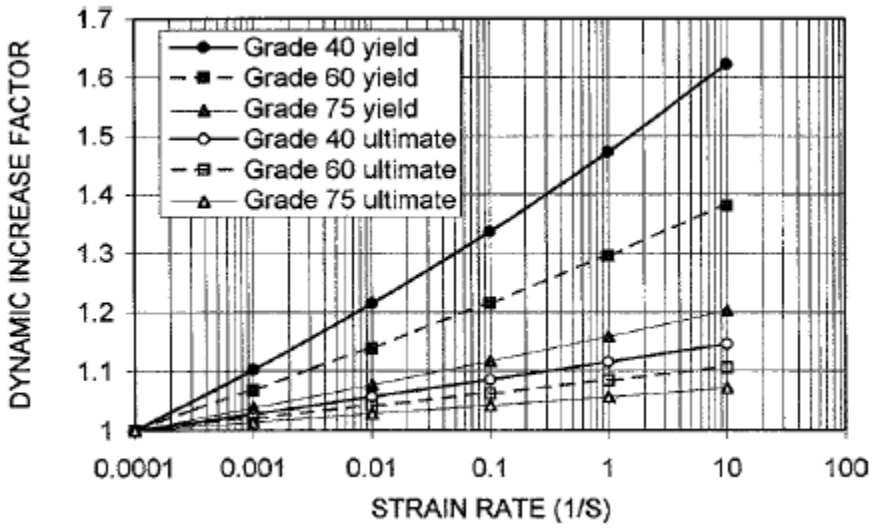

Figure 2.25. Proposed DIF for ASTM A 615 Grade 40, 60, and 75 steel reinforcing bars (assuming yield stress of 48, 69, and 87 ksi, respectively) (Malvar & Crawford, 1998).

Behaviour of concrete under high loading rates

The concrete material has a largely heterogeneous internal structure on both microscopic and macroscopic scales. This heterogeneity, in comparison with steel and aluminium materials, leads to many differences in its manner of deformation (Mainstone, 1975). Experimental works under high loading rates have been conducted on concrete, both in compression and in tension (Pająk, 2011). However, the fact that it is frequently difficult to carry out direct tensile tests on concrete specimens and that the tensile strength of concrete material has constantly been expressed as a function of its compressive strength, also significantly contributes to the scarcity of tensile test data (Fu, et al., 1991).

Compressive strength is more sensitive to changes in strain rate, and the greater the strength of the concrete, the less sensitive the concrete material is to strain rate (Fu, et al., 1991). Although there are many factors which may affect the increase in compressive strength of concrete material as the loading rate is increased, only the concrete quality (or static compressive strength) appears to have a significant effect (Bischoff & Perry, 1991). The quantity of strength increase is typically the greatest for concrete subjected to tension, and smallest for concrete subjected to compression (Takeda & Tachikawa, 1971). According to Suaris & Shah, (1983), the relative flexural strength increase with increasing strain rate is inversely proportional to the static strength, and the tensile strength of concrete is more sensitive to strain-rate than to its compressive strength.

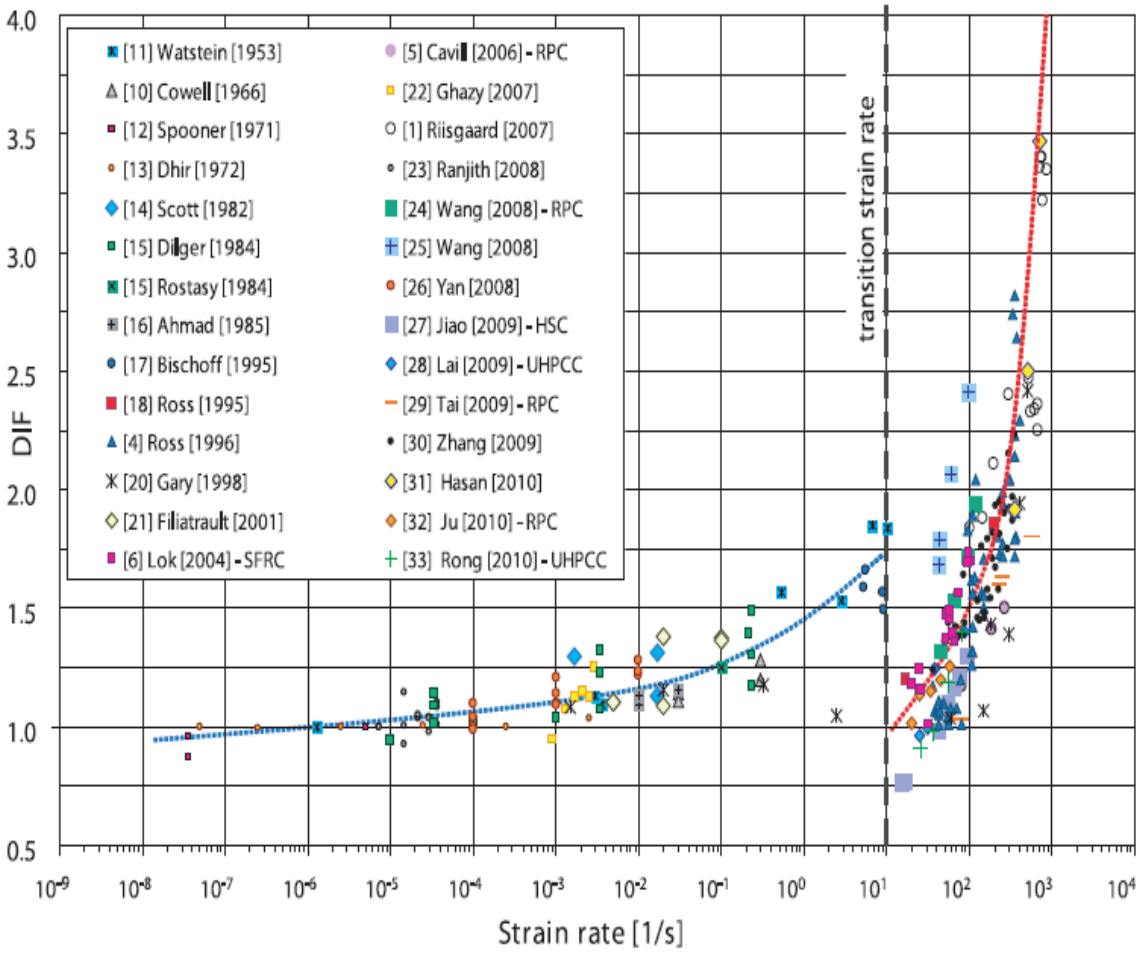

Figure 2.26. Strain rate effect taking into account DIF related to the compressive strength of concrete (Pająk, 2011).

Drop weights have been commonly used to achieve impact strain rates throughout the concrete material, in the order of $10\ s^{-1}$, equivalent to a $250-\mu S$ loading duration. During impact loading (at about $10s^{-1}$) the compressive strength of concrete can be as much as 80% to 100% greater than the static strength; however, there is a large variation in the test results which becomes greater as strain rate increases (Bischoff & Perry, 1991). According to Pająk, (2011), the results presented in Figures 2.26 and 2.27 respectively show an increase in concrete strength both in compression and tension along with the increasing strain rate. The results of concrete in compression in all ranges of strain rates indicate that it should be investigated in two domains of strain rates (Figure 2.26). The strain rate where the DIF values changes drastically is called the transition strain rate (Pająk, 2011). In the left side of the transition strain rate, the DIF achieves the value about 1.8; while on the right side of the transition strain rate, the DIF reaches a value of 3.5. Besides this, different investigators have found and set various boundaries of the transition strain rate of concrete in compression.

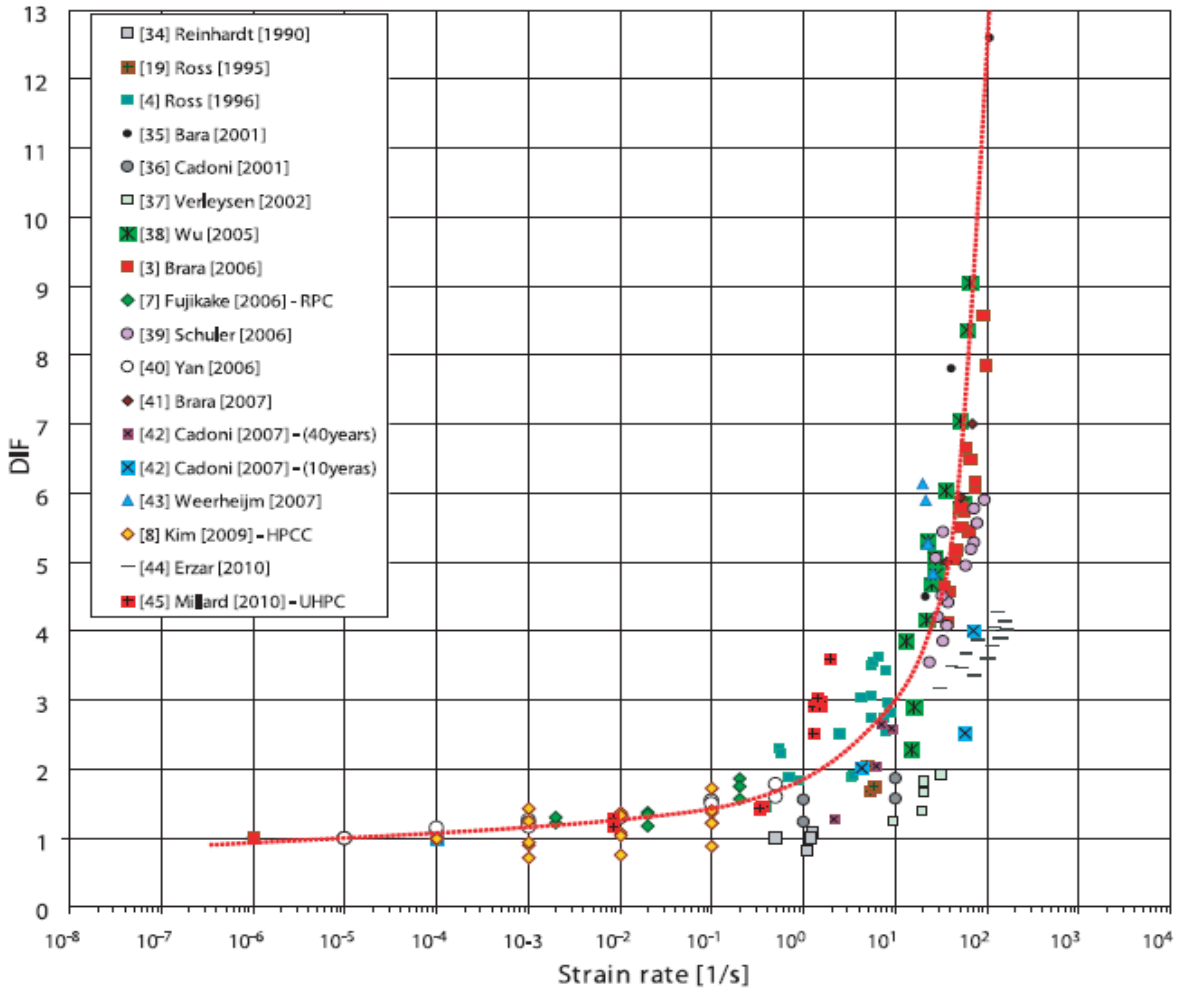

Figure 2.27. Strain rate effect taking into account DIF related to the tensile strength of concrete (Pająk, 2011).

While most of the investigators have also found and set boundaries of the transition strain rate of concrete in tension, some of the investigators noticed a more uniform set of results on concrete in tension than in compression. The dynamic strength of concrete can typically reach a value of 13 times the quasi-static strength (Pająk, 2011). In addition, a shift in the results that might lead to the creation of the transition strain-rate should be observed, depending on the type of the instrument used in testing, hence, some instruments generated results that are less scattered than the others. According to Malvar & Crawford, (1998), for concrete, the DIF can exceed 2 in compression, and exceed 6 in tension. Therefore, the effect of dynamic (impact) loading on the properties of concrete has been shown, and an increase in both compressive and tensile strength has been experienced in every case. Nevertheless, the results might be different depending on the instrument used to dynamically and/or statically perform the test; however, the concrete was always more strain-rate sensitive in tension than in compression.

The comparison between the results of the DIF factors on concrete in compression and tension is shown in Figure 2.28. Finally, some of the DIF formulations for concrete in compression that are accepted by most researchers for their accurate representation of the actual behaviour of concrete are presented. Besides this, DIF formulation in tension is also presented. The data supports the DIF as being a bilinear function of the strain rate (in a log-log plot), with no increases for strain rates below $10^{-6}\,s^{-1}$ and with a slope change at a strain rate of $1s^{-1}$ (Malvar & Crawford, 1998).

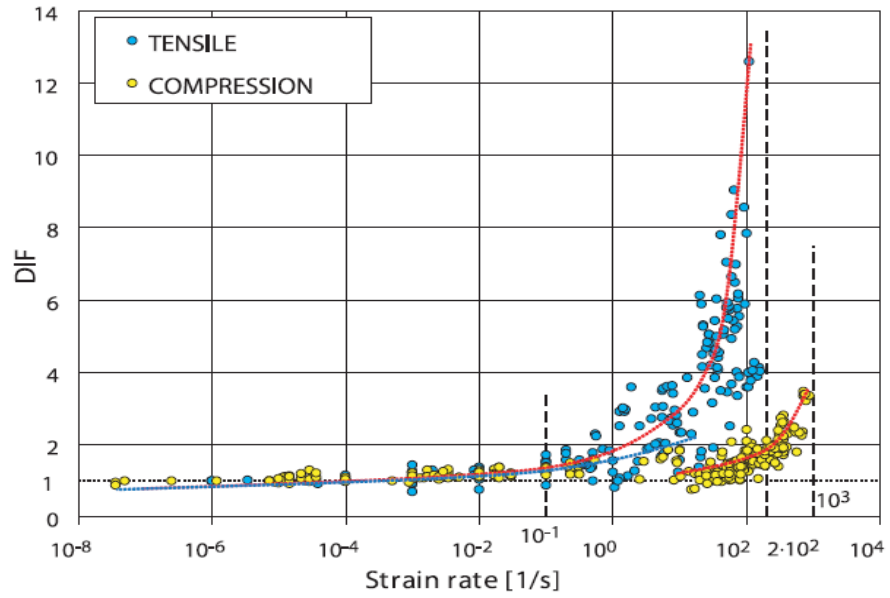

Figure 2.28. Comparison of strain rate effects on tensile and compressive strength of concrete (Pająk, 2011).

The CEB model code 1990 of the dynamic increase factor (DIF) for the compressive strength is given by:

$$f_c/f_{cs} = \left(\frac{\dot{\varepsilon}}{\dot{\varepsilon}_S}\right)^{1.026\alpha_S} \quad \text{for} \quad \dot{\varepsilon} \le 30s^{-1} \qquad (2.4)$$

$$= \gamma_S \left(\frac{\dot{\varepsilon}}{\varepsilon_S}\right)^{1/3} \quad \text{for} \quad \dot{\varepsilon} > 30s^{-1} \qquad (2.5)$$

Where f_c = dynamic compressive strength at $\dot{\varepsilon}$; f_{cs} = static compressive strength at $\dot{\varepsilon}_S$; f_c/f_{cs} = compressive strength dynamic increase factor (DIF); $\dot{\varepsilon}$ = strain rate in the range of $30x10^{-6}$ to $300s^{-1}$; $\dot{\varepsilon}_S = 30x10^{-6}\ s^{-1}$ (static strain rate); $\log\gamma_s = 6.156\alpha_s - 2$; $\alpha_s = 1/(5+9\,f_c/f_{co})$; and $f_{co} = 10MPa = 1540psi$.

Malvar & Crawford, (1998), proposed formulation dynamic increase factor (DIF) for the tensile strength given by:

$$f_t / f_{ts} = \left(\frac{\dot{\varepsilon}}{\dot{\varepsilon}_S} \right)^{\delta} \quad \text{for} \quad \dot{\varepsilon} \leq 1s^{-1} \quad \ldots\ldots (2.6)$$

$$= \beta \left(\frac{\dot{\varepsilon}}{\varepsilon_S} \right)^{1/3} \quad \text{for} \quad \dot{\varepsilon} > 1s^{-1} \quad \ldots\ldots (2.7)$$

Where $f_t =$ dynamic tensile strength at $\dot{\varepsilon}$; $f_{ts} =$ static tensile strength at $\dot{\varepsilon}_S$; $f_t / f_{ts} =$ tensile strength dynamic increase factor (DIF); $\dot{\varepsilon} =$ strain rate in the range of 10^{-6} to $160s^{-1}$; $\dot{\varepsilon}_S = 10^{-6} s^{-1}$ (static strain rate); $\log \beta = 6\alpha - 2$; $\delta = 1/(1 + 8\, f_c / f_{co})$; $f_{co} = 10 MPa = 1540 psi$.

The proposed formulation DIF for the tensile strength in concrete was obtained on the basis of the CEB model code 1990. This proposed formulation was fitted the available data for strain rates below $1s^{-1}$, and for higher strain rates a slope of $1/3$ on a log (strain rate) versus log (DIF) plot was utilised following the CEB formulation (Malvar & Crawford, 1998).

2.6.2. Dynamic behaviour of RC structures under impact loading

Impact loading by its nature has dynamic characteristics, and the effects of inertia forces on the RC structures undergoing impact loading test should be given due consideration. The parameters of dynamic load tests which could affect the experimental findings include the specimen geometry, inertia effects, uniformity of stress and strain along the specimen length (Bischoff & Perry, 1991). If a load is applied dynamically, the resulting displacements of the beam depend on not only upon this load but also upon inertia forces which oppose the accelerations producing them (Clough & Penzien, 2003).

While testing RC beams under impact loading, the system can be considered as a two-degrees-of-freedom model. According to Fujikake, et al., (2009), this model can represent not only the of overall response of the tested RC beam, but also the local response recorded at the contact point between the drop hammer and the RC beam under study with the least degree-of-freedom. Figure 2.29 illustrates the impact testing system with two-degrees-of-freedom. The said model successfully represented the impact loading test of RC beams by taking into consideration local and global failures.

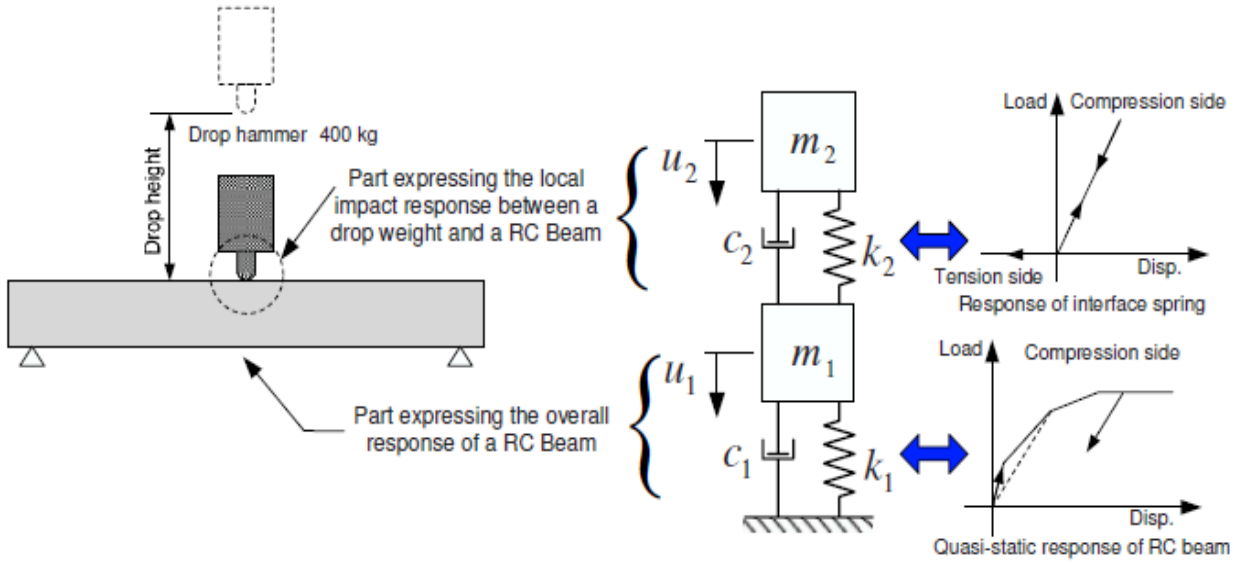

Figure 2.29. Two-degrees-of-freedom mass-spring-damper system model (Fujikake, et al., 2009).

In order to analyse the results of an impact test, one must be able to separate the inertial loading effect from the total load measured by the instrument tup (Bentur, et al., 1986). In addition, one of the most challenging tasks for the impact research is to find the exact bending load (Soleimani, et al., 2007). According to Bentur, et al. (1986), in many instances, only a portion of the total load is effectively involved in bending the beam itself. Thus, the breakdown of forces involved in impact loading is of high interest for the understanding and future analysis of RC structures subjected to impact loading.

In the case of RC beams, the displacements of the specimen inside the supports (clear span) are assumed to be sinusoidal, while the displacements of the specimen are assumed to be linear in the overhanging parts of the beam (Figure 2.30).

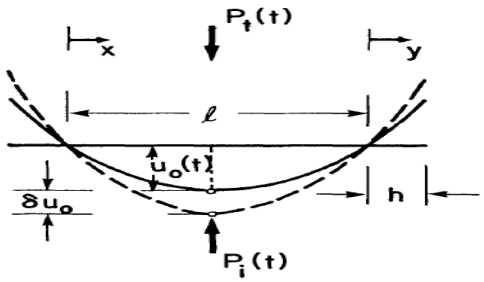

Figure 2.30. Sinusoidal distribution of displacements of a beam subjected to impact loading (Bentur, et al., 1986).

A method developed based on Figure 2.30 above and used by Bentur, et al. (1986), and emphasised by Soleimani, et al. (2007) is presented below :

The displacements can be written mathematically as follows:

$$u(x,t) = u_0(t)\sin\frac{\pi x}{l} \quad \text{(Between the supports)} \quad \ldots\ldots\ldots\ldots\ldots\ldots\ldots\ldots\ldots\ldots\ldots\ldots (2.8)$$

$$u(y,t) = \frac{-u_0(t)\pi}{l} y \quad \text{(Overhanging the supports)} \quad \ldots\ldots\ldots\ldots\ldots\ldots\ldots\ldots\ldots\ldots (2.9)$$

The generalized inertial load $P_i(t)$ must satisfy the following virtual work equation:

$$P_i(t) = \int_0^l \rho A\left(\ddot{u}_0(t)\sin\frac{\pi x}{l}\right)\left(\delta u_0 \frac{\sin \pi x}{l}\right)dx + 2\int_0^h \rho A\left(\frac{-\ddot{u}_0(t)\pi y}{l}\right)\left(\frac{-\delta u_0 \pi y}{l}\right)dy \ldots\ldots\ldots\ldots (2.10)$$

The following expression is the solution of equation 2.10 for a prismatic homogeneous beam:

$$P_i(t) = \rho A \ddot{u}_0(t)\left[\frac{l}{2} + \frac{2\pi^2}{l^2}\frac{h^3}{3}\right] \ldots\ldots\ldots\ldots\ldots\ldots\ldots\ldots\ldots\ldots\ldots\ldots\ldots\ldots (2.11)$$

Where $P_i(t)$ is the generalized inertial load; ρ is mass density of beam material; A is the area of the beam cross-section; $\ddot{u}_0(t)$ is acceleration at the centre of the beam; l is the distance between the supports (clear span) and; h is the portion overhanging the supports.

If the distributed inertial load on the beam can be replaced by a generalized inertial load acting at the mid-point, the system can be considered as a single degree-of-freedom and the actual bending load can be acquired by subtracting the inertial load from the observed tup load.

$$P_b(t) = P_t(t) - P_i(t) \ldots\ldots\ldots\ldots\ldots\ldots\ldots\ldots\ldots\ldots\ldots\ldots\ldots\ldots\ldots\ldots (2.12)$$

Where $P_i(t)$ is the generalized inertial load; $P_t(t)$ is the observed tup load and $P_b(t)$ is the bending load of the beam.

The above equation 2.12 could be used in analysing the behaviour of the beam; if so, one should consider only that part of the external load involved in actually stressing and deforming beam $P_b(t)$, in other words the bending load (Bentur, et al., 1986; Soleimani, et al., 2007). The equation 2.12 enables us to estimate the bending load from the recorded tup load and the computed inertia load.

The bending load can also be estimated from the summation of supports reaction. According to Soleimani & Banthia, (2014), when appropriate load cells are introduced to the supports, the support anvils do not experience inertial forces during a test. Therefore, the true bending load at time t, $P_b(t)$ acting at the mid-span of the beam under study, can also be obtained by summing the reaction forces at the support anvils at time, t (Figure 31).

$$P_b(t) = R_A(t) + R_C(t) \quad \ldots\ldots (2.13)$$

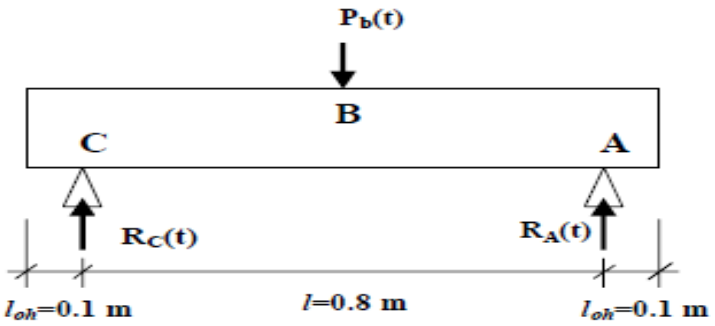

Figure 2.31. Load configuration on RC beams (Soleimani, et al., 2007).

Where $R_A(t)$ is a reaction load at support A at time t and $R_C(t)$ is a reaction at support C at time t.

The bending load can also be directly estimated, based on the expression below (equation 2.20) developed by Metz (2007). The bending load can be estimated on the basis of drop height and travelled distance of the specimen (displacement) after the impact loading, by considering the law of conservation energy, which states that the potential energy (PE) before an event must equal to the kinetic energy (KE) after an event (Nave, 2001).

$$PE = KE \quad \ldots\ldots (2.14)$$

For a simple drop test, the conservation-of-energy equation is:

$$mgh = 1/2\, mv^2 \quad \ldots\ldots (2.15)$$

Where m is mass; g is acceleration of gravity; h is drop height; v is velocity of impact

From the equation 2.15 above, the impact velocity can be expressed as:

$$v = \sqrt{2gh} \quad \ldots\ldots (2.16)$$

By using the work-energy principle, the test engineer or the research in this kind test should be able to estimate the expected force. The net work done during an impact testing is equal to the product of the average force of impact by the distance travelled during impact (Metz, 2007).

$$W_{net} = 1/2\, m v_{final}^{\ 2} - 1/2\, m v_{initial}^{\ 2} \quad \ldots\ldots\ldots\ldots (2.17)$$

The initial velocity $(v_{initial})$ is equal to zero in drop testing, hence, the equation 2.17 can be expressed as:

$$W_{net} = 1/2\, m v_{final}^{\ 2} \quad \ldots\ldots\ldots\ldots (2.18)$$

If the impact distance could be easily measured, then the average impact force F is calculated as follows:

$$F = \frac{W_{net}}{d} \quad \ldots\ldots\ldots\ldots (2.19)$$

Where d is the distance travelled after the impact, that is, the deflection under impact point.

Finally, the simultaneous replacement of equations 2.18 and 2.16 in 2.19 led to the following equation:

$$F = \frac{1/2 m v_{final}^{\ 2}}{d} = \frac{1/2 m\left(\sqrt{2gh}\right)^2}{d} = \frac{mgh}{d} \quad \ldots\ldots\ldots\ldots (2.20)$$

The equation 2.21 can be used to estimate the bending load from the impact loading test, thus the following formula is presented:

$$P_b(t) = \frac{mgh}{d} \quad \ldots\ldots\ldots\ldots (2.21)$$

Therefore, by referring to all those mathematical expressions described above, the bending load and the inertial load can be estimated for the impact loading test of RC structures including beams. However, due to the complexity of impact loading test and its associated behaviour within, it is not possible to accurately estimate the impact capacity of beam under study based only on its cross-sectional properties (Saatci & Vecchio, 2009).

In the same way, other methods and techniques used to evaluate the impact loading have also been reviewed. Figures 2.32 and 2.33 show the scenarios of impact loading applied to the RC beam and the distribution of forces involved in drop testing.

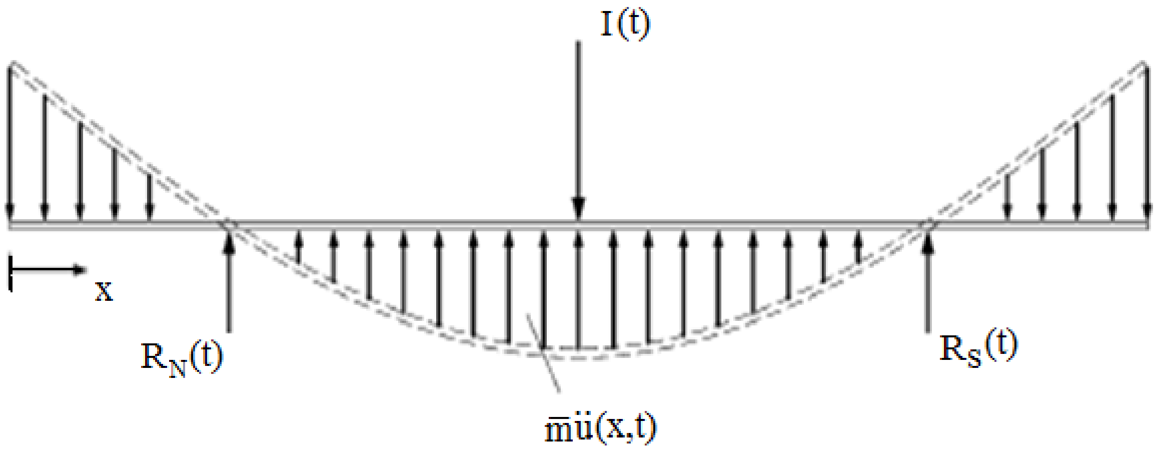

Figure 2.32. Dynamic free body diagram of the tested RC beams subjected to impact loading (Saatci & Vecchio, 2009).

According to Saatci & Vecchio, (2009), through their research on impact loading, the following expressions have been developed to evaluate the impact load results from the dynamic responses.

$$\int_0^L \overline{m}\ddot{u}(x,t)dx + R_N(t) + R_S(t) - I(t) = 0 \quad \ldots\ldots (2.22)$$

Where L is the total length of the specimen; $\overline{m}$ is the mass per unit length; $\ddot{u}(x,t)$ is the acceleration of the specimen; $I(t)$ is the impact force ; $R_N(t)$ and $R_S(t)$ are the support reaction forces at the north and south support, respectively.

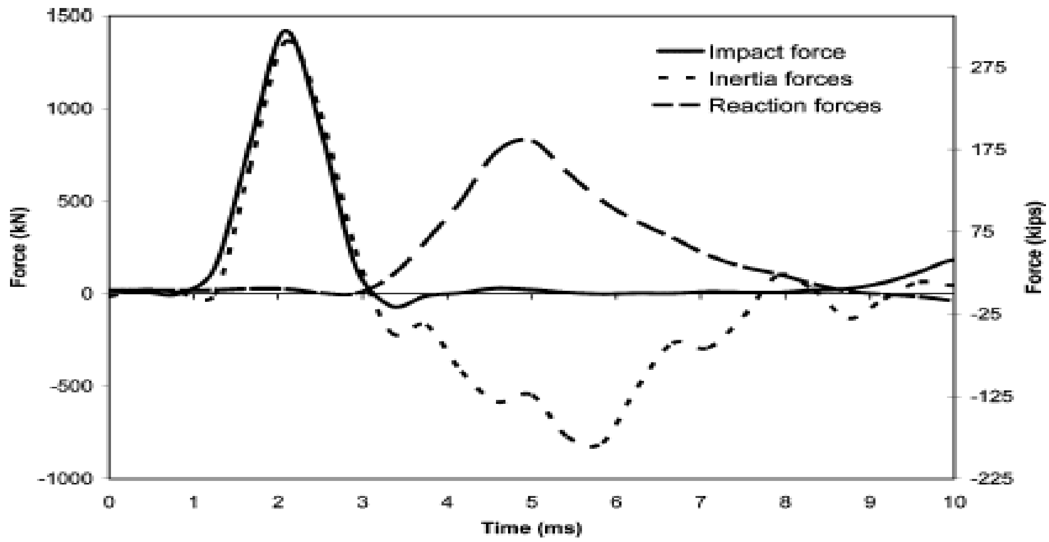

Figure 2.33. Breakdown of forces involved in impact loading testing of RC beams (Saatci & Vecchio, 2009).

The introduction of impact loading to the specimen produced vibrations and caused the RC beam in testing to oscillate up and down and vice versa. The impact force was resisted by inertia force, before its transmission to the supports. According to Saatci & Vecchio, (2009), the phenomena above lead to the formation of the shear plug through the specimen. In their study (Saatci & Vecchio, 2009), they observed that all specimens developed severe diagonal cracks, originating from the impact point propagating downwards with an angle of approximately 45 degrees, forming shear plugs. The aforementioned phenomena should be well explained and understood through the Figure 2.33 above, related to the breakdown of forces involved in drop testing. All quantities in equation 2.22 were measured during the tests; five accelerometers attached at five different locations at the south half of the specimen are used to measure the accelerations, the support reactions $R_N(t)$ and $R_S(t)$ were acquired from the load cell transducers readings, and the impact forces $I(t)$ were computed as the product of the accelerations of the drop-weight times its mass. On the basis of the same equation 2.22, the impact force is resisted by a combination of inertia and reaction forces (Saatci & Vecchio, 2009).

The total reaction force (R) at the supports can be determined using the formula 2.23 below, which can be matched against the test results to find the value of α.

$$R = (1-\alpha)\frac{I}{2} \qquad (2.23)$$

Where I is the impact force; and α is the ratio of the inertia forces to the total impact, and where the inertia force distribution is assumed to be proportional to the elastic displaced shape of the specimen loaded at the mid-span.

The impact setup presented in Figure 2.34 below, has been used to record and estimate the dynamic response and extracted displacements results accordingly. Bending load capacity of a RC beam subjected to impact can be estimated as 2.3 times its static capacity when it has been performed on impact machine similar to the one presented in Figure 2.34 (Soleimani, et al., 2007) . Extensive research work on impact testing has been done at the University of British Columbia in Canada for more than 25 years by Professor N. Banthia and his co-workers, and hence the presented device is one of the best impact machines to use in impact loading research.

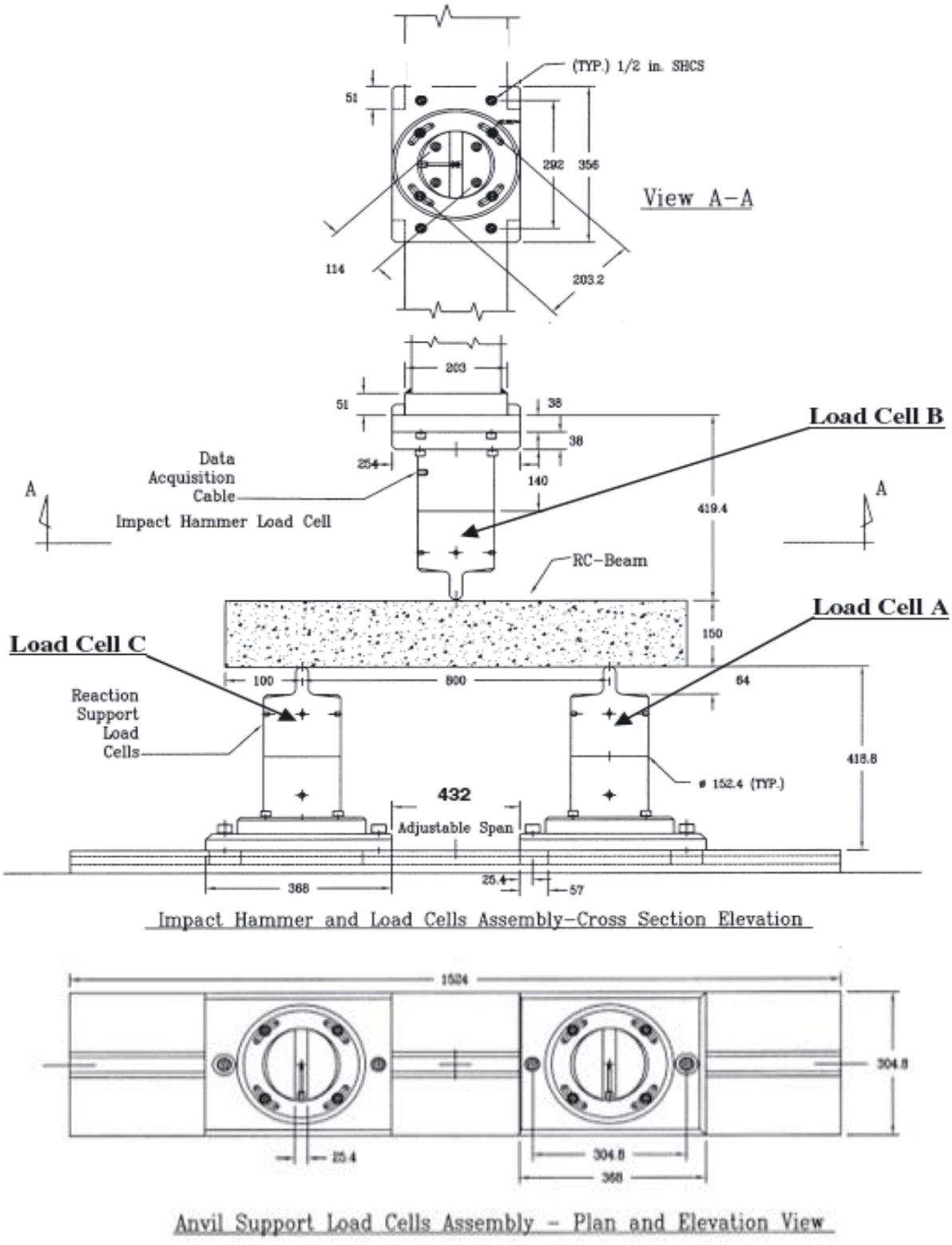

Figure 2.34. The load cell assembly and the specimen in position for impact loading test (Soleimani & Banthia, 2014).

2.7. Past experimental studies conducted on RC beams under impact loading

2.7.1. Non-FRP-strengthened RC beams

Kishi, et al., (2012), carried out a study to develop an impact resistant design method for RC beams following the performance-based design concept based on experimental results. This investigation was conducted on the dynamic response characteristics of RC beams subjected to falling-weight impact loading with different impact energies. A total of 36 RC beams that theoretically exhibit flexure failure under static loading was tested for once-only falling-weight impact loading. The layout of the reinforcement for beams for each series is shown in Figure 2.35.

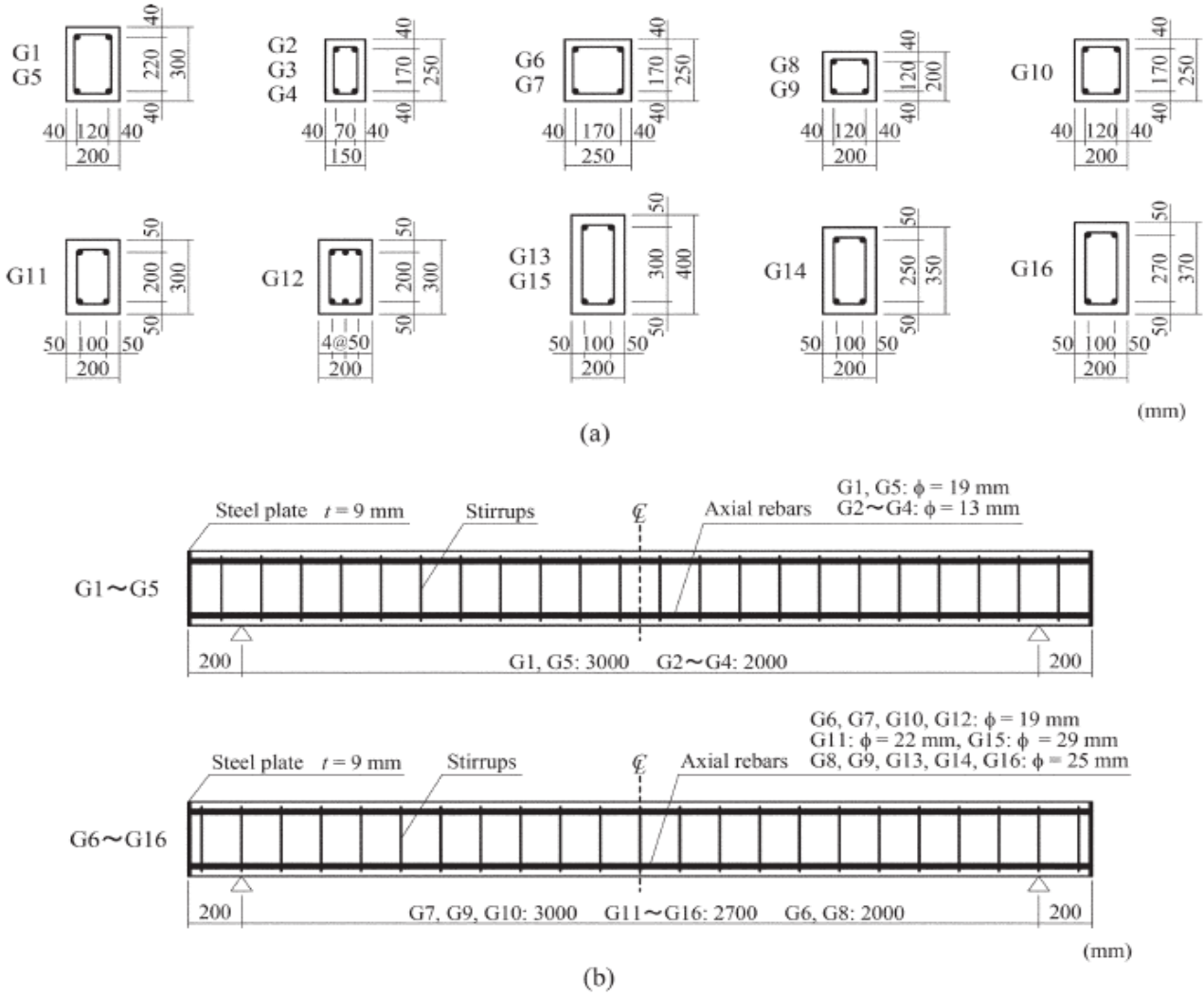

Figure 2.35. Details of beams of each series: (a) cross section of beams; (b) reinforcement layout of beams (Kishi, et al., 2012).

The beams under study were divided into 16 test series with respect to beam dimensions and /or test duration. Thus , the tested beams had varying section parameters. In addition, the variation in diameter and number of longitudinal reinforcing steel in combination with different stirrups spacing were taken into consideration through this experimental study. For all beams, the static shear-flexural capacity ratio $\alpha = V_{usc} / P_{usc}$ is greater than 1, meaning that the beam would statically fail in flexure (Kishi, et al., 2012). Figure 2.36 shows the falling weight impact test apparatus utilised in this study.

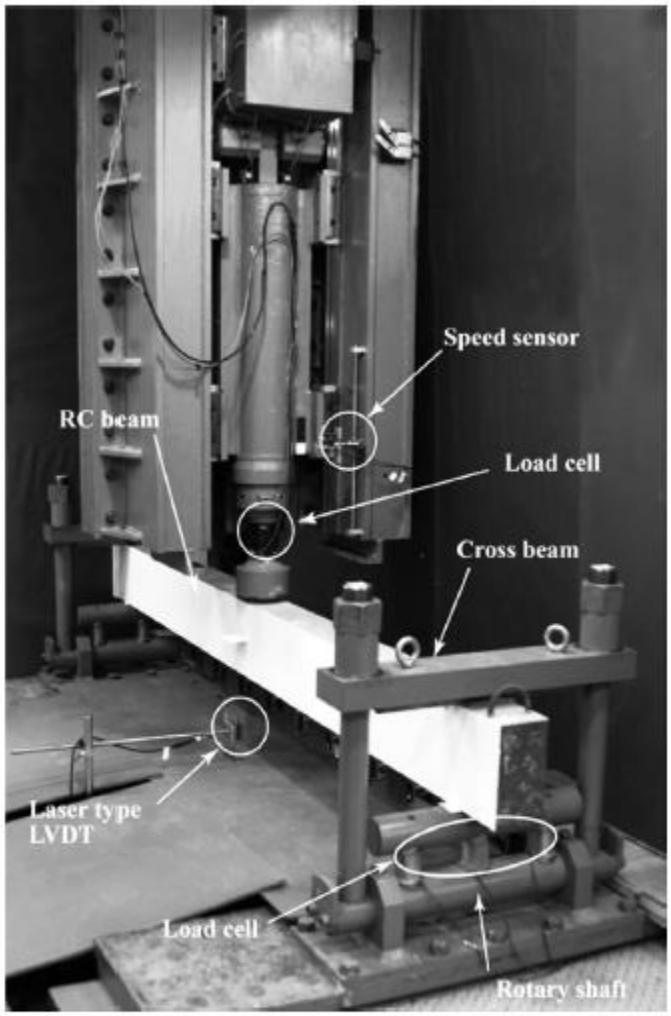

Figure 2.36. Falling-weight impact test apparatus (Kishi, et al., 2012).

In this experiment, the impact velocities V of the weight varied from 3.13 to 7.7 m/s. The minimum and maximum input impact energies were 2.41 and 14.71 kJ, respectively. The impact load was applied to the beams without taking into consideration any limit state. The impact force P was measured by using a load cell transducer installed in the falling weight component with a capacity of 1960, 2940, and 2940 kN for 300, 400, and 500 kg falling weight, respectively, and measuring frequency higher than 4 kHz for all types of weight used in this

study. Each load cell used for measuring the reaction force R at the support had a capacity of 294 kN and a measuring frequency of 2.4 kHz. The dynamic deflection D of the beam were measured at the mid-depth using a laser-type LVDT with a maximum stroke of 200 mm and a measuring frequency of 915 Hz (Kishi, et al., 2012).

Figure 2.37 shows the time history of dynamic responses of various tested beams. Those dynamic responses include impact force P, reaction force R and dynamic deflection D.

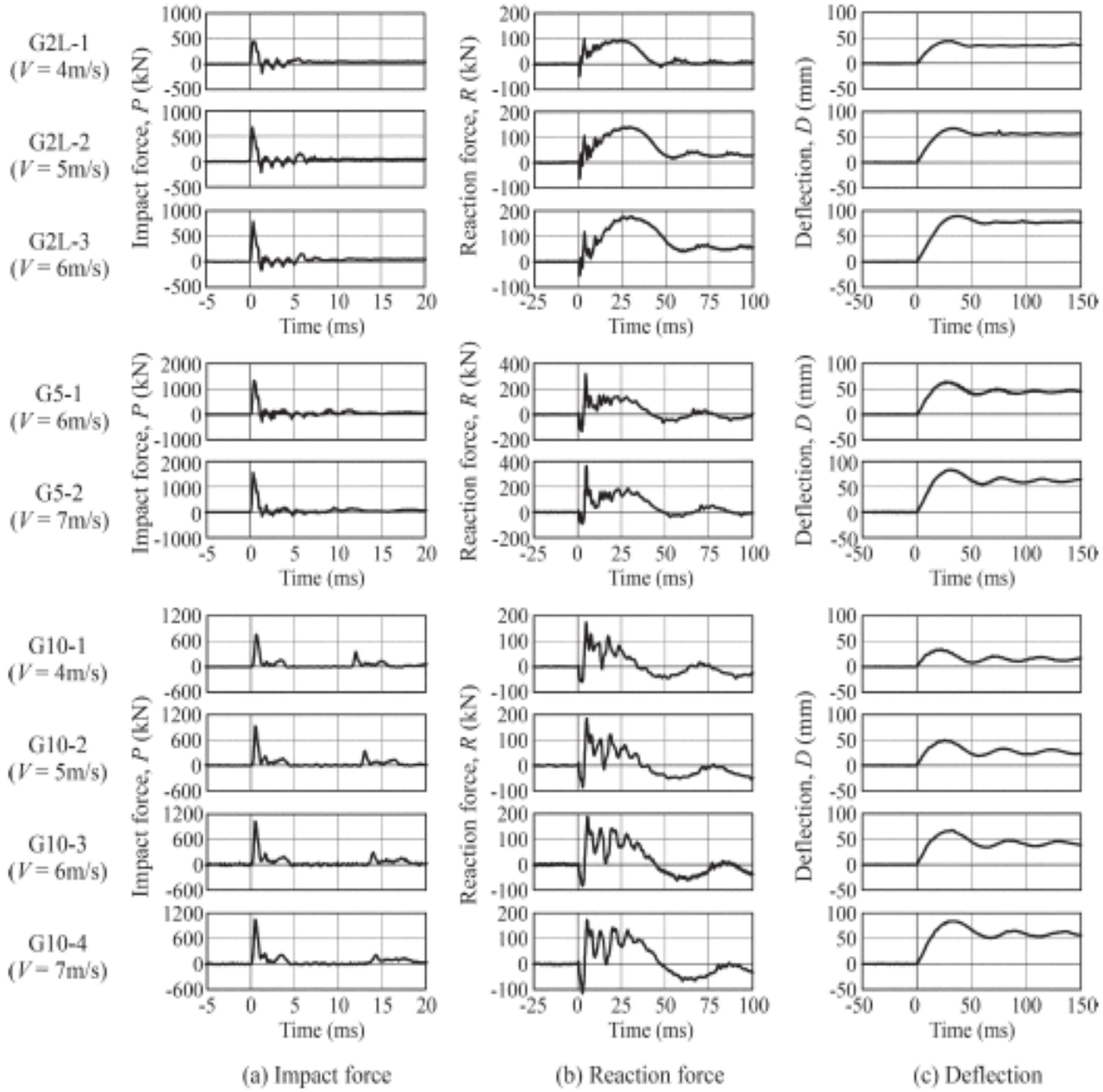

Figure 2.37. Time history responses of series G2L, G5, and G10: (a) impact force P; (b) reaction force R and (c) deflection D (Kishi, et al., 2012).

The following observations should be made on the behaviour of beams in the same series respectively from Figures 2.37 (a), 2.37 (b) and 2.37 (c):

(1). At the starting of impact, the time history displays a triangular shape with high amplitude and short time duration;

(2). At the starting of impact, a negative reaction force is excited due to impact and the main response is made up of half-sine wave or a triangular-shaped component;

(3). The main response exhibits a half-sine wave; after that, the deflection is restrained. The residual deflection δ_{rs} of the beam in the same series has a tendency to increase with each increment of impact velocity V .

Furthermore, it can be seen from the results of this study that the characteristics of the relationship between reaction force R and deflection D are different, depending on the statistic flexural loading capacity P_{usc} of the beam and the magnitude of input impact energy E . Figure 2.38 shows the cracking patterns of RC beams used in this study.

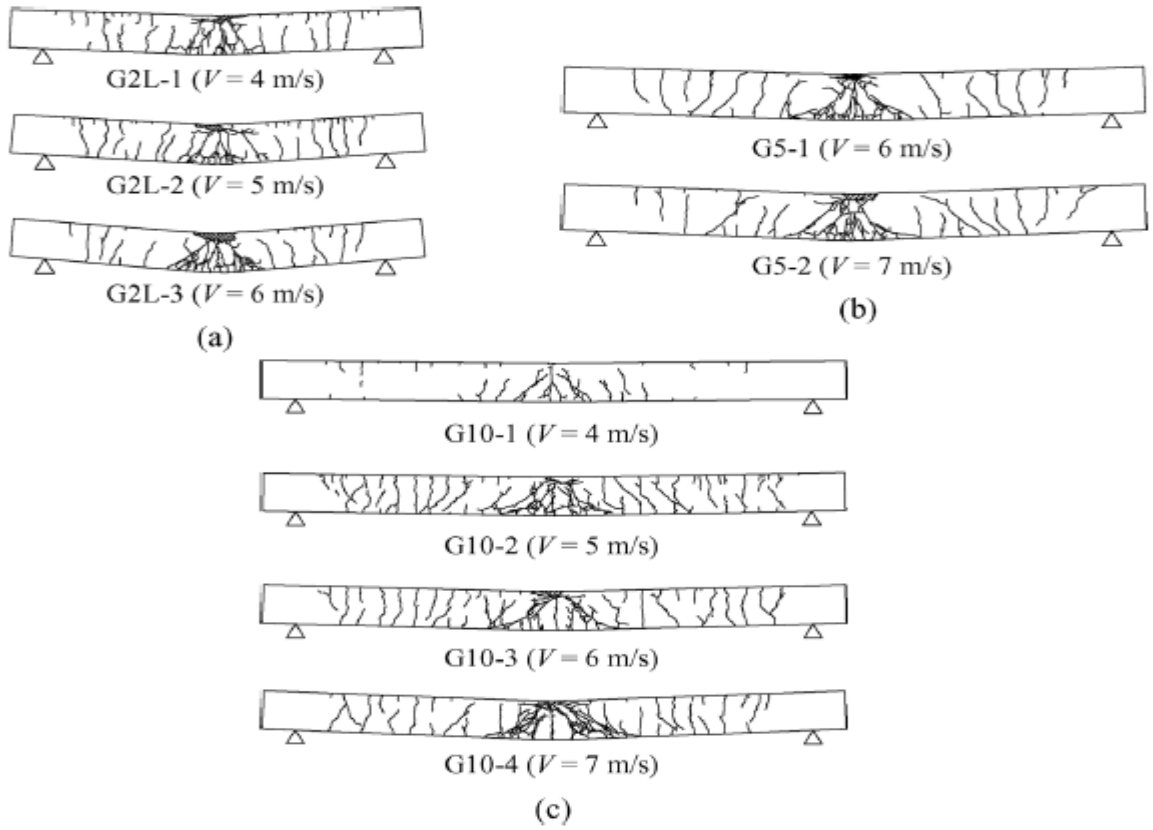

Figure 2.38. Crack patterns in beams of Series G2L, G5, and G10: (a) Series G2L; (b) Series G5 and c) Series G10 (Kishi, et al., 2012).

The following conclusions were drawn from this experimental research:

(i). All beams failed in flexure because the static shear-flexural capacity ratios were greater than 1.5.

(ii). The time history plot of the reaction force result and the shape of the hysteretic loop between the reaction force and the mid-span deflection results vary within the sectional properties of the tested beam and the amount of input energy.

(iii). The maximum and residual deflections are practically proportional with regard to the input impact energy, and the gradients can be empirically formulated with high correlation utilising the inverse of the static flexural load-carrying capacity of the beam.

(iv). The ratio of the maximum to the residual deflection almost achieves 1.5, which might be an important design parameter (Kishi, et al., 2012).

Chen & May, (2009) , conducted a series of experimental studies to assess the high-mass, low-velocity impact behaviour of RC members such as beams and slabs, and to come up with high-quality input data and results to use in the validation of numerical modelling. Fourteen 3.0 m long with 2.7 m clear span and four 1.8 m long with 1.5 m clear span RC beams were subjected to impact loads tests with the use of a drop weight facility. Pin-ended and simply supported systems have been adopted and two types of impactor have been used; these are hemispherical and flat impactors. Figure 2.39 shows the reinforcement layout of RC beams used in this study. For the aforementioned Figure 2.39, all dimensions are in mm.

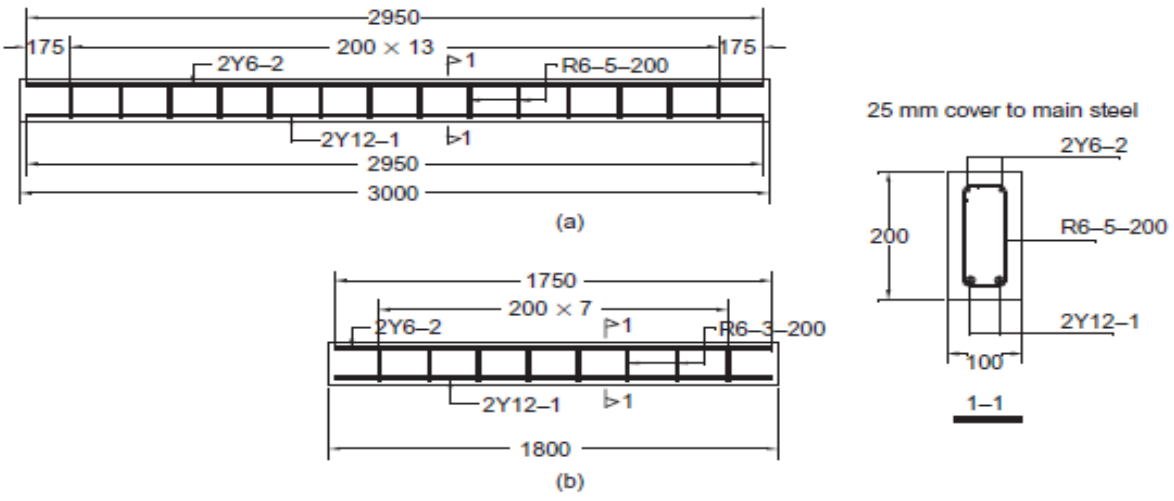

Figure 2.39. Reinforcement details for: (a) 3.0 m beams; (b) 1.8 m beams (Chen & May, 2009).

Two types of classification of tests were adopted: type A tests and type B tests. Type A tests had a 12 mm thick plywood pad placed between a beam and the impactor, while type B tests were used to investigate the effect of the impactor directly striking a beam. It was considered that although strain rate could have some effect on the impact behaviour of beams, the influence would not be significant, owing to the low impact speed. The dynamic properties of the materials were therefore not explicitly tested (Chen & May, 2009). Figures 2.40 shows the impact testing apparatus including support systems and various impactors.

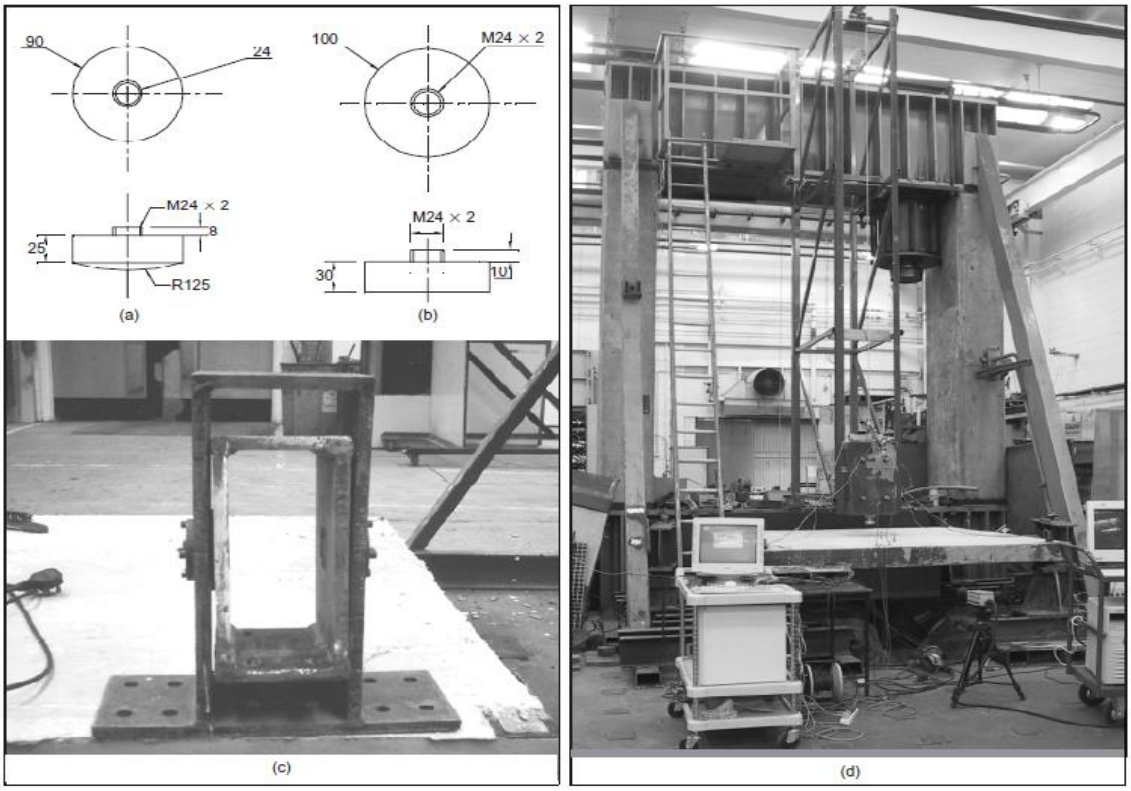

Figure 2.40. Details of impact system: (a) spherical impactor; (b) flat impactor; (c) pin-ended beam support and (d) drop-weight impact apparatus (Chen & May, 2009).

A high-speed video camera was used to record the impact scenarios at a rate of 4500 frames per second with a resolution of 256 x 256 pixels. The load cell transducer, which was placed between the mass and the impactor, was used to measure impact forces. For some tests, in which the impact force was expected to practically exceed the capacity of load cell normally used in this study, the impact force was obtained from the response recorded with the use of accelerometers installed in the striking component. Also, the acceleration at the various critical points on the beam under study was recorded with the use of accelerometers. In some of the tests, the technique of inserting strain gauges inside the bar and attaching them to the reinforcement has been used. This technique allowed the researchers to record the strains in

the reinforcement without jeopardising the bond between the concrete and the embedded reinforcement. Two electronic triggers, separated with 40 mm spacing at the bottom of the guiding leg of the frame, were used to measure the velocity of the striking component (impactor) at the moment of impact (Chen & May, 2009). Table 2.4 lists the maximum impact forces, peak times, the time at which the maximum impact force took place, and modes of failures of various tested RC beams. Figures 2.41 and 2.42 illustrate the correlation between impact load and crack propagation for beam A1 and B3 respectively.

Table 2.4. Maximum impact force, peak time and failure type of RC beam tests (Chen & May, 2009)

Group no.	Test no.	$F_m : kN$	$F_{AVG} : kN$	$(F_m - F_{AVG})/F_{AVG} : \%$	$t_m : ms$	$t_{AVG} : ms$	$(t_m - t_{AVG})/t_{AVG} : \%$	Failure type
A1	1	n/a	230	n/a	n/a	1.8	n/a	a
	2	223		-3.0	2.1		+16.7	a
	3	234		+1.7	1.5		-16.7	a
	4	233		+1.3	2.0		+11.1	a
	5	n/a		n/a	n/a		n/a	a
	6	229		-0.4	1.4		-22.2	a
A1*	7	128	—	—	1.6	—	—	a
A2	8	214	222	-3.6	2.0	1.8	+11.1	a
	9	230		+3.6	1.6		-11.1	a
A3	10	194	—	—	2.0	—	—	a
B1	11	n/a	—	n/a	n/a	—	n/a	b
	12	161		—	1.3		—	b
B1*	13	183	—	—	1.4	—	—	b
B2	14	169	170	-0.6	1.5	—	0	b
	15	171		+0.6	1.5	—	0	b, c
B3	16	654	—	—	0.3	—	—	c
B3*	17	215	—	—	1.0	—	—	c
B4	18	241	—	—	1.0	—	—	c

Notes:

F_m : maximum impact force.

t_m : time of maximum impact force (peak time).

— : Result not available owing to instrument failure.

Failure: type a — flexural failure and no spalling of impact zone; type b — highly yielding or rupture of tension steel, spalling of impact zone; type c — scabbing and spalling.

In all the tests performed throughout this research, the striking component was unrestrained in the vertical direction so that after the first impact it rebounded and then dropped onto the

specimen again. The deformation of the structure member under impact loads and propagation of cracks could thus expand under subsequent strikes. The recorded response of the specimen under the susquent strikes was, however, not as important as under the first impact. Only the behaviour of the RC member subjected to the first impact, which took the duration of about 50 ms for RC beams, was investigated throughout (Chen & May, 2009).

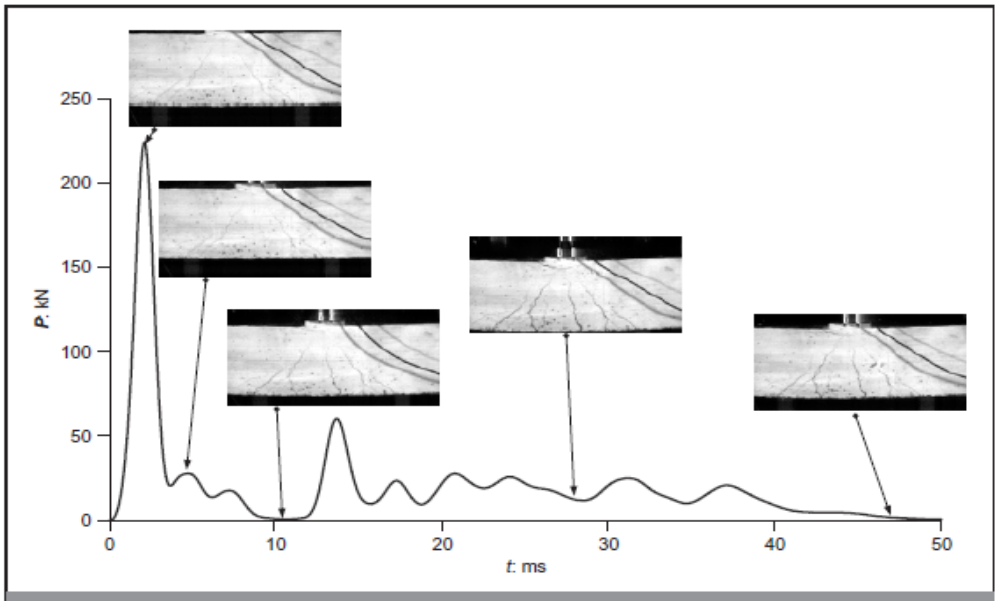

Figure 2.41. Correlation between impact load and crack propagation for beam A1 (Chen & May, 2009).

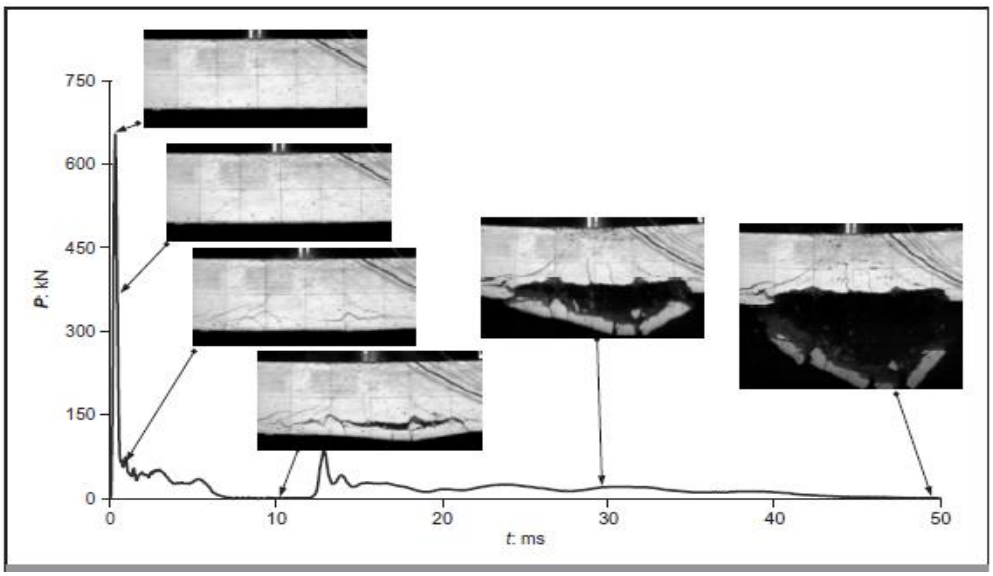

Figure 2.42. Correlation between impact load and crack propagation for beam B3 (Chen & May, 2009).

Figure 2.41 exhibits that a set of diagonal shear cracks initially formed on beam A1 as the impact load reached its maximum at 2 ms. This was also followed by the development of considerable number of vertical flexural cracks. The separation between the striker and RC beam took place at about 10 ms, which is shown by zero impact load, though both the beam and impactor continued their downwards move. At this point spallation of concrete can be noticed directly underneath the impactor. The striking component (impactor) and beam then came back into contact, more cracking occurred and the concrete spalling became more apparent. At a duration of 50 ms the beam and impactor split up again as the latter begun its upwards move (Chen & May, 2009).

On Figure 2.42 it can be noticed, that there was practically no cracking on beam named as B3 before the impact force achieved its maximum at 0.3 ms. Two important diagonal shear cracks were symmetrically formed about the mid-span underneath the impact zone at about 0.5 ms, also some vertical flexural cracks were formed at the bottom and in the central portion of tested the beam. Further, unlike to beam A1, a certain number of horizontal cracks were experienced at the level of the bottom steel bar reinforcement under the impact zone. They eventually joined together to become one crack as long as the time increased whilst the impact load decreased. Around 8 ms contact was lost between the beam under study and the impactor for a short period of time, as the said beam deformed at a quicker rate than the impactor. The opening of the formed horizontal crack became so wide, thus the concrete cover under this type of crack begun to detach, scab or separate, from the remainder of the beam. From 10 ms to 30 ms the impactor and beam contacted again, leading to a relatively small impact load. Spallation also occurred during this period beneath the impact zone. The scabbing of the concrete became more significant between 30 and 50 ms. Finally, a significant amount of the concrete cover on the underside of the beam snapped from a triangular region delimited by two considerable diagonal shear cracks. At about 50 ms the striking component begun its upwards move and impactor lost contact once more (Chen & May, 2009).

Three modes of failure were observed, namely mode a, mode b, and mode c. Mode a was predominantly flexural failure with some concrete crushing underneath the impactor and some shear cracking experienced in the impact zone, see Figures 2.43 (a), 2.43 (b), and 2.43 (c) for beams A1, A2, and A3 respectively. In this mode of failure, less damage occurred than in modes b and c, due to some of the impact energy being utilised in the deformation of the plywood pad (Chen & May, 2009). Mode b was a predominantly localised failure in the vicinity

of the impact and yielding of the tension steel reinforcing bars, as it can be seen in Figures 2.43 (d) and 2.43 (e) for beams B1 and B2 respectively. This typical mode of failure occurred on beams subjected directly to impact loading by the hemispherical impactor. Finally, mode c was alike to the mode a in terms of failure; nevertheless, it was accompanied by loss of the concrete cover to the steel reinforcing bars in tension zone due to the scabbing phenomenon. Scabbing occurred on the bottom side of beams starting at the level of the steel reinforcement, as can be seen in Figures 2.43 (f) and 2.43 (g) for beams B3 and B4 respectively. It occurred on beams subjected directly to impact loading with the flat impactor (Chen & May, 2009).

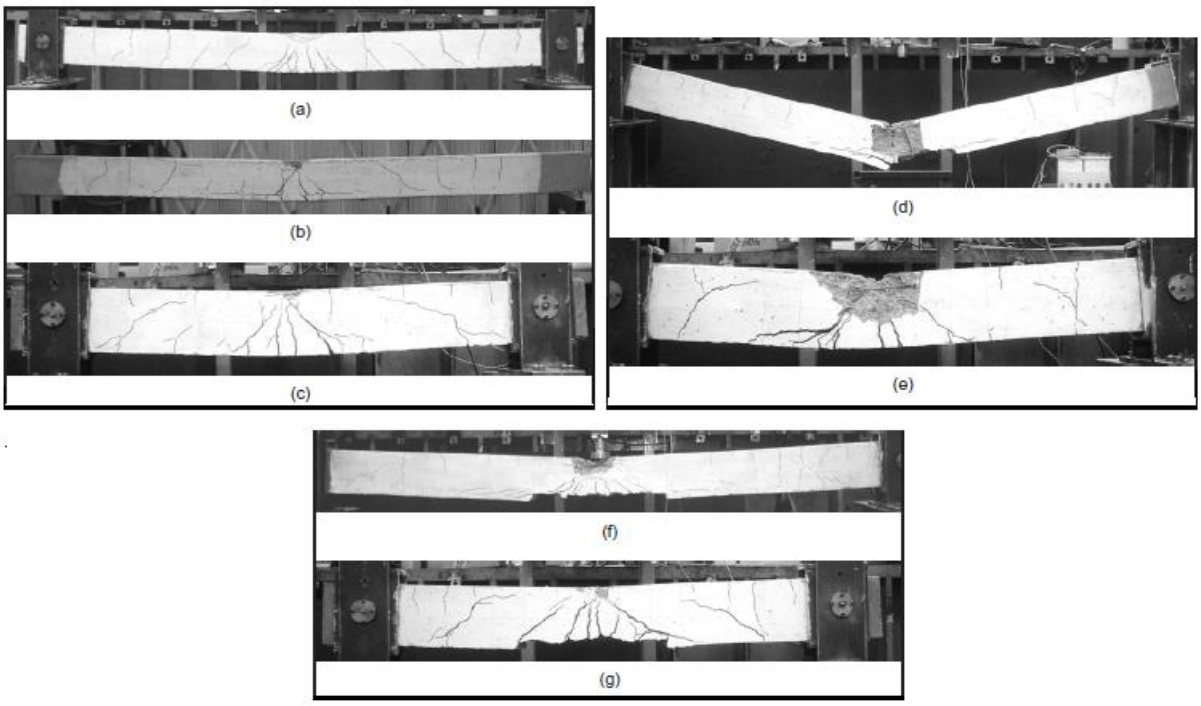

Figure 2.43. Post-test crack pattern of beams: (a) beam A1; (b) beam A2; (c) beam A3; (d) beam B1; (e) beam B2; (f) beam B3 and (g) beam B4 (Chen & May, 2009).

Some of the conclusions drawn from this extensive experimental study are the following:

(i). The beam tests have confirmed the findings of other researchers that beam supports conditions have less influence on the impact force result than the span. It has also been realised that the plywood interface, which was utilised in some of the tests performed in this study, distributes the input force in similar manner to a flat impactor.

(ii). The correlation between the impact response of the tested beams in terms of cracking, spallation and scabbing phenomena, and the load-time histories, has been established on the basis of the records acquired with the high-speed camera.

(iii). Some of the data generated from this study have already been utilised to calibrate numerical models and procedures for the simulation of impact load subjected to RC structures, and further uses may be expected (Chen & May, 2009).

Fujikake, et al., (2009), carried out a drop hammer test on RC beams to investigate the influence of drop height and the effect of the amount of longitudinal steel reinforcing bars to the contribution of the impact responses of RC beams. Twelve RC beams with the size of 250 mm deep, 150 mm wide and 1700 mm long were tested under impact loads. Three different sizes of longitudinally deformed bars namely D13, D16 and D22 have been used with respectively 397 MPa, 426 MPa, and 85 MPa yield strength. 75 mm stirrups spacing for D10 bars with a yield strength of 295 MPa were also used. Three series S1616, S1322 and S2222 of RC beams were formed based on the longitudinal size of bars D16, D13, and D 22 respectively. They were flexure controlled beams, that is, the shear resistance was larger for more than 50% of its bending resistance. A 42 MPa compressive strength concrete was used containing aggregates of 10 mm maximum size. The arrangement of rebar used in various tested beams is shown in Figure 2.44.

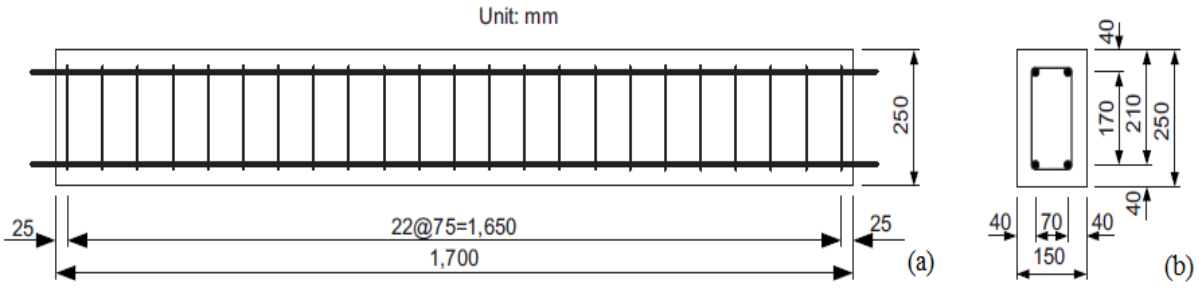

Figure 2.44. Rebar arrangement: (a) side view; (b) cross-sectional view (Fujikake, et al., 2009).

A drop hammer apparatus with a mass of 400 kg was used at the mid-span to test various beams under impact loading. Two different sets of four drop heights were selected for the impact test. These selected sets differed depending on the series of the beams to be tested. Series S1322 and series S2222 beams were tested under an identical set of four drop heights, while series S1616 beams were tested under a different set of four drop heights. A dynamic load cell transducer which was adequately and rigidly connected to the impactor (drop hammer) was used to measure the contact force which was developing between the impactor and the RC beam during the drop test. The mid-span deflection response of various tested RC beams was evaluated and recorded with the use of a typical laser displacement sensor (Fujikake, et al., 2009).

Typical failure modes observed during the impact loading test and their associated drop heights are shown in Figure 2.46. Series S1616 beams showed globally a flexural failure at all the drop heights. For series S1322 and series S2222 beams, the global flexural failure was noticed only at a drop height which did not exceed 0.6 m. Local failure with heavy spallation of concrete near to the impact loading point was noted at the drop height of at least 1.2 m. In addition, it is found that the quantity of longitudinal compressive steel reinforcing bars has a tendency to affect the extent of the local failure; since then the length of the local failure for series S 1322 beams was found to be approximately 20% greater than that for series S2222 beams. Figure 2.45 shows the used drop hammer setup.

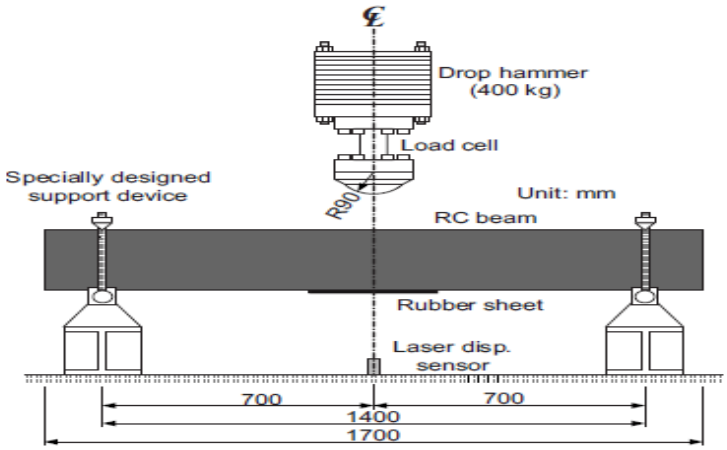

Figure 2.45. Drop hammer impact test setup (Fujikake, et al., 2009).

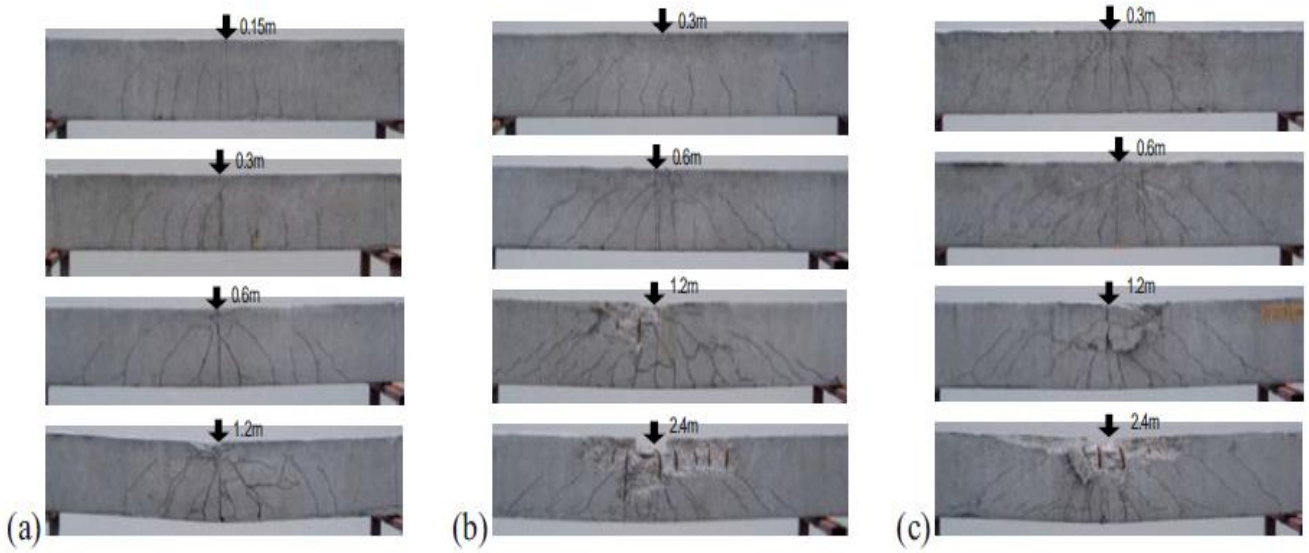

Figure 2.46. Failure modes: (a) S1616 series; (b) S1322 series and (c) S2222 series (Fujikake, et al., 2009).

For the tests performed at an equal drop height, the maximum impact load result and the impulse were however observed to be roughly identical in spite of the differences between various specimens. The flexural rigidities (EI) influence not only the maximum mid-span deflection but also the duration of impact loading and the time taken for the maximum mid-span deflection to occur. Figure 2.47 shows the measured impact loads and mid-span deflections in series S1616 beams. In addition, the results for series S1322 and S2222 were also presented in similar Figures. The measured impact loads are characterised by an initial pulse-like waveform of relatively high amplitude, generally followed by a blunt waveform of relatively low amplitude.

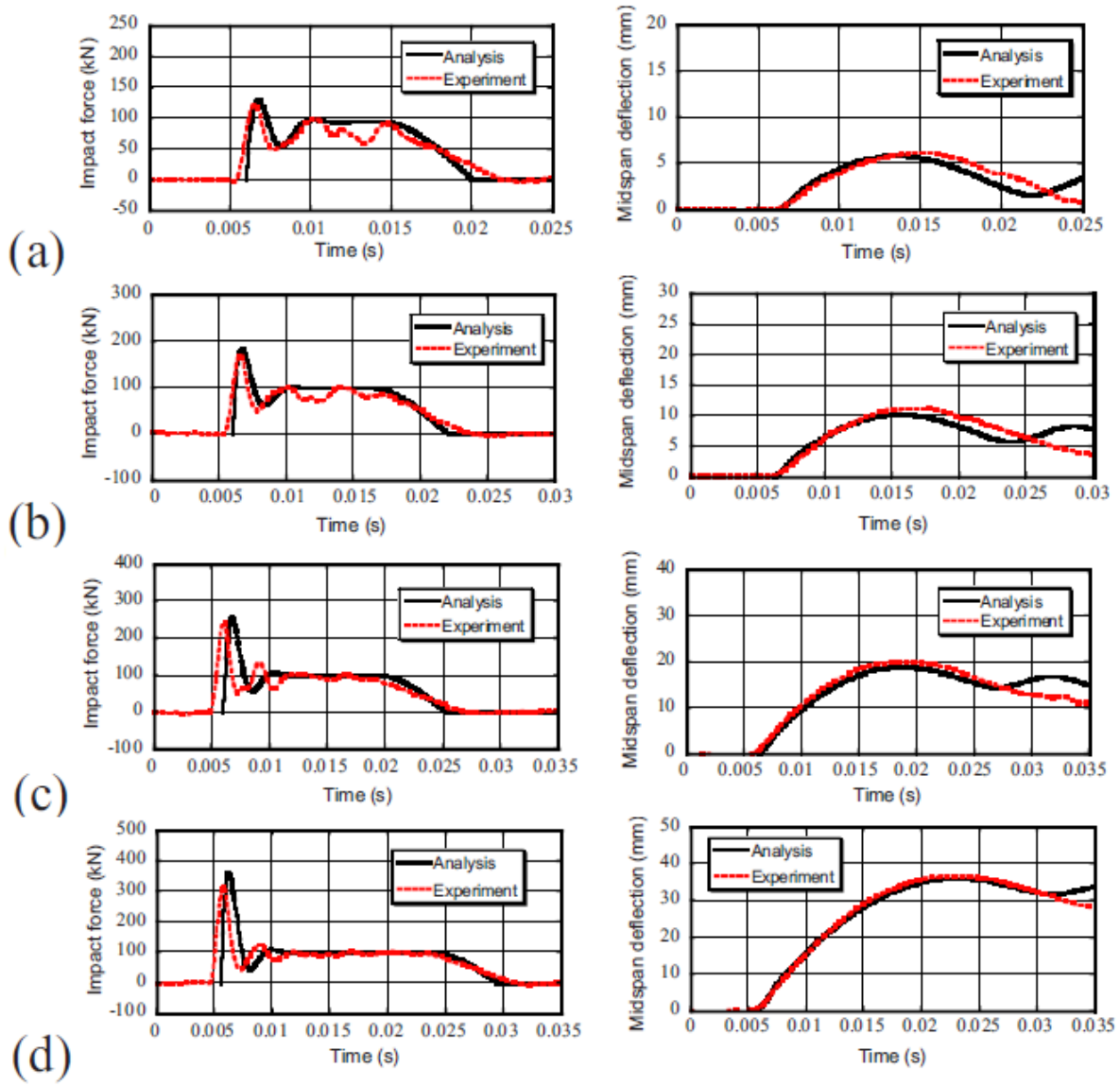

Figure 2.47. Impact responses for S 1616: (a) drop height = 0.15 m; (b) drop height = 0.3 m; (c) drop height = 0.6 m and (d) drop height = 1.2 m (Fujikake, et al., 2009).

Figure 2.48 shows the maximum impact load results, the magnitude of the impulse, the duration of the impact load, the maximum mid-span deflection results, and the time taken for the maximum mid-span deflection acquired respectively at each drop height.

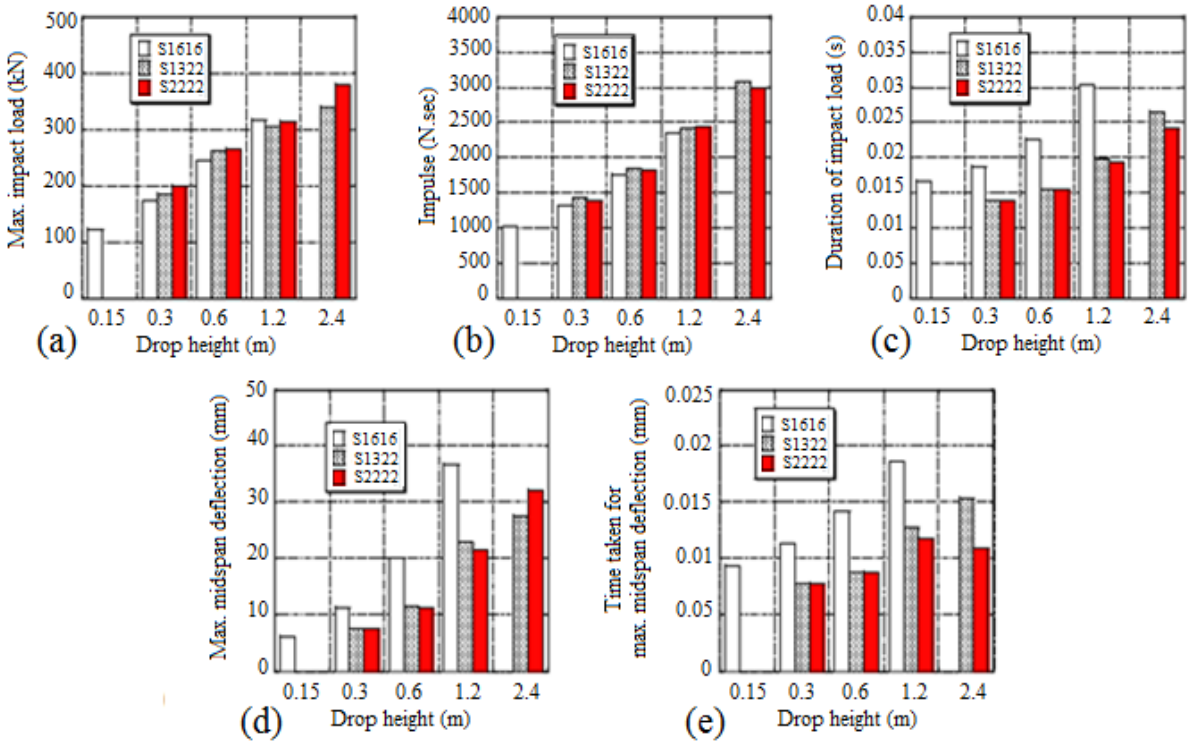

Figure 2.48. Impact responses: (a) maximum impact load; (b) impulse; (c) duration of impact load; (d) maximum mid-span deflection and (e) time taken for maximum mid-span deflection (Fujikake, et al., 2009).

The following conclusions were drawn from this study:

(i). The quantity of longitudinal steel bar reinforcement considerably affected the modes of failure of RC beams subjected to impact loading. The RC beam with the relatively lower amounts of longitudinal steel bar reinforcement showed only overall flexural failure, whilst the RC beam with the relatively higher amounts of longitudinal steel bar reinforcement evinced not only the overall flexure failure but also local failure in the vicinity of the impacted loading point, due to the huge impact force from the loading acting on a single point.

(ii). The quantity of longitudinal steel bar reinforcement in the compression zone influenced the extent of the local failure. The local failure was significantly reduced when heavy longitudinal steel bar reinforcement was used in compression zone. Therefore, the longitudinal compression reinforcement enhances the resistance of the beam's local failures when tested under impact loading.

(iii). The results obtained in terms of maximum impact load, the magnitude of the impulse, the duration of impact load, the maximum mid-span deflection, and the time taken for the maximum deflection were all increased as long as the drop height was increased. The duration of impact load, the maximum mid-span deflection and the time taken for maximum mid-span deflection were influenced by the flexural rigidity of the various tested RC beams.

(iv). The maximum mid-span deflection was found to be an important index for assessing damage levels of RC beams tested under impact loading (Fujikake, et al., 2009).

2.7.2. FRP-Strengthened RC beams

Erki & Meier, (1999), conducted the first documented experimental study on RC beams strengthened with CFRP laminated plates and tested under impact loading. RC beam, simply supported and externally strengthened for flexure, were experimentally tested. In this study, one end of the beam under study was lifted up to and then dropped from a predefined drop height. Impact loading was directly induced in the beam as the dropped end came into contact with the underneath support, which was a damping unit made from a shock absorber. Figure 2.49 shows the experimental test setup and the cross-sectional details of two types of beams.

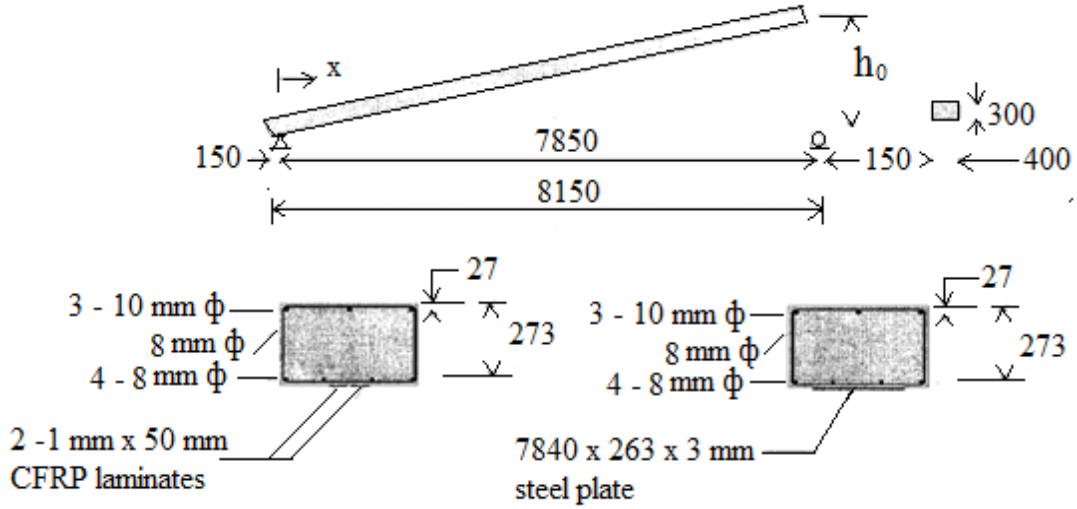

Figure 2.49. (a) Test setup; (b) RC beams strengthened with CFRP laminates and (c) RC beams strengthened with a steel plate (Erki & Meier, 1999).

The assumption was made that after the first release from the specified drop height, but before getting in contact with the damper, the beam under test was not cracked. At that particular

instant when the beam came into contact with the damper, shear and bending moments were prompted by an impulse wave. The generated energy was normally first absorbed by the provided damper and then by the RC beams, as the concrete material cracked and the steel reinforcement yielded. For the G-beams types, energy was most absorbed by yielding phenomena of the external steel plate, and finally by its debonding. For the BF-beams types, the glued CFRP laminates material absorbed energy throughout longitudinal cracks developed in the epoxy adhesive layer and when tension occurred, in the rupture of the used CFRP laminate itself. Debonding and tension failures of the used CFRP laminates can be compared to the release of an extremely stretched elastic band. The deformations of the beams that had been strengthened with CFRP laminates led to the stretching of those strengthening materials and consequently, the produced strain energy was kept and stored in those laminates. The failures of the CFRP laminates were particularly explosive due to the sudden release of the stored strain energy (Erki & Meier, 1999).

Finally, the following concluding remarks are drawn from this study:

(i). The CFRP laminate strengthened RC beams exhibited excellent performances when subjected to impact loading. However, unlike their counterparts externally strengthened with the use of steel plates, the CFRP laminate strengthened RC beams displayed minimal energy absorption behaviour. Therefore, the additional anchorage of the CFRP laminates was recommended as it would significantly enhance the impact resistance capacity of the RC beams.

(ii). The results of these tests showed the debonding and tension failures for CFRP laminates. In one of the tests, one of the two provided CFRP laminates first underwent a debonding failure, which consequently led to the overloading the remaining laminate; this finally failed in tension at a particular point where it bridged over a huge flexural crack within the beam.

(iii). The tensile strength was approximately the same for both the steel plate material and CFRP laminates. A comparison of maximum mid-span deflection results for 2G and BF2 beams tested from 2.2 m and 2 m drop height respectively was made. It was found that before the failures of the CFRP laminates, BF2 beam produced smaller deflection than 2G beam; however, after the failures of CFRP laminates, BF2 beam produced higher deflection (Erki & Meier, 1999).

Tang & Saadatmanesh, (2003), carried out an experimental study to investigate certain basic properties of RC beams strengthened with FRP laminates, such as cracking patterns and failure mechanism, dynamic response, deflection, and distribution of stresses. Five precast concrete beams of 95 mm deep, 203 mm wide and 1980 mm long were tested under impact loading. Each beam had two No 3 longitudinal steel reinforcing bars (ϕ 9.5 mm) and no shear reinforcements were needed as the span/depth ratio was quite large (about 20). Among those five beams, one unstrengthened beam was used as control beam, and the four remaining beams were strengthened on the bottom and top faces with FRP laminates. Two beams were strengthened with Kevlar laminates and the other two with carbon laminates. The following labelling was also adopted: TB1 and TB3 for beams strengthened with Kevlar laminate, TB2 and TB4 for beams strengthening with carbon laminates and TB5 for control beam. Due to the nature of impact loading which generates vibration, the bottom and top faces of the beams under testing would experience the unavoidable cyclic compressive and tensile stresses; thus, the FRP laminate material was glued on both faces. The surfaces of the beams and FRP laminates were adequately cleaned prior to bonding. The sandblasting technique used to clean various beams led to an uneven concrete surface; consequently, it was not practically possible to accurately measure the epoxy thickness. However, an average value of about 1.3 mm thickness of the epoxy adhesive was estimated. Figure 2.50 shows the test setup and placement of instrument.

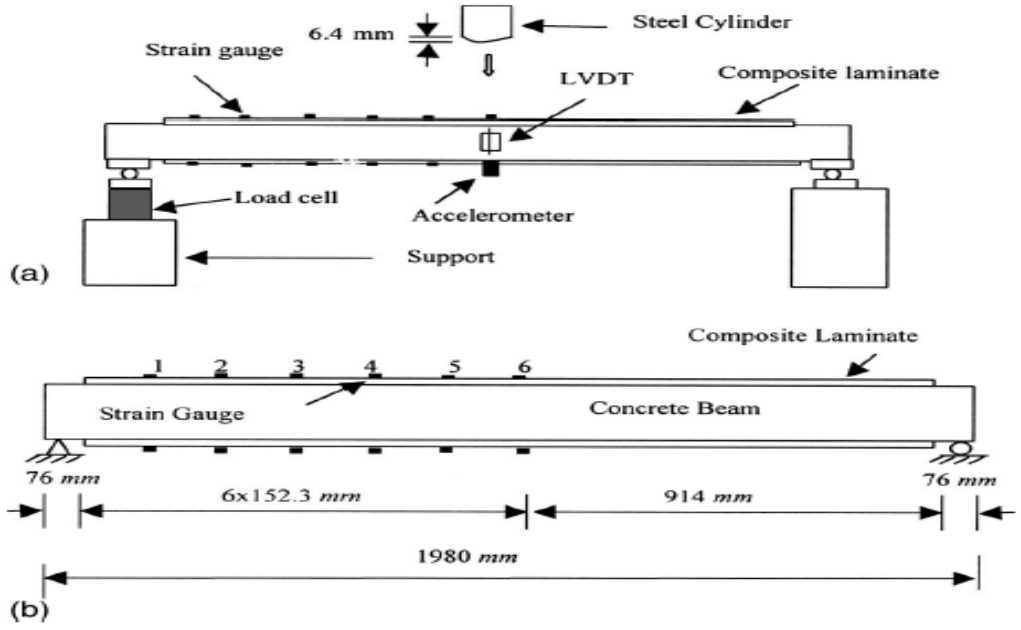

Figure 2.50. (a) Test setup; (b) placement of strain gauge (Tang & Saadatmanesh, 2003).

All tested beams through this experimental study were simply supported. Various beams had a tendency to jump and move away from the supports throughout the impact loading test, thus two 12.7 mm diameter coarse-threaded steel bars were used to adequately tie both ends of the beams to the supports. However, the beams were still be able to rotate during their drop testing. A 222N falling weight steel cylinder was used to induce the impact loading onto the mid-span of each beam from various specified drop heights. Some transducers well used to capture and measure various dynamic responses including LVDTs, load cell, accelerometers and strain gauges; see Figure 2.50. Two LVDTs placed in a parallel way on both sides at the mid-span of the beam to measure the deflection. Two accelerometers were used to measure the acceleration and they were adequately installed at the bottom side of the beam. Also, a load cell was used to measure the reaction force induced at one of the supports. Six strain gauges were mounted onto the FRP laminate at each face of the beam and used to monitor the longitudinal strains distribution alongside the bottom and top surfaces, see Figure 2.50. Finally, a dial calliper was used to measure the residual (permanent) deflection experienced in the mid-span of the beam during the impact loading test (Tang & Saadatmanesh, 2003).

The failure modes of various beams are shown in Figure 2.51. In addition, Figure 2.52 shows the maximum reaction force results from various beams. Reaction force at the support, in the first half-cycle measured by the load cell transducer, was made of two components. One of the components was related to the impact force directly caused by the falling weight steel cylinder; the other component was the inertia force generated by the vibrating motion of the beam. After the formation of the first half-cycle, it was noticed that the reaction force was only induced by the inertia force. In addition, the reaction force was found to increase as the dropping height was increased. Nevertheless the frequency of the vibration decreased as the dropping height increased, thereby the duration of the beam's vibration was also increased (Tang & Saadatmanesh, 2003).

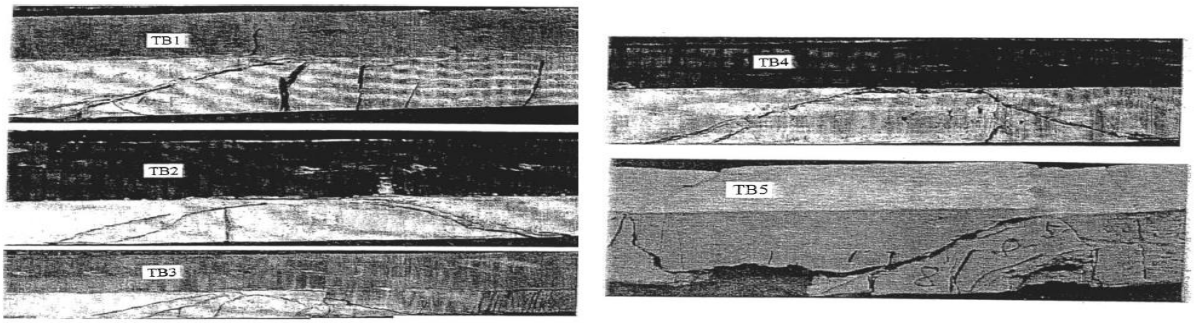

Figure 2.51. Failure modes observed from various beams (Tang & Saadatmanesh, 2003).

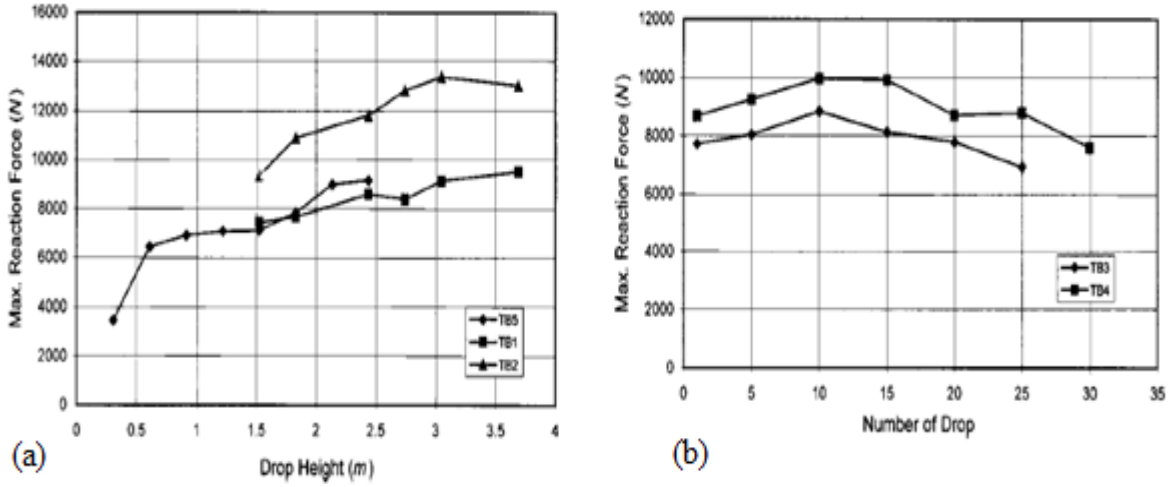

Figure 2.52. Comparison of the maximum reaction force at the supports for: (a) TB1, TB2, and TB5; (b) TB3 and TB4 (Tang & Saadatmanesh, 2003).

The average of the measured deflections from two LVDTs recorded at the mid-span of the beam was taken as its deflection measurement result. As the drop height was increased during the impact loading testing, the deflection was almost linearly increased for beam TB1, TB2, and TB5. Deflection predominantly depends on the stiffness of the beam under testing; therefore the stiffness of the beam is significantly reduced as the number of the performed drop tests increased (Figure 2.53). In fact, the timely change of the stiffness of the beam under loading mostly depended on the formed cracking and its profiles. Referring to Figure 2.51 above; the flexural cracks are formed on the bottom face of the concrete beam and propagated towards the top face, up to the neutral axis. As the FRP laminates were bonded onto both top and bottom faces of the beam, the direct observations of the bending cracks were not possible. The use of carbon and Kevlar laminates resulted in a significant reduction of the formed cracks. The reduction occurred for both the number of cracks and their widths. In RC structures strengthened with FRP laminates material, the deformation owing to the initial impact loading always differs from the deformation prompted by ulterior vibration of the structural member under study. For strengthened RC beams subjected to impact loading, three types of cracks were experienced. Flexural cracks were developed first, followed by shear (diagonal) cracks and final the longitudinal cracking appeared and took place in the bottom FRP laminate. Thus, the global deformation for this kind of RC beam comprises flexural, shear and bearing deformation in the impact loading zone. Generally, the mode of failure was the shear failure in companion with the local concrete crushing of onto the top face of the beam and delamination of the FRP composite material (Tang & Saadatmanesh, 2003).

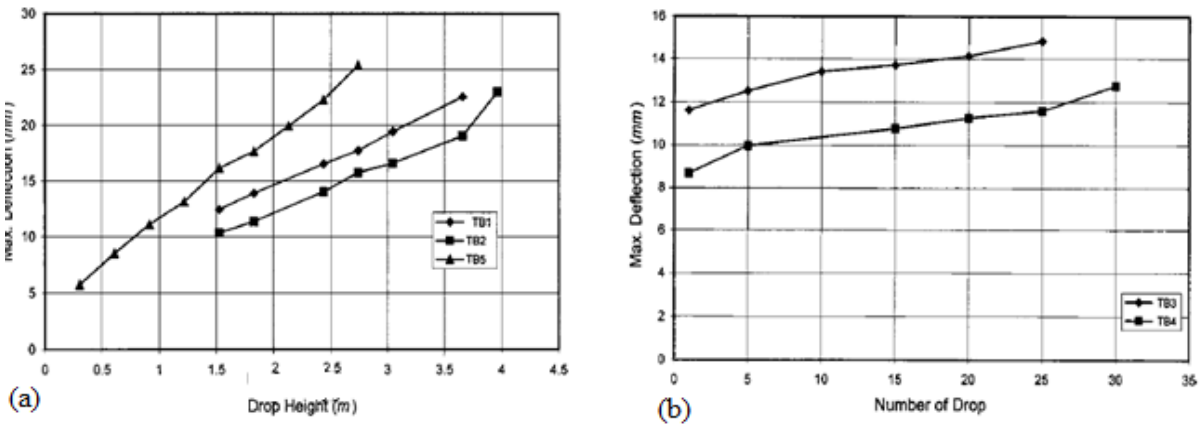

Figure 2.53. (a) The comparative analysis of maximum deflection results from TB1, TB2, and TB5 for different drop heights; (b) the comparative analysis of maximum deflection results from TB3 and TB4 for repeated impact load (Tang & Saadatmanesh, 2003).

According to Tang & Saadatmanesh, (2003), impact loading resulted in the cracking of the beam. At the particular instant when the beam ceased to vibrate, a part of the deflection of the beam could not recover. This type of deflection is normally termed as the residual or permanent deflection. The RC beam strengthened with FRP composite material was not perfectly elastic; and even through no visible cracks were noticed on the concrete face of the RC beam after the removal of the loading, some permanent deflection was still observed on various tested RC beams due to micro-cracking. Therefore, the permanent deformation depends upon to the impact energy, the properties of individual materials, the stiffness of the beam and the width and distribution of induced cracks. Figure 2.54 shows both individual and cumulative residual deflection results from various beams.

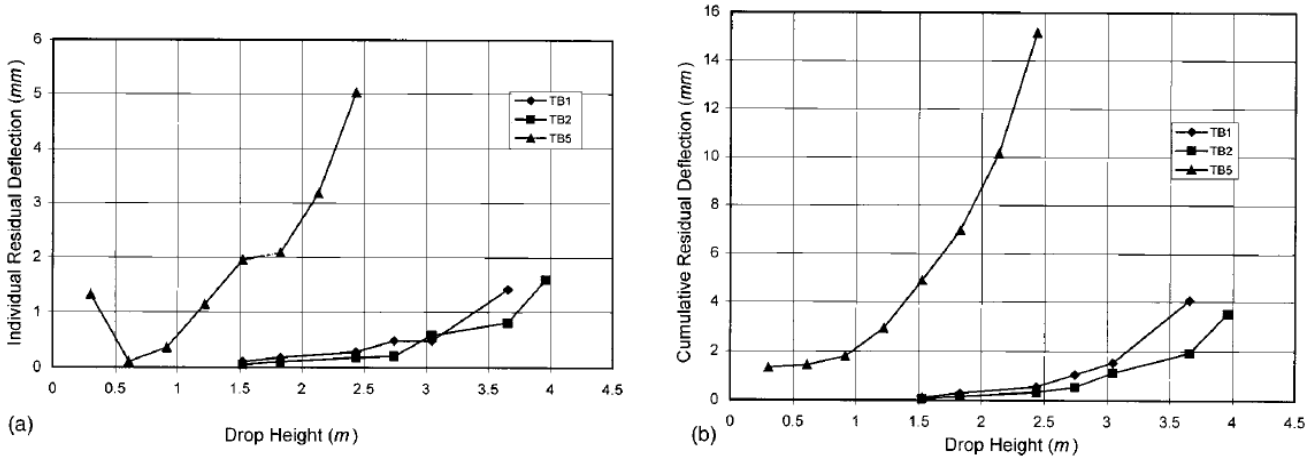

Figure 2.54. (a) Individual residual deflection results from TB1, TB2, and TB5; (b) cumulative residual deflection results from TB1, TB2, and TB5 (Tang & Saadatmanesh, 2003).

The following research conclusions can be extracted from the results of this experimental investigation:

(i). The FRP laminates considerably enhanced the capacity of the RC beams to withstand the impact loads and, consequently reduce the maximum deflection. The benefit in capacity depends not only on the type of the used FRP laminate but also on its properties such weight, thickness, and strength.

(ii). Dynamic response incited by impact loading should be regarded as inevitable considered as the strain generated by the inertia force was enough to induce the cracks into the concrete.

(iii). The stiffer carbon laminate significantly decreased the deflection. As a result of an increasing stiffness, the residual (permanent) was also reduced.

(iv). The suitable use of externally bonded FRP laminates to strengthen RC beams that are subjected to impact loading can be effectively recommended due to its ability to reduce both the width and number of cracks. FRP laminates can also enhance the shear strength of the beam under impact loads by restraining the widening of cracks (Tang & Saadatmanesh, 2003).

Dladla, (2014) and Mundeli, (2014) conducted respectively an experimental study and a numerical study on patch-repaired and FRP-strengthened RC beams under quasi-static loading conditions. For the validation of various numerical models, the emphasis was made on the behaviour of RC beams in terms of modes of failure, load deflections relations, crack pattern and ultimate loads (Mundeli, 2014). All mentioned key points were assessed under four point bending tests on 15 beams experimentally and 5 models numerically. According to Dladla, (2014), fifteen rectangular RC beams with the dimensions of 155 x 254 x 2000 mm were cast. Four sets of retrofitted beams and one set of control beams were tested under quasi-static loading. Each set was made of 3 beams. Sets of the retrofitted beams were formed on the basis of the patch-repair length. These retrofitted beams have a patch repair length of 450, 800, 1300 and 1800 mm respectively for the first, second, third and four set. The selection of the patch repairs lengths took into consideration the effect of principal stress behaviour of beams (Dladla, 2014). The grinding technique was used to simulated the effects of corrosion on deteriorating RC beams. It is not always possible to compare findings from a study performed under quasi-static loading conditions and the one done under consecutive impact loadings. Nevertheless, in

this study on the behaviour of FRP-strengthened RC beams, it was requested to reproduce the same beams as those tested under quasi-static loading conditions. Table 2.5 shows the comparison of debonding loads results from numerical and experimental studies. The results shown in this Table 2.5 are selected and used to compare findings obtained from quasi-static and consecutive impact loading conditions in this experimental research.

Table 2.5. Comparison between debonding loads (Mundeli, 2014).

RC beam type	FEM	Experiments
450 mm-Patched beam	226.2 kN	205±9.7 kN
800 mm-Patched beam	236.8 kN	212.8±12 kN
1300 mm-Patched beam	237.3 kN	193.8±17.7 kN
1800 mm-Patched beam	240.5 kN	210.5±11 kN

2.8. Chapter summary

RC beams are among the key members of any RC structure which is well designed, built, regularly monitored and maintained to fulfil its intended use. RC structures in service deteriorate due to many reasons including corrosion attacks on reinforcing steel bars, leading to the reduction of the rebar cross-sectional area. The latter also leads to the degradation of the structural performance. The deteriorating RC structures in service require appropriate remedial measures to reinstate their load-carrying capacity up to the acceptable performance level (Täljsten, 2006). Nevertheless, the repaired and rehabilitated RC beams are susceptible to further deterioration due to their possible exposure to the harsh environment and/or extreme loading conditions including impact loading. In line with this study, the following topics and subtopics have been reviewed:

(1). The deterioration of RC structures, and repair of corroded RC beams;

(2). FRP composite materials, and strengthening of RC structures;

(3). The effects of loading conditions on the behaviour RC structures including dynamic behaviour of RC structures under impact loading and high loading rate;

(4). Some of the past experimental studies conducted on RC beams under impact loading have also be reviewed and presented for both non-FRP-strengthened and FRP-strengthened RC beams.

Corrosion of the reinforcement steel is one of the main causes of deterioration of RC structures (Zhang, et al., 2010). A number of internal and external factors are involved in the deterioration of RC structures such as: the aging of the structure, environmentally induced degradation, poor initial design and lack of maintenance (Täljsten, 2006). One of the most common reinstatement methods for cracking, delamination and spalling damage is the removal of deteriorated concrete followed by the application of patch repair materials (Beushausen & Alexander, 2009). The repair process must successfully integrate new and old materials, forming a composite system capable of enduring exposure to service loads, environment and time (Vaysburd, 2006).

The rehabilitation and/or the strengthening of existing structures to correct deterioration-related damage, and increase structural load-carrying capacity or ductility has traditionally been performed using conventional techniques and materials (Setunge, et al., 2002). These conventional materials and techniques include (but are not limited) to steel plate bonding, jacketing systems, external prestressing among others. However, some drawbacks and shortcomings have been experienced on RC structures that have been strengthened using traditional/conventional techniques. Thus, the heavy weight of steel materials, corrosion attacks on steel, difficulties of forming joints and intensive labour for surface preparation are the major shortcomings and hinder the use of steel plate as a strengthening material (Nurbaiah, et al., 2010). In addition, the following disadvantages have been observed from jacketing systems: sometimes they are very expensive, time-consuming and need the inevitable interruption of use of the structure while works are being executed (Frangou, et al., 1995). Furthermore, when the important dead load is added to the strengthened structures, significant dimensions change and bulk formwork is needed. When steel jackets were installed and bonded with welding, the following drawbacks were experienced: (i) lack of analytical tool; (ii) time consumption; (iii) relatively high cost; (iv) adequately trained labourers are required and (v) specialised equipment and electric power supply required on site (Frangou, et al., 1995). Steel jackets are also prone to corrosion attacks. Moreover in prestressing method, (i) the external tendons are easily accessible (unlike their internal counterparts), which makes them more vulnerable to fire and sabotage; (ii) external tendons are usually subjected to vibrations and, consequently, their free length should be systematically limited to some extent and (iii) deviation and anchorage zones are mostly cumbersome additions to the cross section of the structure, these elements should be carefully detailed and adequately reinforced (Picard, et al., 1995). The FRP composite materials have been adopted as a strengthening material to overcome those aforementioned drawbacks and shortcomings, and others.

The FRP composite is one of the advanced composite materials normally applied in various including civil engineering, in which the reinforcing fibres are embedded in matrix resin to form a new material with desired properties. FRP composites generally offer many excellent properties in comparison to conventional/traditional materials such as aluminium and steel (Täljsten, 2006). High strength-to-weight ratio, corrosion resistance, low maintenance cost and general versatility of FRP materials make them more attractive and reliable for plate bonding applications (Quantrill & Hollaway, 1998). On contrary, a few drawbacks and shortcomings related to FRP strengthening are reported in literature such as debonding issues. Also, some of the factors that might adversely affect the mechanical properties of FRP strengthening materials are highlighted in literature: highly sensitive to damage from impact collision, ultraviolet radiation, temperature changes and fire (ACI Committee, 1996).

It is obvious that the mechanical properties of individual materials such as steel and concrete, are altered by changing rate of strain (Fu, et al., 1991). For RC structures and members under high loading rates, including dynamic and impact loadings, both concrete and steel are stress/strain rate sensitive: an increase in stress/strain rates would lead to an increase of the elastic modulus, and for both, an increase in the compressive and tensile strengths (Chen & May, 2009). In addition, with an increasing loading rate, the cracking stiffness, ultimate load resistance, and energy absorption of various RC beams were found to experience an increase (Adhikary, et al., 2012). Furthermore, under impact loading studies, the influence of the loading rate on concrete behaviour becomes such an important parameter that it must be inevitably considered in order to produce reasonable results (Cusatis, 2011).

The main differences between a quasi-static constitutive model and its dynamic counterpart for concrete material are precisely expressed by the need to truly understand inertia effects and the effects of strain rate, not only on the deformation, but also on the failure of the concrete target (Li, et al., 2005). Some of the experimental studies reviewed provide useful information to overcome one of the most challenging tasks in impact research which is the estimation of the true bending force (Soleimani, et al., 2007). Hence, by breaking down the forces involved in impact load testing and taking into account reaction force of the supports, the estimation of the true bending force and inertial force could be done (Bentur, et al., 1986; Soleimani, et al., 2007; Metz, 2007; Saatci & Vecchio, 2009; Soleimani & Banthia, 2014).

Fujikake, et al., (2009); Chen & May, (2009); and Kishi, et al., (2012) have carried out extensive studies on non-FRP-strengthened RC beams mostly using drop test machines. In their

studies, insights were provided onto properties and behaviour of RC beams under impact loading. Cracking patterns, displacements, and contacts forces results have been extracted and well analysed from the impact responses. Previously studies carried out on the FRP-strengthened RC beams subjected to impact loading (Erki & Meier, 1999; Tang & Saadatmanesh, 2003) are made on non-patch-repaired beams. However, it has been noticed that, currently, strengthening and rehabilitation projects combine both patch repairs and FRP materials as a solution to the deteriorating RC structures; therefore this research is conducted to assess the behaviour of patch-repaired and FRP-strengthened RC beams under extreme loadings such as impact loading. Dladla, (2014) carried out a research on patch-repaired and FRP-strengthened rectangular beams subjected to quasi-static loading conditions. A comparative analysis is made between the FRP debonding loads obtained from rehabilitated beams subjected to quasi-static loading and those subjected to consecutive impact loading. Moreover, (Mullajee, 2014) conducted a research on patch-repaired and FRP-strengthened T-beams; however, the impact loading was applied on the minor axis of the T-beams to simulate the behaviour of trucks hitting overhead bridges. The current research is conducted on rectangular beams where impact loading is applied on the major axis, that is, the load application is vertically above the various RC beams. The results of this research could be used to validate numerical studies conducted on patch-repaired and FRP-strengthened RC beams and also provide insights on the collision of road users such as vehicle accidents on flyovers, interchanges and overpass bridges.

CHAPTER 3: EXPERIMENTAL STUDY

3.1. Introduction

Fifteen RC beams were cast with the dimensions of 155 x 254 x 2000 mm. They were divided into five groups of three beams. The first group comprised unstrengthened RC beams as control beams. The other four groups comprised FRP-strengthened beams with concrete patch repairs of varying lengths. The patch repair length was 450, 800, 1300, and 1800 mm respectively for the second, third, fourth and fifth group. The grinding technique was used for all RC beams except the control beams, to induce the corrosion effects on steel bars in beams. Damaged RC beams were repaired with concrete-based patch repair materials in the corroded zones, then strengthened with FRP strips and tested under impact loading.

The present research is part of ongoing researches performed under the auspices of the Concrete Material and Structural Integrity Research Unit (CoMSIRU) at the University of Cape Town (UCT). The same number of beams with the same dimensions have been previously cast, tested and assessed under quasi-static loading conditions (Dladla, 2014). In practice, the FRP composite materials are generally used in association with concrete-/cement-based patch repairs to rehabilitate deteriorating RC structures and members, including beams. However, no researches had taken place on RC structures/members that are patch-repaired and strengthened with FRP composite. The behaviour of rehabilitated RC structures/members, subjected to different loading and environmental exposure conditions, is currently being investigated, both numerically and experimentally, through successive researches in CoMSIRU. The present study is an experimental research conducted on path-repaired and rehabilitated RC beams that are subjected to impact loading and it is unique for CoMSIRU.

Due to the complexity of the impact loading testing, all specimens were prepared in the CoMSIRU concrete laboratory at the Department of Civil Engineering. Thereafter they were transported and tested in the Blast and Impact Survivability Research Unit (BISRU) laboratory at the Department of Mechanical Engineering. BISRU has erected a drop testing machine where blast and impact testing take place, mostly for various mechanical engineering fields. Furthermore a blast room in which to conduct the falling impact load tests and an operations room are available and functioning well. A maximum of 5 m drop height and 1000 kg mass can be achieved and used to perform various experimental tests. The research approach is summarised and presented in Figure 3.1.

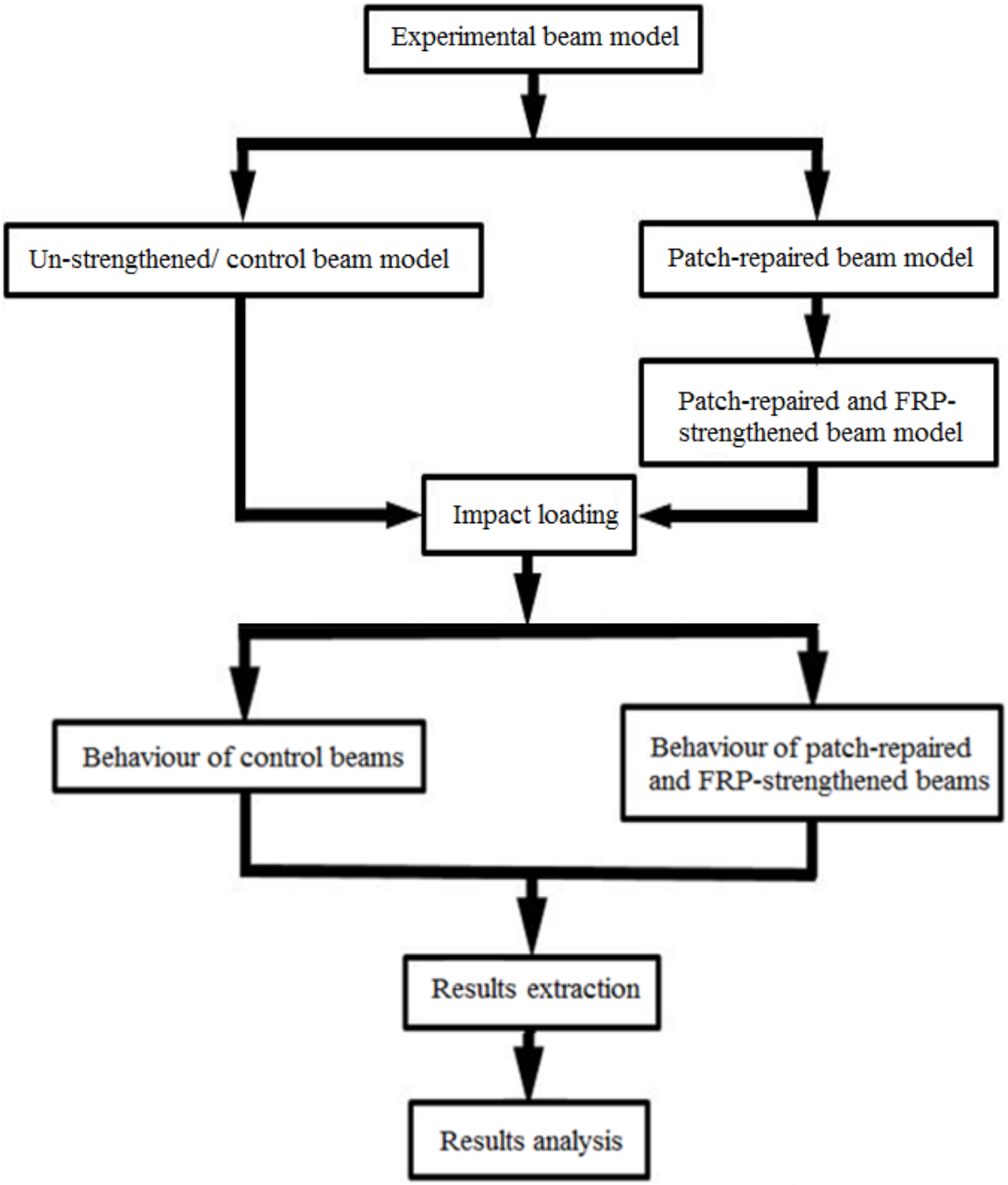

Figure 3.1. Research approach.

3.1.1. Specimen details

The reinforcement detailing and the dimensions of the experimentally tested beams are illustrated in Figure 3.2. As previously mentioned, fifteen RC beams (2000 mm long, 254 mm

deep and 155 mm wide) were cast and tested under impact loading. The main reinforcing steel bars were 20 mm diameter high-strength type and 8 mm diameter high-strength type compressive and shear reinforcing steel bars. A 12 mm diameter steel bar was shaped as a handle for lifting the RC beams from the moulds to the curing place, and from the concrete laboratory to BISRU laboratory. Furthermore, a constant spacing of 80 mm was provided between consecutive stirrups. All fifteen RC beams had the same size and they were cast with the same concrete mix proportions. In the case of damaged RC beams, these had the same damage depth and varying damage length.

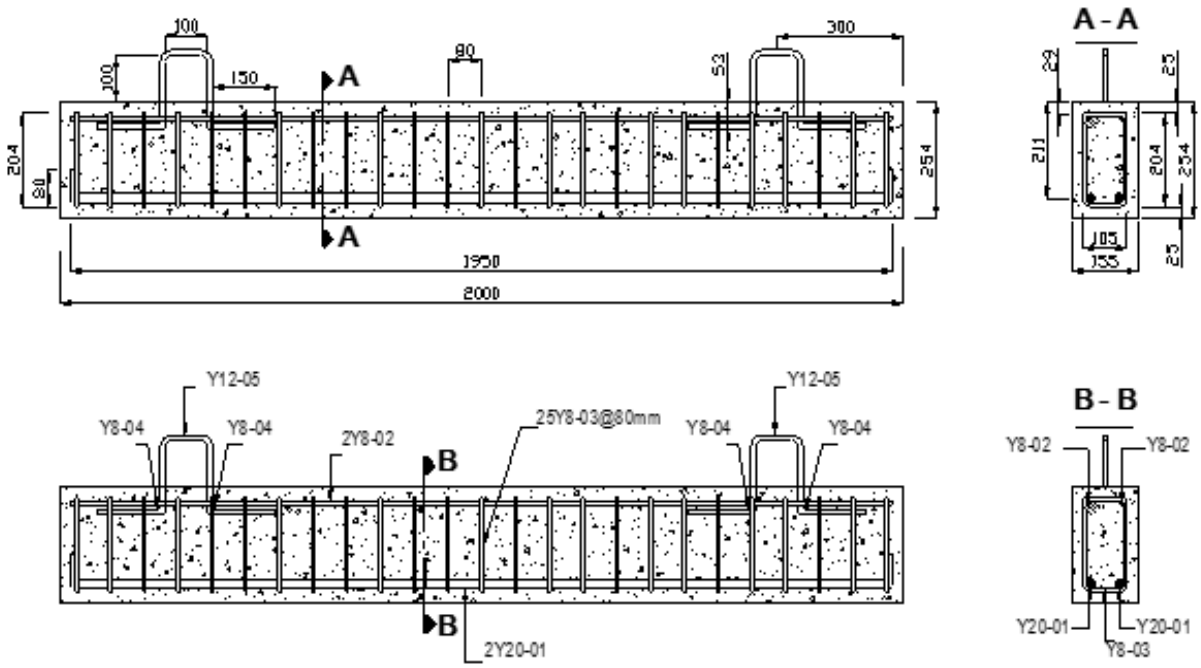

Figure 3.2. Reinforcement layout and dimensions details of RC beam specimens.

As previously mentioned in this research, there were five groups of beams and each group comprised three beams. The repair patch length was the milestone on which the build-up of these groups was based. Therefore the following code was adapted for easy identification of the different RC beams in the experimental test. Unstrengthened beams were used as control beams (CB); with the 450 mm damaged-length patch-repaired and FRP-strengthened beams (SB1), 800 mm damaged-length patch-repaired and FRP-strengthened beams (SB2), 1300 mm damaged-length patch-repaired and FRP-strengthened beams (SB3), and 1800 mm damaged-length patch-repaired and FRP-strengthened beams (SB4). In addition, a 1700 mm long FRP strip was used as a strengthening material for each damaged and patch-repaired RC beam.

3.1.2. Material properties

Various properties of the materials used in this research are presented. As previously mentioned, research of this type is ongoing, and therefore beams with properties similar to the ones previously tested by Dladla, (2014) in CoMSIRU were cast. In this present research, the same concrete mix design, the same patch repair material type and the same strengthening FRP strips type were used. However, due to the changes made by the cement factory which supplies cement to the above-mentioned research unit, the cement used in the previous study (CEM I 52.5N) was replaced by its equivalent (CEM II/A-L, 52.5N). The supplied Klipheuwel sand contained a lot of water due to rainfall, hence that sand was dried in an oven of 15^{o} C for two days in order to control the water content in the final mix (Figure 3.3). Table 3.1 is presented below to briefly illustrate the concrete mix constituent materials. The properties of reinforcing steel, the FRP strengthening and concrete patch repair materials were also tabulated and are presented later in this document.

Table 3.1. Concrete mix proportions per m^3.

Material	**Type**	**Mass (kg/m^3)**
Water	-	195.00
Cement	CEM II/A-L, 52.5 N	433.33
Coarse aggregate	Crushed Greywacke (19mm)	958.00
Fine aggregate	Klipheuwel sand	845.00
w/c ratio 0.45 60ml of admixture per 42 l concrete mixer		

Before casting of beams, a trial concrete mix was used to test the workability of the concrete by slump test method. A slump of 65mm was obtained, therefore, the admixture was used to achieve an average slump of 120 mm. Each beam was cast using same materials, as shown in Table 3.1. A group of three beams was cast at once a day, thus five days were spent on the casting of beams. Two 42 litre-capacity concrete mixers were used in the concrete laboratory at the University of Cape Town to produce the concrete which was cast into rectangular steel moulds four and a half meter long (Figure 3.4). The rectangular steel moulds were properly cleaned with pressurised air, assembled adequately using bolts, appropriately sealed with silicone and suitably oiled to allow an easy demoulding of beams and for future use.

Figure 3.3. Rectangular steel mould.

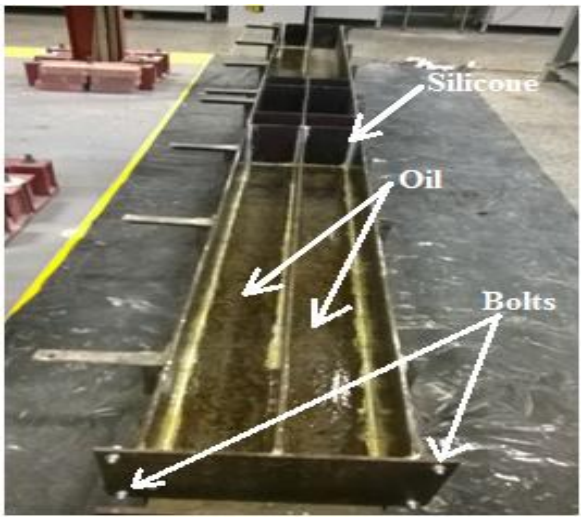

Figure 3.4. Drying sand in the oven.

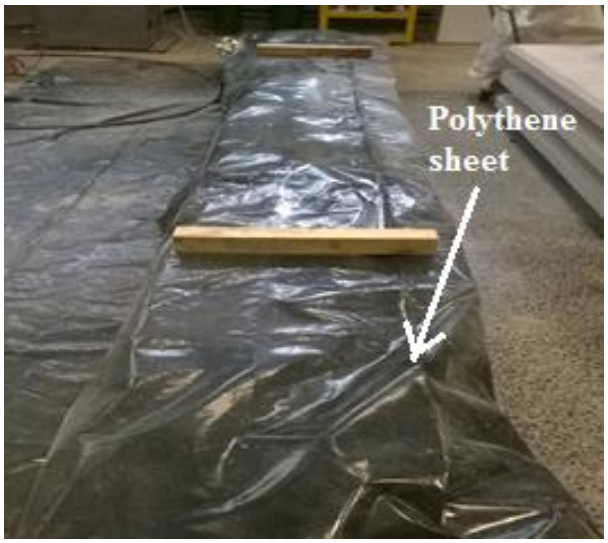

Figure 3.5. Curing of beams after demoulding.

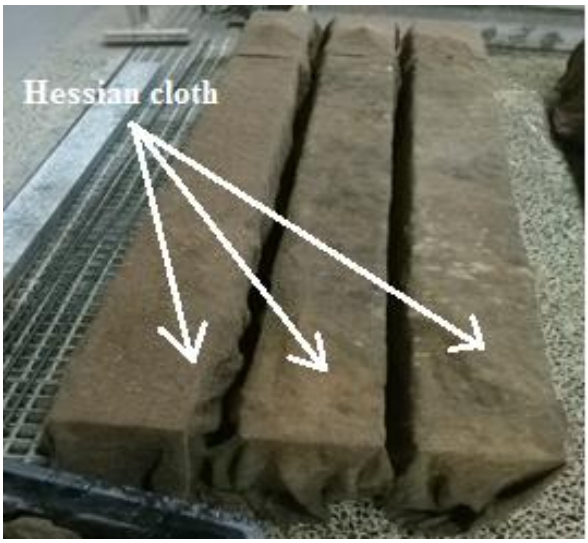

Figure 3.6. Covering of beams after casting.

The concrete was transported from the concrete mixers by wheelbarrows, placed into moulds using a shovel, mechanically compacted using a poker vibrator and levelled with a trowel. After casting, polythene sheets were used to cover the exposed surfaces of beams for three days. After those three days the beams were demoulded and covered with hessian cloth and cured for 28 days. Simultaneously for each batch of concrete, three cubes 100 x 100 x 100 mm size were also cast and cured under laboratory conditions during the 28-day period. Three cubes of the same size were cast for the trial mix and for patch repair material. The obtained compressive strengths of concrete are shown in Table 3.2. On the same Table 3.2, TM stands for trial mix;

PRM stands for patch repair material; and CB, SB1, SB2, SB3, and SB4 stand for various tested RC beams as previously described.

Table 3.2. Concrete compressive strength results.

Age (days)	Item	Cube Nº	Mass (kg)	Compressive Strength (MPa)	Average compressive Strength (MPa)
28	TM	1	2.435	54.20	54.27
		2	2.450	54.80	
		3	2.450	53.80	
	CB	1	2.405	54.00	54.77
		2	2.425	56.00	
		3	2.405	54.30	
	SB1	1	2.410	48.50	48.77
		2	2.460	48.50	
		3	2.390	49.30	
	SB2	1	2.405	59.00	57.00
		2	2.430	57.00	
		3	2.430	55.00	
	SB3	1	2.380	54.50	55.20
		2	2.400	58.40	
		3	2.380	52.70	
	SB4	1	2.380	60.80	58.80
		2	2.340	61.00	
		3	2.400	54.60	
14	PRM	1	2.330	68.20	69.80
		2	2.340	71.20	
		3	2.360	70.00	

The targeted compressive strength of the concrete used to cast all RC beams was 50 MPa according to the foregoing research done.

The documented engineering properties of South African reinforcing steel, and patch repairing and strengthening SIKA materials were summarised respectively in the following Tables 3.3 and 3.4.

Table 3.3. Properties of reinforcing steel (Dladla, 2014).

Size of steel (mm)	Yield strength (MPa)	Ultimate strength (MPa)
20	502	630
8	250	-

Table 3.4. SIKA patch repair and FRP strengthening materials.

Property \ Type	Sikadur-32N (N/mm^2)	Sikacrete-214 (N/mm^2)	Sikadur-30 (N/mm^2)	Sika CarboDur S512 (N/mm^2)	Sikadur-330 (N/mm^2)	SikaWrap-230C (N/mm^2)
Compressive strength @ 14 days & 10°C	42	-	-	-	-	-
Flexural strength @ 14 days & 10°C	42	-	-	-	-	-
Tensile strength @ 14 days & 10°C	25	-	-	-	-	-
E-modulus: Tensile	4000	-	-	16500	234000	-
E-modulus: Flexural	3600	-	-	-	-	-
E-modulus: Compressive	3250	-	-	-	-	-
Compressive strength @ 7 days	-	55	-	-	-	-
Flexural strength @ 7 days	-	5.7	-	-	-	-
Tensile strength @ 28 days	-	5.5	-	-	-	-
Compressive strength @ 7 days & 10°C	-	-	70-80	-	-	-
Shear strength @ 7 days & 15°C	-	-	14-17	-	-	-
Tensile strength @ 7 days & 15°C	-	-	24-27	-	-	-
E-modulus: Compressive @ 23°C	-	-	9600	-	-	-

E-modulus: Tensile @ 23ºC	-	-	11200	-	-	-
Tensile strength	-	-	-	3100	4300	-
Tensile strength @ 7 days & 23ºC	-	-	-	-	-	30
E-modulus: Flexural @ 7 days & 23ºC	-	-	-	-	-	3800
E-modulus: Tensile @ 7 days & 23ºC	-	-	-	-	-	4500

The used FRP strip strengthening materials Sika CarboDur S512 was 1.2 mm thick, 50 mm wide and 1700 mm long; the FRP sheet SikaWrap-230C was 0.128 mm thick, 165 mm wide and 665 mm long and used on both ends of the Sika CarboDur S512. The anchorage of RC beams using FRP sheets was done both ends of FRP strip.

3.1.3. Damage procedure

The combined action of the effects of corrosion attacks and extreme loading conditions (including impact loading), which RC structures are exposed during most of their service life, generally leads to structural deterioration of those RC structures. It is therefore necessary to rehabilitate the deteriorating RC structures. Corrosion of steel bar is one of the major causes of degradation of RC structures, even if it is a slow process. There are various effects of corrosion on RC structures in service, both direct and indirect. The direct effects of corrosion attacks on steel include weak interfacial layer forming between corroded steel and its surrounding concrete matrix, loss of the rebar section and volumetric expansion of corroded steel. Among other direct effects, only the loss of the rebar section was taken into consideration in this present research.

Over time, the naturally slow process of corrosion has extremely negative effects on RC structures in service; however for the purposes of research, the corrosion process is accelerated by various methods and techniques. Examples of these are the impressed current technique, impressed voltage technique, macro-cell corrosion technique, artificial climate environment technique, accelerated AC impedance technique, and electrically accelerating chloride ions diffusing technique (Ahmad, 2009). Due to the time required to effectively apply the different accelerated techniques, the grinding technique was adopted in this study to simulate the effects

of corrosion on RC structures that is, reduction of rebar section. Various damage lengths were induced in the RC beams, including the creation of concrete-free volume in association with the reduction of the steel bars section in the same region for the said RC beams. The concrete-free volume was filled with polystyrene material before the RC beams were cast. According to previous research carried out on similar beams by the same research unit, different damage lengths were selected, based on the principal stress behaviour of the beams under study.

Simulated corrosion effects i.e. reduction of the diameter of the rebar.

In this study, the effects of corrosion were simulated using the grinding technique to create a damaged zone by reducing the main steel bars up to 14% of their initial diameter size. The reduction of the rebar section in relation to the reduction in flexural strength of RC beams, therefore FRP strengthening was needed to restore the flexural capacity of those RC beams. Nevertheless, the percentage of the rebar section reduction was reported to be 5% in the foregoing researches conducted on the same sized RC beams that had been patch-repaired and strengthened with a similar composite material. However, as previously mentioned, every conducted research conducted took into account its particular loading conditions. The lost area of the rebar, using the grinding technique, is calculated below, and shown in Figure 3.7.

To achieve 5% reduction of cross-sectional of the rebar, the ground depth of the steel bar was determined as follows:

With A_s = Rebar cross-sectional area

$r^2 = x^2 + y^2$; Equation of circle centred at the origin $(0,0)$ ……(3.1)

$$y = \pm\sqrt{r^2 - x^2} \quad \text{……..(3.2)}$$

$$A_1 = 2\int_0^q \sqrt{r^2 - y^2}\, dy \quad \text{……...(3.3)}$$

$$= r^2 \arcsin\left(\frac{y}{r}\right) + y\sqrt{r^2 - y^2}\Bigg|_0^h$$

$$= r^2 \arcsin\left(\frac{h}{r}\right) + q\sqrt{r^2 - h^2} \quad \text{……...(3.4)}$$

With A_{lt} = Area of steel bar lost due to grinding

$$= \frac{A_s}{2} - A_1 \quad \ldots\ldots (3.5)$$

Substitute equation 3.4 into equation 3.5

$$A_{lt} = \frac{A_s}{2} - r^2 \arcsin\left(\frac{h}{r}\right) - h\sqrt{r^2 - h^2} \quad \ldots\ldots (3.6)$$

Rearrange equation 3.7

$$\frac{A_s}{2} - A_{lt} = r^2 \arcsin\left(\frac{h}{r}\right) + h\sqrt{r^2 - h^2} \quad \ldots\ldots (3.7)$$

Consider $r = 10mm$ and $A_l = \frac{A_s}{20} = 5\%$ loss of rebar section and substitute into equation 3.7 gives

$$\frac{A_s}{2} - A_{lt} = r^2 \arcsin\left(\frac{h}{r}\right) + h\sqrt{r^2 - h^2}$$

$$\frac{A_s}{2} - \frac{A_s}{20} = 100 \arcsin\left(\frac{h}{10}\right) + h\sqrt{100 - h^2}$$

$$\frac{9}{20} A_s = 100 \arcsin\left(\frac{h}{10}\right) + h\sqrt{100 - h^2}$$

$$141.372 = 100 \arcsin\left(\frac{h}{10}\right) + h\sqrt{100 - h^2}$$

Solving for h, with $A_S = \pi r^2 = 100\pi = 314.16mm^2$

$\therefore h = 8$, therefore

$\therefore r - h = 10 - 8 = 2mm$ Grinding depth.

In this present research, the 14% rebar cross-sectional corresponding to a grinding depth of 4mm was selected based on the classification of induced degree of corrosion in a study carried out by Masoud, et al., (2005). This considered percentage of 14% was classified as severe corrosion, according to those aforementioned authors, and it was reported to have considerable effects on the flexural capacity of deteriorated RC beams.

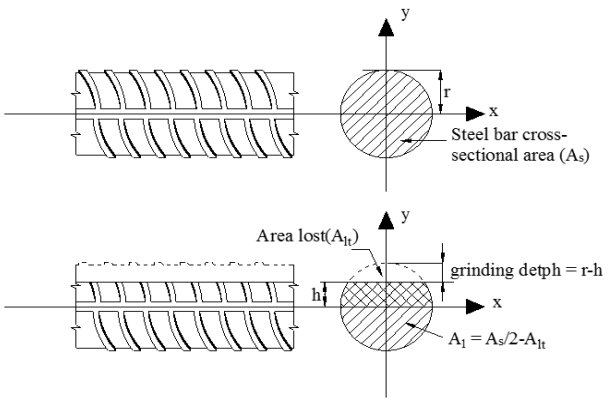

Figure 3.7. Reduction of the steel bar cross-sectional area with grinding technique.

A 4 mm depth was ground-off from the cross-sectional area of main steel bars. The grinding of rebar was kept constant for all RC damaged beams, nevertheless, the ground length varies according to the damaged length of RC beams under study. Furthermore, the damaged lengths are 450, 800, 1300 and 1800 mm respectively, and were equal to the length of reduced rebar cross-sectional area.

Induced damage with varying patch length

In order to induce damage into different RC beams, the polystyrene material was used into the area reserved to receive the patch repair before casting of those RC beams. The depth of that polystyrene material was 105 mm for all RC beams while its length varies proportionally to the length of the damage. Various damaged areas reserved for receiving concrete patch repairs were shown in Figure 3.8, Figure 3.9, Figure 3.10 and Figure 3.11 respectively.

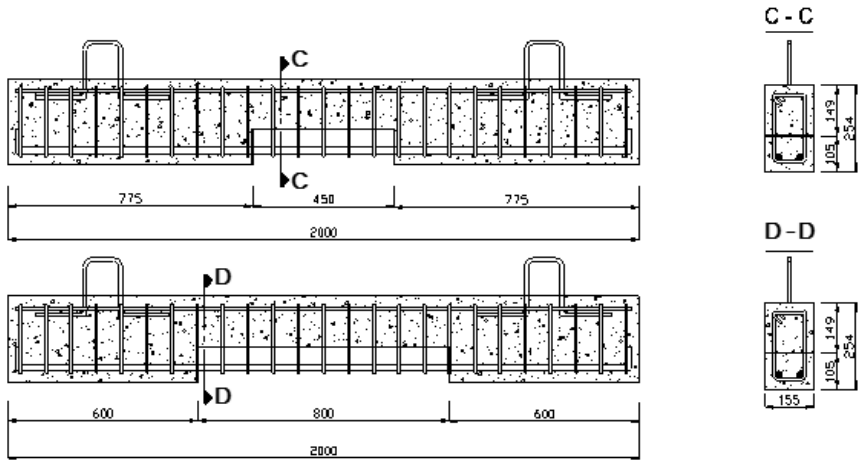

Figure 3.8. 450 & 800 mm long damaged areas reserved to be patch-repaired.

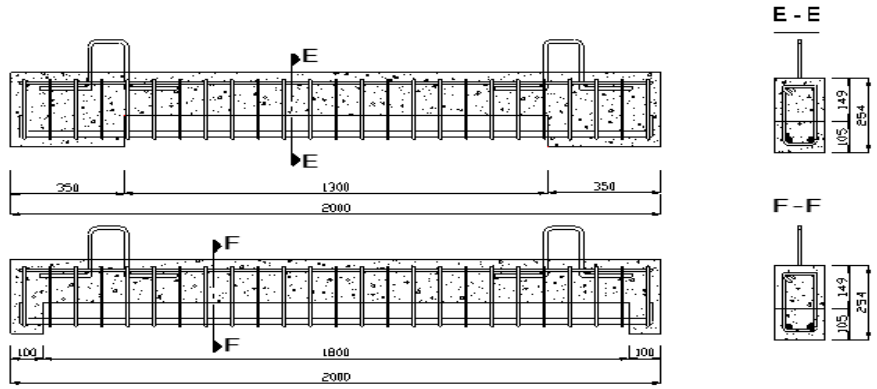

Figure 3.9. 1300 & 1800 mm long damaged areas reserved to be patch-repaired.

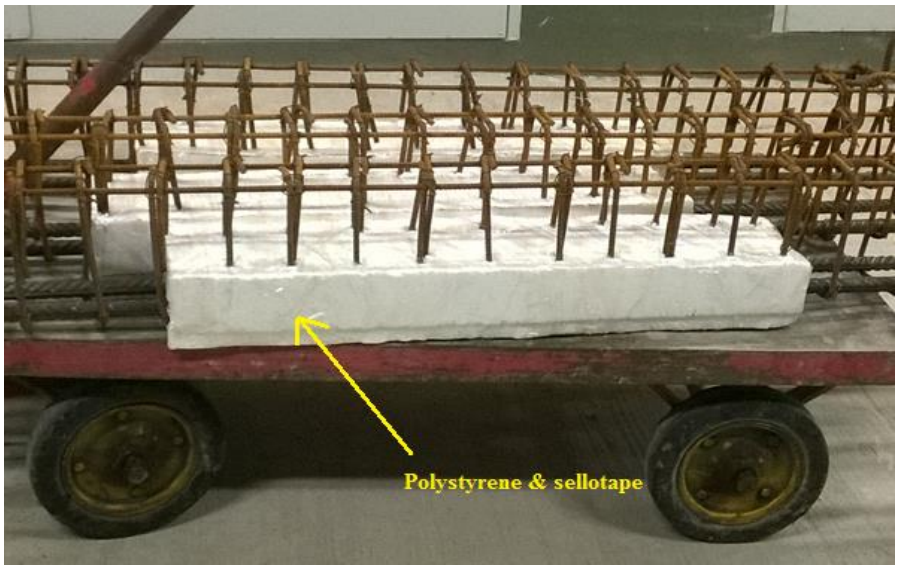

Figure 3.10. Polystyrene material placed into the damaged area and fixed using a sellotape before casting of RC beams.

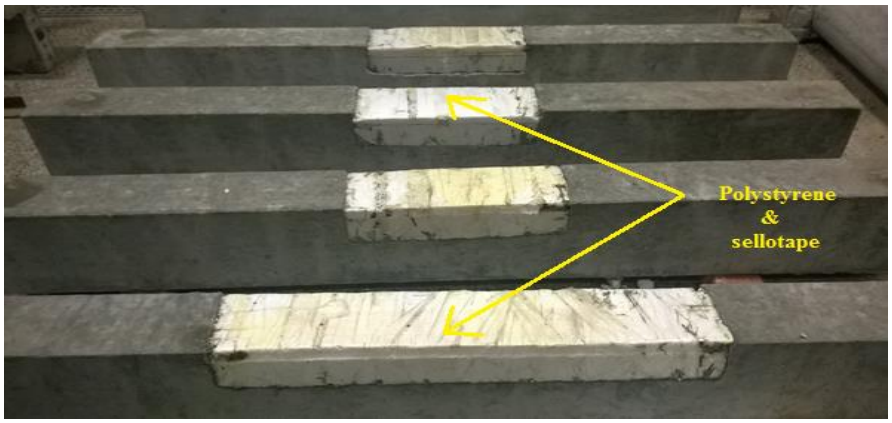

Figure 3.11. Polystyrene material placed into the damaged area and fixed using a sellotape after demoulding of RC beams.

3.2. Repair process

The versatility and successful use of reinforced concrete in different daily activities of a human being, and particularly in construction industry, make concrete the most-highly used man-made material in the world; approximately 12 billion of tonnes are manufactured annually (Broomfield, 2007). Generally, the RC structures in service fulfil their desired and expected functions; however, in some cases, they are exposed to harsh environmental and extreme loading conditions which may lead to the premature failure of those RC structures. It is necessary to effectively maintain and rehabilitate deteriorating RC structures to ensure their continuous safe use at reasonable cost. It has been reported by various asset managers, engineers and researchers that patch repairs in association with FRP composite material, properly address the deficiencies of RC structures especially for localised damage zones. In addition, this type of repair system protects the rehabilitated RC beams against further corrosion attacks or at least mitigate the easy spread of the corrosion into the same RC structures.

In this present research, patch repair was applied to twelve damaged RC beams using Sikacrete-214. After adequate preparation of the damaged area within the RC beams, the free flowing structural repair concrete was sprayed into the above-mentioned zone and levelled with a trowel. Moreover, two hours after casting, curing was started using hessian cloth and this lasted for a period of 14 days, to ensure enough strength before the FRP strengthening application and later the impact loading testing. All repair works were executed by smoothly following the standards and specifications as described and explained in the Sika South Africa (Pty) Ltd. product manual.

3.2.1. Repair preparation and execution

The repair work combined both patch repair and FRP strengthening composite materials to successfully extend the intended service life of RC beams. A series of consecutive activities were performed to effectively and timely accomplish patch repair and FRP strengthening of the rehabilitated RC beams.

Patch repairing preparation and application

After a 28-day period of curing, the polystyrene material was removed from the damaged area of the RC beams. Due to the presence of the sellotape material wrapped around the polystyrene material, an interface with a bright, smooth and hard top surface (similar to ceramic material) was created underneath the concrete. Two sequences of drilling works were done, using two different portable electric drills on the previously created interface, in order to make it rough enough to take the concrete patch repairs (Figure 3.12). The first drilling session was carried out using a relatively large electric drill with a large drill bit, while the second drilling session was conducted using a small portable electric drill with a smaller sized drill bit. The damaged area of the steel bars, including the previously ground rebar, were cleaned with a wire brush and all rust deposits were removed. After a suitably rough surface was achieved, the surface was properly cleaned with pressurised air and later dampened thoroughly with a wet hessian cloth. Both sides of the damaged area of RC beams were supported by a wooden batten and tied together with triangular bent steel clamps (Figure 3.13). In addition, before pouring the patch repair material into the damaged area, silicone material was used to properly seal and fill any empty spots which might be between the wooden battens and the prepared RC beams.

The adequately treated substrate surface was coated with 2 mm thick structural bonding adhesive layer Sikadur-32N, the correct type for bonding fresh concrete to an existing concrete substrate (Figure 3.13). After the three steps, the mixed Sikacrete-214 was poured into the formwork while the adhesive was still tacky. The self-compacting concrete was levelled at the top end of the patch-repaired RC beams (Figure 3.14). Two hours later, the patch-repaired RC beams were covered with hessian cloth to begin the 14-day curing process.

Figure 3.12. Roughen the substrate.

Figure 3.13. Interfaces & formwork preparations.

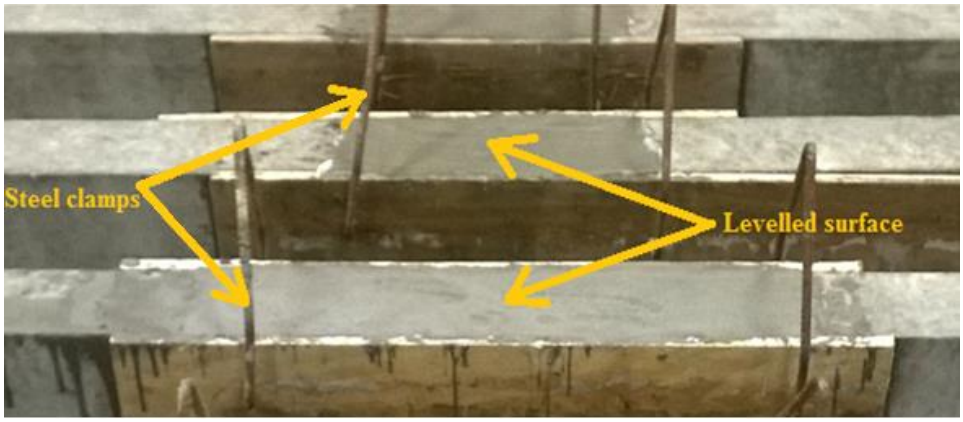

Figure 3.14. Self-compacting concrete patch repair placing and levelling with a trowel.

FRP strengthening preparation and application

After 14 days of curing the patch-repaired RC beams, the bottom surface (reserved to receive the FRP strip) was properly cleaned of all loose material. It is important to note here that FRP composites are not only used as a strengthening material but also as a repair material. According to Soudki, (2011), the external application of FRP composites on deteriorated RC beams allows one to restore and/or increase flexural capacity; reduce the rate of further corrosion attacks and effects by acting as low permeability barrier for future ingress of water and oxygen into concrete; and maintain the bond strength of the rehabilitated RC beams by increasing their external confinement, particularly when FRP sheets are used as wraps.

Figure 3.15. Applicator tool for spreading the bonding adhesive on the concrete substrate.

Therefore, a 2 mm thick adhesive Sikadur-30 type was used to externally bond the FRP strip onto the well-cleaned and prepared concrete substrate. All FRP bonding agents were mixed properly with respect to the time specified by their manufacturing industry until the predicted colour of the mixture was obtained. All uneven surface were levelled using Sikadur-30 FRP bonding agent and the bonding agent was applied with the provided applicator tool (Figure 3.15), enabling us spread constant thickness of the FRP bonding adhesive onto the concrete substrate. One 1700 mm long FRP strip (Sika Carbodur S512) was applied to the prepared surface of each rehabilitated RC beam. At both ends of the FRP strip, a 165 mm wide SikaWrap-230 FRP fabric was used to anchor the FRP strip onto the patch-repaired area of the RC beams. The FRP sheet was wrapped up at both ends of the FRP plate by using a 2 mm thick Sikadur-330 adhesive. The dimensions and details of the FRP strengthening and patch repair materials are summarised and presented in Table 3.5.

Table 3.5. Description of patch-repaired and FRP-strengthened RC beams.

Beam type	FRP strengthened RC beams characterisation											
	Patch length (mm)	Patch height (mm)	Patch width (mm)	FRP strip size (mm)			FRP sheet size (mm)			Adhesive layer thickness (mm) for		
				t	w	L	t	w	L	Patch repair	FRP strip	FRP sheet
SB1	450	105	155	1.2	50	1700	0.128	165	665	2	2	2
SB2	800	105	155	1.2	50	1700	0.128	165	665	2	2	2
SB3	1300	105	155	1.2	50	1700	0.128	165	665	2	2	2
SB4	1800	105	155	1.2	50	1700	0.128	165	665	2	2	2

Figures 3.16 and 3.17 illustrate respectively a typical patch-repaired and FRP-strengthened RC beam. Apart from control beams, other RC beams were patch-repaired and strengthened using CFRP composite materials in this current research. Immediately after strengthening work, all tools were cleaned with recommended Sika products. Both control and rehabilitated RC beams were painted white before testing in order to have an easy visualization of their deformation while testing. This was particularly important for their damage progression, including cracking patterns.

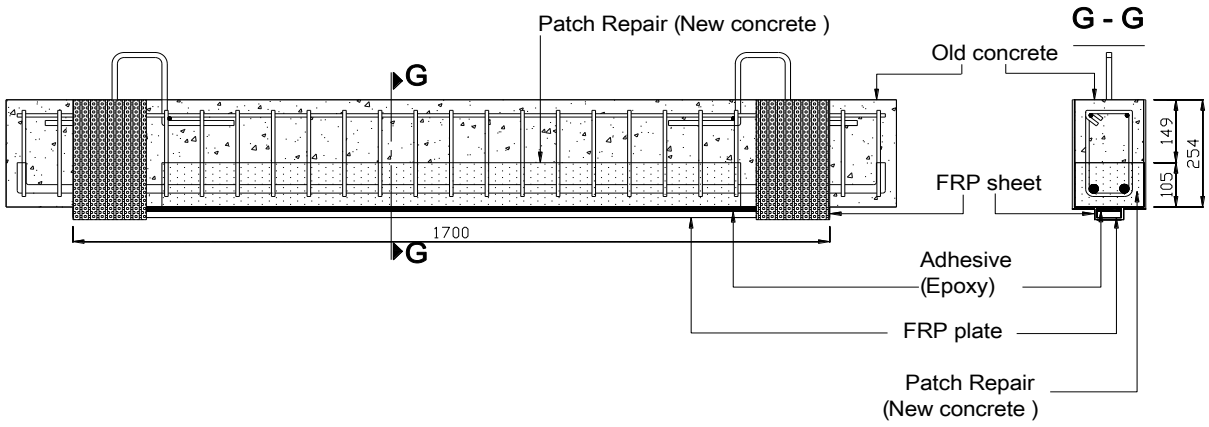

Figure 3.16. Typical patch-repaired and FRP-strengthened RC beams.

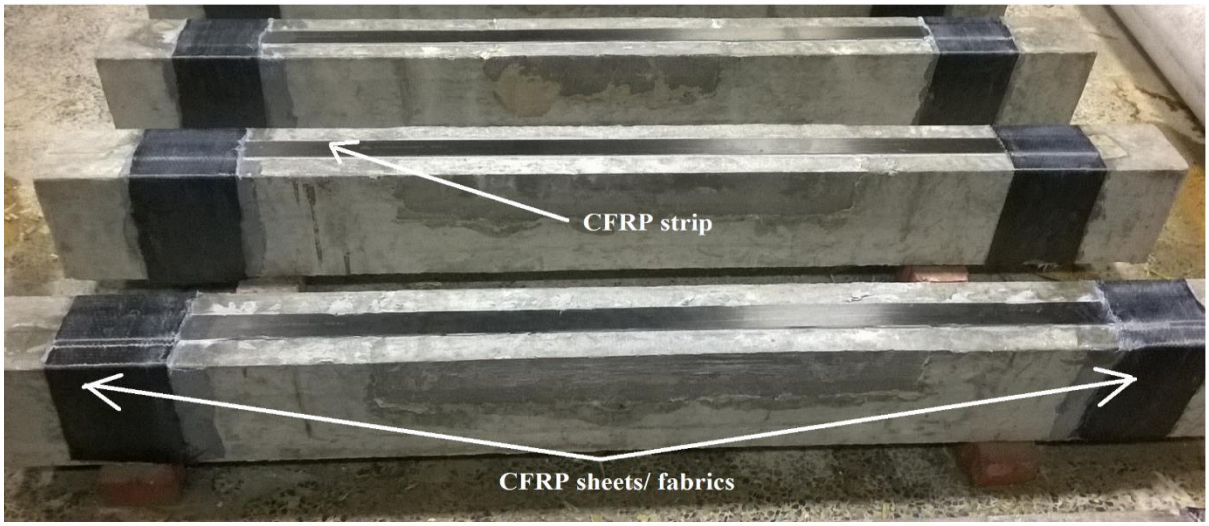

Figure 3.17. CFRP strengthening of various RC beams.

3.3. Testing procedure

A typical drop weight machine, located at the UCT Mechanical Engineering Department, had been modified for testing RC T-beams, and this was modified for a second time to be used for testing rectangular RC beams in this present research. After completing the patch-repairing and FRP strengthening works of the deteriorated RC beams, these rehabilitated RC beams were testing under impact loading. The impact load was applied at the mid-span of a simply supported RC beam (specimen) and it was applied consecutively with respect to varying drop

heights. The appropriate supporting system consisted of heavy steel pedestals at the bottom which were bolted to the strong floor, and a clamping system at the top. This prevented the lifting action of the specimen (RC beam) generated by developed inertial effects, followed by vibrations induced by impact loads. The clamping system had round steel bars at both sides (top and bottom) which allowed specimens to rotate without creating restraint moments at the support that is, a simply support conditions system (Figure 3.21).

The measured and recorded parameters relating to the structural responses of the tested RC beams include the contact force response and beam deflection response. In addition, the entire sequence was recorded with a high-speed camera (HSC), and thus, the progression of damage resulting from consecutive impact loading could be observed and assessed. Figure 3.18 describes the positioning of a RC beam during the drop test. Each beam was tested in the following dimensions: 1485 mm clear span and 257.5 mm overhanging on both sides of the supports. The position of the striking head of the drop weight machine was indicated with an arrow at the top side of the beam in its mid-span.

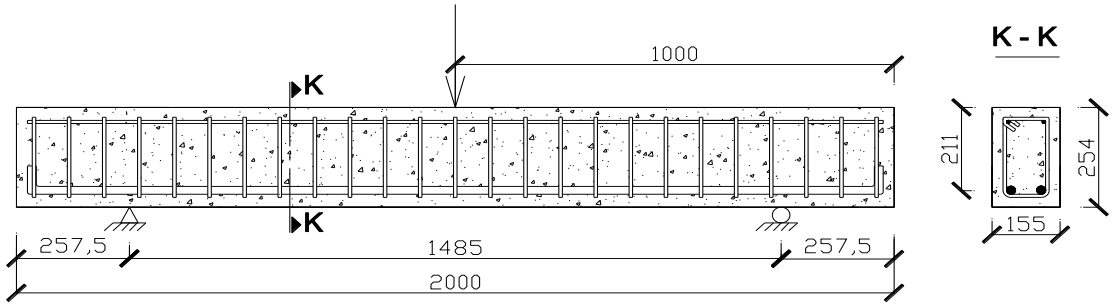

Figure 3.18. Specimen dimensions and positioning of the end supports during the drop test.

3.3.1. Data acquisition system and instrumentation

In this study, two different transducers were utilised (featuring a load cell attached to the impact hammer), along with Photron-ultima APX-RS high-speed camera to record and store the structural responses from different RC beams as they were subjected to the impact loading tests. Figure 3.19 shows the data acquisition system. A 200 kN load cell transducer capacity was used at a sampling rate of 20000 Hz to record the contact forces. A HSC with a resolution of 18000 frames per second (fps) and 512 x 256 pixels has been used at a sampling rate of 20000 Hz to record the impact loading scenario.

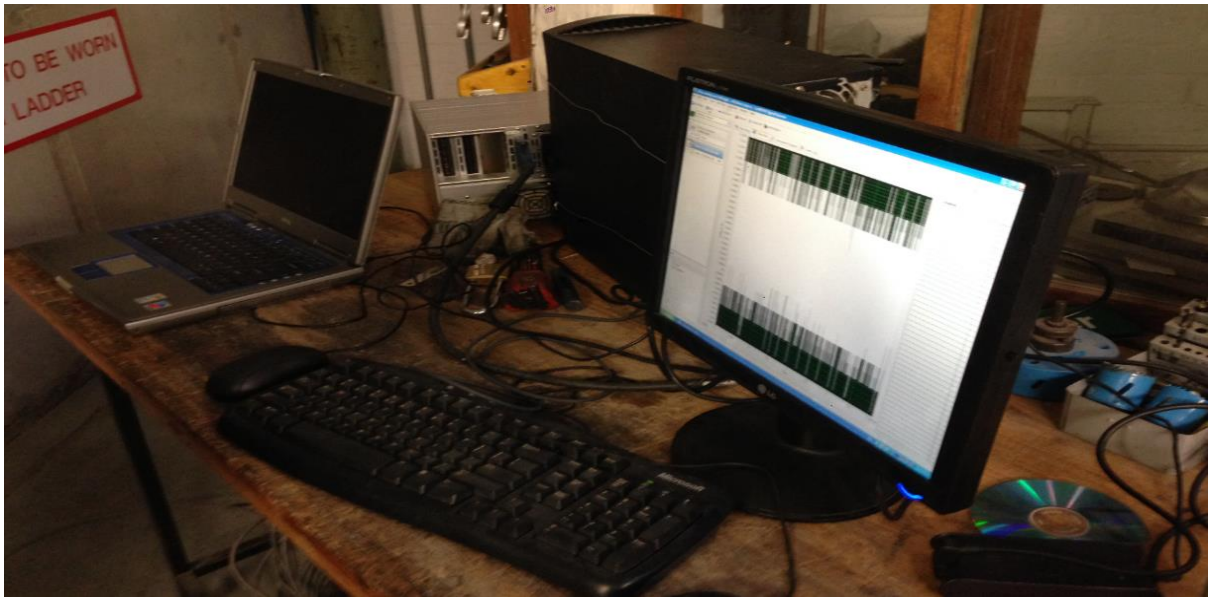

Figure 3.19. Data acquisition system.

The data acquisition system consisted of a load cell transducer connected to personal computer via a signal conditioning module (package) in combination with the virtual instrument software produced by National Instruments Corporation (NI). This was used to record and store the contact force response. A HSC connected to a laptop computer in combination with Photron FASTCAM Viewer (PFV) software was used to record the entire impact loading event in order to gain insight into the progression of damage, including the cracking patterns and mode(s) of failure, and also to eventually extract deflections at points of interest.

3.3.2. Impact loading testing

Prepared and ready RC beam specimens were put into place and tested under impact loading using drop weight machine. A drop hammer with a recorded mass of 332.403 kg was dropped onto the top of the specimen at its mid-span and from different heights. The striking impact hammer was 170 mm square, and it had a hemispherical shape with 500 mm radius (Figure 3.20). The striking hammer was modified to fit the rectangular RC beams, as it had been manufactured to be used on T-beams.

In order to monitor and assess the behaviour of patch-repaired and FRP-strengthened RC beams under consecutive impact loading with relatively low velocity, the following drop heights (h): 150 mm, 300 mm, 400 mm, 500 mm , 600 mm, 700 mm, 800 mm and 1000 mm were selected. The contact force, the progression of damage including cracking patterns and mode(s) of

failure, and resulting deflection response were recorded from the aforementioned drop heights. All data were collected through appropriate data acquisition system as previously mentioned and presented. Furthermore, Matlab software and Photron FASTCAM Analysis (PFA) software were used to analyse recorded and collected data. Figure 3.21 shows impact loading testing setup with a beam in position.

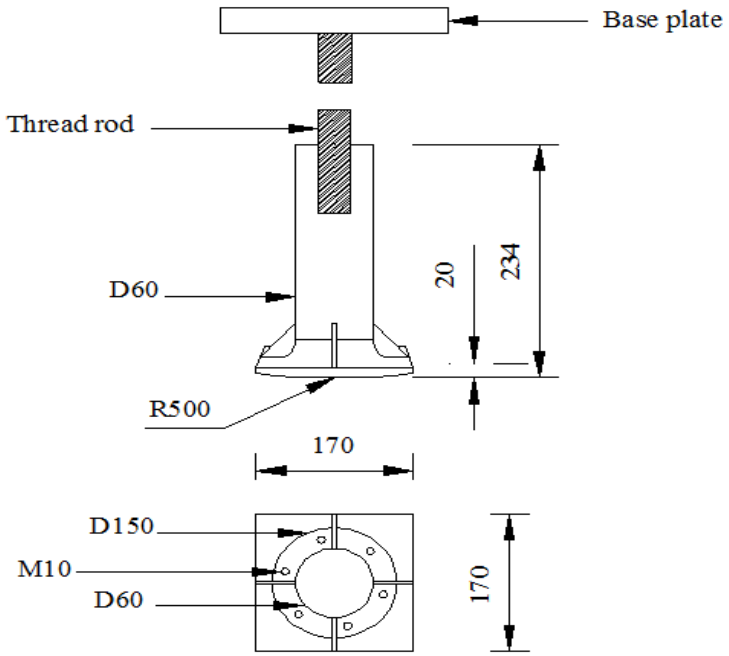

Figure 3.20. Modified striking impact hammer.

One of the most challenging tasks for impact researchers is to be able to estimate the true bending force (Soleimani, et al., 2007). The following procedure was proposed to overcome this challenge:

(i). Use of PFA software to extract displacement data from the HSC footage at the mid-span of each tested RC beam ;

(ii). Use of Matlab software (especially the curve fitting technique) to extract the displacement function from displacement results;

(iii). Double differentiation of the displacement function to obtain the acceleration function with the use of Matlab software;

(iv). Use of the acceleration function together with the properties of the tested RC beam (density, cross-sectional area, clear span and overhanging length) and compute the inertia forces in excel spreadsheet (refer to equation 2.11);

(v). The true bending forces could be obtained by subtracting the inertia forces from the contact forces recorded by using a load cell. The bending forces can also be computed based on the ratio of the drop height to the associated maximum deflection (refer to equation 2.21).

Furthermore, a target point was chosen in mid-span of the tested RC beam within the HSC footage. The full project that is, three-step process, prior to the extraction of the displacements response was then done with PFA software. The chosen target point went through a three-step process from which the displacements response were acquired. This full project includes the tracking, exporting and saving the displacement response from the aforementioned point (Appendices C.1.1 & C.1.2).

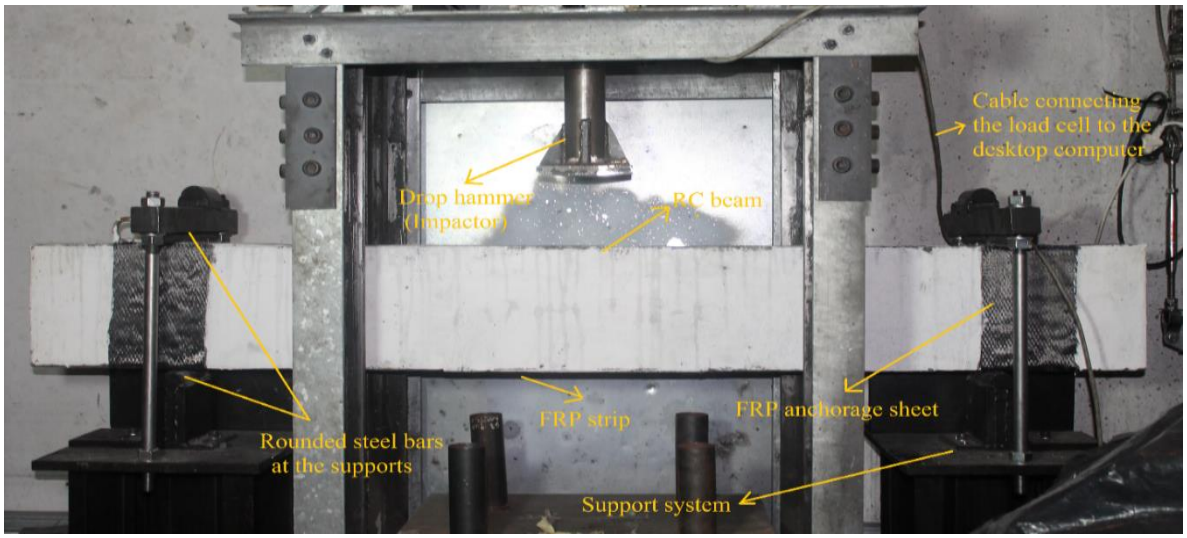

Figure 3.21. FRP-strengthened RC beam (SB1_2) in the position on the impact machine for testing.

The procedure described above, together with the preliminary analysis of the recorded contact forces, constitute the pre-analysis. In addition, the pre-analysis of the results was followed by the final analysis using Matlab graphics to present different results obtained through figures. Also, various tables were used to present the results. A comparative analysis of the obtained results from the control beams and patch-repaired and FRP-strengthened RC beams was made through the aforementioned analysis.

3.4. Chapter summary

The methodology described in this chapter was developed in order to carry out the study on the behaviour of FRP-strengthened and concrete patch-repaired RC beams under impact loading. As mentioned earlier, the research is ongoing kind and the first task was to reproduce RC beams with similar characteristics, especially in terms of target strength and size. From the initial stage of preparation of materials prior to the casting of RC beams, to the final stage of testing and analysis, all the activities and methods used were described in this chapter.

The preparation of individual materials used in this study was highlighted, and this mainly included the drying the sand in the oven at 15^{o} C for a period of two days. The properties of materials used were also presented, and these included the compressive strength of both concrete and patch repair materials. The grinding technique, used to simulate the effects of corrosion on steel bars, was briefly presented. In addition, the test setup was described in detail including the manufactured supporting system and modified drop hammer.

The method of testing, the data acquisition process and the way forward to the analysis were presented. The prepared RC beams (both controls, patch-repaired and FRP-strengthened) were tested under impact loading by using a drop test machine to achieve the research objectives in this study. The results obtained on the basis of the proposed methodology are discussed, analysed and presented in the following chapter.

CHAPTER 4: RESULTS ANALYSIS AND DISCUSSION

4.1. Introduction

The present experimental study was a part of an ongoing investigation conducted on RC beams that were patch-repaired and strengthened with FRP materials and subjected to different loading conditions. The impulse force recorded from a striking head (impactor) by a load cell transducer was used to study the behaviour of simply supported concrete patch-repaired and FRP-strengthened RC beams. In total, 15 RC beams were tested under impact loading. These comprised three undamaged beams as controls (CB) and 12 patch-repaired and FRP-strengthened beams (SB). The SB were further classified as SB1, SB2, SB3, and SB4, corresponding to 450 mm, 800 mm, 1300 mm and 1800 mm patch repair length respectively. The following Table 4.1 summarises the beam types and drop height of the impactor from which various drop tests were performed.

Table 4.1. Drop height for all performed impact loading tests.

Drop test / Beam type		Drop height (mm)							
		Test Nº 1	**Test Nº 2**	**Test Nº 3**	**Test Nº 4**	**Test Nº 5**	**Test Nº 6**	**Test Nº 7**	**Test Nº 8**
CB	1	150	300	399	498	606	705	800	1004
	2	150	303	400	500	599	701	803	1000
	3	150	304	402	502	599	700	700	1002
SB1	1	150	300	401	503	598	700	798	1000
	2	150	298	398	498	600	700	800	1003
	3	150	300	400	501	601	701	799	1002
SB2	1	150	300	397	498	599	703	800	1003
	2	150	301	398	499	597	698	802	1001
	3	150	301	399	500	599	700	800	1000
SB3	1	150	302	403	501	600	699	798	998
	2	150	300	401	499	602	699	801	1001
	3	150	300	400	501	599	700	799	999
SB4	1	150	297	399	502	600	698	801	1001
	2	150	300	400	499	601	700	800	1000
	3	150	300	400	501	600	700	802	1001

The impact load testing was carried out by using a drop weight machine and following the procedure presented and detailed in **Chapter 3: Experimental Study** of this dissertation. Each RC beam was subjected to eight consecutive impact loading tests. In addition, two transducers (a load cell and a HSC), together with a signal conditioning package in combination with computers (desktop and laptop), were used to capture and record the structural responses of the RC beams. These contact forces and deflection responses were respectively captured and recorded with a load cell and HSC transducers. The recorded contact forces and deflection responses, together with their respected derivative and associated parameters, were analysed and discussed accordingly.

The recorded contact force responses, combined the inertial forces and true bending forces together. Also, deflection responses included maximum and residual or permanent deflections. In this study, the focus was made on maximum values due to time constraints and the huge amount of data required to be recorded with the HSC. Consequently, the secondary pulses and their associated deflection responses were not computationally covered here. However, their effects on the global behaviour of the tested beam were taken into consideration. The data analysis was done using PFA and Matlab software tools.

The extracted data from the experimental investigation were presented and discussed according to the following research parameters and observations:

a) the recorded contact force response, inertial and bending forces;
b) the deflection (vertical displacement) response that was associated with the forces in (a);
c) the progression of damage, including the cracking pattern and the mode(s) of failure;
d) the effects of varying patch length on the recorded contact force, deflection response and the propagation of damage;

4.2. Recorded contact forces, inertia and bending forces results

The recorded contact forces representing the dynamic response were directly captured with the use of the load cell transducer, following the introduction of the impulse force through the tested RC beams. The impact loading history was recorded and analysed accordingly. The recorded contact force loading history combined both maximum contact forces and rebound

forces. However, as previously mentioned, the current study focuses on maximum values. Figure 4.1 describes the typical loading history of impact force which includes the first pulse and secondary pulses.

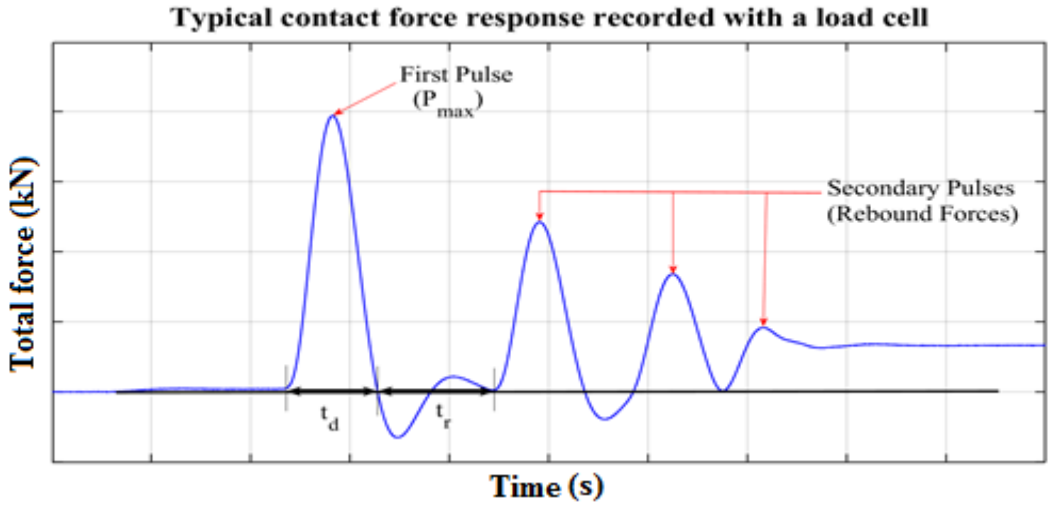

Figure 4.1. Typical recorded contact force response extracted from a load cell transducer.

The impact load directly applied on a simply supported beam led to the formation of the first pulse which corresponds to the magnitude of the maximum contact force (P_{max}). Moreover, the impact hammer bounced back after the formation of the first pulse, thus the secondary pulses were also formed. Thereafter, the tested beam was subjected to free-vibration motion until it stopped oscillating. However, there was a transition period between the first pulse and secondary pulses which corresponds to the rebound time (t_r). The transition period was made of a negative phase directly followed by a positive phase, due to the drift phenomena of a load cell after receiving a sudden loading. During the negative phase, the impact hammer lost contact with the RC beam under testing, while the inertial effects (in association with the dead load applied to the load cell) led to the formation of the positive phase. The major impact loading event corresponded to the duration (t_d) of the first pulse formation. The duration (t_d) was largely the same irrespective of the number of the drop tests and type of tested RC beam. It was found to be equal to 0.095 s ≈ 95 ms (Figures 4.2 and 4.3). The magnitude of the maximum contact force (P_{max}) was related to the drop height (h) and the current stiffness of the tested beam. The duration of the transition period, also called rebound time (t_r) reflected the energy released after the major impact loading event (first pulse). Therefore, the released energy depended on the current flexural rigidity and stiffness of the tested beam. Generally, in this study, the recorded contact force history lasted for a maximum duration of 1.2 s ≈ 1200

ms. The results of recorded maximum contact force from both CB and SB were discussed and presented individually. In addition, a comparative analysis between the results from CB and SB beams was presented for their respective contact force results.

Many researchers, engineers and asset managers identify impact loading as one of the most extreme form of load (Fujikake, et al., 2006; Fujikake, et al., 2009). Moreover, when impact loading comes into contact with a structure, adverse effects might be experienced during the very short period of time. The structure under study was known to produce considerable inertia forces when subjected to impact loading. In this regard an attempt was made to estimate the inertia forces and bending forces from the total forces also commonly called recorded contact forces. However, after the computation of inertial forces, and considering the results of recorded contact forces, a decision was made to also compute the bending forces. The computation of inertia and bending forces was made on the basis of the deflection response. The process was explained in previous Chapter 3 and the formulae are reviewed in Chapter 2. The bending force led to insight into the flexural behaviour of various tested beams. The inertial forces (P_i) and bending forces (P_b) are discussed in relation to the drop height.

4.2.1. Contact force response results of CB

The following discussion is on the recorded contact force results of CB group. The CB group comprised CB1, CB2 and CB3. All available results regarding the control beams are presented in Appendices (A.1.1 and A.1.2) in form of loading history at the end of this dissertation. However, the contact force results from CB 1 were selected to represent the typical loading history of control beams. Thus, Figure 4.2 illustrates the contact force history from undamaged RC beam CB1.

While Figure 4.2 shows the region of interest within this study, it did not take into account the entire contact force history. The area of interest comprises the recorded maximum contact force of the tested RC beam. The entire contact force history is presented in Appendix A.1.1. From CB1 results, three secondary pulses following the primary pulse were recorded from the first drop test performed from 150 mm drop height. The recorded contact force response from the first drop test was short, compared to the remaining seven drop tests. Also, the duration of the first pulse formation associated with the first drop test was short compared to the other remaining durations of the other first pulses. This was due to fewer effects on both stiffness and flexural capacity of tested RC beam CB1 after the first drop test. The formed cracks were

very small and they closed immediately after the end of the first drop test performed on the RC beam CB1.

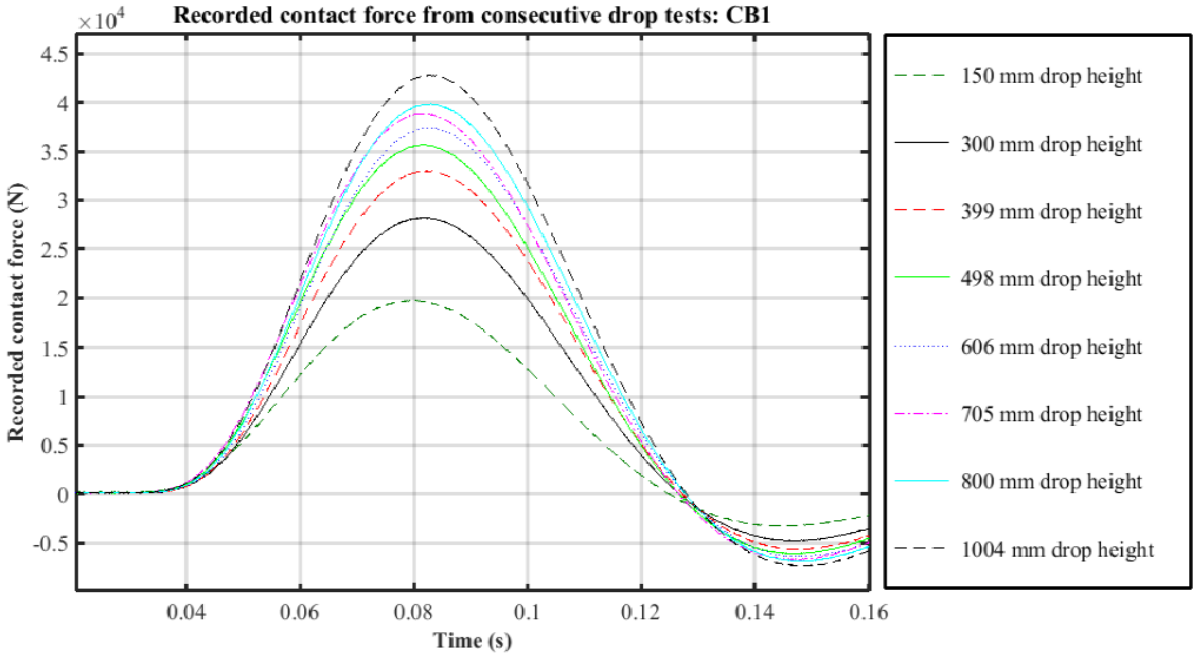

Figure 4.2. Recorded contact force responses from a load cell transducer: CB1.

As it can be seen in Figure 4.2 above, maximum contact forces increased as drop heights increased. The same observation was made regarding all tested control beams. The degradation of the concrete surface at impact point, in combination with the deterioration of stiffness of tested CB, resulted in an overall increase of the impact loading event (both first pulse and secondary pulses). The increase of the drop height led to the development of various effects of inertial forces and, consequently, the rebound time also increased.

Table 4.2 summarises the average of recorded contact force and computed force results obtained from the CB group. As can be seen in Table 4.2, from the first drop test to the second drop test, the recorded maximum contact force (P_{max}) increased drastically by 29.99% and progressively increased up to the last drop test. This considerable increase might be attributed to the doubled drop of height. Nevertheless, the recorded maximum contact force increased slightly from the fifth drop test up to the seventh drop test, as stiffness and flexural rigidity decreased. However, a relatively significant increase of contact force was observed from the last drop test. This increase might be attributed to the double increment of the drop height and the associated impulse force.

Table 4.2. Recorded contact and computed forces results: CB.

Drop Tests Results / Beam Type	Test Nº	Drop height (mm)	Recorded contact forces	Computed forces		Rebound time (t_r) of P_{max} in (s)
			P_{max} (N)	P_b (N)	P_i (N)	
CB	1	150	19746	105676	56313	0.219565
	2	302	28204	193324	88572	0.320437
	3	400	32990	199357	99940	0.362915
	4	499	35686	175976	132320	0.372067
	5	603	37405	187110	136192	0.378795
	6	703	38889	191473	147963	0.371322
	7	802	39866	185728	144693	0.362088
	8	1002	42815	187361	134565	0.377842

The deterioration in stiffness of tested RC beam was associated with the energy release. In this regard, the first drop test was done from a small drop height, the associated small amount of energy was released, and it took a shorter time to rebound. Hence the increase of rebound time as the drop height increased might be associated with the energy release, due progressive concrete cracking and concrete crushing propagating from the vicinity of the impact point. The rebound time may also be increased due to continuous extension of formed cracks into the tested RC beam as a resulting of consecutive drop tests. However, the rebound time reached its maximum at the fifth drop test and decreased at both sixth and seventh drop tests. It increased slightly at the last drop test and this might be attributed to the considerable degradation of the stiffness after the fifth drop test.

4.2.2. Contact force results of SB

The SB family comprises SB1, SB2, SB3 and SB4 groups. Among the available average contact force results from FRP-strengthened RC beams, SB1, SB2 and SB3 results are presented in Table 4.3. It should be noted that the results for SB4 were not available due to the load cell which broke down during the testing period. The typical contact force response from FRP-strengthened RC beam is shown in Figure 4.3. Figure 4.3 also illustrates the recorded contact force response obtained from a concrete patch-repaired and FRP-strengthened RC

beam SB2_1. It is also important to remember that this current study emphases maximum values. In addition, various graphs of impact loading history are presented in Appendices A.2.1, A.3.1, A.3.2, A.4.1 and A.5.1.

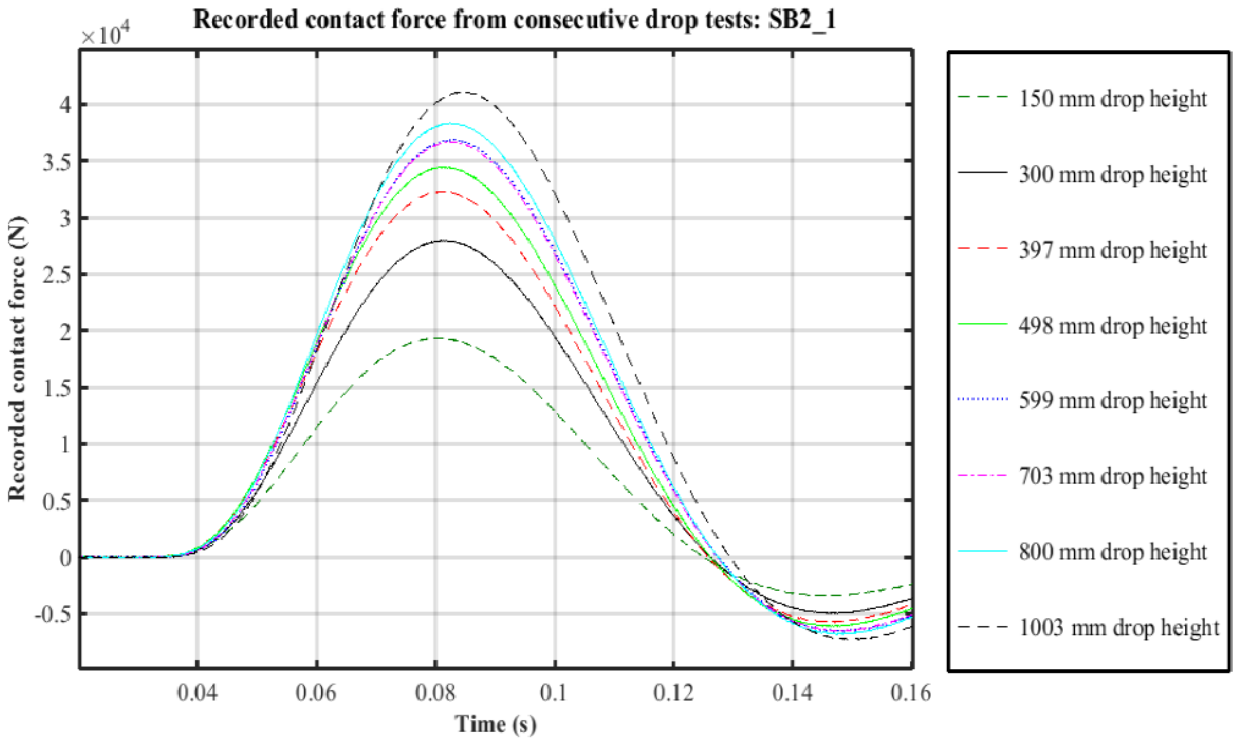

Figure 4.3. Recorded contact force responses from a load cell transducer: SB2_1.

An increase of 27.62% to the recorded contact force from the first drop test to the second drop test was observed from SB2. Similar to results obtained from the undamaged beam CB, the contact force response from SB1, SB2 and SB3 increased as the drop height increased. However, as can be seen in results from SB1 and SB2, after the seventh and sixth drop test respectively, a small decrease of contact force results was experienced. This decrease might be associated with the total debonding of FRP strip that was observed after the sixth and fifth drop tests respectively from SB1 and SB2. No decrease of contact force results was observed from SB3. Nonetheless, a considerable increase of contact force was experienced in the last drop tests. Thus, degradation of the stiffness was also considerable as the last drop height was significantly increased. The results of maximum contact force obtained from SB did not differ very much from the results obtained from CB. Therefore, using the FRP strengthening materials, the restoration of flexural capacity was achieved.

Table 4.3. Recorded contact and computed forces results: SB1, SB2, SB3 and SB4.

Drop Tests Results / Beam Type	Test Nº	Drop height (mm)	Recorded contact forces	Computed forces		Rebound time (t_r) of P_{max} in (s)
			P_{max} (N)	P_b (N)	P_i (N)	
SB1	1	150	-	105722	61026	-
	2	299	27842	151505	71497	0.312781
	3	400	32287	175368	107611	0.370124
	4	501	35139	183544	126595	0.394466
	5	599	36076	191303	133581	0.374966
	6	700	38166	188387	136617	0.386105
	7	799	37776	193834	141830	0.321386
	8	1002	40979	194296	140827	0.352676
SB2	1	150	19375	134607	37364	0.219094
	2	301	26768	155907	91125	0.318359
	3	398	31534	167263	105268	0.368248
	4	499	34165	175628	125411	0.388175
	5	598	36713	185527	122451	0.392810
	6	701	36682	192230	148452	0.336297
	7	801	38342	194727	168901	0.349261
	8	1002	41096	186643	146364	0.355232
SB3	1	150	19590	119695	62695	0.221462
	2	302	-	161060	96502	-
	3	403	-	176694	105138	-
	4	501	35002	189746	132220	0.401650
	5	600	36897	199876	133536	0.401840
	6	699	38049	198018	136959	0.390512
	7	798	39143	200130	142298	0.384061
	8	998	41487	213911	168749	0.368674
SB4	1	150	-	118072	67385	0.217192
	2	297	-	163852	103474	0.320012
	3	399	-	174161	108204	0.385655
	4	502	-	191096	128377	0.403571
	5	600	-	193683	134783	0.411227
	6	698	-	199853	143544	0.374770
	7	801	-	201063	145822	0.375744
	8	1001	-	212348	151994	0.381024

The rebound time increased by 31.18 % after the first drop test from SB2. This can be attributed to the high impulse force introduced to the tested RC beam SB2 and, consequently, the stiffness and the flexural capacity degraded accordingly. From SB1, SB2 and SB3 results, the rebound time progressively increased as the drop height increased. A decrease in rebound time was observed after the fifth drop test from SB3. As it was the case on the results of contact force from SB1 and SB2, the decrease in rebound time was observed after the total debonding of FRP strips from the concrete soffit took place. Thus, the stiffness and flexural capacity were considerably deteriorated after the sixth, fifth and fifth drop tests respectively from SB1, SB2 and SB3. The rebound time increases afterward but did not reach previously peak value. The integrity of the strengthened beams was compromised when FRP debonding took place, following the shear plug failure and concrete crushing which occurred in the vicinity of the impact point.

4.2.3. Inertia and bending forces results

Inertia and bending forces results: CB

The inertial and bending forces results are shown in Table 4.2. These results were also later presented through various figures. The general tendency was that both inertial and bending forces increased as the drop height increased. On the on hand, bending forces increased rapidly from the first drop test to the second drop test. However from the third test the increment became relatively slighter and even few negative increments were observed. This might be due to the ratio of drop height to maximum deflection. Thus, the elastic deformations associated with that particular drop test were less or closer to those obtained from the previous drop test. On the other hand, the similarities from the first to the second drop test were found to increase considerably for both bending and inertial forces results. After the fourth drop test, a slight increment of inertial force was experienced. In addition, some negative increments were also obtained. This was attributed to a considerable deterioration of stiffness as a result of consecutive drop tests.

Inertial and bending forces results: SB

The inertial and bending forces results from all SB are presented in Table 4.3. These results are also later shown and analysed through various figures. Similar to the results presented above from CB, the obtained results from SB general exhibited an increase as the drop height

increased. The biggest increment in both bending and inertial forces was observed in most the cases from the second drop test. However, a few exceptions were also experienced. This might be attributed to the complexity of the impact load testing from which the behaviour of beams from one group might be a little different from others. Moreover, the following ascending order of SB behaviour, in terms of degradation for both flexural capacity and stiffness can be established: SB1, SB2, SB4 and SB3. The above classification is made on the basis of the average of bending force results.

4.2.4. Comparative analysis

Recorded contact force

CB results exhibited slightly higher values both on the first and last drop tests. The following order can be established based on the last drop tests results in ascending order: SB1, SB2 and SB3. This shows that the patch repair and FRP strengthening method performed well under impact loading. Thus, different layers composing patch-repaired and FRP-strengthened RC beam worked together and behaved almost as a monolithic specimen. In addition, degradation of stiffness due to consecutive drop tests was almost the same, despite the type of the beam under test. Figures 4.4, 4.5 and 4.6 show the recorded contact force results, the rebound time results, and the recorded contact force versus maximum deflection results respectively from all available data.

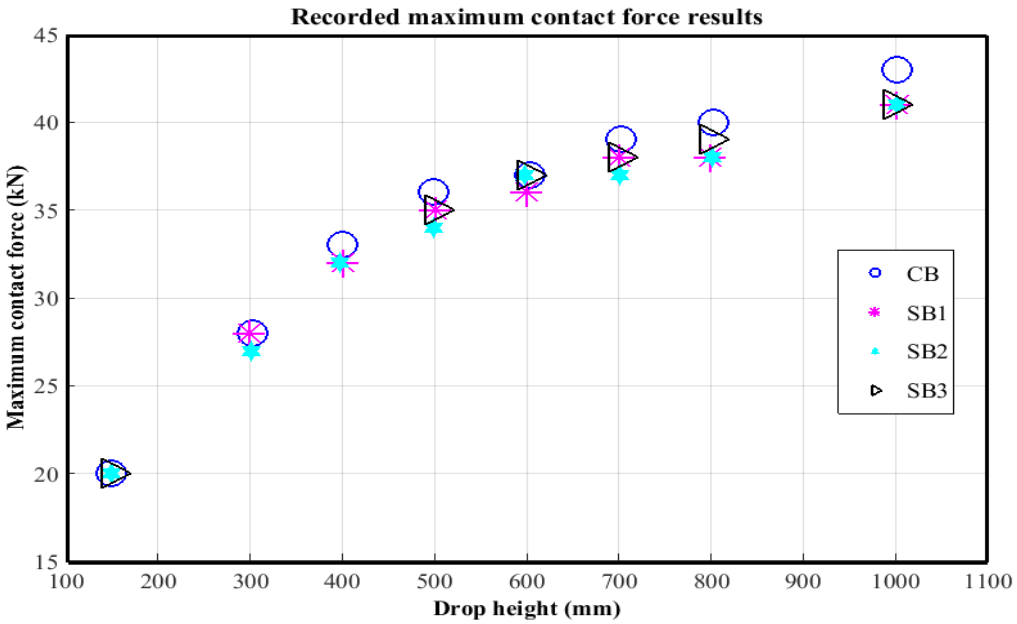

Figure 4.4. Maximum contact force results recorded with a load cell transducer.

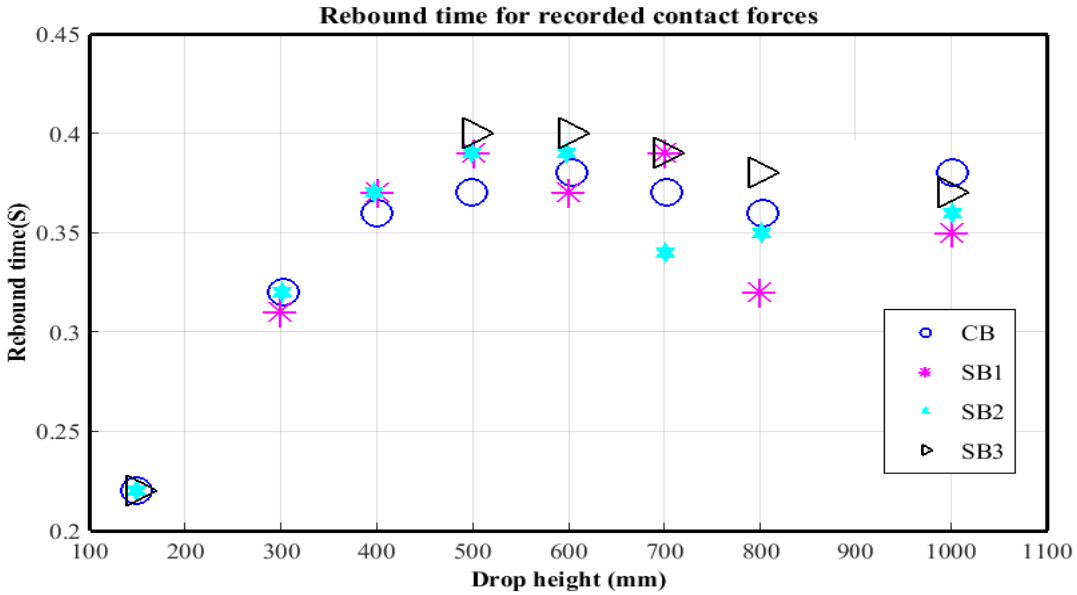

Figure 4.5. Rebound time results obtained from various drop heights.

An increase in both recorded contact force and maximum deflection results can clearly be seen as the drop height increased. On the basis of the results presented in Figure 4.6, it can be seen that the used patch repair and strengthening techniques achieved their intended use as the differences between CB and SB results were rather small. The 14% reduction of cross-sectional area from main reinforcing steel bars was adequately compensated with the used FRP materials.

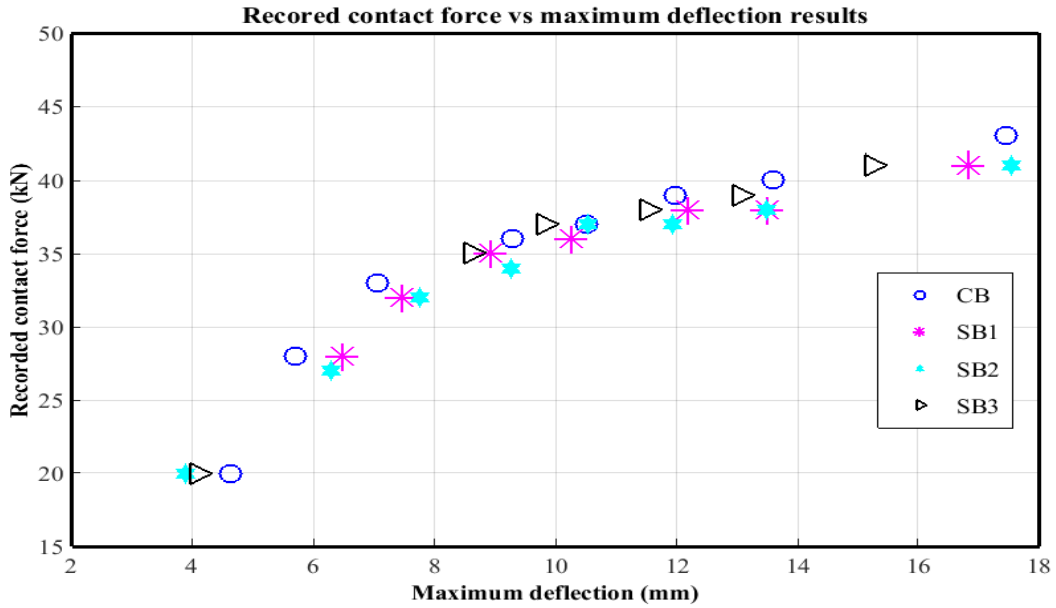

Figure 4.6. Recorded contact force vs maximum deflection results.

The obtained results from both CB and SB showed a continuous increase of the rebound time generally up to the end of the fifth drop test. An exception was made in results of SB1 where the maximum rebound time was reached at the end of the fourth drop test. Thus, in most cases, the debonding of the FRP strip from the soffit of RC beams started after the fifth drop test. FRP debonding gradually increased, and consequently the created opening widened due to consecutive drop tests; most of the time the FRP system failed after the sixth drop test. Generally, during this study, it can be seen that the patch-repaired and FRP-strengthened RC beams experienced a lower rebound time than that of control beams. Thus control RC beams were more flexible than strengthened RC beams.

Inertial and bending forces

It was always crucial and challenging to be able to estimate the distribution of impact loads; one portion of these loads was involved in bending and the other portion was attenuated by inertial forces. Figure 4.7 shows maximum inertia force results obtained from both CB and SB. Figure 4.8 shows all the inertia force and the associated maximum deflections results. Irrespective of the type of the tested beam, inertial forces increased as drop height increased. In addition, the general tendency was that SB family exhibited higher values than CB. This might be attributed to the FRP strip that was used to compensate the reduced steel bar area in the tensile zone. Thus, as the cross-sectional area of SB was a bit higher than that of CB, the associated flexural capacity was also higher. The forces resisting to the impulse, expressed in terms of inertial forces, were higher from SB than CB.

Bending forces were normally extracted from total forces. Thus, a similar trend to what seen in the inertial force was also noticed in results of bending forces. An exception was made on second and third drop tests where CB values were higher than SB values. Otherwise, bending force results from SB family were higher than those from CB. Furthermore, it is important to remember that the bending force results depended on the ratio of drop height to the associated maximum deflection. The elastic deformations expressed in terms of maximum deflections results were higher in CB group than in SB family. Therefore flexural rigidity and bending stiffness deteriorated more in CB than in SB. Figure 4.9 shows maximum bending force results obtained from both CB and SB. Figure 4.10 shows all the bending force and the associated maximum deflections results.

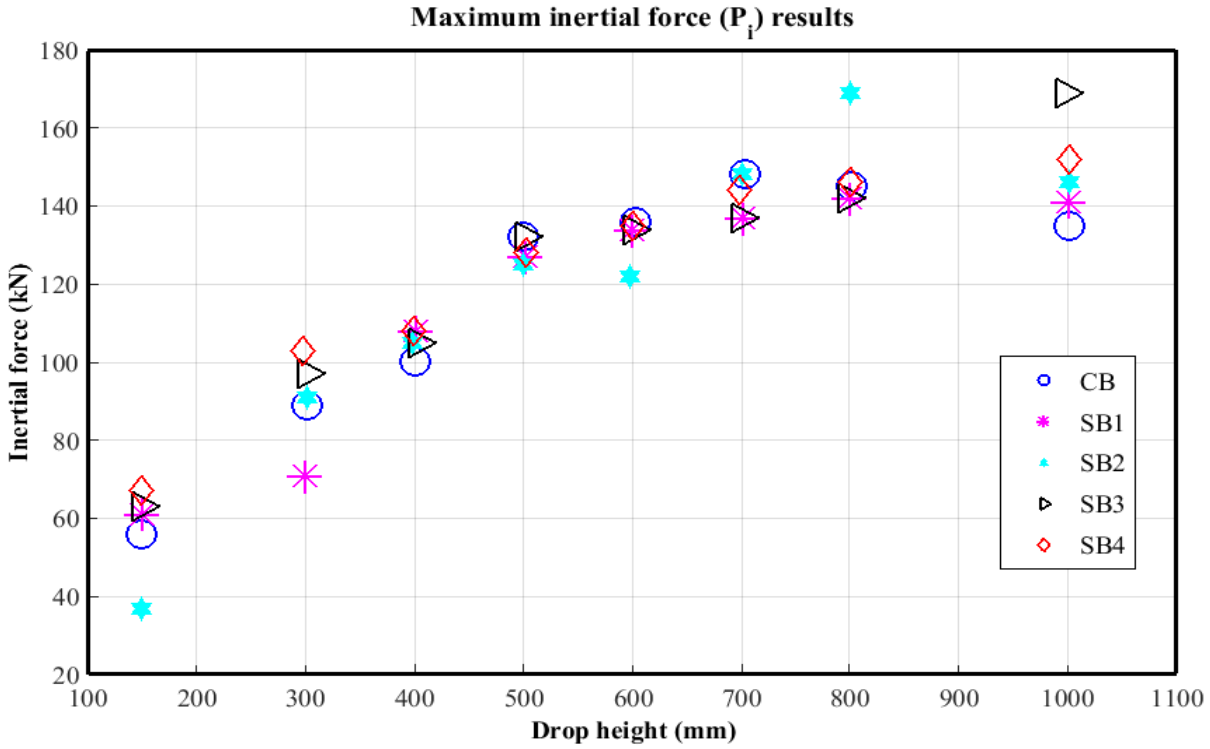

Figure 4.7. Maximum inertial force results obtained from various drop heights.

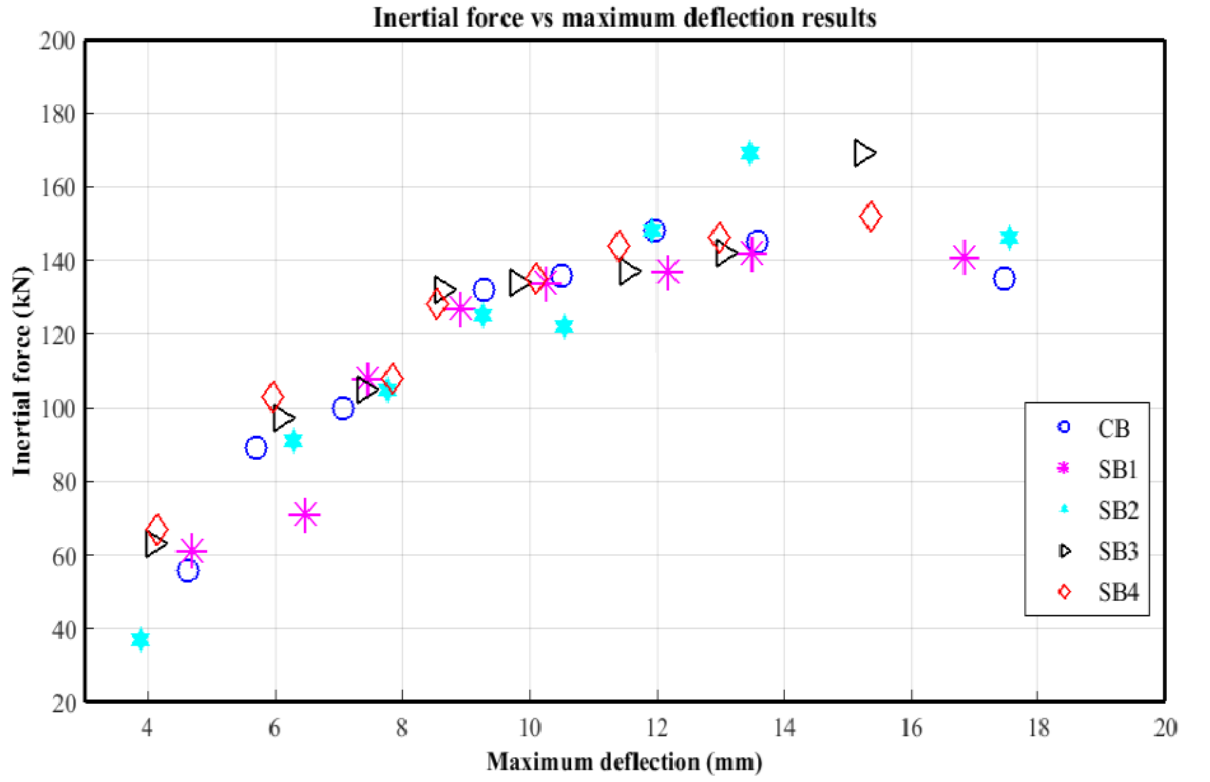

Figure 4.8. Inertial force vs maximum deflection results

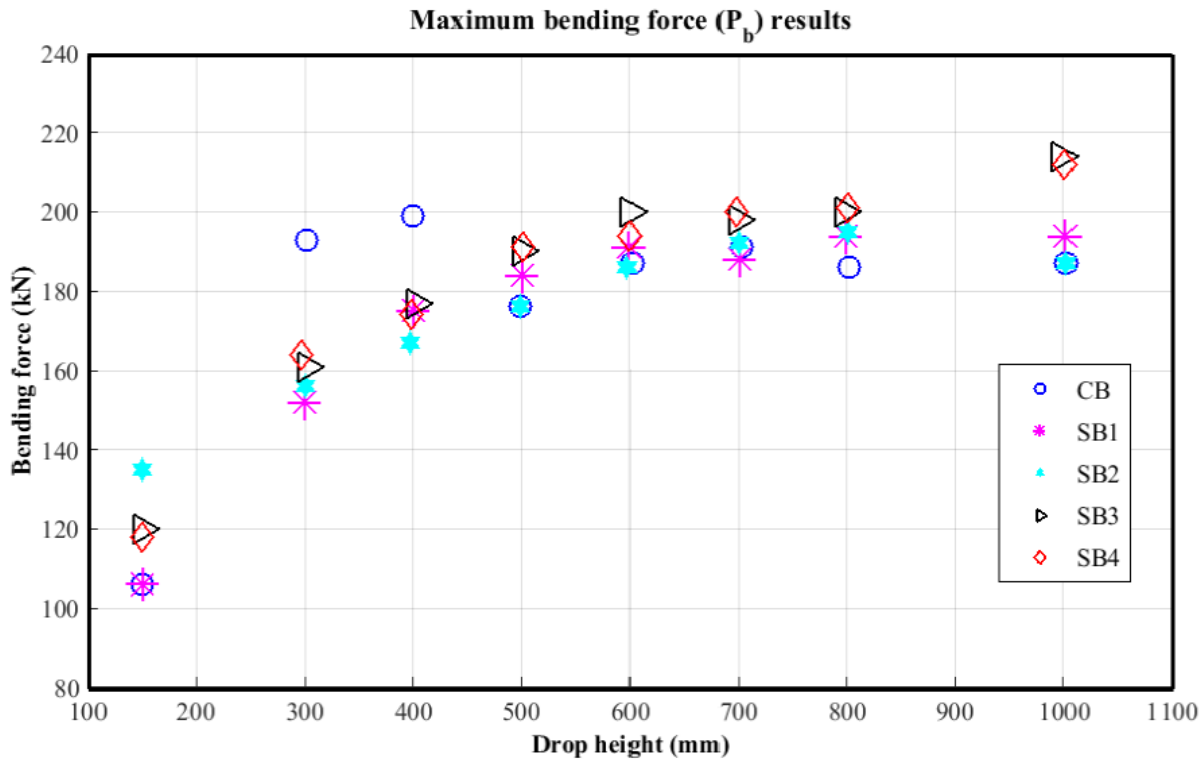

Figure 4.9. Maximum bending force results obtained from various drop heights.

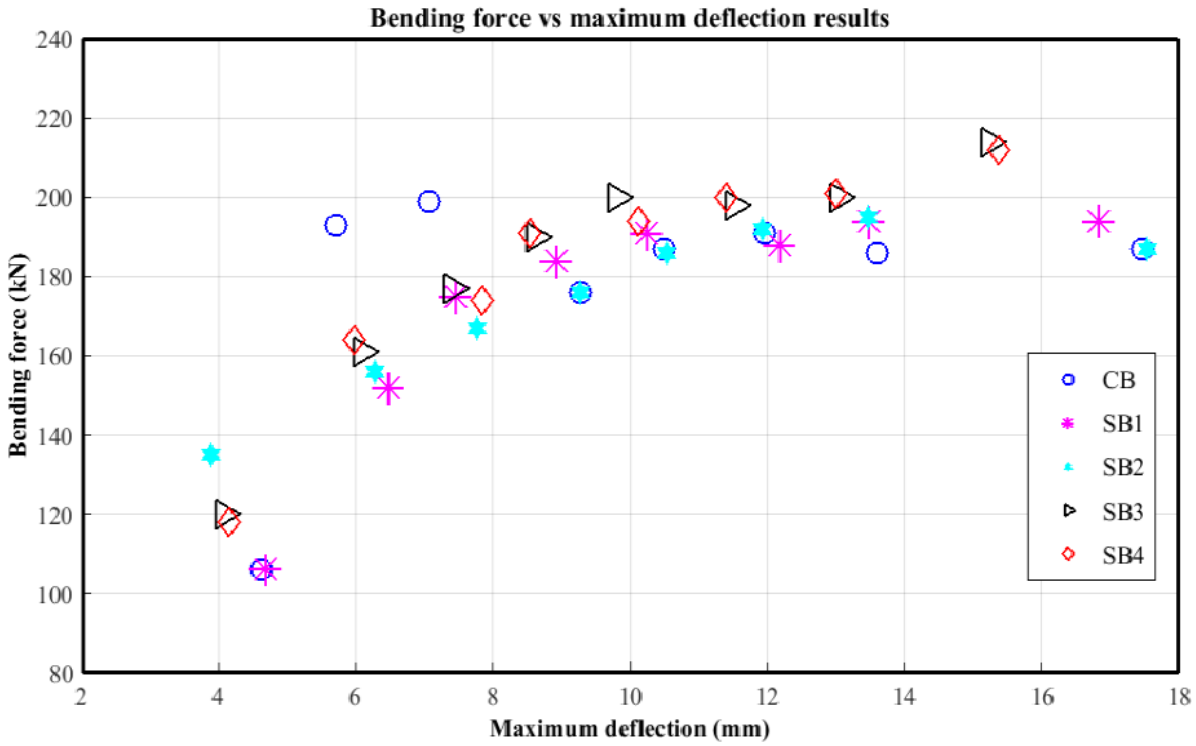

Figure 4.10. Bending force vs maximum deflection results

4.3. Deflection responses

Deflection responses were taken at the mid-span of each tested RC beam. They were extracted from HSC footage with the use of PFA software tool. A typical deflection response extracted from a targeted point in the mid-span of RC beam is shown in Figure 4.11.

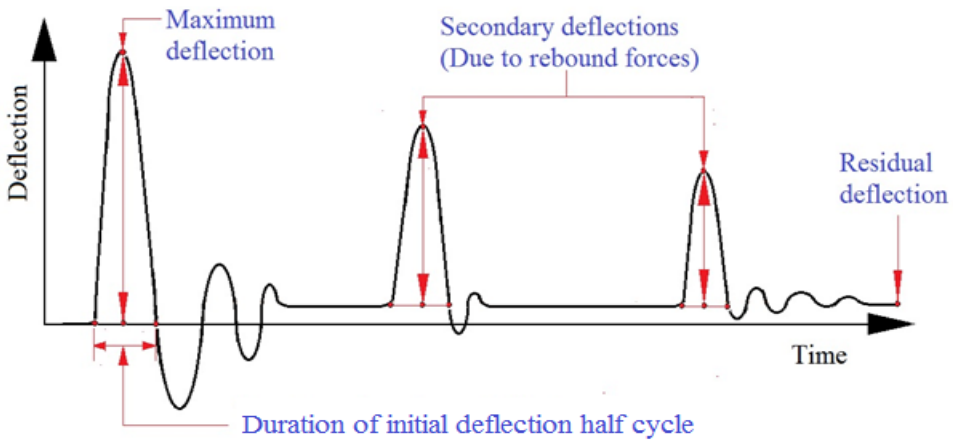

Figure 4.11. Typical deflection response extracted from HSC footage.

The residual deflection (δ_{rs}) as well as deflection half cycle duration provided insight into the stiffness of the tested RC beam (Tang & Saadatmanesh, 2003; Grandić, et al., 2011). The cumulative residual deflection ($\sum \delta_{rs}$) results were also presented and can be used to describe how much or to what extent the stiffness was degraded after any drop test (Tang & Saadatmanesh, 2003). The total deflection (D_{max}) after any particular drop test represents the summation of maximum deflection at that drop test and the residual deflection experienced from the previous drop test. It combines the recovered and non-recovered deflection results, and gives a global picture of the extent to which a RC beam under testing is deformed, both elastically and plastically. Thus, the summation of deflections observed in any particular drop test was expressed in terms of total deflection. The maximum deflection (δ_{max}), in combination with the bending force of any particular drop test, foresaw a general trend on both bending stiffness and flexural capacity results of the tested RC beam. Thus deflection response results might be used to describe the general behaviour of various tested RC beams.

It should be important to recall that in some cases, due to time constraint and data storage limitations, only data containing maximum deflection were saved and stored. The residual deflection results were also evaluated by averaging the deflection values in the region of the

ending part of deflection response results. Where only a portion of deflection data was saved, the average value was estimated to be the residual deflection, starting directly from the far end of maximum deflection peak. As it can be easily seen in Figure 4.11 above, the average value of deflection response results in between maximum deflection peak and first secondary deflection peak did not differ much from the average value of deflection response results located on the ending part of the whole deflection history. The comparative analysis of the results obtained from both control and strengthened beams was based on deflection responses. The results of deflection response, including various related parameters from different tested RC beams were discussed and presented.

4.3.1. Deflection response of CB

Table 4.4 shows the average of maximum, residual, cumulative residual and total deflections and the associated half cycle duration results from CB. A big increase of maximum deflection was observed from the first drop test to the second drop test for each beam of the CB group. In general, maximum deflection increased as drop height increased. However, an exception was made on the seventh drop test of CB2. This might be attributed to two successive drop tests (i.e. 6^{th} and 7^{th} test) that were accidentally performed on the same drop height. Thus, flexural capacity and stiffness of tested RC beam decreased as drop height increased.

Table 4.4. Maximum, residual, cumulative residual and total deflections and its half cycle duration results: CB.

Drop Tests Results / Beam Type	**Test Nº**	**Drop height (mm)**	δ_{max} **(mm)**	δ_{rs} **(mm)**	$\sum\delta_{rs}$ **(mm)**	D_{max} **(mm)**	**Duration of** δ_{max} **in (s)**
CB	1	150	4.633	0.755	0.755	4.633	0.013218
	2	302	5.714	0.508	1.263	6.469	0.011980
	3	400	7.071	0.420	1.683	7.579	0.012417
	4	499	9.282	1.185	2.868	9.702	0.013885
	5	603	10.505	1.916	4.784	11.690	0.015149
	6	703	11.971	3.002	7.786	13.887	0.016285
	7	802	13.599	3.479	11.265	16.601	0.017414
	8	1002	17.463	6.489	17.754	20.942	0.020235

Except for deflection half cycle duration associated with maximum deflection resulting from the first drop test, deflection half cycle duration increased as the drop height increased (Figure 4.13).

The magnitude of residual deflection from the first three drop tests was relatively closer irrespective of the type of beam tested. However, the magnitude of the residual deflection was substantially different for the remaining drop tests. This can be attributed to a progressive deterioration in stiffness of tested RC beam as the impact loading was cumulatively applied, up to the final drop test. The resulting plastic deformation from various consecutive impact loading tests rose with the number of the drop test. A considerable loss of stiffness after the final drop test was observed, resulting in an average of cumulative residual deflection of 16.694 mm for the whole CB group.

Residual deflection results showed lower to higher values respectively from CB3, CB1 and CB2. Thus, the cumulative residual deflection results of CB provided a general picture on how the tested RC beam deteriorated in stiffness of as the number of drop tests increased. The average value of 0.8% of cumulative residual deflection was gained after the first drop test from CB1 and CB3. The average value of 61.2% of cumulative residual deflection was recorded after the seventh drop test. This led to the remaining average stiffness of 38.8% from CB before the last drop test. It was also noticed that CB3 was stiffer and less flexible compared to two other control beams.

Similar to the maximum, residual and cumulative residual deflections results, the total deflection results exhibited a higher value in CB2 compared to the remaining control beams. The total deflection combines both maximum and residual deflections, hence it provides insight into both elastic and plastic deformations of tested beams. As it can be seen in Table 4.4 above, the total deflection increased as the drop height increased. This was attributed to progressive deterioration of both flexural capacity and stiffness due to consecutive drop tests. In any case, independently to the type of deflection considered, the CB2 results presented higher deformations than the other remaining control beams; CB2 was more flexible.

4.3.2. Deflection response of SB

Table 4.5 shows maximum, residual, cumulative residual and total deflections and the associated half cycle duration results from SB. Various figures were used to present the results.

Table 4.5. Maximum, residual, cumulative residual and total deflections and its half cycle duration results: SB1, SB2, SB3 and SB4.

Drop Tests Results / Beam Type	Test Nº	Drop height (mm)	δ_{max} (mm)	δ_{rs} (mm)	$\sum\delta_{rs}$ (mm)	D_{max} (mm)	Duration of δ_{max} in (s)
SB1	1	150	4.681	0.798	0.798	4.681	0.011148
	2	299	6.474	0.447	1.245	7.272	0.011657
	3	400	7.452	0.364	1.609	7.899	0.011711
	4	501	8.918	0.715	2.324	9.282	0.012578
	5	599	10.243	1.772	4.096	10.958	0.013957
	6	700	12.166	2.815	6.911	13.938	0.015913
	7	799	13.482	2.839	9.750	16.297	0.018246
	8	1002	16.842	4.780	14.530	19.681	0.019946
SB2	1	150	3.889	0.521	0.521	3.889	0.013190
	2	301	6.291	0.521	1.042	6.812	0.011742
	3	398	7.762	0.507	1.549	8.283	0.012037
	4	499	9.273	0.985	2.534	9.780	0.013203
	5	598	10.545	2.535	5.069	11.530	0.014650
	6	701	11.931	2.838	7.907	14.466	0.015899
	7	801	13.480	4.355	12.262	16.318	0.017326
	8	1002	17.541	7.831	20.093	21.896	0.020539
SB3	1	150	4.088	0.582	0.582	4.088	0.011208
	2	302	6.085	0.563	1.145	6.667	0.011130
	3	403	7.408	0.260	1.405	7.971	0.011305
	4	501	8.621	0.737	2.142	8.881	0.012524
	5	600	9.808	1.232	3.374	10.545	0.012990
	6	699	11.524	2.973	6.347	12.756	0.015435
	7	798	13.049	2.353	8.700	16.022	0.017475
	8	998	15.240	4.012	12.712	17.593	0.018561
SB4	1	150	4.146	0.493	0.493	4.146	0.011517
	2	297	5.977	0.173	0.666	6.470	0.011247
	3	399	7.845	0.497	1.163	7.658	0.011350
	4	502	8.547	0.719	1.882	9.044	0.012035
	5	600	10.113	2.110	3.992	10.832	0.014096
	6	698	11.411	3.272	7.264	13.521	0.015789
	7	801	12.999	3.920	11.184	16.271	0.017328
	8	1001	15.372	5.854	17.038	19.292	0.018376

The lowest values in maximum, cumulative residual and total deflections were observed from SB, while the highest values in maximum, cumulative residual and total deflections were obtained from SB2. Thus, the lowest and the highest degree of degradation of both flexural capacity and stiffness were respectively observed from SB3 and SB2. The time taken for the formation of the maximum deflection, that is, deflection half cycle duration, increased as the drop height increased. However, in most of the cases (three out of four), the decrease in deflection half cycle duration was only observed after the second drop tests. Thus, as the impact loading was consecutively applied to tested beam, various damages were introduced in the said beam. These damages progressively increased in size, leading to an increase of deflection half cycle duration and deterioration of stiffness. For all strengthened beams, maximum, cumulative residual and total deflections increased as the drop height increased. Thus, parameters such as flexural capacity and stiffness deteriorated as consecutive drop tests were performed on SB.

Finally, the highest average of the value of 4.780 mm, 7.831 mm, 4.012 mm and 5.854 mm residual deflection was observed respectively from SB1, SB2, SB3 and SB4. Thus, the stiffness of tested RC beam has significantly reduced. In addition to that, an average value of 67.10%, 61.03%, 68.44% and 65.64% of cumulative residual deflection was obtained after the seventh drop test respectively from SB1, SB2, SB3 and SB4. This led to the reduction of the stiffness up to 32.90%, 38.97%, 31.56% and 34.36% before the last drop test respectively from SB1, SB2, SB3 and SB4. Besides the display of highest values of all type of deflection results, SB2 also exhibited a higher reduction of stiffness after the seventh drop test.

4.3.3. Comparative analysis

Figure 4.12 shows the maximum deflection results from all tested RC beams. The maximum deflection increased almost linearly as the drop height increased. The elastic deformations increased as drop height increased. Consequently, the flexural capacity and stiffness deteriorated as consecutive drop tests were introduced onto the tested beam. The maximum deflection results from CB were practically the same compared with those obtained from SB. However, some exceptions were made on last drop tests, where SB3 and SB4 results were found to be relatively lower than CB. Thus, the reduced area of steel bars, together with the intentionally damaged concrete area, was compensated accordingly through patch repairs and FRP strengthening applications.

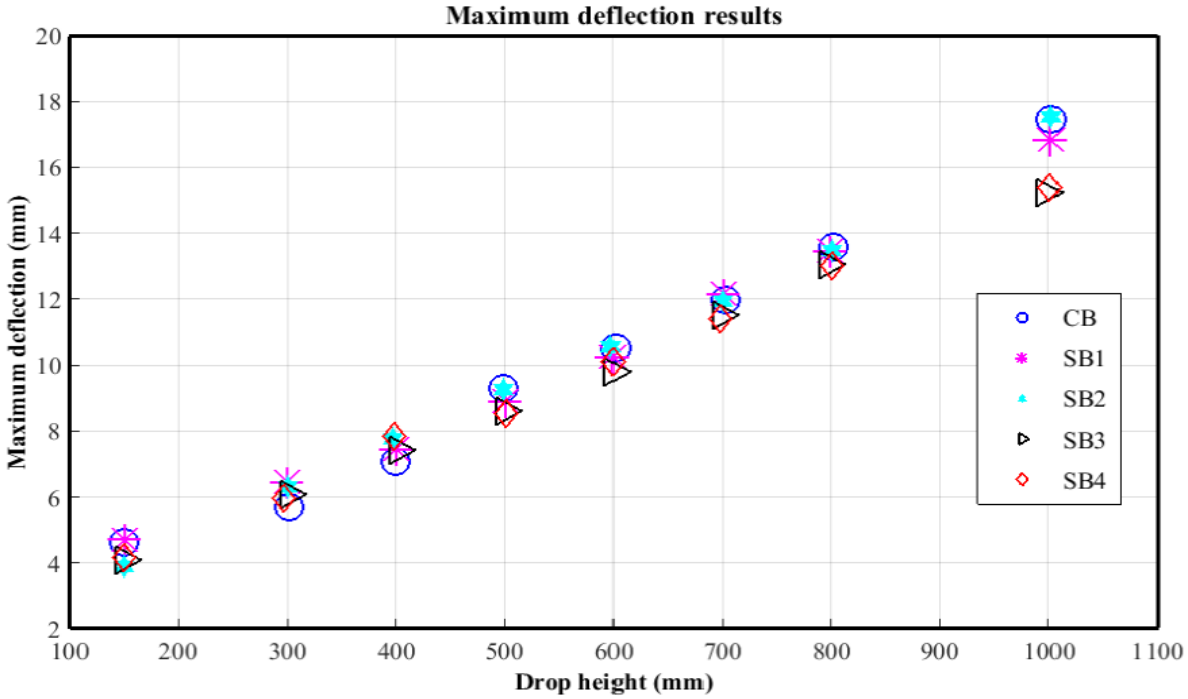

Figure 4.12. Maximum deflection results obtained from various drop heights.

In general, apart from the first drop tests, the duration of maximum deflection formation known as deflection half cycle duration increased as drop height increased. Figure 4.13 shows deflection half cycle results obtained from CB. Figures 4.14, 4.15, 4.16 and 4.17 show deflection half cycle duration results obtained from SB1, SB2, SB3 and SB4 respectively.

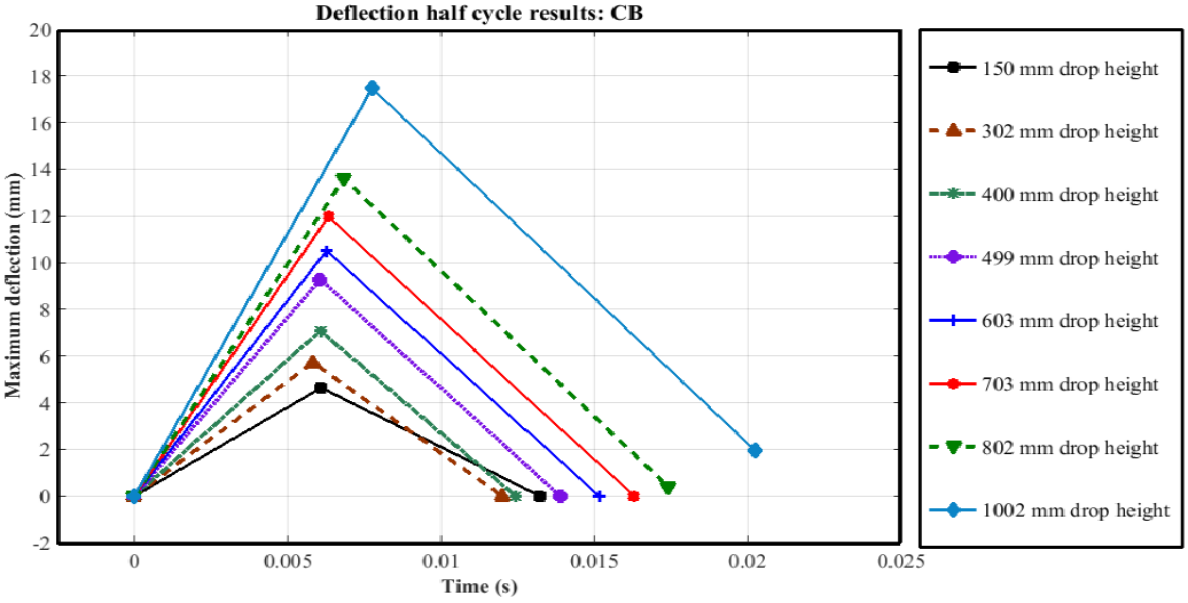

Figure 4.13. Deflection half cycle results obtained from various drop heights: CB.

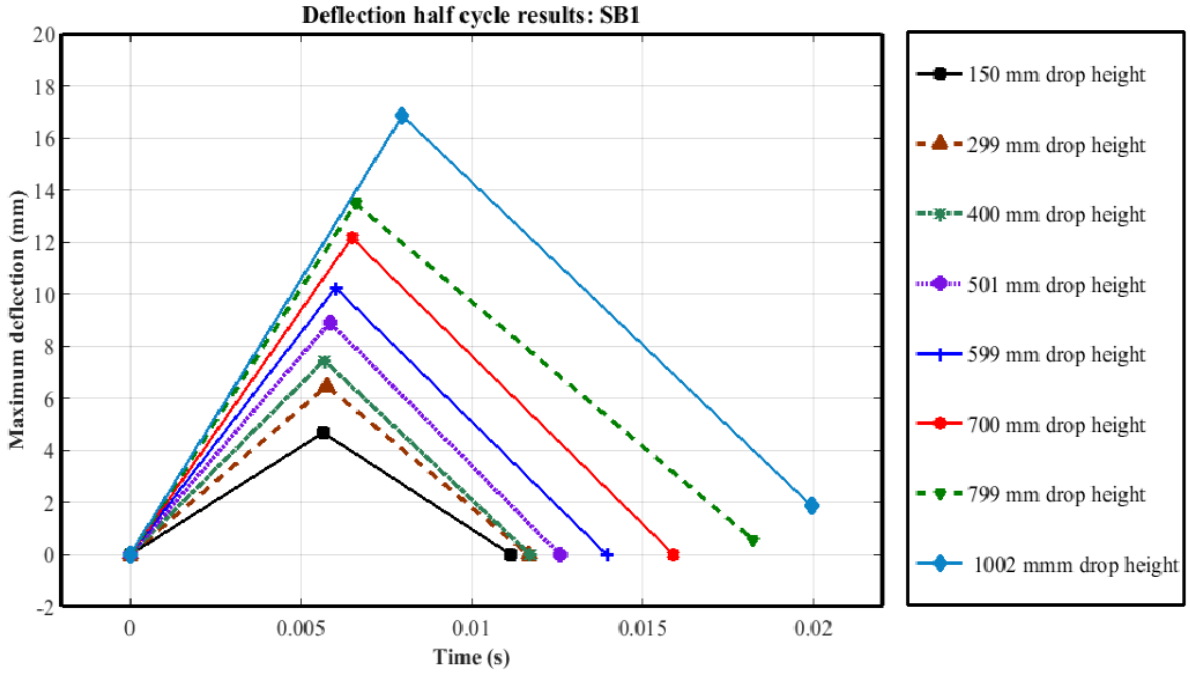

Figure 4.14. Deflection half cycle results obtained from various drop heights: SB1.

Furthermore, in some cases after the fourth drop test, some maximum deflection did not fully recover, consequently they failed to research the initial point. Therefore some non-recovered deflection results were also presented in various deflection half cycle figures. Thus stiffness and flexural capacity degraded as drop height increased, and consequently, deflection half cycle duration increased.

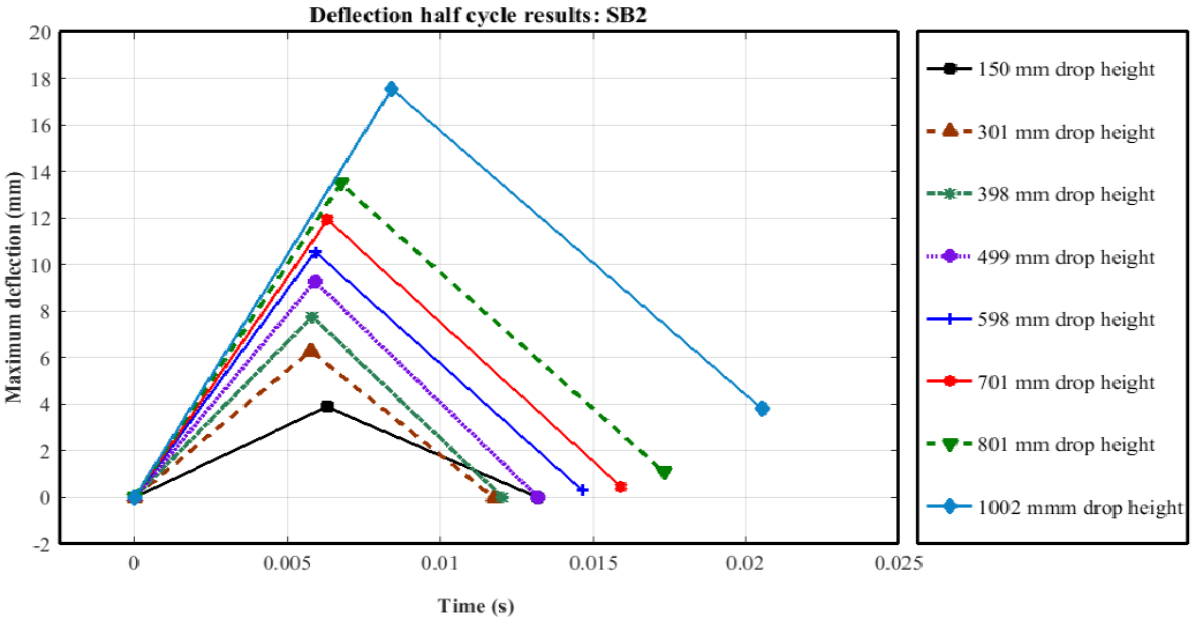

Figure 4.15. Deflection half cycle results obtained from various drop heights: SB2.

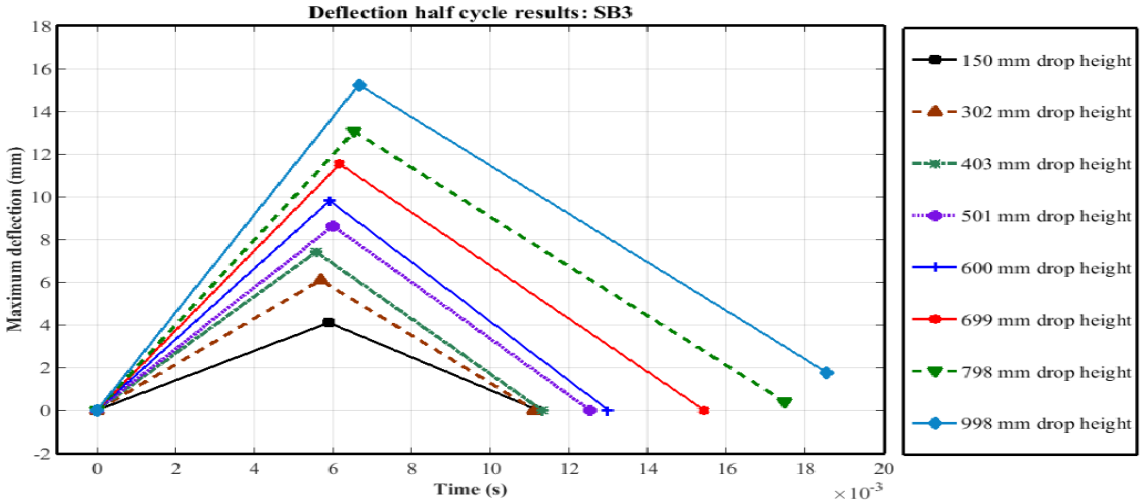

Figure 4.16. Deflection half cycle results obtained from various drop heights: SB3.

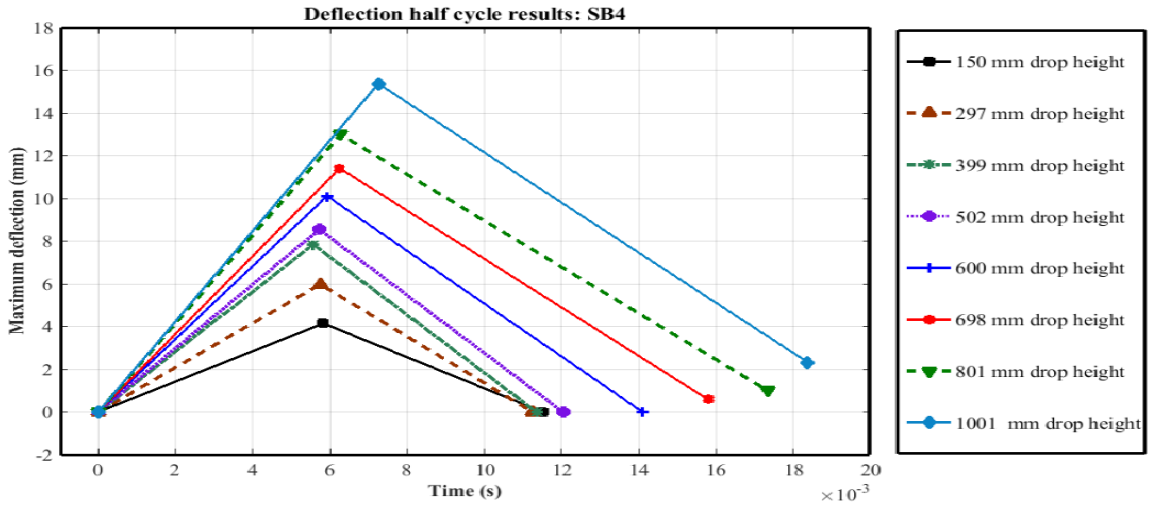

Figure 4.17. Deflection half cycle results obtained from various drop heights: SB4.

The adverse effects of consecutive impact loading on tested beams, especially on stiffness parameter, can also be regarded in terms of both residual and cumulative residual deflections. Figures 4.18 and 4.19 respectively show the residual deflection results and cumulative residual deflection results obtained from all tested RC beams at various drop heights.

The progressive degradation of the stiffness of tested beam from individual drop tests was described based on residual deflection results. The total deterioration of stiffness after any particular test(s) was described on the basis of cumulative deflection results. In the first four drop tests, irrespective of the type of tested beam, residual deflection and cumulative residual deflection results were relative lower, as compared to the results obtained from the remaining drop tests. This might be attributed to the magnitude of the impact loading introduced onto tested beams as the drop heights were relatively lower. Thus, the damages created at this stage

were of relative significance. Therefore, both stiffness and flexural capacity were not considerably degraded after the first four drop tests. From the fifth to the last drop test, both residual deflection and cumulative residual deflection results significantly increased as the drop height increased. Except for SB2 results, in general the other SB results were lower when compared to results from CB at any drop height. Hence, both stiffness and flexural capacity deteriorated considerably at this stage. This was attributed to cumulatively performed drop tests and their relatively higher drop heights.

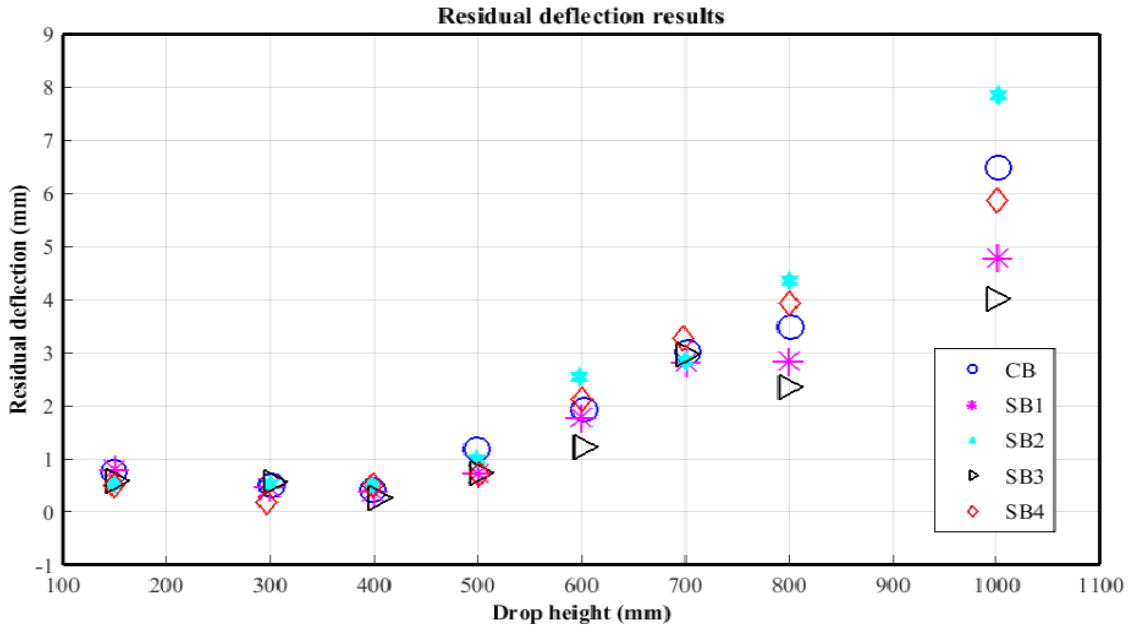

Figure 4.18. Residual deflection results obtained from various drop heights.

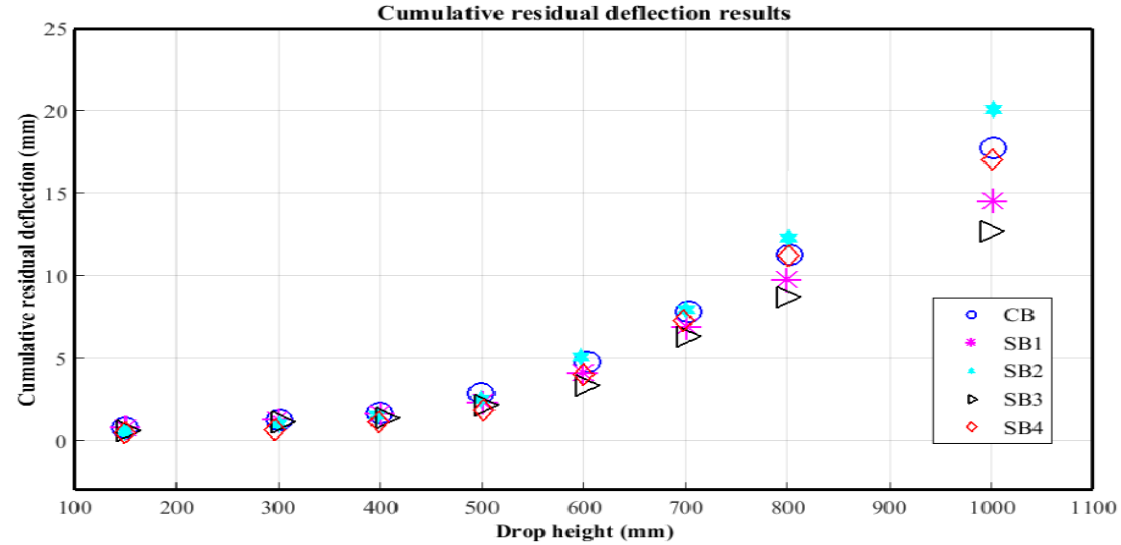

Figure 4.19. Cumulative residual deflection results obtained from various drop heights.

Figure 4.20 shows total deflection results obtained from all tested RC beams at various drop heights. Generally, for both recovered and non-recovered deflections, CB results exhibited higher values compared with those obtained from SB, except for SB2 results. Therefore, both flexural rigidity and stiffness deteriorated considerably in SB2 and CB than the remaining groups of beams.

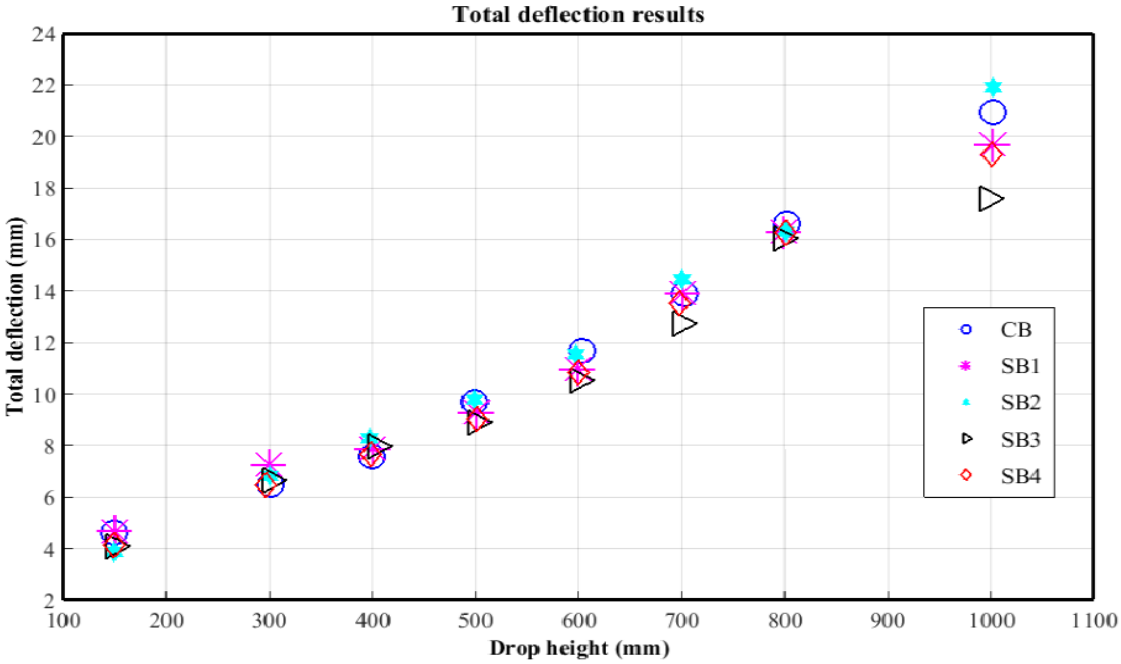

Figure 4.20. Total deflection results obtained from various drop heights.

4.4. Progression of damage and mode(s) of failure

The progression of damage is discussed in terms of cracking pattern and mode(s) of failure. The formed cracks were mainly flexural, flexure-shear and shear cracks. Impact loading caused flexural cracks to begin on the bottom edge of the tested RC beams and progress upwards towards the neutral axis. In addition, some flexural cracks were formed on the top edge of the tested RC beams, due to the development of inertial forces, and these cracks progressed downwards towards the neutral axis. The flexure-shear cracks mainly originated from the previously formed flexural cracks. The energy release associated with the developed flexural cracks, in combination with the substantially developed stresses around the end of those flexural cracks, led to the formation of flexure-shear cracks. Furthermore, shear cracks were often observed in the vicinity of the end supports. Tested RC beams mainly failed in concrete crushing in the vicinity of the impact point, the formation of shear plugs and FRP debonding for strengthened RC beams.

The tested RC beams were subjected to eight consecutive drop tests. Various progressions of damage included both cracking pattern and mode(s) of failure and these, depending on the type of beam that was being tested, were observed accordingly and well elucidated. The cracking pattern of any tested beam under impact loading was described and presented. All observations related to the progression of damage during the impact load testing have been properly marked and recorded using a HSC transducer. Figure 4.21 illustrates the major observations made during the drop testing of the different beams.

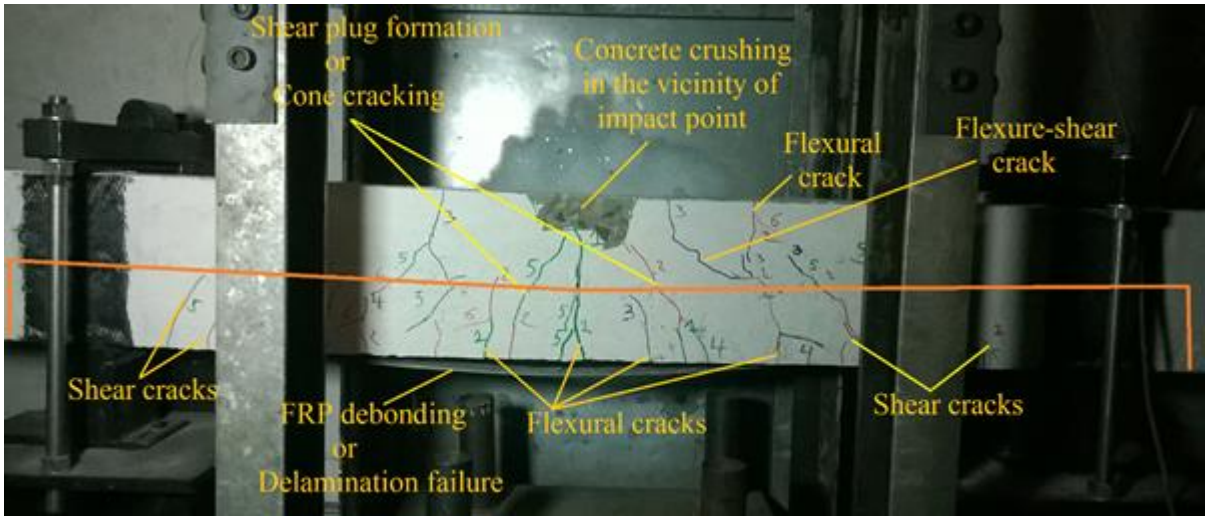

Figure 4.21. Typical progression of damage including cracking profiles and mode(s) of failure observed during drop testing of patch-repaired and FRP-strengthened RC beam (SB4_1).

During the drop testing, flexural cracks started on the bottom edge of the tested RC beam and propagated upwards towards the neutral axis. These cracks were directly caused by the bending forces of the applied impact loading. However the other flexural cracks started from the top edge of the tested RC beam and propagated downwards towards the neutral axis. These last-formed flexural cracks were mainly caused by support conditions at both ends, along with the negative bending phenomena produced through inertial forces. In addition, shear cracks were formed near to the end supports due to the generated tensile stresses that were greater than the tensile strength of the concrete. Finally, flexure-shear cracks were also formed and most of the time they were initiated by flexural cracking. The formation of the flexural cracks led to the increase of shear stress above these cracks. Thus, when the tensile stress of the concrete in the tested beam was exceeded by the combined shear and tensile stress, the development of flexure-shear cracks took place.

Furthermore, various modes of failure were observed, depending on the RC beam being tested. Hence, the concrete crushing failure took place in the compression zone, due to the consecutive striking of the impact hammer in the mid-span of the tested RC beam, and the energy released at the impact point. The FRP-strengthened RC beams failed in debonding due to the excess stresses created between the various adhesives products that had been used to fasten the FRP composites to the concrete beam soffit.

Photographs were taken to illustrate the cracking pattern and modes of failure. In order to properly monitor and assess the progression of damage and associated modes of failure, the following theoretical drop heights (h) were selected: 150 mm, 300 mm, 400 mm, 500 mm, 600 mm, 700 mm, 800 mm, and 1000 mm. The real drop heights, from which various tests were performed, are summarised in Table 4.1. Directly after each drop test, each crack that appeared was marked and labelled with the number of the strike by which it was formed. The numbering of the cracks has followed this order: after the first drop test (h = 150mm) the formed cracks were named as crack number 1, up to and including crack number 8 which was associated with the last drop test (h = 1000mm). In addition, different markers of various colours were used in order to separate the differently formed cracks in combination with their associated drop heights during the experimental testing (except for CB1). The drop test number, from which a particular crack was formed, was also indicated alongside that crack. In the case of patch-repaired and FRP-strengthened RC beams, the patch-repaired zone is indicated by an orange line. Nevertheless, the following discussion about the progression of damages and mode(s) of failure of RC beams subjected to impact loading is more qualitative than quantitative.

4.4.1. Progression of damage and mode of failure of CB

The cracking pattern caused by the first two drop tests was dominated by the formation of many flexural, some flexure-shear and a few shear cracks. These formed flexural cracks started on both upper and lower edges of the tested beams. Nevertheless, most of them started from the bottom edge and grew progressively upwards towards the neutral axis. They were mainly located at the mid-span of the tested beams, up to the quarter length of the clear span from both supports. Also, they were small and immediately closed after their formation. In relation to the third and four drop tests, most of the formed cracks were flexural and flexure-shear cracks. These flexural cracks started forming at both edges of the tested beams. Very few shear cracks were formed. A particular observation was made on CB3: one of the formed flexural cracks

almost spanned the height of that beam. With respect to the fifth and sixth drop tests, very few flexural cracks were formed. Those flexural cracks started on both edges. Most of the formed cracks were flexure-shear cracks. Some cracks, almost horizontally oriented, were observed joining previously formed cracks. The observations made on the progression of damage and the cracking pattern resulting from the seventh and eighth drop tests were the same as those noticed after the fifth and sixth drop tests. Figure 4.22 illustrates the cracking pattern profiles and modes of failure observed from CB group. Moreover, cracking patterns and modes of failure of the other remaining beams of CB group are presented in Appendix B1.

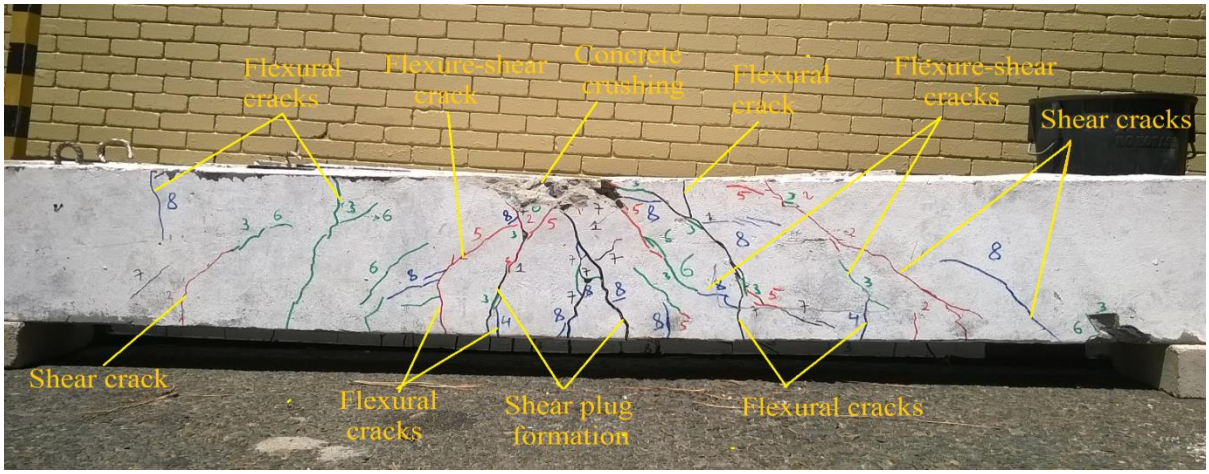

Figure 4.22. Progression of damage observed during drop testing of CB3.

All control beams failed in concrete crushing in the vicinity of the impact point. The CB had also all experienced the formation of the shear plug. Furthermore, two out of three beams experienced a wider crack, almost vertically oriented, directly under the impact point after their respective drop testing. In addition, from CB3 one of the shear plug cracks was wider than the other and obliquely oriented.

4.4.2. Progression of damage and mode of failure of SB

Progression of damage and mode of failure of SB1

After the first drop tests, most of the formed cracks were flexural cracks. These formed flexural cracks started on both edges of SB1_2 and SB 1_3, while the SB1_1 flexural cracks formed from the bottom edge only. This could be attributed more to the developed substantial inertial forces from SB1_2 and SB1_3 than those forces developed from SB1_1 after the first two drop tests. Regarding the third and the fourth drop tests, many flexure-shear, few flexural and few

shear cracks were formed. These flexural cracks started forming on both edges of the tested beams. From the fifth and sixth drop tests, few flexural cracks were formed on SB1_1 and SB1_2. These created flexural cracks started from both edges. Flexure shear cracks were also formed from SB1_2 and SB1_3. Almost horizontally oriented cracks, joining previously formed cracks, were observed from SB1_1 and SB1_3. At the end of the seventh and eighth drop tests, most of the formed cracks were flexure-shear cracks. A few flexural cracks were also formed from SB1_1 and they started from both edges. Furthermore, almost horizontally oriented cracks were observed joining previously created cracks at SB1_1 and SB1_3. Figure 4.23 shows the observation made on the progression of damage through SB1. In addition, the cracking pattern and mode of failure of the remaining beams of the SB1 group are presented in Appendix B2.

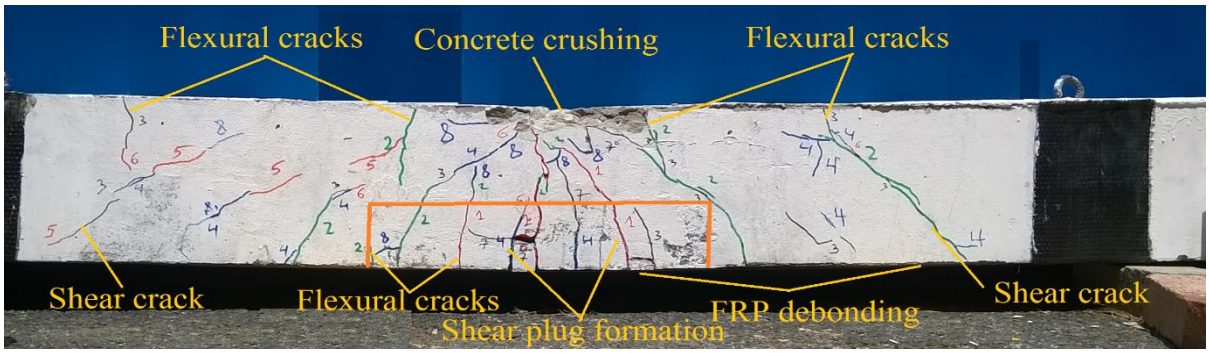

Figure 4.23. Progression of damage observed during drop testing of SB1_3.

The SB1 group failed in concrete crushing in the vicinity of the impact point. Considerable concrete spalling almost broke off from SB1_2 and SB1_3 respectively after the last drop test. It also failed with the formation of the shear plug. The FRP debonding started from the third, fourth and fifth drop test respectively for SB1_2, SB1_1 and SB1_3. Total FRP debonding was observed after the sixth drop test for both SB1_1 and SB1_2, and after the seventh drop test for SB1_3. Thus the bonding strength was higher in SB1_3 than it was in the other beams of the same group.

Progression of damage and mode of failure of SB2

After the first two drop tests, most of the formed cracks were flexural cracks. These flexural cracks started from both edges. Also, a few shear cracks were observed from SB2_3. The observations made at the end of the third and fourth drop tests included the formation of many flexure-shear cracks and some flexural cracks. These flexural cracks formed from both edges

for SB2_2 and SB2_3; they only started from the top edge from SB2_1. Furthermore, few shear cracks were formed from SB2_1 and SB2_3. At the end of the fifth and sixth drop tests, many flexural cracks were observed from SB2_1 and SB2_2. These formed flexural cracks started from the top edge for SB2_1 and from both edges for SB2_2. In addition, some shear cracks were formed from SB2_2. Flexure shear cracks were also observed from SB2_1 and SB2_1. From the seventh and eighth drop tests, most of the formed cracks were flexure cracks. Some flexural cracks were formed. These flexural cracks started forming from the top edge only for SB2_3 and from both edges for SB2_2. Also, almost horizontally oriented cracks were observed joining previously created cracks on SB2_1 and SB2_3. The observations made on the progression of damage including cracking pattern and mode of failure of tested RC beam SB2 are shown in Figure 4.24. Moreover, the cracking pattern and modes of failure of the remaining beams of the SB2 group are presented in Appendix B3.

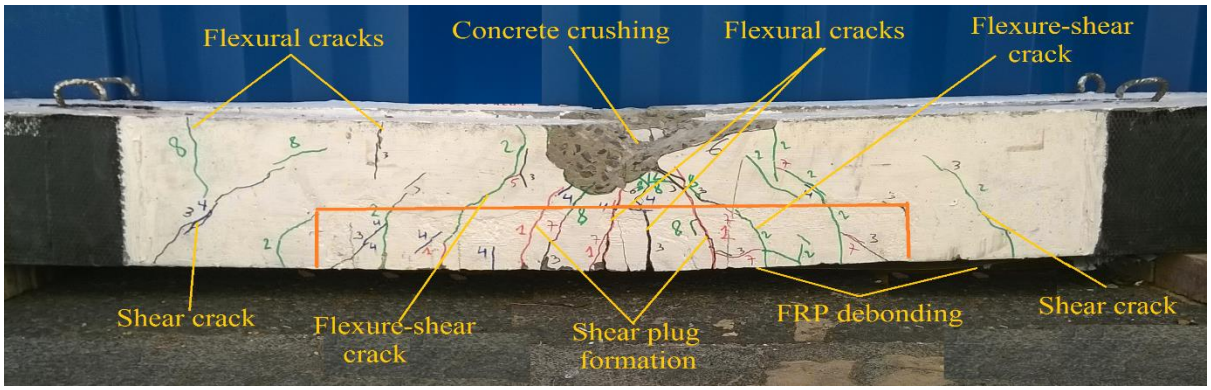

Figure 4.24. Progression of damage observed during drop testing of SB2_3.

Globally, SB2 group failed in concrete crushing in the vicinity of the impact point and formation of the shear plug. In addition, considerable concrete spalling was noticed at SB2_3 and substantial concrete spalling almost broke away from SB2_1. Also some cracks, which had been created beneath the impact point, were wide open and it was noted that an almost vertically oriented crack formed on SB2_2. The FRP debonding started from the third drop test for SB2_1, and from the fourth drop test for both SB2_2 and SB2_3. The total FRP debonding was observed after the fifth, the sixth and the seventh drop test respectively for SB2_1, SB2_2 and SB2_3. Thus for SB2_3 the epoxy adhesive layer between the FRP strip and the concrete substrate from lasted longer here than it did for their peers.

Progression of damage and mode of failure of SB3

Cracking patterns and modes of failure of SB3 are briefly shown in Figure 4.25. In addition, cracking patterns and modes of failure of the other remaining beams of the SB3 group are presented in Appendix B4.

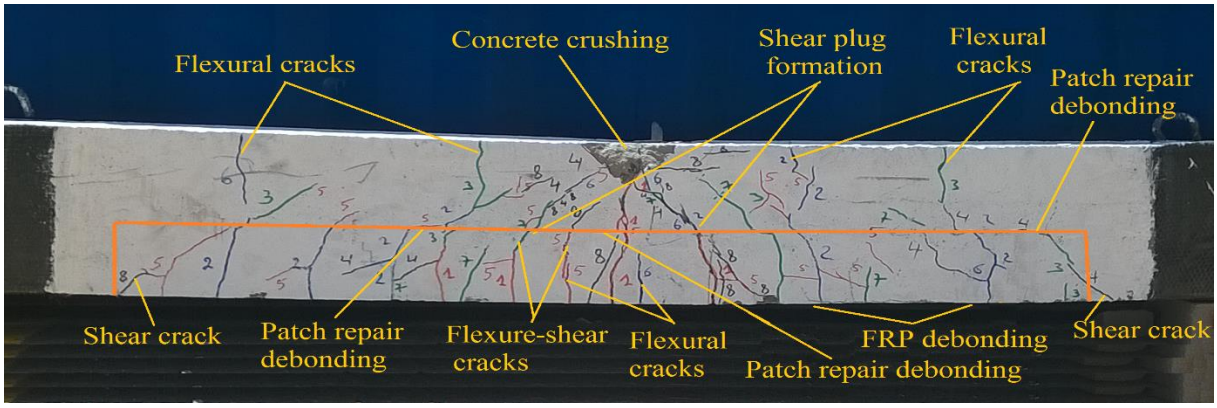

Figure 4.25. Progression of damage observed during drop testing of SB3_3.

In accordance with the first two drop tests, most of the cracks formed were flexural cracks and these started from both edges, except for those observed at SB3_1, where the flexural cracks only started from the bottom edge. In addition, some flexure-shear cracks were also formed. Few shear cracks were formed and observed from SB3_3. In relation to the third and fourth drop tests, many flexure-shear cracks and some flexural cracks were formed. These flexural cracks started from both edges of the tested beams. In addition, few shear cracks were observed at SB3_3. At the end of the fifth and sixth drop tests, the following observations was made: most of the cracks were flexure-shear cracks. Few flexural cracks were formed at either SB3_1 or SB3_2. Some almost horizontally oriented cracks were observed at SB3_1. Also, a few shear cracks were noticed within SB3_3. At the end of the seventh and eighth drop tests, almost all of the formed cracks were flexure-shear cracks. Few flexural cracks were observed from SB3_3 after the seventh and eight drop tests. In addition, few almost horizontally oriented cracks were observed joining previously created cracks.

Generally, the SB3 group failed in concrete crushing in the vicinity of impact point and the formation of the shear plug. It is worth noting that one of the cracks, comprising the shear plug, was wider than the other for both SB3_1 and SB3_2. In addition, considerable spalling of concrete was noticed within SB3_1. The FRP debonding started from the third drop test for both SB3_1 and SB3_2 and from the fifth drop test for SB3_3. The total FRP debonding was observed after the fifth, sixth and seventh drop test respectively for SB3_1, SB3_2 and SB3_3.

Therefore, the epoxy adhesive layer between FRP strip and concrete substrate lasted longer for SB3_3. However, the FRP debonding spread to three-quarters of the shear span between the anchorage FRP sheets for SB3_3.

Progression of damage and mode of failure of SB4

Cracking pattern and mode of failure of SB4 are briefly described in Figure 4.26. In additionally to that, the cracking patterns and modes of failure of the other remaining beams of the SB4 group are presented in Appendix B5.

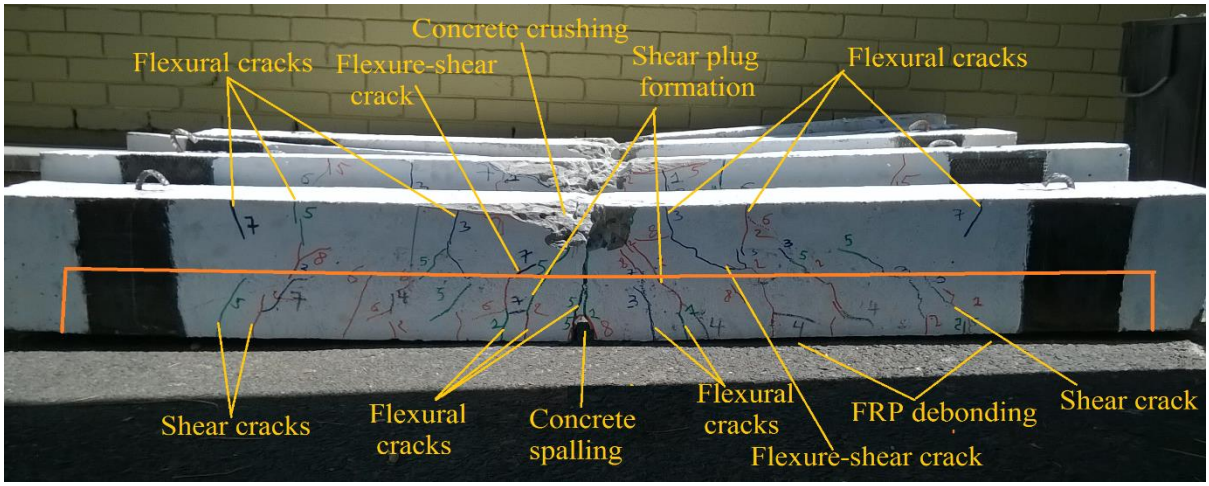

Figure 4.26. Progression of damage observed during drop testing of SB4_1.

After the first two drop tests, the tested beams experienced the formation of many flexural, some flexure-shear and few shear cracks. These flexural cracks started to form from both edges, with many of them occurring on the lower edge. In addition, some of these flexural cracks spanned the entire height of the tested beams; these cracks were located under the impact point. Most of the cracks that formed during the third and fourth drop tests were flexure-shear cracks. Some flexural cracks were also formed and they started from both edges of SB4_1 and SB4_3. A few shear cracks were observed from SB4_2. Cracks that were almost horizontally oriented, and which joined previously formed cracks, were also observed. In addition, a full horizontally oriented crack was observed in the adhesive layer between the concrete patch and the old concrete of the beam. Regarding the fifth and sixth drop tests, the formed cracks were mostly dominated by flexure-shear cracks. A few flexural cracks were also observed. These flexural cracks started to form from the bottom edge (except those from SB4-1 which started from both edges). After these two drop tests, that is, fifth and sixth test, some few shear cracks were also

observed from SB4_1. In the last two drop tests, most of the cracks formed were flexure-shear with few flexural cracks. Additionally, very few shear cracks were observed from SB4_2. A considerable portion of concrete spalled from the distal face of the impact point within both SB4_1 and SB 4_3.

Tested beams from the SB4 group failed in concrete crushing in the vicinity of the impact point, with substantial concrete spalling of materials. Furthermore, the SB4 group also failed in the formation of the shear plug. The FRP debonding started from the third drop test for SB4_2, and from the fourth drop test for both SB4_1 and SB4_3. Total FRP debonding was observed after the sixth drop test for all beams of the SB4 group. Therefore, the epoxy adhesive layer between FRP strip and concrete substrate failed more quickly for SB4_1.

4.4.3. Comparative analysis

Generally, during this experimental study, the formed flexural cracks started mainly from the bottom edge for most of the tested RC beams. But some of these cracks also started forming from both edges (top and bottom) due to the combined action of direct impact loading and the associated developed inertial forces. All the tested beams presented many flexural cracks, some flexure-shear cracks and few shear cracks. However, the extent of cracking profiles presented some slight differences. Moreover, all tested beams failed in concrete crushing in the vicinity of the impact point, causing concrete spalling on the distal side of the impact point. In addition, FRP debonding failure was observed for the patch-repaired and FRP-strengthened beams. On the one hand, five out of twelve FRP-strengthened beams (that is, 41.7%) exhibited the start of FRP debonding after the third drop test. Five out of twelve FRP-strengthened beams (that is, 41.7%) displayed the start of FRP debonding after the fourth drop test. Two out of twelve FRP-strengthened beams (that is, 16.7%) exhibited the start of FRP debonding after the fifth drop tests. On the other hand, two out of twelve FRP-strengthened beams i.e. 16.7% displayed the end (total) of FRP debonding after the fifth drop test. Seven out of twelve FRP-strengthened beams (that is, 58.3%) exhibited the end (total) of FRP debonding after the sixth drop test. Three out of twelve FRP-strengthened beams (that is, 25%) displayed the end (total) of FRP debonding after the third drop test. Thus, the earliest FRP debonding was observed from the third drop test, while the last FRP debonding was observed from the fifth drop test. The earliest total FRP debonding was observed from the fifth drop test, while, the last total FRP debonding was observed from the seventh drop test.

Furthermore, the increase of the patch length for the FRP-strengthened RC beams led to fewer cracks being formed when visualised from the front view. Therefore, the following classification of more cracks that formed, from lower to higher, might be established starting with SB4, SB3, SB2 and SB1. Table 4.6 shows the qualitative comparison of damage induced in various tested beams that had been subjected to consecutive drop tests. The aforementioned comparison was made with respect to the extent of crushed concrete in compression zone that is, on the proximal side of the impact point; the extent of concrete broke-off in tension zone - that is, on the distal side of the impact point; the cracking profile of the tested beams from the front view; the extent of FRP debonding induced in CFRP strips; and the extent of damage in CFRP sheets - that is, the cut-off of CFRP sheets used as anchorage.

Table 4.6. Qualitative comparison of damage and their damage extents observed from various tested beams.

Beam type	Extent of crushing in compression zone	Extent of concrete broke-off in tension zone	Extent of cracking profile from the front view	Extent of FRP debonding induced in CFRP strips	Extent of damage induced in CFRP sheets
CB	*****	*	*****	-	-
SB1	***	**	*****	*****	*
SB2	***	**	****	*****	-
SB3	***	*	****	*****	-
SB4	***	*	****	*****	-

* The various forms of damage were rated out of five, with five being the worst in terms of damage induced.

4.5. Effects of varying patch repair length

The evaluation of the effects of varying patch repair lengths on the behaviour of various patch-repaired and FRP-strengthened beams was examined on the basis of various results. These were mainly the recorded contact forces, deflection response and propagation of damage, and included cracking patterns and modes of failure.

Table 4.7 shows the available results of recorded contact forces obtained from the patch-repaired and FRP-strengthened RC beams. The same Table 4.7 displays only the results of the last four drop tests. These results were chosen because of the considerable drop heights in association with the high impulse load, which led to a noticeable difference in results. However,

the differences in the results of the first four drop tests were relatively small. The full recorded contact force results are shown in Table 4.3. On the basis of those results, it can be seen that the recorded contact force increased as the patch length increased. This can be attributed to the higher compressive strength recorded when patch repair materials were used than results obtained from concrete used to produce beams prior to repair and FRP strengthening activities (Table 3.2). Thus the longer the patch length, the higher the associated compressive strength, and consequently, the recorded contact forces also increased.

Table 4.7. Recorded contact force results obtained from last 4 drop tests.

Beam type / **Results**	**SB1 (450mm patch length)**	**SB2 (800mm patch length)**	**SB3 (1300mm patch length)**	**SB4 (1800mm patch length)**	**Test Nº**
Recorded contact force (N)	36076	36713	36897	-	5
	38166	36682	38049	-	6
	37776	38342	39143	-	7
	40979	41096	41487	-	8

The effects of the patch-repair length based on deflection results can also be discussed. These results included but were not limited to maximum deflection, cumulative residual and total deflection. It is important to recall that some parameters such as flexural capacity and stiffness were previously discussed in this study, based on the aforementioned deflection results. Table 4.8 shows maximum deflection, cumulative deflection and the total deflection results for the last 4 drop tests. Also, the full results were presented in Table 4.5 and discussed through various figures within this dissertation. The results of the last 4 drop tests provided insight into the general picture of the remaining deflection results. The averages of maximum deflection, cumulative residual deflection and total deflection are presented in Table 4.9.

On the basis of the average deflection results, it can be seen that SB2 exhibited higher values in all cases. Thus, in general, the following ascending order (in terms of deflection results) can be established: SB3, SB4, SB1 and SB2. Furthermore, except for SB2 results, the perception was that the longer the patch length, the lower the maximum deflection results. However the general view, based on the three previously mentioned deflection types, does not allow adequate deduction of the effects of patch repair length on various strengthened beams.

Table 4.8. Maximum, cumulative residual and total deflections results: Last 4 drop tests.

Beam type / Results	SB1	SB2	SB3	SB4	Test Nº
Maximum deflection δ_{max} **(mm)**	10.243	10.545	9.808	10.113	5
	12.166	11.931	11.524	11.411	6
	13.482	13.480	13.049	12.999	7
	16.842	17.541	15.240	15.372	8
Cumulative residual deflection $\sum \delta_{rs}$ **(mm)**	4.096	5.069	3.374	3.992	5
	6.911	7.907	6.347	7.264	6
	9.750	12.262	8.700	11.184	7
	14.530	20.093	12.712	17.038	8
Total deflection D_{max} **(mm)**	10.958	11.530	10.545	10.832	5
	13.938	14.466	12.756	13.521	6
	16.297	16.318	16.022	16.271	7
	19.681	21.896	17.593	19.292	8

Table 4.9. Average of maximum, cumulative residual and total deflections results.

Beam type / Results	SB1	SB2	SB3	SB4
Average maximum deflection δ_{max} **(mm)**	10.032	10.089	9.478	9.551
Average cumulative residual deflection $\sum \delta_{rs}$ **(mm)**	5.158	6.372	4.551	5.460
Average total deflection D_{max} **(mm)**	11.251	11.622	10.565	10.904

The aforementioned Table 4.6 shows the qualitative comparison on damage and the extent observed on various tested beams, including patch-repaired and FRP-strengthened beams. The qualitative comparison was made on the basis of the following observations: the extent of crushed concrete in the compression zone; the extent of concrete that broke off in the tension zone; the cracking profile of the tested beams from the front view; the extent of FRP debonding induced in CFRP strips; and the extent of damage in CFRP sheets. Among all the observations on patch-repaired and FRP-strengthened beams listed above, noticeable differences were obtained on both the extent of concrete broken off in the tension zone and the extent of cracking profile as observed from the front view. A greater amount of concrete broke off (through

concrete spalling and scabbing) in SB1 and SB2 than in SB3 and SB4. Thus the first two patch-repaired lengths - that is, the shorter patch lengths, lost more concrete than the last two patch-repaired lengths - that is, the longer patch lengths. The following ascending order, with regard to the extent of cracking profile, can be established: SB4, SB3, SB2 and SB1. The differences in the extent of cracking profile as observed from the front view were slight. Moreover, these cracking profiles, as observed from the front view, increased in density as the patch length decreased. This might be attributed to the compressive strength and plastic ability of patch repair materials.

4.6. Assessment of composite action between various layers of materials of patch-repaired and FRP strengthened beams.

A typical patch-repaired and FRP-strengthened RC beam had four layers with three horizontally oriented interfaces and two vertically oriented interfaces (Figures 3.16 and 3.17). No visible and noticeable cracks were observed on any interfaces, except for the SB4 group, where a few small cracks (micro-cracks) were observed between patch repair and the old concrete of those beams. Debonding of FRP strips from the concrete soffit was the major mode of failure for patch-repaired and FRP-strengthened RC beams. The debonding of FRP strips took place on the interface between FRP strip and the concrete layers that is, both old concrete and patch repairs, but the rest of the interfaces remain intact during and after the consecutive drop tests. As it was previously discussed, on the one hand the earliest FRP debonding was observed after the third drop test, while the earliest total FRP debonding was observed after the fifth drop test. On the other hand, the last FRP debonding was observed after the fifth drop test, while the last total debonding was observed after the seventh drop test. Hence, in this study patch-repaired and FRP-strengthened RC beams within the first two drop tests can last without any FPR strip delamination. Moreover, the highest percentage of FRP debonding (that is, 41.7 %) was observed after both third and fourth drop tests, while the highest percentage of total (end) FRP debonding (that is, 58.3%) was observed after the sixth drop test. Figure 4.27 shows the bending loads from which both first and total FRP debonding occurred.

On the basis of the results presented in Figure 4.27, it can be seen that, except for the results from SB2, there were very few differences in the bending forces relating to the first FRP debonding of the remaining patch-repaired and FRP-strengthened RC beams. As it was

previously discussed, SB2 exhibited higher elastic deformations (maximum deflections) so consequently the bending forces related to both first and last (total) FRP debonding would be the lowest. Thus the layers of SB2 disintegrated more easily at the lowest bending forces than the other patch-repaired and FRP-strengthened RC beams.

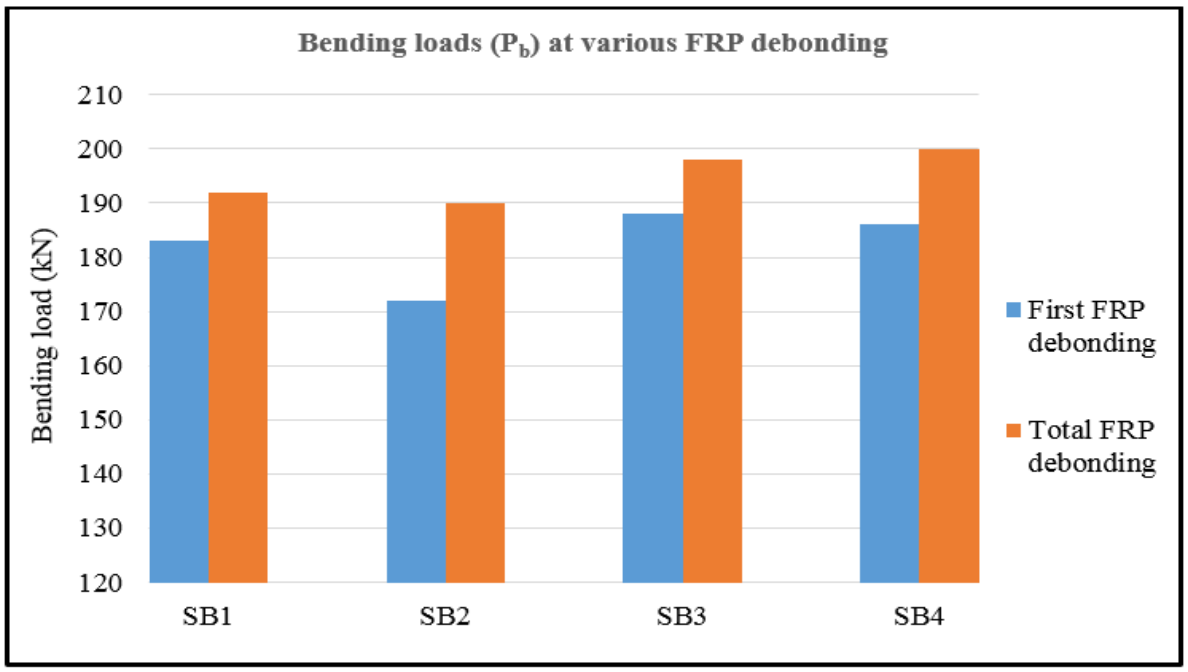

Figure 4.27. Bending loads (P_b) associated to various FRP debonding.

Apart from the failures observed from the interface between FRP strips and concrete layers, some cracks in the concrete layers were observed. The horizontally oriented cracks were seen to join previously formed flexural cracks and flexure-shear cracks. Those cracks were observed mostly in control beams; and a very small number of them were also observed in the patch-repaired and FRP-strengthened beams. However, these last types of cracks did not adversely affect the composite action between various layers in this current impact loading study.

4.7. The comparison to the findings from previously tested RC beams of the similar size subjected to quasi-static loading.

As previously mentioned, the current research is part of an ongoing study, and follows an experimental study made on the same number and on similar-sized RC beams that were subjected to quasi-static loading (Dladla, 2014). In addition, Mundeli, (2014) performed a numerical study on RC beams of the same size and –that are FRP-strengthened and patch-

repaired with concrete based material. Through the said numerical study, five models were investigated under quasi-static loading using Abaqus/ CAE software (Mundeli, 2014). These two experimental studies were performed with the common objective of assessing the behaviour of patch-repaired and FRP-strengthened RC beams. However, comparing the results obtained from the quasi-static loading and the impact loading testing of RC beams does not appear to be feasible, due to the differences in nature of the loading conditions and the associated methods of testing. Thus, the direct comparison between most of the findings obtained from these two type of experimental studies was not practical. Nevertheless, findings, such as cracking patterns and mode(s) of failure, are discussed here.

Results of experimental studies performed under both loading conditions led to the FRP debonding of patch-repaired and FRP-strengthened RC beams. Table 4.10 shows various loads associated with the FRP debonding from both quasi-static loading studies and the impact loading testing results. Apparently the values from quasi-static loadings were found to be higher than those from the impact loading. However the impact loading was performed as eight consecutive drop tests. Thus, the results presented in Table 4.10 were obtained from at least the third drop test, without accumulatively taking into account the first two previously performed drop tests on the same tested RC beams. If an accumulative summation was taken into account of all bending forces related to all performed drop tests (up to the appearance of the first FRP debonding) the values in Table 10 would not be the same.

Table 4.10. Comparison between various loads related to FRP debonding.

Results / Beam Type	Quasi-static loading		Impact loading
	Average debonding loads (kN)		Bending forces at first FRP debonding (kN)
	FEM Results	Experiment Results	
SB1 (450mm patch length)	226.2	205.0	183
SB2 (800mm patch length)	236.8	212.8	172
SB3 (1300mm patch length)	237.3	193.8	188
SB4 (1800mm patch length)	240.5	210.5	186

In both experimental studies, all tested RC beams failed in concrete crushing in the compression zone. In quasi-static loading tests, the concrete crushing failure occurred within/ near the maximum moment region. During the process of impact loading, the concrete crushing failure took place in the vicinity of the impact point. All tested RC beams under impact loading

exhibited more concrete spalling than those obtained under quasi-static loading tests. Apart from the shear plug failure experienced from the impact loading tested RC beams, both types of testing experienced flexural, flexure-shear and shear cracks. Some important flexural cracks were obtained under both loading conditions in the regions surrounding their respective points of loadings applications.

4.8. Chapter summary

In this chapter, the results obtained from 120 drop tests are analysed, discussed and presented. The discussion and interpretation of results focuses on the following points: recorded contact forces; inertial and bending forces; deflection results (including maximum deflections and half cycle duration, residual and cumulative residual deflections, and total deflection); progression of damage including cracking patterns and mode(s) of failure. In addition, the effects of varying patch repair lengths and the composite action between various layers under impact loading were discussed based on the aforementioned points.

In line with this chapter, deterioration of flexural rigidity and stiffness was discussed based on both recorded contact force and deflection results. Both flexural rigidity and stiffness degraded as the drop height increased. On the one hand, recorded contact force results exhibited relatively higher values from SB than CB. Thus, patch-repaired and FRP-strengthened beams were more rigid and less flexible than control beams. In addition, those results show that the longer the patch repair length, the higher the recorded contact force values. On the other hand, deflection results displayed almost equal values from CB rather than SB. Moreover, the final drop test results from SB3 and SB4 exhibited lower values than those from the remaining beam groups. Both elastic and plastic deformations were higher in the control beams than in the patch-repaired and strengthened beams, except for SB2. Hence, both flexural rigidity and stiffness deteriorated far more in CB than SB, with an exception for SB2. Furthermore, both inertial and bending forces increased as drop height increased, irrespective of the type of tested beam.

The effects of varying patch repair length on stiffness, through both recorded contact force and deflection results, were also discussed. In addition, its effects on the propagation of damage were also assessed. It was observed that the recorded contact force increased as the patch-repair length increased. The deflection results did not allow us to clearly express the effects of varying

patch-repair length. However, the tendency was that the patch repair length increased with the decrease in deflection results (except for SB2). Regarding propagation of damage, small differences were noticed in the extent of cracking patterns observed from the front view. The patch repair length increased as the extent of the observed cracking pattern from the front view decreased.

The assessment of the composite action between the different layers of patch-repaired and FRP-strengthened beams was also performed. Generally, under consecutive impact loading, various layers withstood strongly, except for the earlier start and end (total) of FRP debonding observed after the third drop test and the fifth drop test respectively. This was also true for the last start and end (total) of FRP debonding which was observed after the fifth drop test and the seventh drop test respectively. More that the half of the FRP-strengthened beams experienced total FRP debonding after the sixth drop test, while 41.7% of those beams exhibited the start of FRP debonding after both third and fourth drop tests. The various layers stayed together and worked well under consecutive impact loading. Very few small and horizontally oriented cracks were observed on the interfaces of old concrete and patch-repaired materials. SB2 presented lower bending forces associated with both first and total (end) of FRP debonding failure.

Finally, the comparison between some of the findings obtained under quasi-static and impact loadings was made. Due to the complexity of such a comparison, the focus was made on cracking pattern and mode(s) of failure. Under both loading conditions, all tested RC beams exhibited crushing of concrete in the compression zone and FRP debonding failures.

CHAPTER 5: CONCLUSIONS AND RECOMMENDATIONS

5.1. Conclusions

Concrete structures, and RC structures in particular, enable human beings to safely and reliably accomplish their daily activities. These structures include (but are not limited to) bridges, flyovers and interchanges, harbours and buildings. RC structures in service are subjected to various loading conditions such as impact loading, in combination with harsh or extreme environmental conditions, and their life span is likely to be shorter than anticipated. Impact loading will potentially endanger the RC structure, especially if engineers and researchers do not take this into consideration at the design stage. In addition, some of the RC structures in service are now old and need urgent maintenance if they are to fulfil their serviceability requirements. Rehabilitation of RC structures should be considered as a viable solution to these kind of structures. However, appropriate measures should be taken to avoid repairing already-repaired structures, or repairing a structure that has failed prematurely due to poor design (re-design) and poor workmanship. If rehabilitation techniques are adequately studied and applied, from the design or the re-design level up to implementation, that is, by taking into account all the necessary precautions including adequate workmanship and periodic quality control, rehabilitation is a cost-effective and durable solution for deteriorating RC structures.

The main objective of this research was to experimentally study the behaviour of FRP-strengthened RC beams with concrete patch repairs when they are subjected to impact loading. The dynamic response obtained from fifteen RC beams, namely contact force response and deflection response, was analysed, discussed and presented. The following research objectives were achieved by studying the behaviour of FRP-strengthened RC beams under impact loading:

- The investigation of the flexural rigidity and bending stiffness of tested RC beams and the associated deflection responses;
- The assessment of the effects of varying patch repair lengths on stiffness, and the resulting deflections and cracking patterns of patch-repaired and FRP-strengthened RC beams;
- The investigation of the propagation of damage including cracking patterns and the mode(s) of failure of patch-repaired and FRP-strengthened RC beams;

- The assessment of the composite action between various layers of materials of patch-repaired and FRP-strengthened RC beams under impact loading.

Twelve RC beams were consciously damaged by taking 4 mm uniformly out from the diameter of the main reinforcing bars. This corresponded to 14 % loss of the cross-sectional area in the tensile zone of FRP-strengthened RC beams. Concrete-based patch repairs and FRP adhesive materials, together with FRP composite material, were used to repair and rehabilitate twelve RC beams prior to impact loading testing. Appropriate conclusions, based on discussions presented in Chapter 4, were drawn from this experimental study in association with the research objectives.

5.1.1. Investigation on the flexural rigidity and bending stiffness and associated deflection responses

Both flexural rigidity and stiffness of controls and patch-repaired and FRP-strengthened RC beams were discussed and analysed, on the basis of contact forces and associated deflection responses. Also, an attempt was made to analyse and discuss the computed bending and inertial forces which were associated with both drop heights and maximum deflection responses. Nevertheless, regardless of the intensive calculations made to obtain the results of bending and inertia forces, the discussion and analysis of flexural rigidity was based on the maximum and residual deflections results. It should also be noted that the drop height increased with the increase in the number of drop tests. Consequently, the flexural rigidity and bending stiffness deteriorated as long as the drop height increased and consecutive drop tests were applied to tested RC beams.

1) An average of 64.5% of residual deflection was obtained after the seventh drop test. This led to the remaining residual deflection of 35.5% before the last drop test. The last drop test contributed considerably to the deterioration of stiffness of more than 30%, regardless of the type beam being tested. The increment in drop height was a governing parameter while assessing the stiffness and associated deflection response from beams subjected to consecutive impact loading.
2) Regardless of the type of RC beam tested, deflection half cycle duration increased as the drop height increased, except for the first drop test. Furthermore, it has clearly shown that when the drop height increases, the deflection half cycle duration

increases as a result of flexural rigidity decrease. The combined application of concrete based patch repairs and FRP strengthening method would be a good approach to repair and rehabilitate any deteriorating RC beams subjected to consecutive impact loading.

3) The control beams were more flexible than the patch-repaired and FRP-strengthened RC beams, with an exception made for SB2 results. Thus, the flexural rigidity and stiffness from patch-repaired and FRP-strengthened RC beams were globally higher than those obtained from control beams. Flexural rigidity and stiffness increased as the patch repair length increased. The brittle behaviour of FRP strengthening materials and their effects on the overall behaviour of strengthened RC beams was also confirmed on the basis of maximum deflection results.

5.1.2. Assessment of the effects of varying patch repair length on the stiffness, the resulting deflection and the cracking patterns

Patch lengths of 450 mm, 800 mm, 1300 mm and 1800 mm were prepared in advance of the concrete based patch repairs respectively for SB1, SB2, SB3 and SB4 beam groups. FRP sheets, epoxy adhesive layers and FRP sheets of the same size, same length, and thickness were applied to the intentionally damaged area. The utilised concrete based patch repairs exhibited an average compressive strength of 69.80 MPa, while the old concrete to be patch-repaired had an average compressive strength of 54.94 MPa. In addition, the maximum aggregate size used in this study was 9 mm and 19 mm respectively, for concrete based patch repairs and old concrete. This assessment of the effects of varying patch repair lengths of various results and parameters was made on the basis of contact recorded forces, deflection results and observations on the propagation of damage.

1) The patch repair length increase can substantially take a part to the increase of recorded contact force under consecutive impact loading. Thus, the length of patch-repair material can contribute positively to the overall compressive strength of patch-repaired and FRP-strengthened RC beams. Therefore, the longer the patch length, the higher the associated compressive strength. Consequently, the flexural rigidity increases.
2) The patch repair length increases with the decrease in the associated cracking profiles. Therefore, the combination of patch repair and FRP strengthening methods

might increase the ability of rehabilitated RC beams to withstand the easy cracking propagation and consequently reduce the cracking density.

3) The increase of patch repair length can lead to the reduction of both elastic (maximum deflection) and plastic (residual deflection) deformations of rehabilitated RC beams, with the exception of SB2. Therefore, the varying patch-repair lengths can contribute to the increase of stiffness of patch-repaired and FRP-strengthened RC beams.

5.1.3. Investigation on propagation of damage including the cracking patterns and the mode(s) of failure

Eight consecutive drop tests were applied from various drop heights to each of the fifteen control and rehabilitated RC beams. Propagation of damage, including cracking patterns and the mode(s) of failure, was assessed with an emphasis on qualitative aspects. Flexural, flexure-shear and shears cracks were observed on various beams. Both local and global failures were observed from various tested beams. Shear plug (cone cracking), concrete crushing and spalling, FRP debonding were also observed. The findings were in clear agreement with those obtained from previous researches of this kind, both in cracking patterns and mode(s) of failure of RC beams, and this includes the FRP-strengthened RC beams.

1) Regardless of the type of RC beam tested, all RC beams developed flexural cracks in the vicinity of the mid-point of the clear span, followed by the formation of shear plug starting from the impact point. In addition some flexure-shear cracks, mostly propagating from previously formed flexural cracks and a few shear cracks in the vicinity of supports, were observed.
2) All tested RC beams failed locally in concrete spalling and concrete crushing propagated from the impact point towards its surroundings. Also, pieces of concrete broke off on the distal side of the impact point in 53.3% of all tested RC beams. As the drop height increased after the performed consecutive drop tests, the quantity and the density of concrete crushing and spalling increased.
3) All patch-repaired and FRP-strengthened RC beams failed globally in FRP debonding with 16.7% of FRP-strengthened RC beams evincing an earlier total (end) FRP debonding failure after the fifth drop test. Many of the FRP-strengthened RC beams (that is, 58.3%) experienced their total (end) FRP debonding after the

sixth drop test. A quarter of the FRP-strengthened RC beams (that is, 25.0%) continued to resist and exhibited their total (end) FRP debonding after the seventh drop test.

4) All tested RC beams failed globally in permanent bending with the production of important residual deflections.

5.1.4. The assessment of the composite action between various layers of beam material under impact loading

The patch-repaired and FRP-strengthened RC beams tested in this experimental study were composed of various successive layers of materials: a layer of old concrete, the first epoxy adhesive layer, a layer of concrete-based patch repair, the second epoxy adhesive layer, a layer of FRP strip, the third epoxy adhesive layer and a layer of FRP sheet.

1) Apart from the observed FRP debonding which generally started from the third and fourth drop tests (>40%), patch-repaired and FRP-strengthened RC beams can work well under consecutive impact loading. Nevertheless, few short micro-cracks were observed at the interface between the old concrete and patch-repaired layer that is, along the first epoxy layer. Two out of the twelve patch-repaired and FRP-strengthened RC beams experienced such micro-cracks.
2) Patch-repaired and FRP-strengthened RC beams can perform well under consecutive impact loading without considerable defects (no FRP debonding) up to the second drop tests. Thus, depending on the magnitude of the impact load and the number of drop tests considered, various layers composing the patch-repaired and FRP-strengthened RC beams can to some extent withstand severe loadings such as impact loads. At this level, composite RC beams behave as monolithic structural elements.
3) More than 50% of the patch-repaired and FRP-strengthened RC beams subjected to consecutive impact loading experience their total (end) FRP debonding after the fifth drop test. Thus, patch-repaired and FRP-strengthened RC structures, including beams, should withstand a number of consecutive loads; in addition, the embedding of adequate monitoring systems in these structures (to track and record the level of a particular incident) will minimise future rehabilitation work and consequently the cost.

5.2. Recommendations

The use of FRP materials is gaining in popularity as a strengthening material and a considerable number of researchers and asset managers recognise the importance of fully understanding the behaviour of these materials. Thus more researches and studies, experimental, analytical and numerical, and under different loading conditions and environments, should be carried out in this field. Therefore, on the basis of the discussions, findings and conclusions of the current research, the following recommendations for future research and studies are proposed:

- Despite the fact that the tested RC beams had been designed for quasi-static loading, they performed well under extreme loadings such as impact loading. Thus, the combined use of concrete-based patch repairs and FRP strengthening materials should be adopted to rehabilitate deteriorating RC beams that are subjected to various loadings, including consecutive impact loading.
- Various adhesives (epoxies) have to be used to bond together different layers of the tested patch-repaired and strengthened RC beams. Few small cracks were observed along the created interfaces between old concrete, patch repairs and CFRP composite materials. Therefore, following the carefully conducted surface preparation work, various SIKA adhesives (epoxies) used for the tests should be recommended for future rehabilitation of RC beams that are subjected to consecutive impact loading.
- The use of strain gauges on the main reinforcing bars and on FRP strips under the same loading conditions are recommended to more accurately acquire data for understanding the deformation of the tested beams, not only at the mid-span but also at the other critical points. The distribution of longitudinal strains alongside the tested beams should also be analysed.
- The use of non-contact LVDTs to measure deflection at the mid-span of the tested beams might lead to the recording of accurate data which can be compared to the results obtained through using PFA software tool. The data from these LVDTs might take less time for their analysis compared to PFA software tool.
- The use of high capacity load cells, one attached to the drop hammer and the other two on the supports, would enable future researches to obtain a more reliable structural response on contact forces, bending forces and inertia forces. It will also allow researchers to save time for analysis and get more accurate data than

computing the bending forces from data extracted from HSC using PFA and Matlab software tools. Also, additional high capacity load cells should be provided to replace those which may break down during data gathering, due to the nature of the research.

- In a real situation, the impact loading can be applied on RC structures in service at various speeds and with differing weights. Therefore, effort should be made so that the impact loading testing can be done not only with drop height variations but also with varying the mass of the drop hammer from a constant drop height.
- Numerical and analytical studies should be conducted under impact loading on RC structures, so that the mechanisms involved in the degradation of those RC structures which are subjected to impact events would be well analysed and understood. These numerical studies may be also extended to cyclic or repetitive loading, to fully understand the behaviour of patch-repaired and FRP-strengthened RC structures.

BIBLIOGRAPHY

Abbas, A. A., Pullen, D. A. & Costovos, D. M., 2010. Structural response of RC wide beams under low-rate and impact loading. *Magazine of Concrete Research,* Volume 62, pp. 723-740.

ACI Committee, 4., 1996. *State-of-the-Art Report on Fiber Reinforced Plastic (FRP) Reinforcements for Concrete Structures,* Chicago: American Concrete Institute.

ACI Committee, 4., 2008. *Guide for the Design and Construction of Externally Bonded FRP Systems for Strengthening Concrete Structures.* Farmington Hills: American Concrete Institute.

Adhikary, D. S., Bing, L. & Fujikake, K., 2012. Dynamic behavior of reinforced concrete beams under varying rates of concentrated loading. *International Journal of Impact Engineering,* pp. 24-38.

Ahmad, S., 2009. Techniques for inducing accelerated corrosion of steel in concrete. *The Arabian Journal for Sciences and Engineering,* Volume 34, pp. 95-104.

Alkhairi, F. M. & Naaman, A. E., 1993. Analysis of Beams Prestressed with Unbonded Internal or External Tendons. *Journal of Structural Engineering,* Volume 119, pp. 2680-2700.

Alkhrdaji, T., 2004. *Keys to success: Structural repair and strengthening techniques for concrete facilities.* [Online]
Available at:
http://cenews.com/article/4146/keys_to_success_structural_repair_and_strengthening_techniques_for_concrete_facilities
[Accessed 15 February 2014].

Alkhrdaji, T., 2013. *Strengthening of Concrete Structures Using Reinforced Concrete Enlargement Systems.* s.l.:s.n.

Alkhrdaji, T. & Thomas, J., 2009. *Structural Strengthening Using External Post-Tensioning Systems.* [Online]
Available at: http://www.structuraltechnologies.com/article/structural-strengthening-using-external-post-tensioning-systems
[Accessed 16 February 2014].

Almusallam, T. H. & Al-Salloum, Y. A., 2001. Ultimate strength prediction for RC beams externally strengthened by composite materials. *Composites. Part B: Engineering,* Volume 32, pp. 609-619.

An, W., Saadatmanesh, H. & Ehsani, M. R., 1991. RC Beams Strengthened with FRP Plates. II: Analysis and Parametric Study. *Journal of Structural Engineering,* Volume 117, pp. 3434-3455.

Arslan, G., Sevuk, F. & Ekiz, I., 2008. Steel plate contribution to load-carrying capacity of retrofitted RC beams. *Construction and Building Materials,* Volume 22, pp. 143-153.

Aykac, S. et al., 2013. Strengthening and Repair of Reinforced Concrete Beams Using External Steel Plates. *Journal of Structural Engineering,* Volume 139, pp. 929-939.

Azizinamini, A. & Gull, J., 2012. *Improved Inspection Techniques for Steel Prestressing / Post-tensioning Strand,* Miami: Florida International University.

Badawi, M. & Soudki, K., 2005. Control of Corrosion_Induced Damage in Reinforced Concrete Beams Using Carbon Fiber-Reinforced Polymer Laminates. *Journal of Composites for Construction,* Volume 9, pp. 195-201.

Bakis, C. E. et al., 2002. Fiber-Reinforced Polymer Composites for Construction-State-of-the-Art Review. *Journal of Composites for Construction,* Volume 6, pp. 73-85.

Bangash, M. Y. H., 1989. *Concrete and concrete structures: numerical modelling and applications.* London: Elsevier Science.

Banthia, N., Mindess, S. & Pigeon, M., 1989. Impact testing of Concrete Using a Drop-weight Impact Machine. *Experimental Mechanics,* Volume 29, pp. 63-69.

Barros, J. A. O. & Dalfré, G. M., 2013. Assessment of the Effectiveness of the Embedded Through-Section Technique for the Shear Strengthening of Reinforced Concrete Beams. *Strain,* 49(1), pp. 75-93.

Barr, P., 1990. *Guidelines for design and assessment of concrete structures subjected to impact,* London: UK Atomic Energy Authority, Safety and Reliability Directorate, HMSO.

Bentur, A., Berke, N. & Diamond, S., 1997. *Steel Corrosion in Concrete: Fundamentals and civil engineering practice.* 1st ed. London: CRC Press.

Bentur, A., Mindess, S. & Banthia, N., 1986. The behaviour of concrete under impact loading: Experimental procedures and method of analysis. *Materials and Structures,* 19(5), pp. 371-378.

Beushausen, H.-D. & Alexander, M. G., 2009. Concrete repair. In: G. Owens, ed. *Fulton's Concrete Technology*. Midrand, South Africa: Cement & Concrete Institute, pp. 311-330.

Bischoff, P. H. & Perry, S. H., 1991. Compressive behaviour of concrete at high strain rates. *Materials and Structures/Matériaux et Constructions,* Volume 24, pp. 425-450.

Broomfield, J. P., 2007. *Corrosion of steel in concrete: Understanding , investigation and repair*. 2nd ed. New York, USA: Taylor & Francis.

Büyüköztürk, O. & Hearing, B., 1998. Failure Behaviour of Precracked Concrete Beams Retrofitted with FRP. *Journal of Composites for Construction,* Volume 2, pp. 138-144.

Capozucca, R., 1995. Damage to reinforced concrete due to reinforcement corrosion. *Construction and Building Materials,* Volume 9, pp. 295-303.

Chaallal, O., Mofidi, A., Benmokrane, B. & Neale, K., 2011. Embedded Through-Section FRP Rod Method for Shear Strengthening of RC Beams: Performance and Comparison with Existing Techniques. *Journal of composites for construction,* Volume 15, pp. 374-383.

Chalioris, C. E., Papadopoulos, C. P. & Pourzitidis, C. N., 2013. Application of a Reinforced Self-Compacting Concrete Jacket in Damaged Reinforced Concrete Beams under Monotonic and Repeated Loading. *Journal of Engineering,* Volume 2013, pp. 1-12.

Chalioris, C. E. & Pourzitidis, C. N., 2012. Self-Compacting Concrete Jacketing-Tests and Analysis. *AASRI Procedia,* Volume 3, pp. 624-629.

Charif, A., 1983. *Structural behaviour of reinforced concrete beams strengthened by epoxy bonded steel plates. PhD Thesis.* Sheffield: The University of Sheffield.

Chelapati, C. V., Kennedy, R. P. & Wall, I. B., 1972. Probabilistic assessment of hazard for nuclear structures. *Nucl Eng Des,* pp. 333-364.

Chen, Y. & May, I. M., 2009. Reinforced concrete members under drop-weight impacts. *Structures and Buildings,* 162(SBI), pp. 45-56.

Chlosta, M., 2012. *Feasibility study on fiber reinforced polymer cylindrical truss bridges for heavy traffic. Master's thesis.* Delft: Delft University of Technology.

Clough, R. W. & Penzien, J., 2003. *Dynamics of Structures.* Third ed. Berkeley: Computers & Structures.

Comité, E. -. I. d. B., 1993. *CEB-FIP Model Code 1990.* London: Thomas Telford Services Ltd.

Crains, J., Du, Y. & Law, D., 2008. Structural performance of corrosion-damaged concrete beams. *Magazine of Concrete Research,* Volume 60, pp. 259-370.

Cusatis, G., 2011. Strain-rate effects on concrete behavior. *International Journal of Impact Engineering,* Volume 38, pp. 162-170.

De Lorenzis, L. & Teng, J. G., 2007. Near-surface mounted FRP reinforcement: An emerging technique for strengthening structures. *Composites-Part B: Engineering,* Volume 38, pp. 119-143.

Dladla, T., 2014. *The behaviour of patch repaired and strengthened beams: An experimental investigation. MSc Thesis.* Cape Town: University of Cape Town.

Einde, L. V. D., Zhao, L. & Seible, F., 2003. Use of FRP composites in civil structural applications. *Construction and Building materials,* pp. 389-403.

El Maaddawy, T. & Soudki, K., 2005. Carbon-Fiber-Reinforced Polymer Repair to Extend Service Life of Corroded Reinforced Concrete Beams. *Journal of Composites for Construction,* Volume 9, pp. 187-194.

El-Hacha, R. & Rizkalla, S. H., 2004. Near-Surface-Mounted Fiber-Reinforced Polymer Reinforcements for Flexural Strengthening of Concrete Structures. *ACI Structural Journal,* Volume 101, pp. 717-726.

El-Hacha, R., Wight, R. G. & Green, M. F., 2001. Prestressed fibre-reinforced polymer laminates for strengthening structures. *Progress in Structural Engineering and Materials,* Volume 3, pp. 111-121.

Erki, M. A. & Meier, U., 1999. Impact Loading of Concrete Beams Externally Strengthened with CFRP Laminates. *Journal of Composites for Construction,* Volume 3, pp. 117-124.

Esfahani, M. R., Kianoush, M. R. & Tajari, A. R., 2007. Flexural behaviour of reinforced concrete beams strengthened by CFRP sheets. *Engineering Structures,* pp. 2428-2444.

FIB, B., 2001. *Externally bonded FRP reinforcement for RC structures.* Lausanne, Switzerland: International Federation for structural Concrete (fib).

FIB, B., 2007. *FRP reinforcement in RC structures,* Lausanne, Switzerland: International Federation for structural Concrete (fib).

Field, J. E. et al., 2004. Review of experimental techniques for high rate deformation and shock studies. *International Journal of Impact Engineering,* pp. 725-775.

Frangou, M., Pilakoutas, K. & Dristos, S., 1995. Structural repair/ strengthening of RC columns. *Construction and Building Materials,* Volume 9, pp. 259-266.

Fu, H. C., Erki, M. A. & Seckin, M., 1991. Review of Effects of Loading Rate on Reinforced Concrete. *Journal of Structural Engineering,* Volume 117, pp. 3660-3679.

Fujikake, K., Li, B. & Soeun, S., 2009. Impact Response of Reinforced Concrete Beam and Its Analytical Evaluation. *Journal of Structural Engineering* , Volume 135, pp. 938-950.

Fujikake, K., Senga, T., Ueda, N. O. T. & Katagari, M., 2006. Study on Impact response of Reactive Powder Concrete Beam and Its Analytical Model. *Journal of Advanced Concrete Technology,* Volume 4, pp. 99-108.

Fullard, K., 1991. *Interpretation of low-velocity damage tests on concrete slabs.* Manchester, Proceedings of the international conference on earthquake, blast and impact.

Gao, B., Leung, K. Y. C. & Kim, J.-K., 2007. Failure diagrams of FRP strengthened RC beams. *Composite Structures,* pp. 493-508.

Garden, H. N. & Hollaway, L. C., 1998. An experimental study of the failure modes of reinforced concrete beams strengthened with prestressed carbon composite plates. *Composites Part B,* Volume 29, pp. 411-424.

Garden, H. N. & Mays, G. C., 1999. Structural strengthening of concrete beams using prestressed plates. In: L. C. Hollaway & M. B. Leeming, eds. *Strengthening of reinforced concrete structures-Using Externally-bonded FRP composites in structural and civil engineering.* Boca Raton, Florida: Woodhead Publishing and CRC Press LLC, pp. 135-155.

Grandić, D., Bjegović, D. & Grandić, I. Š., 2011. *Deflection of reinforced concrete beams simultaneously subjected to sustained load and reinforcement corrosion.* Como: s.n.

Grote, D. L., Park, S. W. & Zhou, M., 2001. Dynamic behavior of concrete at high strain rates and pressures: I. experimental characterization. *International Journal of Impact Engineering,* Volume 25, pp. 869-886.

Hollaway, L., 1993. *Polymer Composites for Civil and Structural Engineering.* First ed. London: Springer Limited.

Hussain, M. et al., 1995. Flexural Behaviour of Precracked Reinforced Concrete Beams Strengthened Externally by Steel Plates. *ACI Structural Journal,* Volume 92, pp. 14-23.

ISIS, C., 2004. *An Introduction to FRP Strengthening of Concrete Structures.* Winnipeg, Manitoba: ISIS Canada.

Jumaat, Z. M. & Alam, A., 2006. Problems Associated with Plate Bonding Methods of strengthening Reinforced Concrete Beams. *Journal of Applied Sciences Research,* Volume 2, pp. 703-708.

Jumaat, Z. M. & Alam, A. M., 2007. Plate bonded strengthened RC beams with end and intermediate anchors. *International Journal of Engineering and Technology,* 4(2), pp. 185-193.

Kapasny, L. & Zembo, S., 1993. *The influence of the reinforcement corrosion on the load-bearing capacity of the reinforced concrete structures.* Bratislava, RILEM Publications.

Kar, A. K., 1978. Local effects of Tornado-Generated Missiles. *Journal of the Structural Division,* Volume 104, pp. 809-816.

Karbhari, M. V. & Zhao, L., 2000. Use of composites for 21st century civil infrastructure. *Computer methods in applied mechanics and engineering,* pp. 433-454.

Kennedy, R. P., 1976. A review of procedures for the analysis and design of concrete structures to resist missile impact effects. *Nucl Eng Des,* pp. 183-203.

Kishi, Norimitsu, Hiroshi & Mikami, 2012. Empirical Formulas for designing Reinforced Concrete Beams under Impact Loading. *ACI Structural Journal,* 109(4), pp. 509-519.

Klaiber, F. W. & Wipf, T. J., 2000. Strengthening and Rehabilitation. In: W. C. a. L. Duan, ed. *Bridge Engineering Handbook.* Wai-Fah Chen and Lian Duan ed. Boca Raton, Florida: CRC Press, pp. 50.1-38.

Kollar, P. L. & Springer, S. G., 2003. *Mechanics of composite structures.* New York: Cambridge University Press.

Krauser, L., 2006. Repairs, modifications, and strengthening with post-tensioning. *PTI Journal,* Volume 4, pp. 24-40.

Li, Q. M. & Chen, X. W., 2003. Dimensional formulae for penetration depth of concrete target impacted by a non-deformable projectile. *International Journal of Impact Engineering.,* pp. 93-116.

Li, Q. M., Reid, S. R., Wen, H. M. & Telford, A. R., 2005. Local impact effects of hard missiles on concrete targets. *International Journal of Impact Engineering,* pp. 224-284.

MacDonald, M. D. & Calder, A. J. J., 1982. Bonded steel plating for strengthening concrete structures. *International Journal of Adhesion and Adhesives,* Volume 2, pp. 119-127.

Mackechnie, J. R. & Alexander, M. G., 2001. *Repair principles for corrosion-damaged reinforced concrete structures,* Cape Town.: Department of Civil Engineering. University of Cape Town.

Mainstone, R. J., 1975. Properties of materials at high rates of staining or loading. *Matériaux et Constructions,* 8(2), pp. 102-116.

Malumbela, G., 2010. *Measurable parameters for performance of corroded and repaired RC beams under load. PhD Thesis.* Cape Town: University of Cape Town.

Malvar, L. J., 1998. Review of Static and Dynamic Properties of Steel Reinforcing Bars. *ACI Materials Journal,* pp. 609-614.

Malvar, L. J. & Crawford, J. E., 1998. *Dynamic Increase Factors for Concrete,* Orlando, Florida: Directorate for Information Operations and Reports, 1215 Jefferson Davis Highway, Suite 1204, Arlington Va 22202-4302.

Masoud, S., Soudki, K. & Topper, T., 2005. Postrepair Fatigue Performance of FRP-Repaired corroded RC Beams: Experimental and Analytical Investigation. *Journal of Composites for Construction,* Volume 9, pp. 441-449.

Matthys, S., 2000. *Structural behaviour and design of concrete members strengthened with externally bonded FRP reinforcement. PhD Thesis.* Ghent: Ghent University.

Mazumdar, S. K., 2002. *Composites Manufacturing : Materials, Product, and Process Engineering.* Boca Raton, Florida: CRC Press.

Meier, U., 1995. Strengthening of structures using carbon fibre/epoxy composites. *Construction and Building Materials,* Volume 9, pp. 341-351.

Metz, R., 2007. Impact and Drop Testing with ICP Force Sensors. *Sound and Vibration,* pp. 18-20.

Motavalli, M. & Czaderski, C., 2007. FRP Composites for Retrofitting of Existing Civil Structures in Europe: Stae-of-the-Art Review. *Composites & Polycon,* pp. 1-5.

Muda, C. Z. et al., 2013. A review - Local failure on Concrete Target due to Projectile Impact. *International Journal of Scientific & Engineering Research,* 4(1).

Mullajee, A. F., 2014. *The Performance Assessment of Patch Repaired and CFRP Strengthened RC T-beams under Transverse Impact Loading.MSc Thesis.* Cape Town: University of Cape Town.

Mundeli, S., 2014. *Behavior of RC beams patch repaired and strengthened with FRP composites: A numerical study.* Cape Town: University of Cape Town.

Nave, C. R., 2001. *HyperPhysics Mechanics,* Athens: National Science Teachers Association.

Nezamian, A. & Setunge, S., 2004. *Comparison between ACI 440 and FIB 14 design guidelines in using CFRP for strengthening of a concrete bridge headstock.* Calgary, Canadian Society for Civil Engineering.

Nurbaiah, M. N., Hanizah, A. H., Nursafarina, A. & Nur, A. M., 2010. *Flexural Behaviour Of RC Beams Strengthened With Externally Bonded (EB) FRP Sheets Or Near Surface Mounted(NSM) FRP Rods Method.* Kuala Lumpur, Institute of Electrical and Electronics Engineers.

Oehlers, D. J., 1992. Reinforced concrete beams with plates glued to their soffits. *Journal of Structural Engineering,* Volume 118, pp. 2023-2038.

Oehlers, D. J. & Ali, M. M. S., 1998. Debonding of steel plates glued to RC flexural members. *Progress in Structural Engineering and Materials,* Volume 2, pp. 185-192.

Oh, H. B., Cho, Y. J. & Park, G. D., 2003. Static and Fatigue Behaviour of Reinforced Concrete Beams Strengthened with Steel Plates for Flexure. *Journal of Structural Engineering,* Volume 129, pp. 527-535.

Pająk, M., 2011. The influence of the strain rate on the strength of concrete taking into account the experimental techniques. *Architecture Civil Engineering Environment Journal*, pp. 77-86.

Picard, A., Massicotte, B. & Bastien, J., 1995. Relative Efficiency of External Prestressing. *Journal of Structural Engineering,* Volume 121, pp. 1832-1841.

Potyrala, P. B. & Rius, J. R. C., 2011. *Use of Fibre Reinforced Polymers in Bridge Construction. State of the Art in Hybrid and All-Composite Structures.* Barcelona, Spain: Universitat Politecnica de Catalunya.

Quantrill, R. J. & Hollaway, L. C., 1998. The flexural rehabilitation of reinforced concrete beams by using the use of prestressed advanced composite plates. *Composite Science and Technology,* Volume 58, pp. 1259-1275.

Rahimi, H. & Hutchinson, A., 2001. Concrete Beams Strengthened with Externally Bonded FRP Plates. *Journal of Composites for Construction,* Volume 5, pp. 44-56.

Richardson, M. O. M. & Wisheart, J. M., 1996. Review of low-velocity impact properties of composite materials. *Composites Part A,* pp. 1123-1131.

Riisgaard, B. et al., 2007. *Dynamic Increase Factors for High Performance Concrete in Compression using Split Hopkinson Pressure Bar.* Catania, Italy, CRC Press.

Rizkalla, S., Hassan, T. & Hassan, N., 2003. Design recommendations for the use of FRP for reinforcement and strengthening of concrete structures. *Progress in Structural Engineering and Materials,* 5(1), pp. 16-28.

Ryall, M. J., 2001. *Bridge Management.* 1st ed. Oxford: Butterworth Heinemann.

Saadatmanesh, H. & Ehsani, M. R., 1991. RC Beams Strengthened with GFRP Plates. I: Experimental Study. *Journal of Structural Engineering,* Volume 117, pp. 3417-3433.

Saatci, S., 2007. *Behaviour and modelling of reinforced concrete structures subjected to impact loads. PhD Thesis.* Toronto: University of Toronto.

Saatci, S. & Vecchio, J. F., 2009. Effects of Shear Mechanisms on Impact Behavior of Reinforced Concrete Beams. *ACI Structural Journal,* Volume 106, pp. 78-86.

Sangi, A. J., 2011. *Reinforced concrete structures under impact loads.PhD Thesis.* Edinburg: Heriot-Watt University.

Seible, F., 2001. Designing with FRP Composites in the Civil Structural Environment. In: J. G. Teng, ed. *FRP Composites in Civil Engineering.* Hong Kong: Elsevier, pp. 73-84.

Setunge, S. et al., 2002. *Review of strengthening techniques using externally bonded fiber reinforced polymer composites,* Brisbane: CRC Construction Innovation.

Setunge, S. et al., 2002. *User Friendly Guide for rehabilitation or Strengthening of Bridge Structures Using Fiber Reinforced Polymer Composites,* Brisbane: CRC Construction Innovation.

Shiu, W. J., 2008. *Impact de missiles rigides sur structures en béton armé: analyse par la méthode des éléments discrets. PhD Thesis.* Grenoble: Université Joseph Fourier.

Sika, 2013. *Product Manual 2013/14.* Westmead, Pinetown: Sika South Africa.

Soleimani, S., Banthia, N. & Mindess, S., 2007. *Behaviour of RC beams under impact loading: some new findings.* Catania, Italy, CRC Press.

Soleimani, S. M. & Banthia, N., 2014. A Novel Drop Weight Impact Setup for Testing Reinforced Concrete Beams. *Experimental Techniques,* 38(3), pp. 72-79.

Soudki, K., 2011. Using fibre reinforced polymer (FRP) composites to extend the service life of corroded concrete structures. In: V. M. Karbhari & L. S. Lee, eds. *Service life estimation and extension of civil engineering structures.* Cambridge, UK: Woodhead Publishing Limited, pp. 75-95.

Suaris, W. & Shah, S. P., 1983. Properties of Concrete Subjected to Impact. *Journal of Structural Engineering,* 109(7), pp. 1727-1741.

Swamy, R. N., Jones, R. & Bloxham, J. W., 1987. Structural behaviour of reinforced concrete beams strengthened by epoxy-bonded steel plates. *The Structural Engineer,* Volume 65, pp. 59-68.

Szabó, Z. K. & Balázs, G. L., 2007. Near surface mounted FRP reinforcement for strengthening of concrete structures. *Periodica Polytechnica: Civil Engineering,* Volume 51, pp. 33-38.

Tachibana, S., Masuya, H. & Nakamura, S., 2010. Performance based design of reinforced concrete beams under impact. *Natural Hazards and Earth System Sciences,* pp. 1069-1078.

Takeda, J. & Tachikawa, H., 1971. *Deformation and fracture of concrete subjected to dynamic load.* Tokyo: Society of Materials Science.

Täljsten, B., 2006. *FRP Strengthening of Existing Concrete Structures: Design Guidelines.* 4th Edition ed. Lulea: Division of Structral Engineering, Lulea University of Technology, ISBN 91-89580-03-6, Sweden.

Täljsten, B. & Anders, C., 2001. *CFRP-strengthening: concrete beams strengthened with near surface mounted CFRP laminates.* London, Thomas Telford Ltd.

Tang, T. & Saadatmanesh, H., 2003. Behavior of Concrete Beams Strengthened with Fiber-Reinforced Polymer Laminates under Impact Loading. *Journal of Composites for Construction,* Volume 7, pp. 209-218.

Tavakkolizadeh, M. & Saadatmanesh, H., 2003. Fatigue Strength of Steel Girders Strengthened with Carbon Fiber Reinforced Polymer Patch. *Journal of Structural Engineering,* Volume 129, pp. 186-196.

Thermou, G. E., Pantazopoulou, S. J. & Elnashai, S. A., 2007. Flexural Behaviour of Brittle RC Members Rehabilitated with Concrete Jacketing. *Journal of Structural Engineering,* Volume 133, pp. 1373-1384.

Toutanji, H., Zhao, L. & Zhang, Y., 2006. Flexural behaviour of reinforced concrete beams externally strengthened with CFRP sheets bonded with an inorganic matrix. *Engineering Structures,* pp. 557-566.

Tuakta, C., 2005. *Use of Fiber Reinforced Polymer Composite in Bridge Structures. Master's Thesis.* Cambridge: Massachusetts Institute of Technology.

Vandoros, K. G. & Dritsos, S. E., 2008. Concrete jacket construction detail effectiveness when strengthening RC columns. *Construction and Building Materials,* Volume 22, pp. 264-276.

Vaysburd, A., Emmons, P. H. & Bisonnette, B., 2009. *Concrete repair: Research and practice.* London, Taylor & Francis Group.

Vaysburd, A. M., 2006. Holistic system approach to design and implementation of concrete repair. *Journal of Cement and Concrete Composites,* pp. 671-678.

Vidal, T., Castel, A. & François, R., 2007. Corrosion process and structural performance of 17 year old reinforced concrete beam stored in chloride environment. *Cement and Concrete Research,* pp. 1551-1561.

Waghmare, S. P. B., 2011. Materials and Jacketing Technique for retrofitting of Structures. *International Journal of Advanced Engineering Research and studies,* Volume 1, pp. 15-19.

Wakabayashi, M. et al., 1980. *Dynamic loading effects on the structural performance of concrete and steel materials and beams.* Istanbul, International Association for Earthquake Engineering.

White, T. W., Soudki, K. A. & Erki, M.-A., 2001. Response of RC Beams Strengthened with CFRP Laminates and Subjected to a High Rate of Loading. *Journal of Composites for Construction,* Volume 5, pp. 153-162.

Zhang, F., Pan, J. & Lin, C., 2009. Localised corrosion behaviour of reinforcement steel in simulated concrete pore solution. *Corrosion Science,* pp. 2130-2138.

Zhang, R., Castel, A. & François, R., 2010. Concrete cover cracking with reinforcement corrosion of RC beam during chloride-induced corrosion process. *Concrete and Cement Research,* pp. 415-425.

Zhao, X.-L. & Zhang, L., 2007. State-of-the-art review on FRP strengthened steel structures. *Engineering Structures,* pp. 1808-1823.

APPENDICES

APPENDIX A: RECORDED CONTACT FORCE HISTORY DIAGRAMS AVAILABLE RESULTING FROM VARIOUS TESTED RC BEAMS.

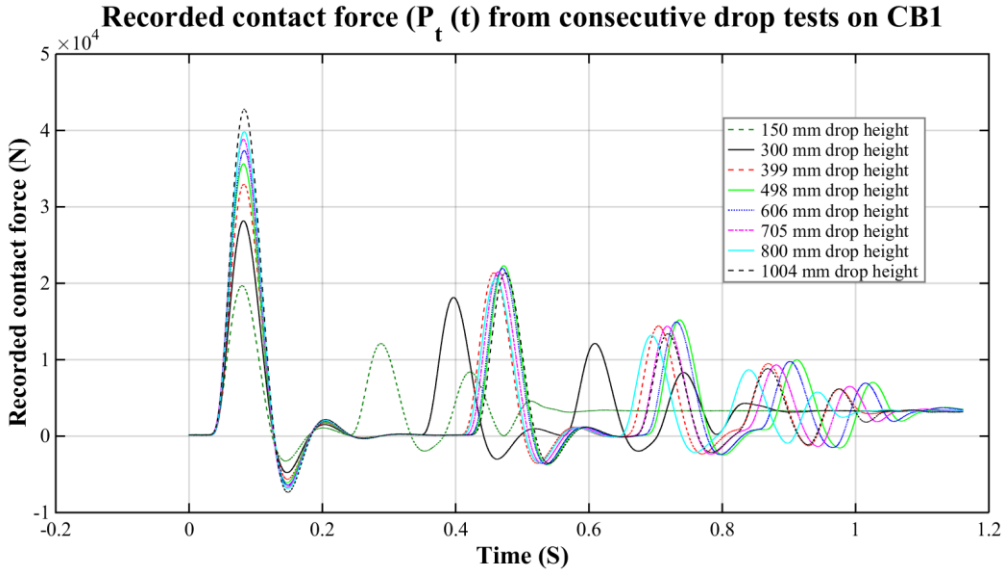

APPENDIX A. 1. 1. Recorded contact force response from CB1.

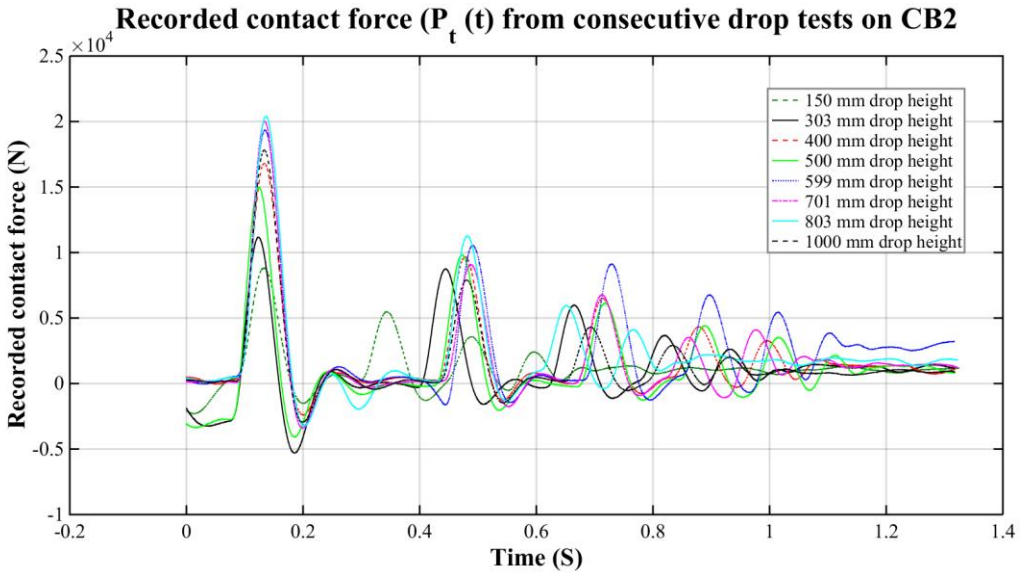

APPENDIX A. 1. 2. Recorded contact force response from CB2.

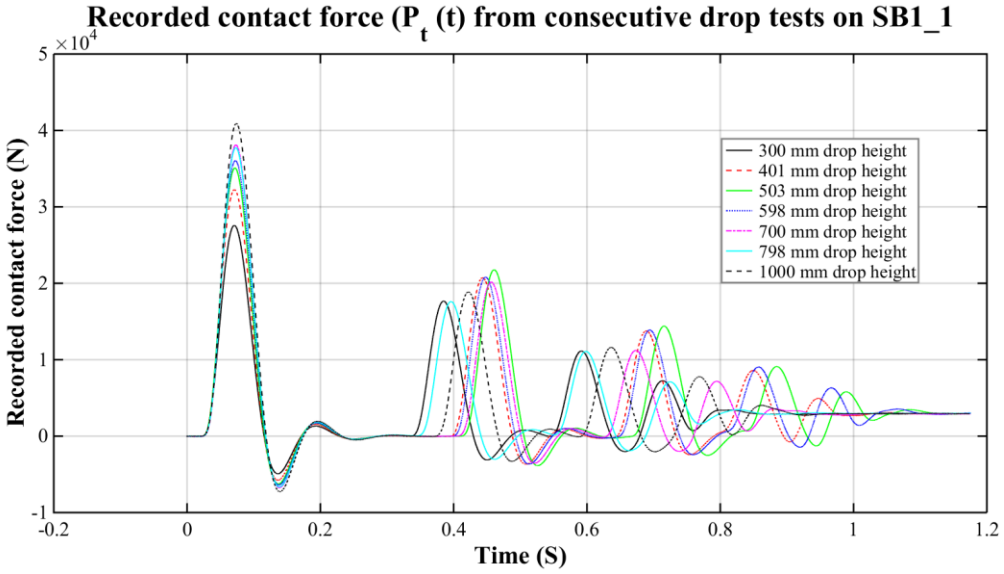

APPENDIX A. 2. 1. Recorded contact force response from SB1_1.

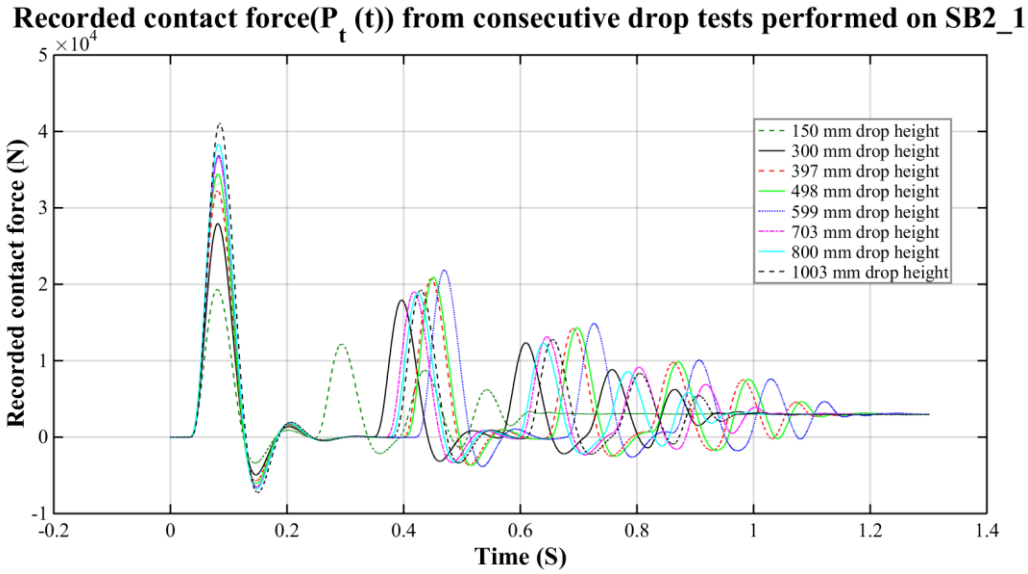

APPENDIX A. 3. 1. Recorded contact force response from SB2_1.

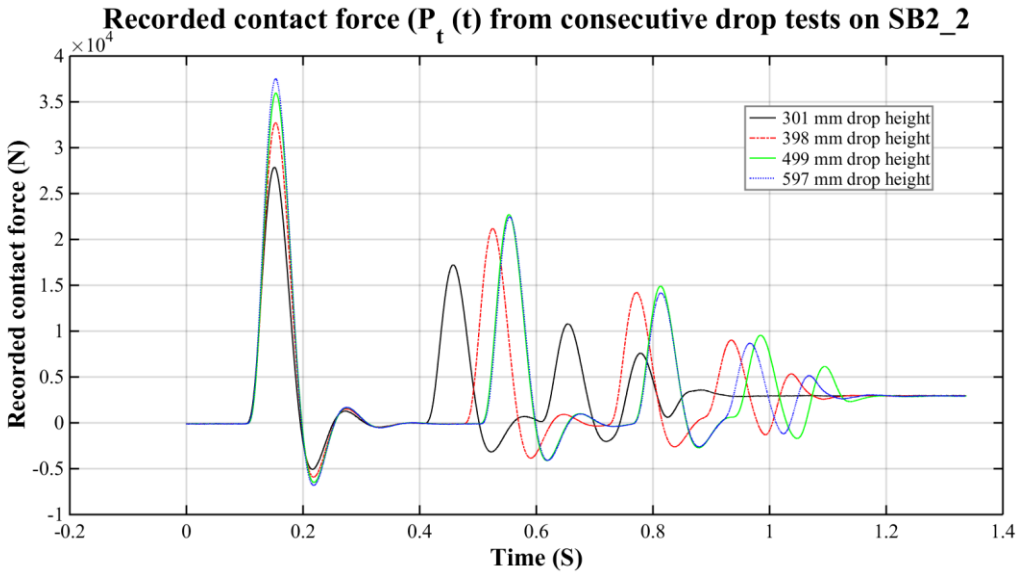

APPENDIX A. 3. 2. Recorded contact force response from SB2_2.

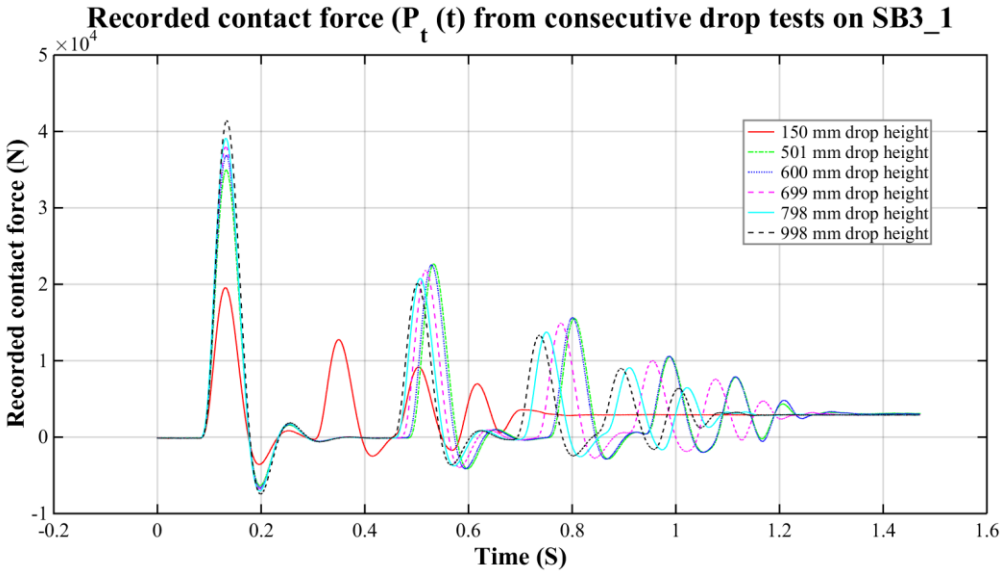

APPENDIX A. 4. 1. Recorded contact force response from SB3_1.

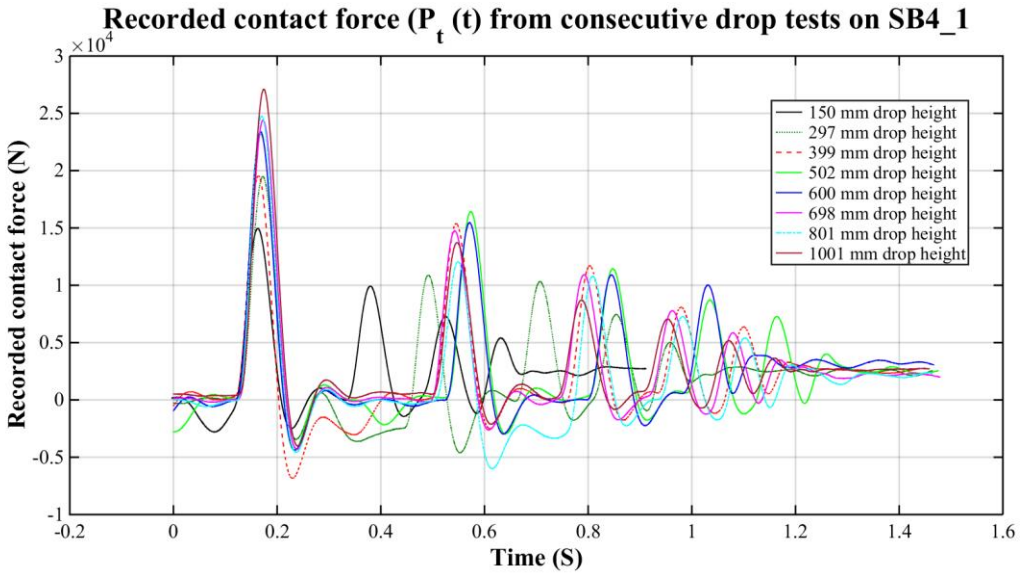

APPENDIX A. 5. 1. Recorded contact force response from SB4_1.

APPENDIX B. PROGRESSION OF DAMAGE OBSERVED FROM DROP TESTING OF VARIOUS RC BEAMS.

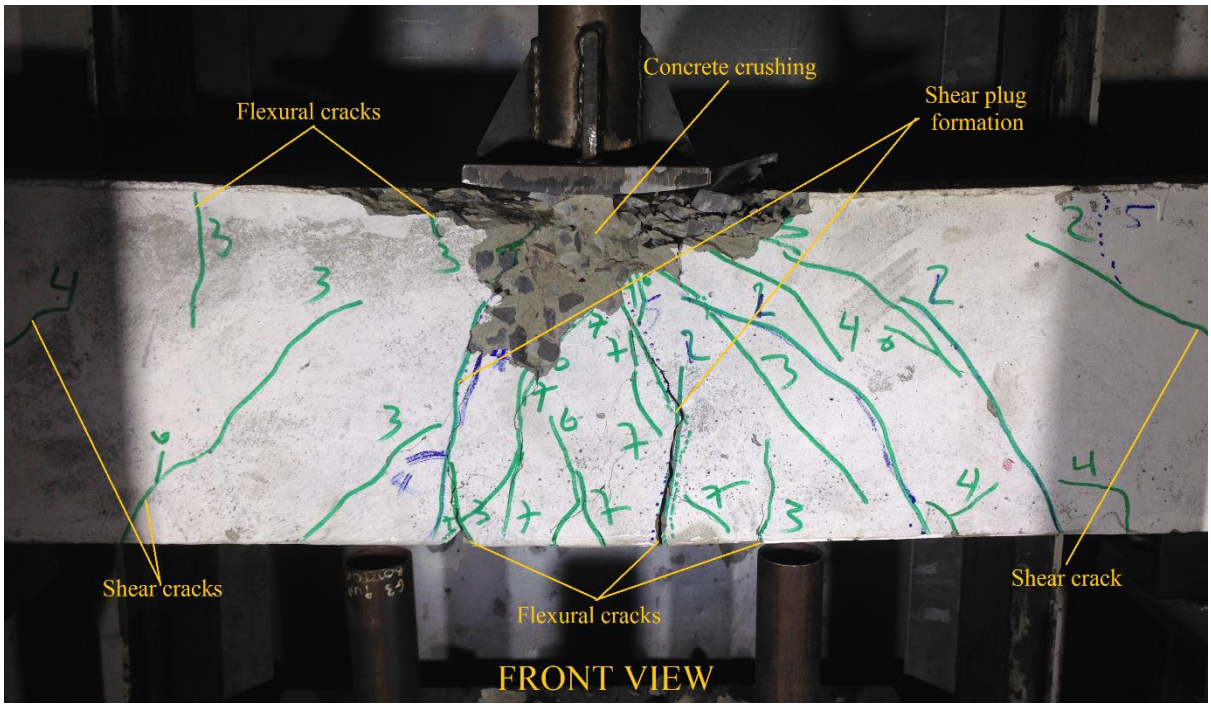

Appendix B. 1. 1. Cracking profiles and mode of failure observed from CB1.

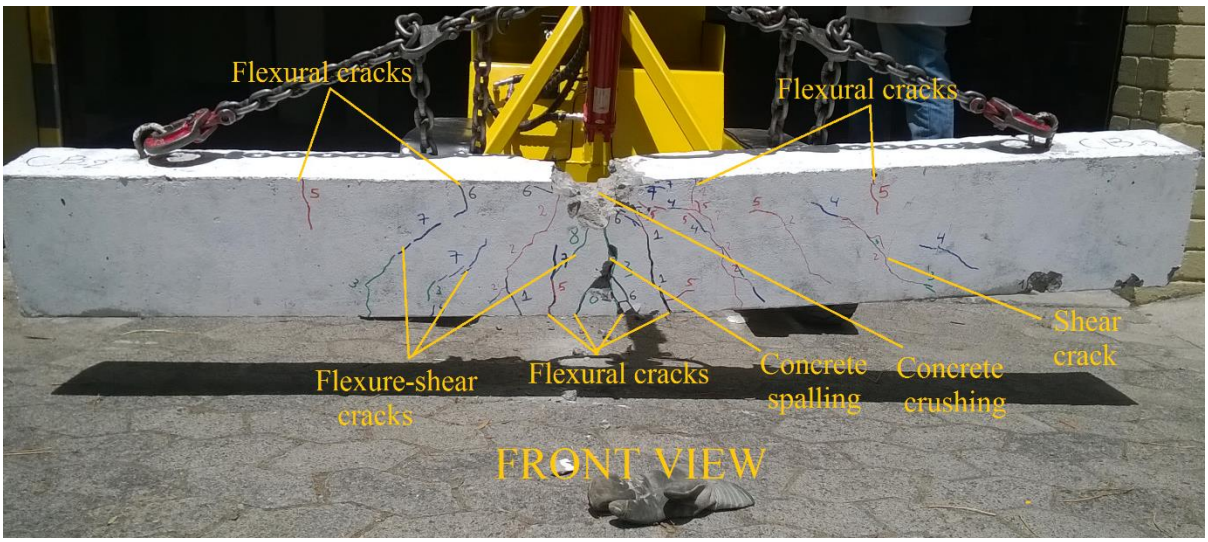

Appendix B. 1. 2. Cracking profiles and mode of failure observed from CB2.

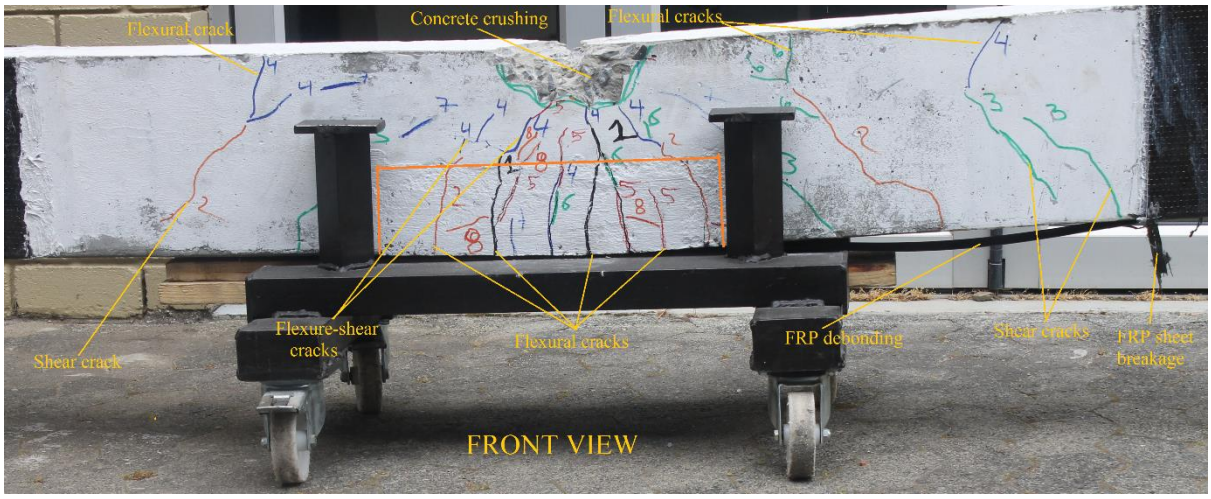

Appendix B. 2. 1. Cracking profiles and mode of failure observed from SB1_1 (a).

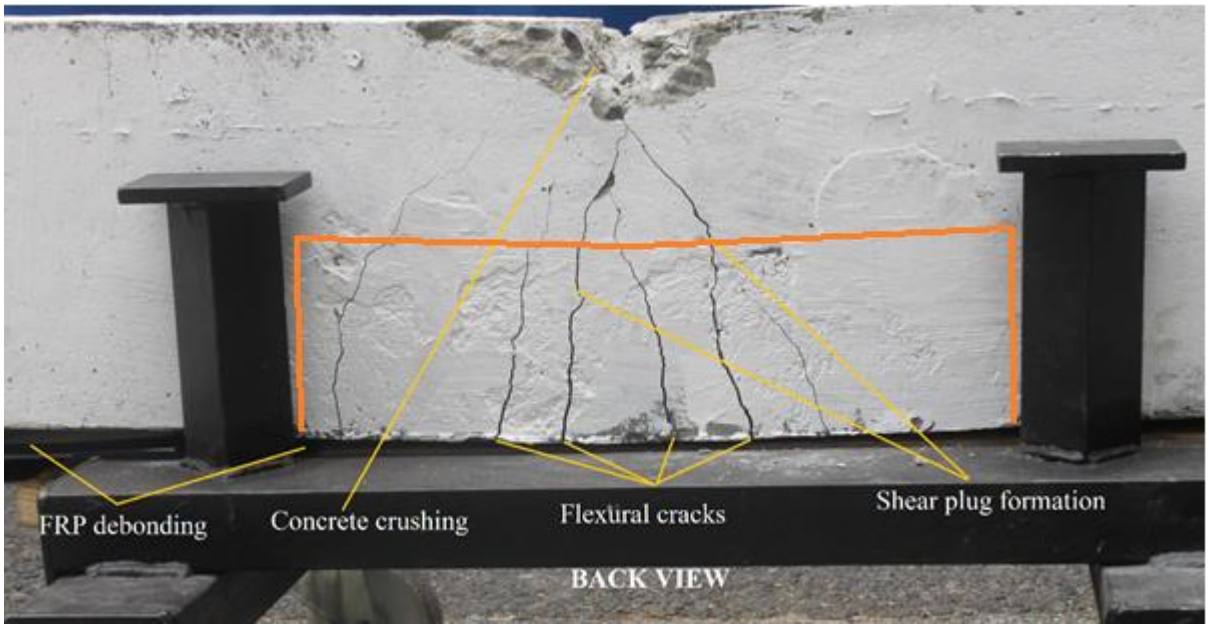

Appendix B. 2. 2. Cracking profiles and mode of failure observed from SB1_1 (b).

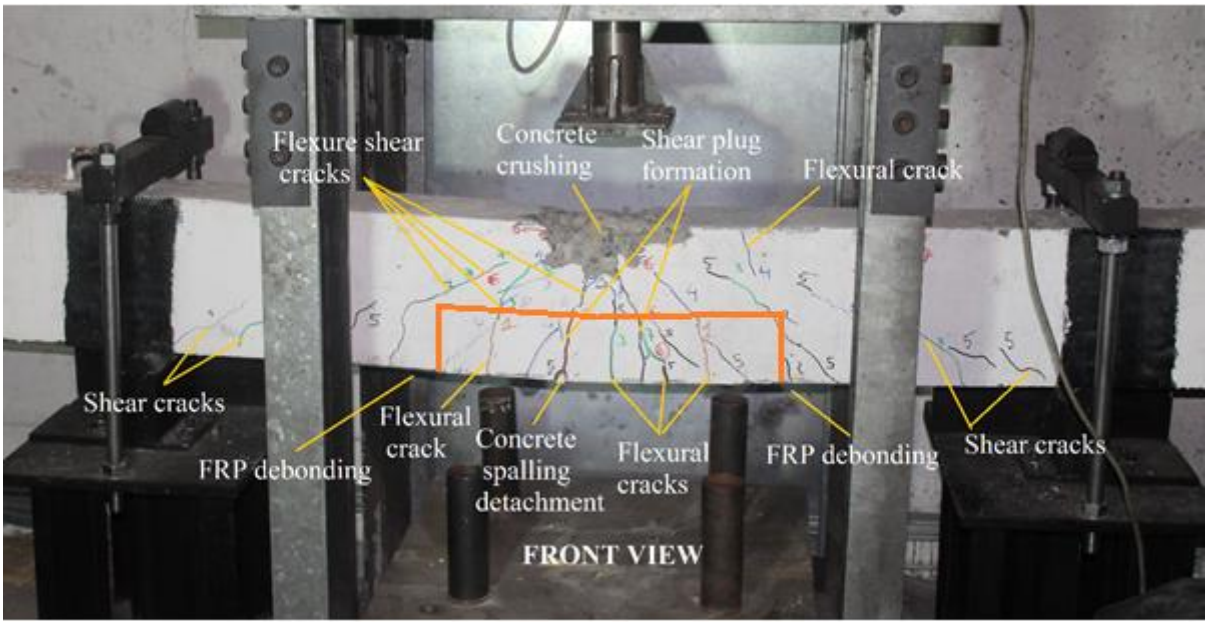

Appendix B. 2. 3. Cracking profiles and mode of failure observed from SB1_2 (a).

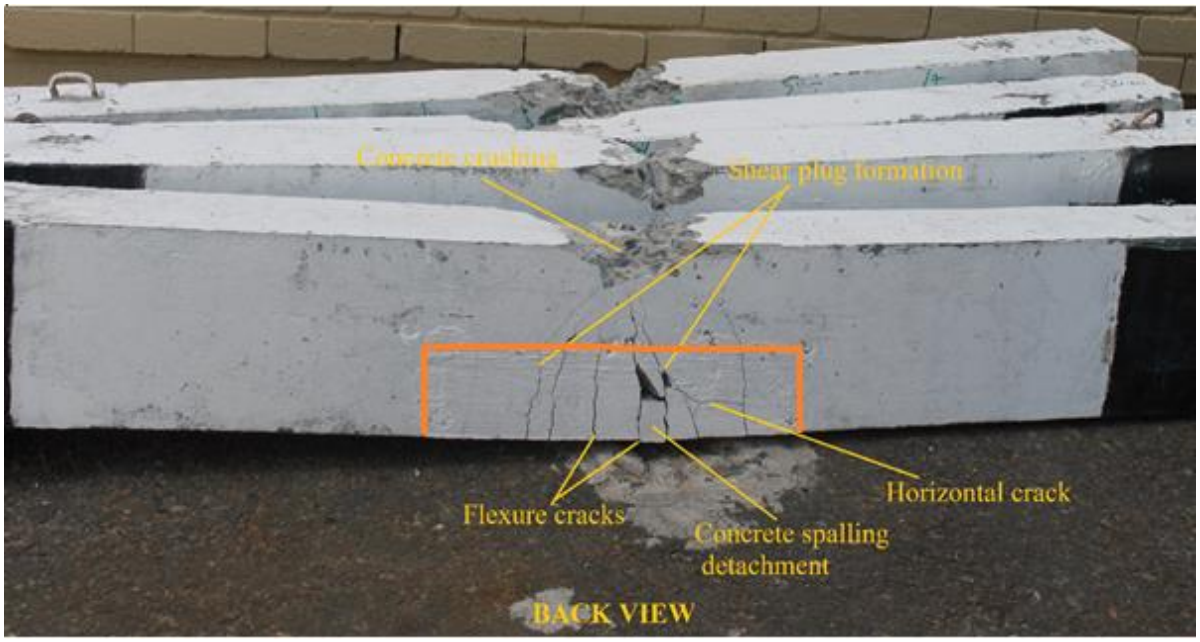

Appendix B. 2. 4. Cracking profiles and mode of failure observed from SB1_2 (b).

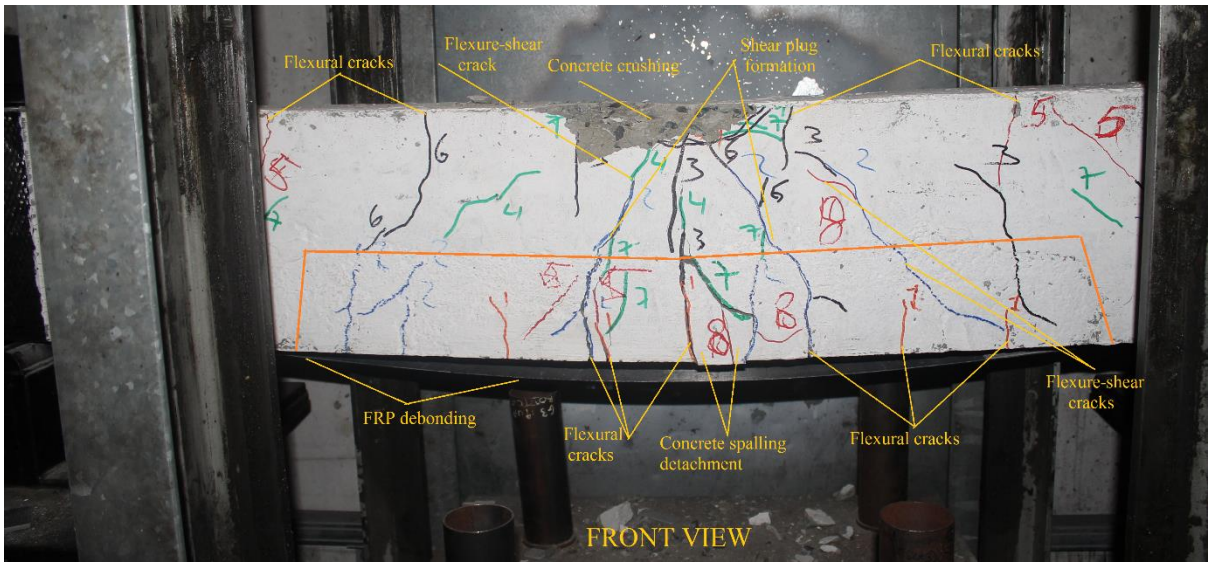

Appendix B. 3. 1. Cracking profiles and mode of failure observed from SB2_1.

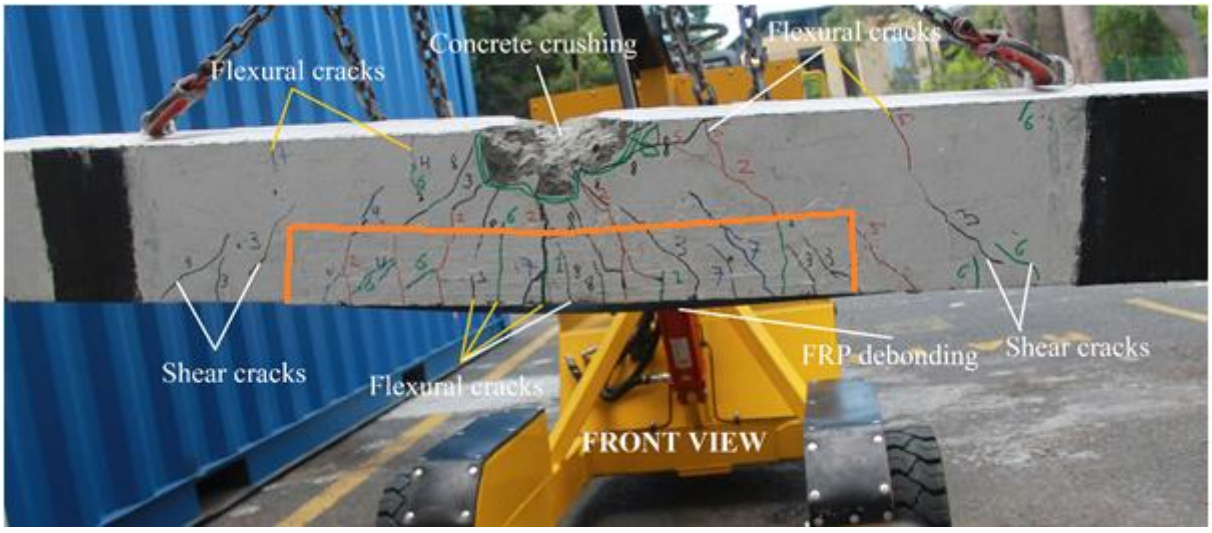

Appendix B. 3. 2. Cracking profiles and mode of failure observed from SB2_2 (a).

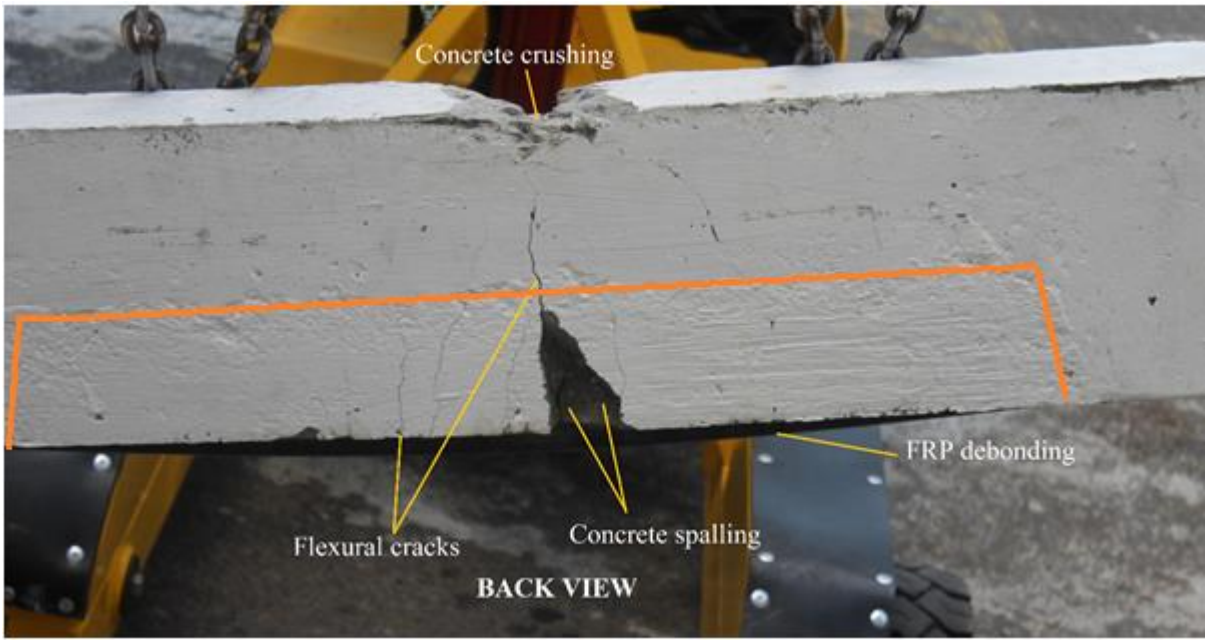

Appendix B. 3. 3. Cracking profiles and mode of failure observed from SB2_2 (b).

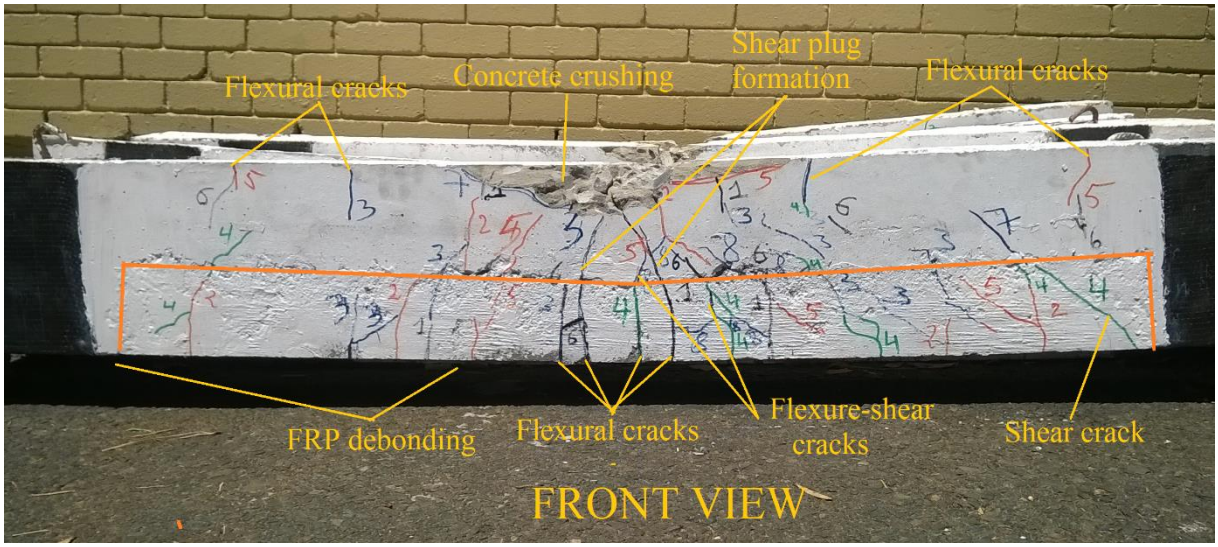

Appendix B. 4. 1. Cracking profiles and mode of failure observed from SB3_1.

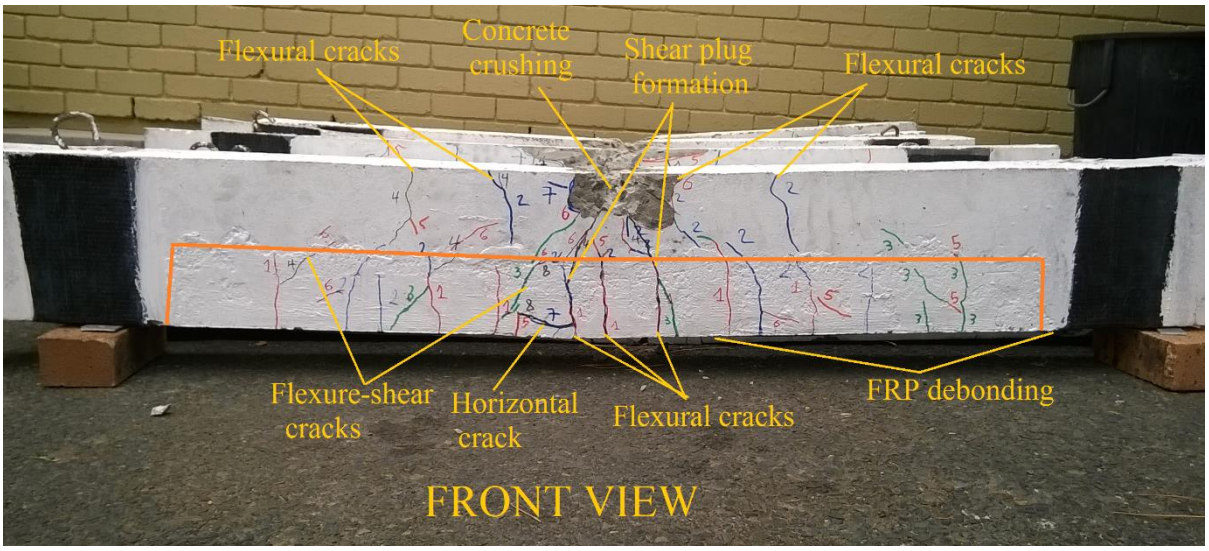

Appendix B. 4. 2. Cracking profiles and mode of failure observed from SB3_2.

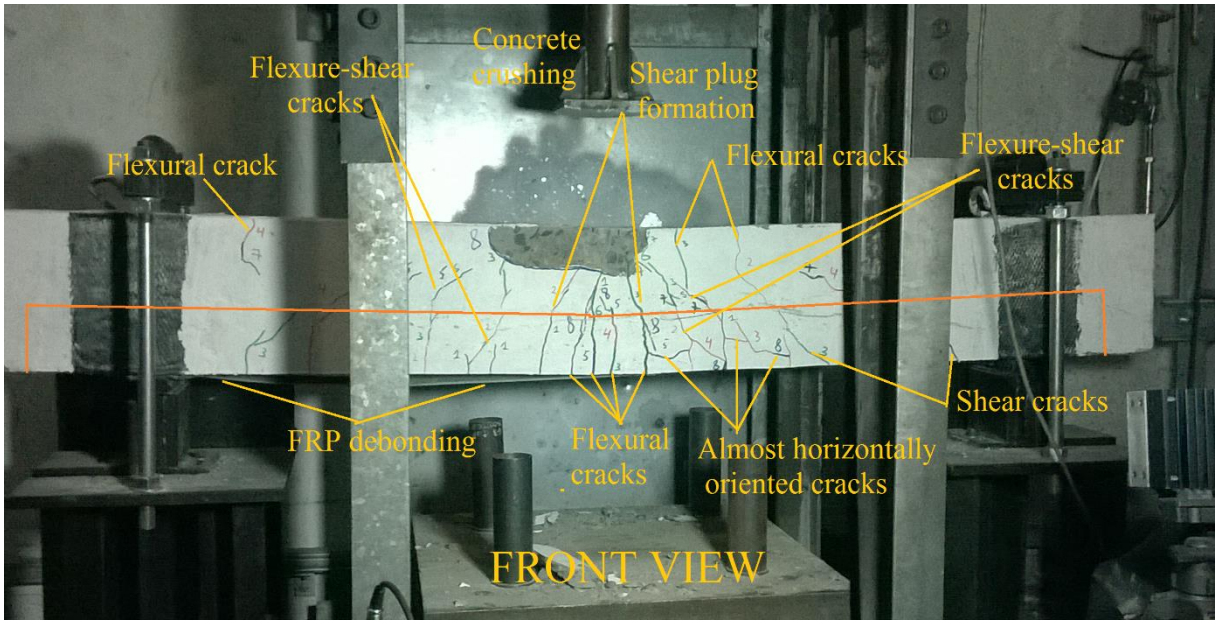

Appendix B. 5. 1. Cracking profiles and mode of failure observed from SB4_2.

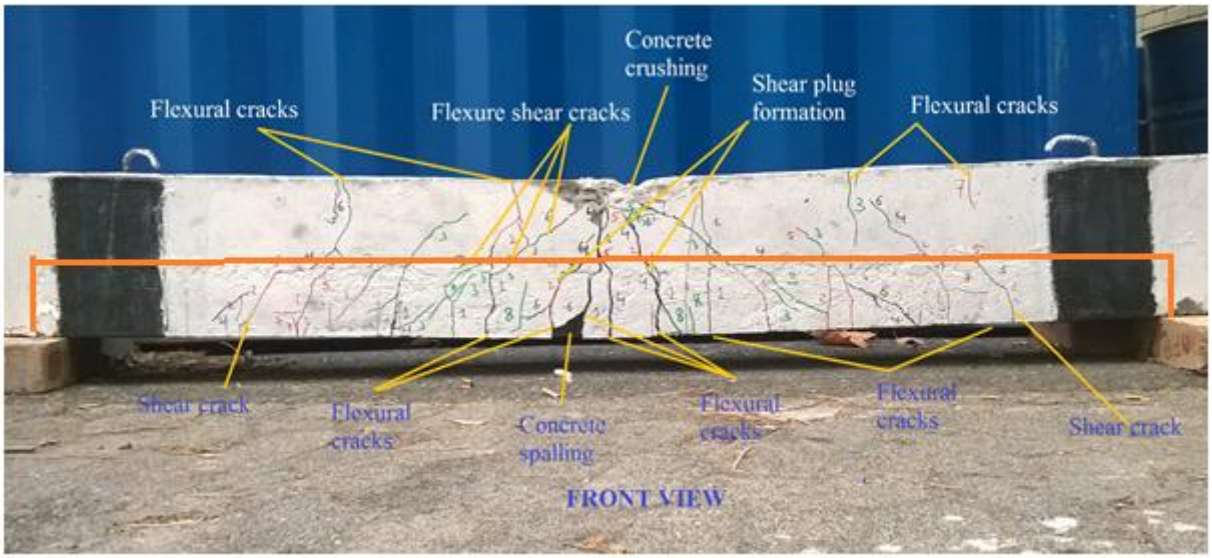

Appendix B. 5. 2. Cracking profiles and mode of failure observed from SB4_3.

APPENDIX C. EXAMPLE OF EXTRACTION OF DISPLACEMENTS RESULTS FROM HSC FOOTAGE WITH THE USE OF PFA SOFTWARE

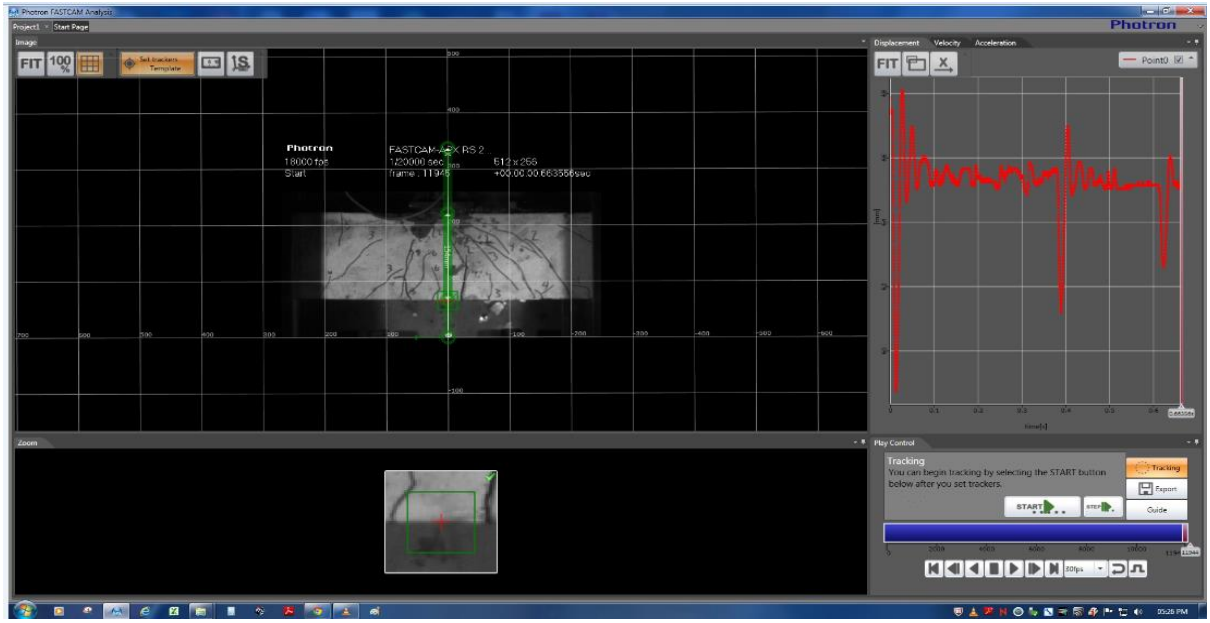

Appendix C. 1. 1. Typical extraction of displacement response with the use of PFA software: End of tracking step from CB1.

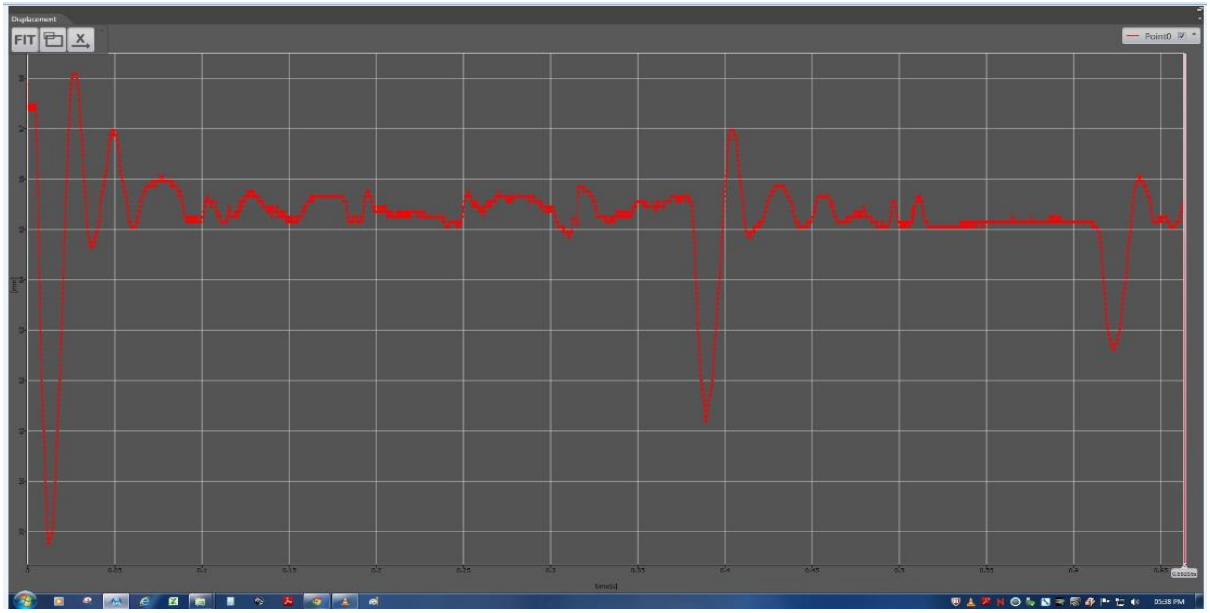

Appendix C. 1. 2. Detailed typical extraction of displacement response with the use of PFA software: End of tracking step from CB1.

EBE Faculty: Assessment of Ethics in Research Projects

Any person planning to undertake research in the Faculty of Engineering and the Built Environment at the University of Cape Town is required to complete this form before collecting or analysing data. When completed it should be submitted to the supervisor (where applicable) and from there to the Head of Department. If any of the questions below have been answered YES, and the applicant is NOT a fourth year student, the Head should forward this form for approval by the Faculty EIR committee: submit to Ms Zulpha Geyer (Zulpha.Geyer@uct.ac.za; Chem Eng Building, Ph 021 650 4791). Students must include a copy of the completed form with the thesis when it is submitted for examination.

Name of Principal Researcher/Student: P. HABIMANA Department: Civil Eng.

If a Student: Degree: Str. Engineering (Msc) Supervisor: Prof. Pilate Moyo

If a Research Contract indicate source of funding/sponsorship:

Research Project Title: Damage detection in Composite structures

Overview of ethics issues in your research project:

Question 1: Is there a possibility that your research could cause harm to a third party (i.e. a person not involved in your project)?	YES	NO
Question 2: Is your research making use of human subjects as sources of data? If your answer is YES, please complete Addendum 2.	YES	NO
Question 3: Does your research involve the participation of or provision of services to communities? If your answer is YES, please complete Addendum 3.	YES	NO
Question 4: If your research is sponsored, is there any potential for conflicts of interest? If your answer is YES, please complete Addendum 4.	YES	NO

If you have answered YES to any of the above questions, please append a copy of your research proposal, as well as any interview schedules or questionnaires (Addendum 1) and please complete further addenda as appropriate.

I hereby undertake to carry out my research in such a way that

- there is no apparent legal objection to the nature or the method of research; and
- the research will not compromise staff or students or the other responsibilities of the University;
- the stated objective will be achieved, and the findings will have a high degree of validity;
- limitations and alternative interpretations will be considered;
- the findings could be subject to peer review and publicly available; and
- I will comply with the conventions of copyright and avoid any practice that would constitute plagiarism.

Signed by:

	Full name and signature	Date
Principal Researcher/Student: Signed by candidate	Signed by candidate	24/01/2014

This application is approved by:

Supervisor (if applicable):	Signed by candidate	24/1/2014
HOD (or delegated nominee): Final authority for all assessments with NO to all questions and for all undergraduate research.	Signed by candidate	27/01/14
Chair : Faculty EIR Committee For applicants other than undergraduate students who have answered YES to any of the above questions.		